2009

The development of a pore pressure and fracture gradient prediction model for the Ewing Banks 910 area in the Gulf of Mexico

Jeffrey Steven Fooshee
Louisiana State University and Agricultural and Mechanical College

THE DEVELOPMENT OF A PORE PRESSURE AND FRACTURE GRADIENT PREDICTION MODEL FOR THE EWING BANKS 910 AREA IN THE GULF OF MEXICO

A Thesis

Submitted to the Graduate Faculty of the
Louisiana State University and
Agricultural and Mechanical College
in partial fulfillment of the
requirements for the degree of
Master of Science in Petroleum Engineering

in

The Department of Petroleum Engineering

by

Jeffrey S. Fooshee
B.S., Louisiana State University and Agricultural and Mechanical College, 2000
May 2009

ACKNOWLEDGEMENTS

First, I would like to thank Dr. John Rogers Smith for his patience and guidance throughout my graduate studies. His knowledge and experience provided tremendous benefit to growth in both my career and studies. His advice has been invaluable.

Thanks to Petroleum Engineering Department Chair Dr. Stephen Sears, Dr. Mileva Radonjic and Dr. Richard Hughes for agreeing to participate on my final examination committee.

I would also like to thank W&T Offshore, Inc., my ex-employer for allowing the continued use of this data set to perform this research. All of this data was acquired while employed at W&T and after resigning, they allowed me to continue using the data set. Without their permission, this research would not be possible.

Also, I would like to thank my current employer, BOPCO, LLC for allowing me to devote a lot of my time at the office working towards this degree.

Very special thanks to my wife, Kristin, for her patience and support during my pursuit of this degree. As a working professional, this degree demanded an extraordinary amount of time away from home. I can not imagine having the ability to complete this degree without her strength and support along the way.

TABLE OF CONTENTS

LIST OF TABLES

LIST OF FIGURES

ABSTRACT

The purpose of this project is to develop a pore pressure and fracture gradient prediction strategy for the Ewing Banks 910 (EW 910) area. Petrophysical and measured pressure data for eight wells previously drilled in the EW 910 area will be examined and reviewed. This strategy will help design future drilling and completion operations in the aforementioned area.

Two pore pressure prediction strategies and one fracture gradient prediction strategy will be reviewed and applied to the available data.

The first pore pressure prediction strategy reviewed was developed by W. R. Matthews. This strategy utilizes a geologic age specific overlay which indicates the normally pressured compaction trendline for the appropriate geologic age. After plotting the observed resistivity/conductivity data on the geologic age specific overlay, formation pore pressures can be predicted. A simple calibration of the data is required to implement this method.

The second pore pressure prediction strategy reviewed was developed by Ben Eaton. Eaton developed a simple relationship that predicts the formation pore pressure knowing the normally pressured compaction trendline, the observed resistivity/conductivity data and a relationship for formation overburden stress.

The fracture pressure prediction strategy reviewed was also developed by Ben Eaton. The data required for this prediction strategy is formation overburden stress, pore pressure and formation Poisson's ratio. A relationship for the overburden stress and Poisson's ratio can be developed or one of Eaton's published relationships can be used. Ultimately, the Eaton fracture gradient prediction strategy results in a simple and accurate relationship provided an accurate estimate of pore pressure is available.

The two formation pore pressure prediction strategies were applied to the petrophysical data. The resulting formation pore pressure prediction was compared to the measured pressure

data obtained from the eight offset wells. After analyzing each pore pressure model against the available pressure data, the Eaton pore pressure prediction strategy was chosen as the best model to implement in future operations.

The fracture gradient prediction strategy was implemented using the formation pore pressures estimated by the Eaton pore pressure prediction strategy. The fracture gradients predicted were within range of the fracture gradients suggested by the offset data.

1. INTRODUCTION

1.1 Research Objectives

An accurate prediction of the sub-surface pore pressures and fracture gradients is a necessary requirement to safely, economically and efficiently drill the wells required to test and produce oil and natural gas reserves. Pore pressures are easily predicted for normally pressure sediments. It is the prediction of pore pressures for the abnormally pressured (i.e. over-pressured) sediments that is more difficult and more important. An understanding of the pore pressure is a requirement of the drilling plan in order to choose proper casing points and design a casing program that will allow the well to be drilled most effectively and maintain well control during drilling and completion operations. Well control events such as formation fluid kicks, lost circulation, surface blowouts and underground blowouts can be avoided with the use of accurate pore pressure and fracture gradient predictions in the design process.

The purpose of this project is to develop a pore pressure and fracture gradient prediction strategy for the Ewing Banks 910 (EW 910) area. Petrophysical and measured pressure data for eight wells previously drilled in the EW 910 area will be examined and reviewed. The pore pressure and fracture gradient prediction strategy will be useful when designing future drilling and completion operations in the aforementioned area.

1.2 Ewing Banks 910 Area Overview and Drilling History

EW 910 is a federally-regulated block located offshore South Louisiana. The water depth ranges from 550' to 700' in this and neighboring blocks. The geologic ages of the subsurface sediments in this area are Pleistocene and Pliocene. The eight wells included in this review are located in four blocks: EW 910, EW 953, EW 954 and South Timbalier 320 (ST 320). Six wells (four located in EW 910, one located in EW 954 and one located in ST 320) were drilled from one eight-well template and are produced to the surface through a four-pile production facility.

The single well drilled in EW 953 and the other remaining well drilled in EW 910 (EW 910 No. 4) were both non-commercial and never produced. Figure 1.1 is a plan view of the surface and bottom-hole locations for the eight wells analyzed. Since the EW 910 A1BP, EW 910 No. 4 and EW 953 No. 1 wells were drilled as straight holes, their surface and bottom-hole locations are essentially the same. The remaining six wells were drilled from the same template as the EW 910 A1BP, therefore their surface locations are essentially the same as that of the EW 910 A1BP.

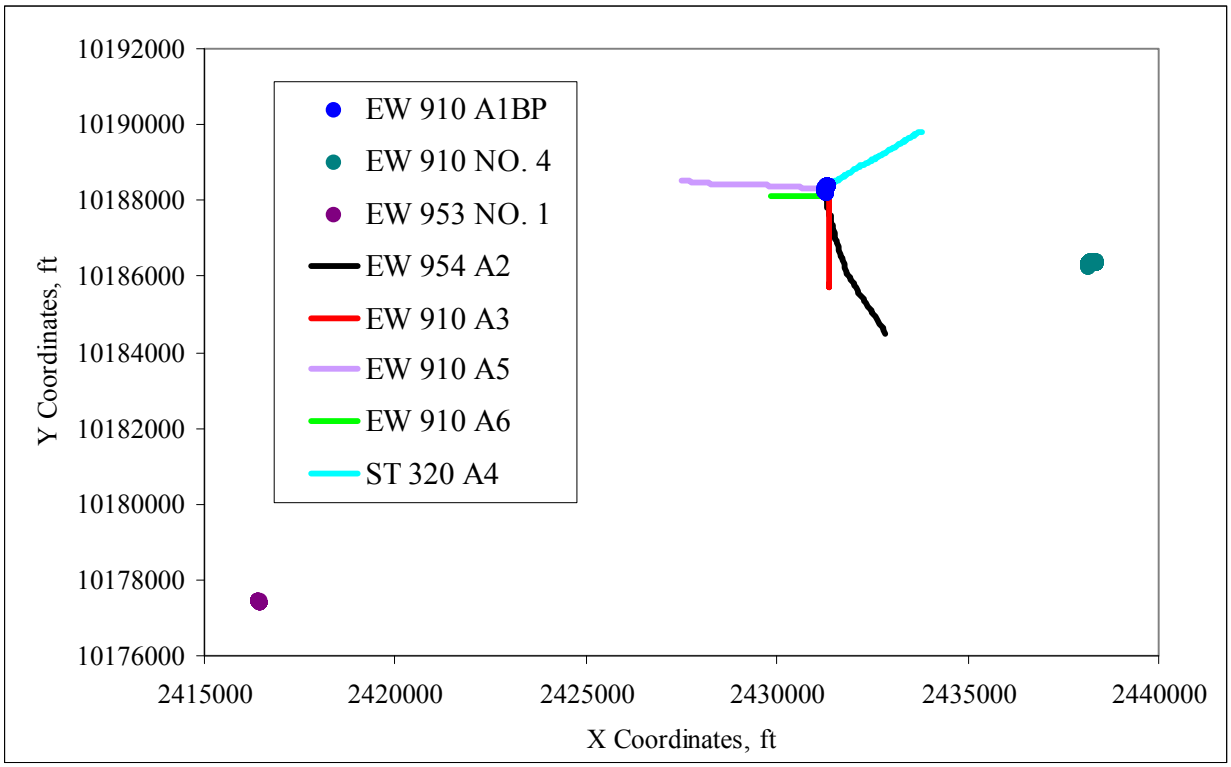

Fig. 1.1: Plan View of Eight Wells Analyzed in EW 910 Area

As can be seen in Fig. 1.1, the EW 953 No. 1 well is approximately 3.5 miles (~18400') southwest and the EW 910 No. 4 is approximately 1.4 miles east-southeast (~7300') of the EW 910 Platform. As can be expected due to the long distances between wells, there is a significant difference in pore pressure regimes.

Figure 1.2 is an arbitrary seismic line starting at the EW 953 No. 1 well and moving NE through the platform wells before ending at the EW 910 No.4 well. The yellow lines signify the

wellbore paths. This seismic view demonstrates the significant faulting that occurs between the wells.

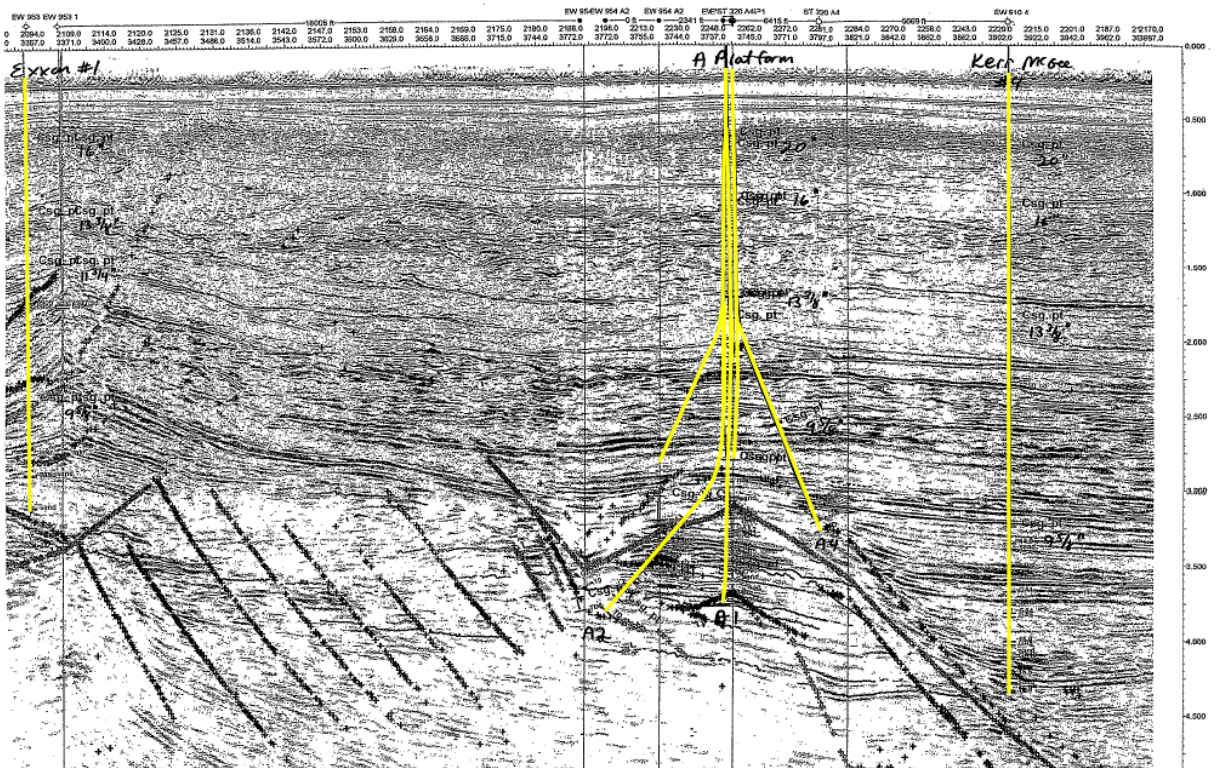

Fig. 1.2: SW – NE Arbitrary Seismic Line

Drilling operations began in October 1984 when Exxon spudded the EW 953 No. 1 well with the Glomar Pacific semi-submersible drilling rig. It took 134 days to reach total depth (10800') and the wellbore was plugged and abandoned due to non-commercial hydrocarbon reserves. Kerr McGee (KMG) drilled an exploratory well, later renamed A1BP, in EW 910 in June 1996 and determined reservoir extent by drilling two more exploratory wells in 1997. The first delineation well drilled into the southern block of EW 954, the A2, was successful, but the No. 4 well in the far eastern region of EW 910 was non-commercial and was plugged and abandoned. After construction of a four-pile production facility, KMG mobilized ENSCO 22, a 3000-hp platform rig, and drilled the remaining four wells from the production facility beginning in April 1999.

The methods utilized in the project to develop a pore pressure and fracture gradient prediction strategy require petrophysical log data. Table 1.1 is a summary of the available log data obtained while drilling these eight wells.

Table 1.1: Summary of Available Log Data in EW 910 Area

Well	RES/COND	SONIC	NEU/DEN	RFT/MDT	SWCs	PWD
EW 953 No. 1	1700-10800’	2000-10750’	3000-10750’	Yes	No	No
EW 910 A1BP	3000-12600’	11700-12600’	9000-11600’	Yes	No	No
EW 954 A2	5500-12900’	8500-14000’	10000-14000’	Yes	No	No
EW 910 A3	4900-12700’	10100-12700’	10100-12700’	Yes	No	Yes
ST 320 A4	3400-10600’	8000-10600’	8000-10600’	No	No	Yes
EW 910 A5	5000-12100’	10100-12100’	10100-12100’	No	No	Yes
EW 910 A6	4900-11300’	NA	10100-11300’	No	No	Yes
EW 910 No. 4	5500-14550’	10500-14550’	10500-14550’	No	Yes	No

1.3 Description of Pore Pressure and Fracture Gradient Prediction Strategies Applied

Two pore pressure prediction strategies and one fracture gradient prediction strategy will be reviewed and applied to the available data. The two pore pressure prediction strategies require petrophysical data, specifically formation resistivity or conductivity, to predict pore pressures. The fracture gradient prediction strategy requires an accurate estimate of pore pressure.

The first pore pressure prediction strategy reviewed was developed by W.R. Matthews[14]. This strategy utilizes a series of geologic age specific overlays, which indicate the normally pressured compaction trendlines for the respective geologic age. After plotting the observed resistivity/conductivity data on the geologic age specific overlay, the pore pressures can be predicted. A simple calibration of the data was required to establish the normal pressure trendline implemented in this method.

The second pore pressure prediction strategy reviewed was developed by Ben Eaton[9]. Eaton developed a simple relationship that will predict the pore pressure knowing the normally

pressured compaction trendline, the observed resistivity/conductivity data and a relationship for the overburden stress versus depth.

The fracture pressure prediction strategy reviewed was also developed by Ben Eaton[7]. The data required for this prediction strategy is formation overburden stress, pore pressure and Poisson's ratio of the formation. A relationship for the overburden stress and Poisson's ratio can be developed based on field data, or one of Eaton's generalized relationships can be used. Generally, the Eaton fracture gradient prediction strategy results in a simple and accurate relationship provided an accurate estimate pore pressure prediction is available.

1.4 Description of Prediction Method Analysis

The workflow implemented to analyze and ultimately choose the best pore pressure and fracture gradient prediction strategy is outlined below. This workflow was performed for each of the eight offset wells.

1. Identify, acquire and review offset well data including;
    - Petrophysical data
    - Drilling records
    - Measured pressure data
2. Construct pore pressure prediction model using petrophysical data.
3. Include offset well data in the pore pressure prediction model.
4. Calibrate pore pressure prediction model, if necessary.
5. Analyze pore pressure prediction model against data obtained from reviewing drilling records and select or develop an accurate pore pressure prediction model.
6. Construct fracture gradient prediction model using an accurate pore pressure prediction model.
7. Analyze fracture gradient prediction model against data obtained from reviewing drilling records.

1.5 Overview of Thesis

This chapter discusses the necessity of an accurate pore pressure and fracture gradient prediction strategy, the objective of this research project, an overview of the EW 910 area and the drilling history, a brief description of the applied prediction strategies, a description of the workflow implemented to analyze the prediction strategies and finally an overview of this thesis.

Chapter 2 discusses the literature that was reviewed to gain knowledge of different pore pressure and fracture gradient prediction strategies.

Chapter 3 includes a review of the available offset well data.

Chapter 4 applies the Matthews approach to estimating pore pressure from petrophysical data to all eight wells.

Chapter 5 applies the Eaton method of estimating pore pressures from petrophysical data for all eight wells.

Chapter 6 compares the results of the Matthews and Eaton approaches and determines which pore pressure strategy is the best model to use in planning future drilling operations.

Chapter 7 utilizes the pore pressure predictions in applying Eaton's fracture gradient prediction strategy to all eight wells.

Chapter 8 summarizes the results of this project and offers recommendations for improvement of results.

2. LITERATURE REVIEW

A literature review was performed to gain knowledge of different pore pressure and fracture gradient prediction methods in an effort to find the best strategy for this area. This review, however, is not fully exhaustive as there are a vast number of strategies that have been developed since the middle of the twentieth century. This review is limited to a few pore pressure prediction strategies and two fracture gradient prediction strategies.

While implementing the multiple pore pressure and fracture gradient prediction strategies, an effort was made to verify or determine the petrophysical data required for a sound prediction strategy. Those methods will also be included in the literature review.

2.1 Pore Pressure Prediction Strategies

Bourgoyne et al[4] clearly summarized four mechanisms for generating abnormal pore pressures, or overpressures; Compaction, Diagenesis, Differential Density and Fluid Migration.

The most common overpressure generating mechanism is compaction. When sediments are deposited in a deltaic depositional environment (the most common depositional environment) the sediments are initially unconsolidated and remain in suspension with the carrying fluid, typically sea water. As the depositional process continues, the sediments come into contact with each other and are able to support the weight of the sediments being deposited above them by the grain-to-grain contact points. Throughout this process, the formation continues to remain in hydraulic communication with the fluid source above. As the depositional process continues, the weight of the overlying sediments begins to compact the sediments, causing the sediments to realign, resulting in a reduced porosity and expulsion of fluid from the formation. As long as the pore fluid can escape as quickly as required by the natural compaction process, the formation pore space will remain in hydraulic communication with the fluid source and the pore pressure is solely the hydrostatic pressure generated from the density of the pore fluid. However, if the

natural compaction process is faster than the rate of the pore fluid expulsion, abnormal formation pressures will be generated due to some of the load being placed upon the sediments being supported by the pressure in the pore fluids.

The second overpressure generating mechanism explained by Bourgoyne et al is diagenesis. Diagenesis is defined as "the physical, chemical or biological alteration of sediments into sedimentary rock at relatively low temperatures and pressures that can result in changes to the rock's original mineralogy and texture". It includes compaction, cementation, recrystallization, and perhaps replacement, as in the development of dolomite. In Gulf of Mexico sedimentary basins, one diagenetic process is the conversion of montmorillonite clays to illites, chlorites and kaolinite clays during compaction when in presence of potassium ions. Water is present in clay deposits as both free water and bound water. The bound water has significantly higher density. During diagenesis, as the bound water becomes free water, the higher density bound water must undergo a volume increase as it desorbs. If the free water is not allowed to escape (i.e. rapid compaction, precipitates caused from diagenesis, caprock, etc.), then the pore pressure will become abnormally pressured. Diagenesis typically occurs under bottom-hole temperatures of at least 200° F.

The third overpressure generating mechanism described by Bourgoyne et al is differential density. This mechanism occurs when a formation contains a pore fluid with a density significantly less than the normal pore fluid density for the area. If the structure has significant dip, then the extension of the structure up dip will result in higher pore pressure gradients than experienced down dip where the pressure gradient is known. Although the up dip pore pressure will be lower in absolute pressure, the pressure gradient will be higher requiring a higher hydrostatic gradient to control the pore pressure. The following example is included for clarification:

Example 1

Reservoir A has a known normal pressure gradient of 0.465 psi/ft at 10000'. The reservoir contains dry gas with a fluid gradient of 0.1 psi/ft. To accelerate the reserves, an additional well will be drilled 3000' away, but due to the significant dip of the reservoir, will penetrate the reservoir 1000' higher on structure. The pore pressure gradient at the reservoir penetration point is calculated as follows:

$P_{F-2} = P_{F-1} - \Delta TVD$ x Fluid Gradient

P_{F-2} = 4650 psi – 1000 ft x 0.1 psi/ft

P_{F-2} = 4550 psi

P_{F-2} Gradient = P_{F-2} / TVD_2

P_{F-2} Gradient = 4550 psi / 9000 ft = 0.505 psi/ft

The fourth and final overpressure generation mechanism elucidated by Bourgoyne et al is fluid migration. This mechanism occurs when overpressured formations have a communication path to a normally pressured formation and the normally pressure formation becomes charged. The hydraulic communication path can be man-made or naturally occurring.

Karl Terzaghi[21] developed a simple relationship between pore pressure and the effective stress of the rock. Even though his relationship was determined empirically, it was proven later that it can be derived analytically from 1-D compaction theory. Terzaghi noted: "The stresses in any point of a section through a mass of soil can be computed from the total principal stresses σ_1, σ_2, σ_3, which act in this point. If the voids of the soil are filled with water under a stress μ, the total principal stress consists of two parts. One part, μ, acts in the water and in the solid in every direction with equal intensity. It is called the neutral stress (or the porewater pressure). The balance $\sigma_i' = \sigma_i - \mu$ represents an excess over the neutral stress μ, and it has its seat exclusively in the solid phase of the soil. This fraction of the principal stress will be called the *effective principal stress.* (…) A change in the neutral stress μ produces practically no volume change and

has practically no influence on the stress conditions for failure. Porous materials (such as sand, clay and concrete) react to a change of μ as if they were incompressible and as if their internal friction were equal to zero. All the measurable effects of a change of stress, such as compression, distortion and a change of shearing resistance are exclusively due to changes in the effective stress σ'_i."

The above statement indicates that this is a conceptual stress. Only the effects of an effective stress change are measurable, not the effective stress itself. Terzaghi determined the following mathematical relationship: $\sigma_{ei} = \sigma_i - P_F$.

Therefore, pore pressure can be calculated from the difference between principal and effective stresses acting in a given direction. In the case of drilling for oil and gas, the principal stress in the vertical direction is the overburden stress, which can be determined by a number of published correlations or by integration of the bulk density log data. The unknown variable is the corresponding conceptual effective stress. In general, overpressuring during the compaction process is associated with a slower porosity decrease with depth. If the assumption is made that vertical strains dominate during the compaction process, then Terzaghi's principle would imply that the effective vertical stress is the exclusive cause of shale porosity variations. Therefore, pore pressure is determined from the effective vertical stress and the overburden stress by the following relationship:

$$P_F = \sigma_{OB} - \sigma_{EV} \qquad \textit{(Equation 2.1)}$$

where P_F is the pore pressure, σ_{OB} is the overburden stress and σ_{EV} is the effective vertical stress, all with units of *psi*.

One of the early papers published on pore pressure interpretation was authored by Hottman and Johnson[13]. The authors included a description of the pore pressure, overburden stress and effective vertical stress relationship described by Terzaghi. They recognized the

significance of Terzaghi's relationship and developed an empirical relationship between fluid pressure gradient (FPG) and the electrical log properties. The data sets used for the development of the techniques were taken from Tertiary sediments located in Southern Louisiana and the Upper Texas Gulf Coast. The geologic age of the acquired data set was Miocene and Oligocene.

The pore pressure and acoustic data used in the interpretation technique is included in Table 2.1.

Table 2.1: Pressure and Acoustic Log Data – Overpressured Miocene-Oligocene Formations, South Louisiana and Upper Texas Gulf Coast per Hottman and Johnson[13]

Parish or County and State	Well	Depth (ft)	Pressure (psi)	FPG (psi/ft)	$dT_{ob(sh)} - dT_{n(sh)}$ (microsec/ft)
Terrebonne, La	1	13387	11647	0.87	22
Offshore Lafourche, La	2	11000	6820	0.62	9
Assumption, La	3	10820	8872	0.82	21
Offshore Vermillion, La	4	11900	9996	0.84	27
Offshore Terrebonne, La	5	13118	11281	0.86	27
East Baton Rouge, La	6	10980	8015	0.73	13
St. Martin, La	7	11500	6210	0.54	4
Offshore St. Mary, La	8	13350	11481	0.86	30
Calcasieu, La	9	11800	6608	0.56	7
Offshore St. Mary, La	10	13010	10928	0.84	23
Offshore St. Mary, La	11	13825	12719	0.92	33
Offshore Placquemines, La	12	8874	5324	0.60	5
Cameron, La	13	11115	9781	0.88	32
Cameron, La	14	11435	10292	0.90	38
Jefferson, Tx	15	10890	9910	0.91	39
Terrebonne, La	16	11050	8951	0.81	21
Offshore Galveston, Tx	17	11750	11398	0.97	56
Chambers, Tx	18	12080	9422	0.78	18

A chart of the data presented in Table 2.1 is shown as Figure 2.1. Figure 2.1 is a plot illustrating the relationship of the difference between the interval transit time of the observed shale and the interval transit time of the normally pressured shale section $(dT_{ob(sh)} - dT_{n(sh)})$ values and Formation Pressure Gradient (FPG).

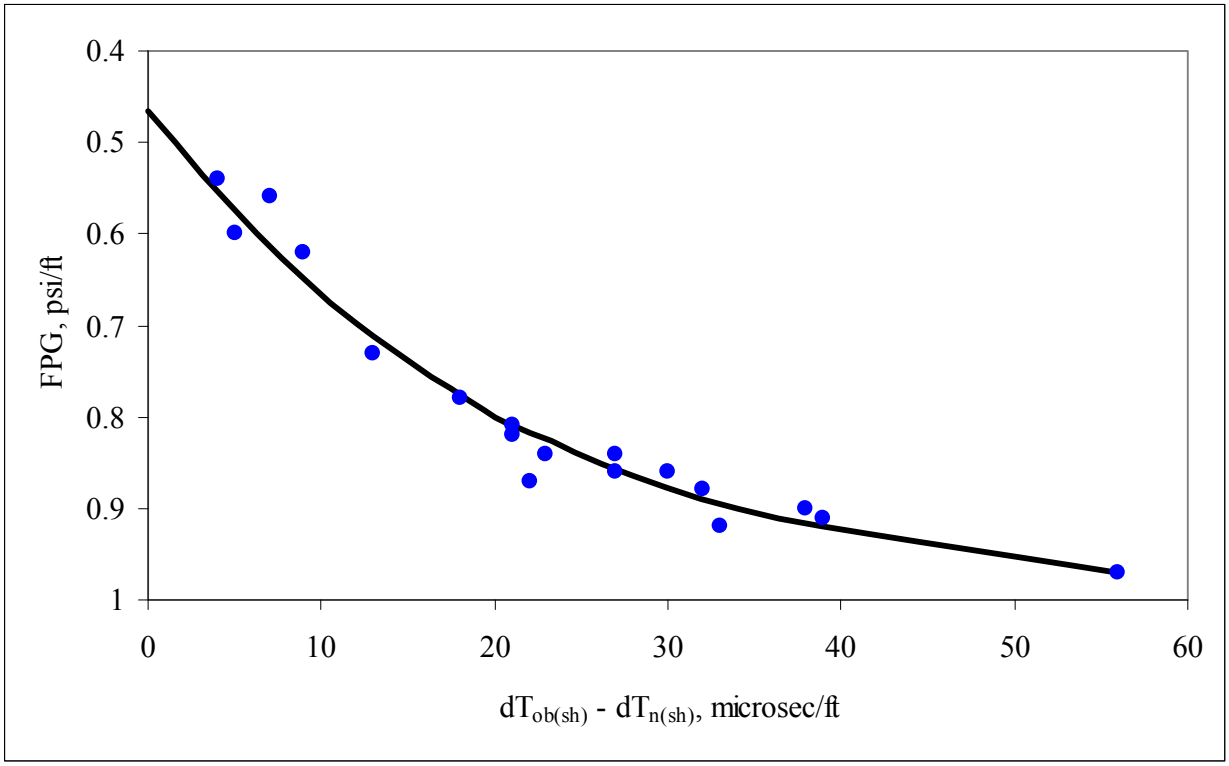

Fig. 2.1: Relation Between Shale Acoustic Parameter $dT_{ob(sh)}$ - $dT_{n(sh)}$ and Reservoir FPG per Hottman and Johnson[13]

The authors developed the following procedure to estimate pore pressures knowing acoustic travel time for shale formations.

1. The "normal compaction trend" for the area of interest is established by plotting the logarithm of $dT_{(sh)}$ vs. depth. (The authors included such a plot for the Miocene and Oligocene formations from the South Louisiana and Upper Texas Gulf Coast. It is reproduced as Figure 2.2)
2. A similar plot is made for the well in question.
3. The top of the overpressured formation is found by noting the depth at which the plotted points diverge from the trendline.
4. The fluid pressure gradient of a reservoir at any depth is found as follows:
    - The divergence of adjacent shales from the extrapolated normal line is measured.

- The fluid pressure gradient (FPG) corresponding to the $(dT_{ob(sh)} - dT_{n(sh)})$ value is found using the solid black line in Figure 2.1.

5. The FPG value is multiplied by the depth to obtain reservoir pressure.

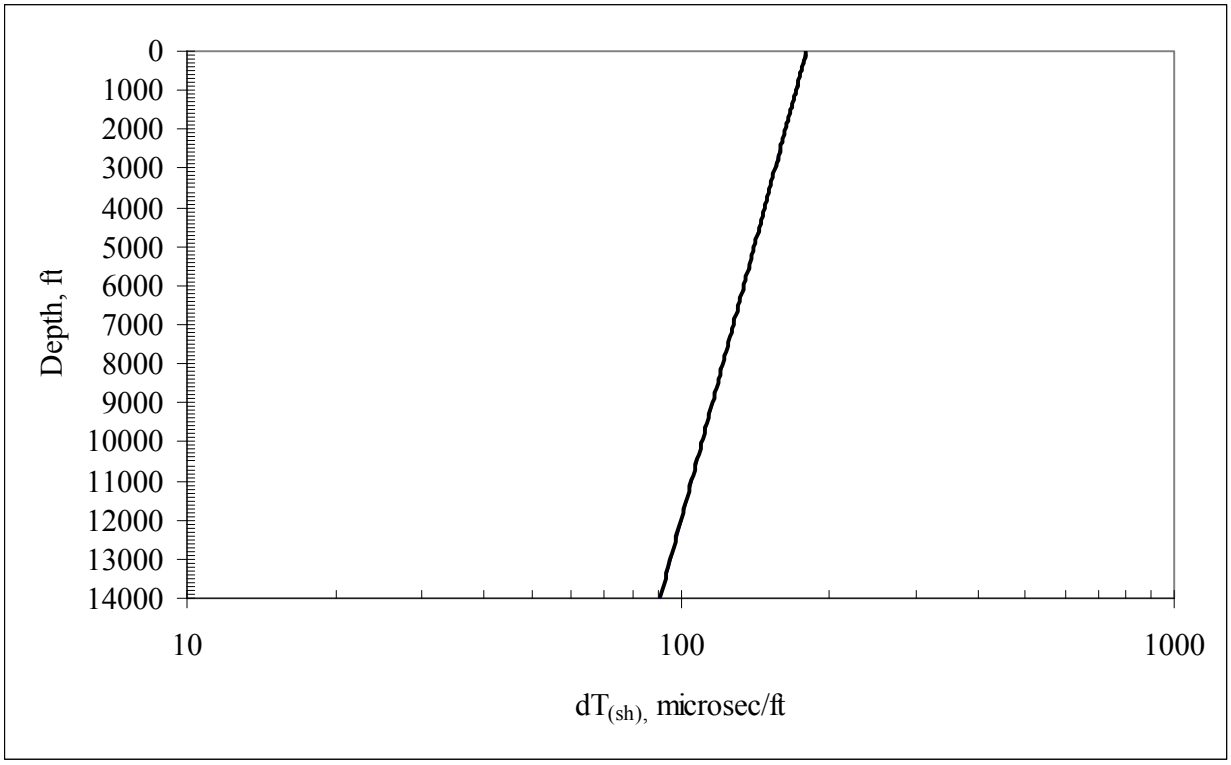

Fig. 2.2: Shale Travel Time vs Burial Depth for Miocene and Oligocene Shales, South Louisiana and Upper Texas Gulf Coast per Hottman and Johnson[13]

Hottman and Johnson also developed a technique for estimating pore pressures from formation resistivity properties. The procedure is similar to the formation acoustic property method in that formation properties (resistivity) of the abnormally pressured section are compared against a normal compaction trendline derived from offset well data. The pore pressure and formation resistivity data used in the interpretation technique is shown in Table 2.2.

Table 2.2: Pressure and Shale Resistivity Data – Overpressured Miocene-Oligocene Formations, South Louisiana and Upper Texas Gulf Coast per Hottman and Johnson[13]

Parish or County and State	Well	Depth (ft)	Pressure (psi)	Formation Pressure Gradient (psi/ft)	Shale Resistivity Ratio (ohm-m)
St. Martin, La	A	12400	10240	0.83	2.60
Cameron, La	B	10070	7500	0.74	1.70
Cameron, La	B	10150	8000	0.79	1.95
Cameron, La	C	13100	11600	0.89	4.20
Cameron, La	D	9370	5000	0.53	1.15
Offshore St. Mary, La	E	12300	6350	0.52	1.15
Offshore St. Mary, La	F	12500	6440	0.52	1.30
Offshore St. Mary, La	F	14000	11500	0.82	2.40
Jefferson Davis, La	G	10948	7970	0.73	1.78
Jefferson Davis, La	H	10800	7600	0.70	1.92
Jefferson Davis, La	H	10750	7600	0.71	1.77
Cameron, La	I	12900	11000	0.85	3.30
Cameron, La	J	13844	7200	0.52	1.10
Cameron, La	J	15353	12100	0.79	2.30
Lafayette, La	K	12600	9000	0.71	1.60
Lafayette, La	K	12900	9000	0.70	1.70
Lafayette, La	L	11750	8700	0.74	1.60
Lafayette, La	M	14550	10800	0.74	1.85
Cameron, La	N	11070	9400	0.85	3.90
Terrebonne, La	O	11900	8100	0.68	1.70
Terrebonne, La	O	13600	10900	0.80	2.35
Jefferson, Tx	P	10000	8750	0.88	3.20
St. Martin, La	Q	10800	7680	0.71	1.60
Cameron, La	R	12700	11150	0.88	2.80
Cameron, La	R	13500	11600	0.86	2.50
Cameron, La	R	13950	12500	0.90	2.75

Using the above data set, the authors generated a plot relating the Formation Pressure Gradient (FPG) to the ratio of the Normally Pressured Shale Resistivity and the Observed Shale Resistivity $(Rn_{(sh)}/Rob_{(sh)})$. This plot is shown as Figure 2.3.

The following procedure to estimate the pore pressure using shale resistivity data was outlined by Hottman and Johnson:

1. The normal "compaction trend" for the area of interest is established by plotting the logarithm of shale resistivities in normal pressured sections from offset well data.

2. A similar plot is made for the well in question.
3. The top of the overpressured formations is found by noting the depth at which the plotted points diverge from the normal trend line.
4. The pressure gradient of a reservoir at any depth is found as follows:
    - The ratio of the extrapolated normal shale resistivity to the observed shale resistivity is determined.
    - The fluid pressure gradient corresponding to the calculated ratios is found by using the solid black line in Figure 2.3.
5. The reservoir pressure is obtained by multiplying the FPG value by the depth.

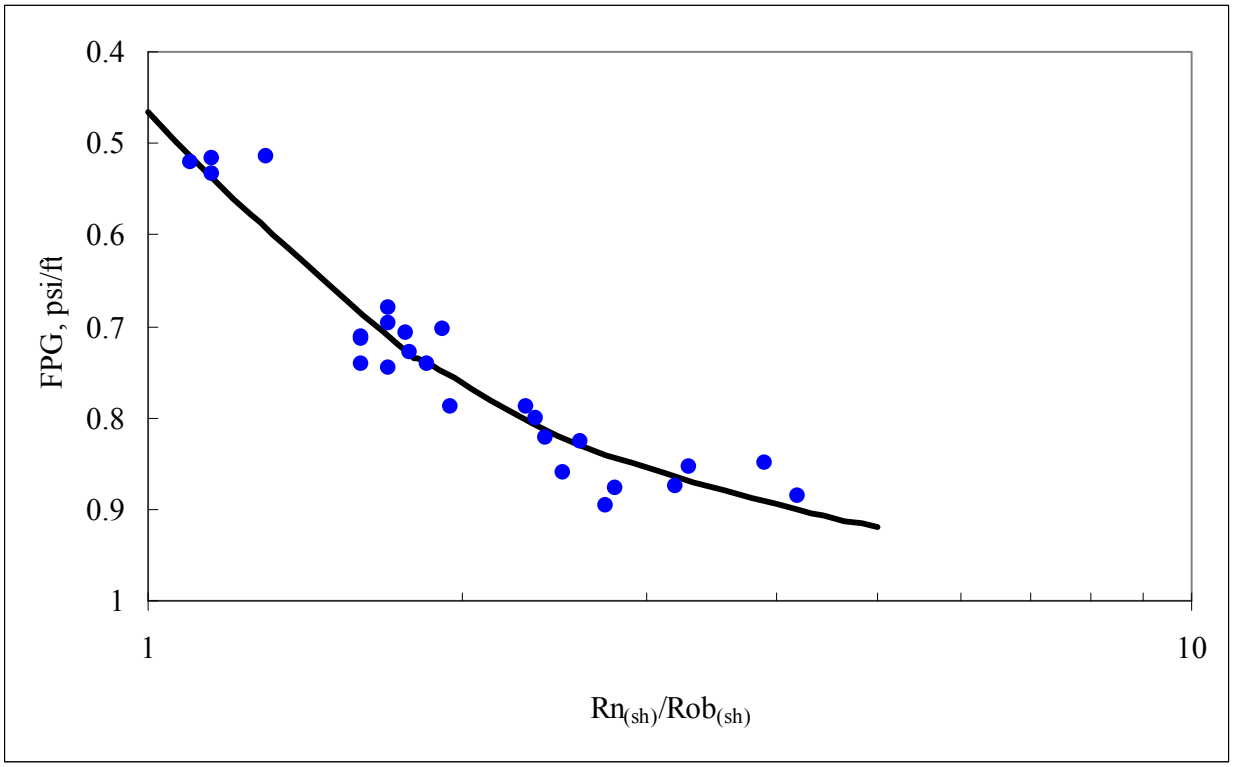

Fig. 2.3: Relation Between Shale Resistivity Parameter $Rn_{(sh)}/Rob_{(sh)}$ and Reservoir Fluid Pressure Gradient per Hottman and Johnson[13]

Hottman and Johnson believed that if their techniques were used in similar geologic environments with which the authors obtained the pressure data, pore pressures can be predicted to within 0.5 ppg equivalent mud weight (EMW). The authors discussed the following

limitations to their methods in determining pore pressure from both formation acoustic and resistivity data:

- Variations in shale clay mineralogy and clay content can make interpretations difficult. To ensure an accurate interpretation, care must be taken in selecting proper data points. Only shales with low SP deflection and uniform resistivity or sonic values should be selected.
- If zones of considerable depth contain fresh or brackish water, the variation in resistivity may render the resistivity approach useless. In such cases, use the sonic interpretation technique if available data exists.
- In general, the correlation of acoustic travel time versus depth is more easily established than resistivity since there are more factors that influence formation resistivity such as: salinity of the contained fluid, mineral composition and temperature. The data collection did not isolate these factors. The development of the empirical approach is inclusive of all factors. If any of these factors are significantly different than the data set, the approach may prove invalid.

In 1972 Eaton[9] published a technique for pore pressure prediction. Eaton recognized that Hottman and Johnson's basic relationship is correct, but can be improved. Hottman and Johnson's relationships, in the simplest terms, are as follows:

$$P_F / D = f\left(Rn_{(sh)} / Rob_{(sh)}\right) \qquad \textit{(Equation 2.2)}$$

$$P_F / D = f\left(dTob_{(sh)} - dTn_{(sh)}\right) \qquad \textit{(Equation 2.3)}$$

After rearrangement of the terms, the relationships are as follows:

$$Rn_{(sh)} / Rob_{(sh)} = f\left(P_F / D\right) \qquad \textit{(Equation 2.4)}$$

$$dTob_{(sh)} / dTn_{(sh)} = f\left(P_F / D\right) \qquad \textit{(Equation 2.5)}$$

Though Hottman and Johnson recognized Terzaghi's relationship to be true, their relationships did not follow the same form. Specifically, there was no way to distinguish the effects of the

three variables in Terzaghi's pore pressure relationship. Their relationship related pore pressure to just one petrophysical parameter, whether it was formation resistivity or interval transit time.

Eaton noted that the technique developed by Hottman and Johnson utilized just a single line drawn through the FPG versus the petrophysical parameter data and that data was considerably scattered. This led Eaton to expand on Hottman and Johnson's relationships. Eaton combined Terzaghi's and Hottman and Johnson's relationships by solving Terzaghi's relationship for pressure and dividing all of the variables by depth as follows:

$$P_F / D = \sigma_{OB} / D - \sigma_{EV} / D \qquad \textit{(Equation 2.6)}$$

Eaton postulates that the parameters derived from petrophysical log data are dependent variables primarily controlled by the pore pressure gradient and overburden stress gradient groups. He believed that Hottman and Johnson's relationships should be expanded to account for the effect of the overburden stress gradient. Up to this point, it was argued that the overburden stress gradient is constant for a given area and of no significance. Eaton refutes this argument saying that overburden stress gradients are functions of burial depth in areas where compaction and abnormal pressures are caused by increasing overburden loads with deeper burial. The overburden stress is a function of burial depth and formation bulk density by the following relationship:

$$\sigma_{ob} = \int \rho_b dD \qquad \textit{(Equation 2.7)}$$

where ρ_b is the formation bulk density.

Eaton initially developed the following empirical relationship iteratively, and it predicts the abnormal pressure behavior of Hottman and Johnson fairly well as seen in Figure 2.4:

$$P_F / D = \sigma_{OB} / D - 0.535\left(\frac{Rob_{(sh)}}{Rn_{(sh)}}\right)^{1.5} \qquad \textit{(Equation 2.8)}$$

If Eaton's empirical relationship is examined closely, the 0.535 term preceding the resistivity parameter is the effective stress gradient when the overburden stress gradient is 1.0 psi/ft and the normal pressure gradient is 0.465 psi/ft. Therefore Eaton's empirical relationship can now be more generically described as

$$P_F / D = \sigma_{OB} / D - \left(\sigma_{OB} / D - P_{F(n)} / D\right) * \left(\frac{Rob_{(sh)}}{Rn_{(sh)}}\right)^{1.5} \qquad \textit{(Equation 2.9)}$$

where $P_{F(n)}$ is the area-specific normal pore pressure gradient.

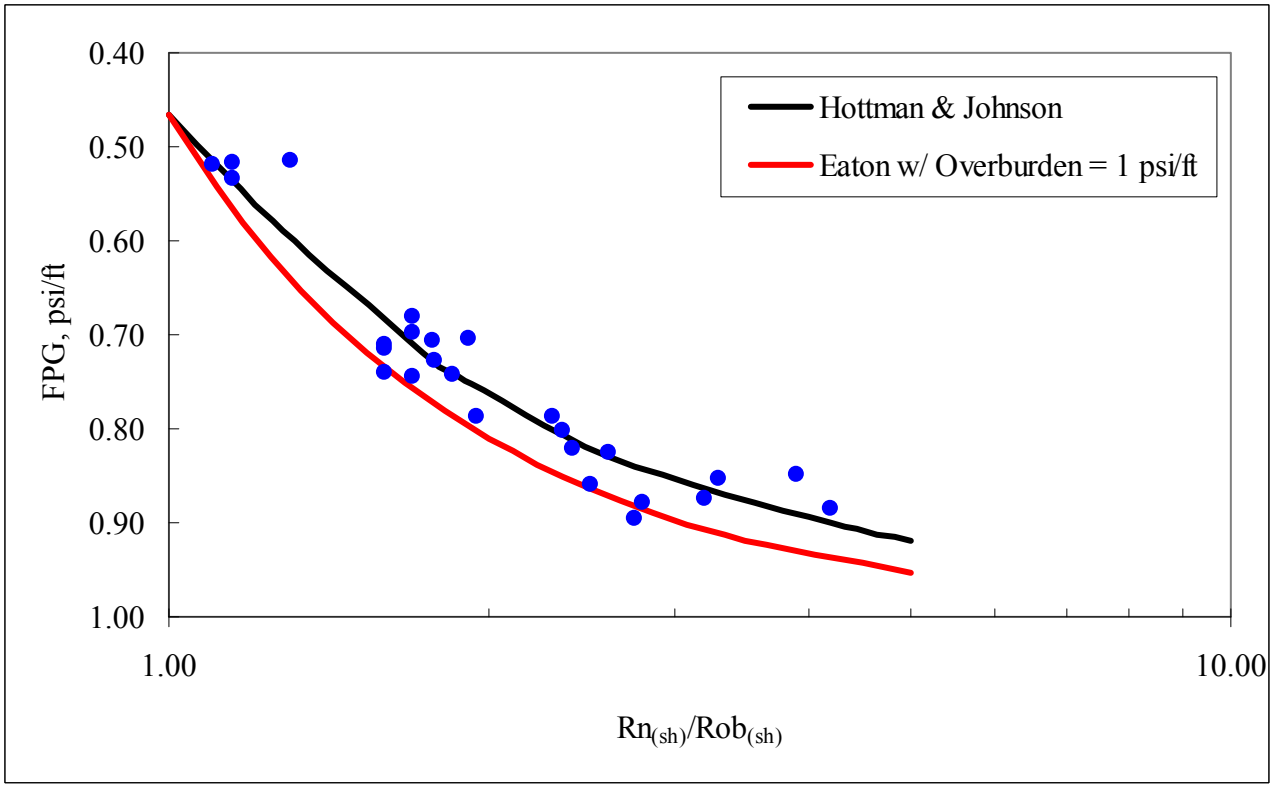

Fig. 2.4: Comparison Between Hottman and Johnson's Relationship and Eaton's Relationship per Eaton[9]

Eaton claimed that Equation 2.9 could be implemented in any area. However, the exponent on the resistivity parameter term was questioned by Eaton. After evaluation of more data, he decided that an exponent with a value of 1.2 should be more precise. Figure 2.5 is a comparison of measured pressure data and Eaton's relationship with varying exponents.

It was this comparison that led Eaton to believe an exponent of 1.2 should be used. Eaton's equation for abnormal pore pressure prediction is as follows:

$$P_F / D = \sigma_{OB} / D - \left(\sigma_{OB} / D - P_{F(n)} / D\right) * \left(\frac{Rob_{(sh)}}{Rn_{(sh)}}\right)^{1.2} \qquad \textit{(Equation 2.10)}$$

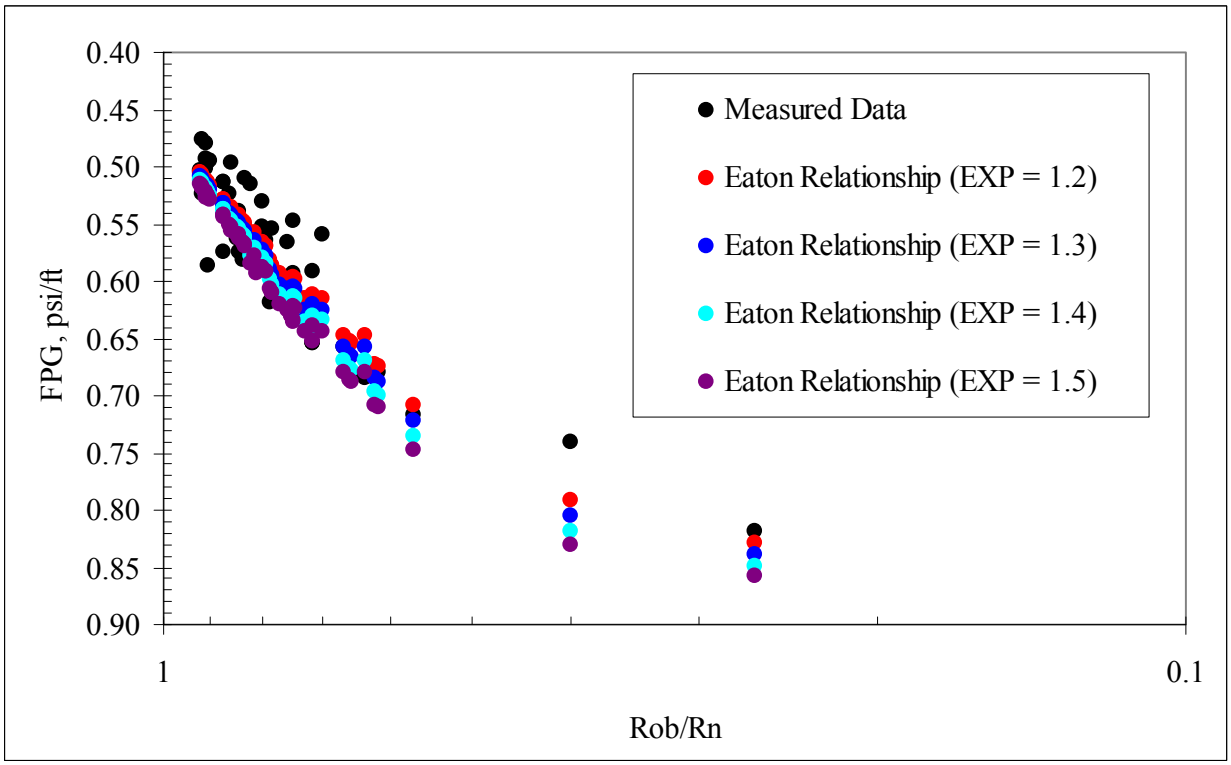

Fig. 2.5: Eaton Relationship Calculated With Varying Exponents Compared to Measured Pressure Data

Knowing that conductivity, *C*, and resistivity, *R*, are related by the relationship

$$C = \left(\frac{1000}{R}\right) \qquad \textit{(Equation 2.11)}$$

Eaton's equation can be rewritten as follows in terms of conductivity:

$$P_F / D = \sigma_{OB} / D - \left(\sigma_{OB} / D - P_{F(n)} / D\right) * \left(\frac{Cn_{(sh)}}{Cob_{(sh)}}\right)^{1.2} \qquad \textit{(Equation 2.12)}$$

Eaton also developed a similar equation that can be used with interval transit time data. This equation can be used for both sonic log and seismic data. It is as follows:

$$P_F / D = \sigma_{OB} / D - \left(\sigma_{OB} / D - P_{F(n)} / D\right) * \left(\frac{dTn_{(sh)}}{dTob_{(sh)}}\right)^3 \qquad \textit{(Equation 2.13)}$$

Eaton's relationships described above were thought (at least at the time of development) to predict pore pressures to within 0.5 ppg EMW for any geologic environment as long as care is taken to provide quality input data.

W. R. Matthews[14] published a series of technology articles in the early 1970s. This series discussed how to utilize electric well logs as a drilling tool. The main product of this publication series relevant to this research was the development of a series of conductivity (or resistivity) versus depth overlays specific to a specified geologic age. The overlays were developed by establishing a normal compaction trendline from measured pressure data. The abnormally pressured trendlines were established by relating the ratio of observed conductivity, *Cob,* to the conductivity of the normally pressured section, *Cn*, similar to both Hottman and Johnson and Eaton's techniques. The specific overlay relevant to this project is the Pliocene/Pleistocene overlay and should be used with semi-log plotting paper. The original Matthews conductivity ratio, *Cob/Cn*, versus pore pressure gradient relationship was limited to a maximum pore pressure of 0.6 psi/ft. MI Drilling Fluids[14] expanded on the research and published an overlay with pore pressure gradient values up to 0.883 psi/ft (17 ppg EMW). Figure 2.6 is an electronic version of this conductivity versus depth overlay for the Pliocene/Pleistocene geologic environment. Equations were developed for each pore pressure gradient line and included on a semi-log plot in MS EXCEL. The following procedure should be used when utilizing the overlays:

1. Plot conductivity values of "clean shales" versus depth.
2. From the plot, determine a normal compaction trend line. The 8.5 ppg EMW line corresponds with the normal compaction trend line on the conductivity plot. Line up the overlay with the normal compaction trend line. Since this is an electronic version, "lining

up" the normal compaction trendline with the normally pressured conductivity values is accomplished by a "shifting factor" within the spreadsheet. Essentially, the "shifting factor" changes the y-intercept of the equations for the pore pressure gradient lines.

3. Once the normal compaction trendline and normally pressure conductivity data are lined up, the departure of the conductivity data on the plot indicates the pore pressure environment.
4. If there are anomalies present with the conductivity and formation pressure relationship, a "shift" of the trendlines may be necessary. There are numerous potential reasons of why the pressure and conductivity do not match (change of formation water salinity, crossing faults with different pressure regimes on either side, diagenesis, etc.), so an investigation must be performed to understand why a "shift" is required.

When this method was developed, extensive personal computer usage was not yet available. This method provided a simple and quick examination of pore pressures. Matthews did not conclude a prediction variance.

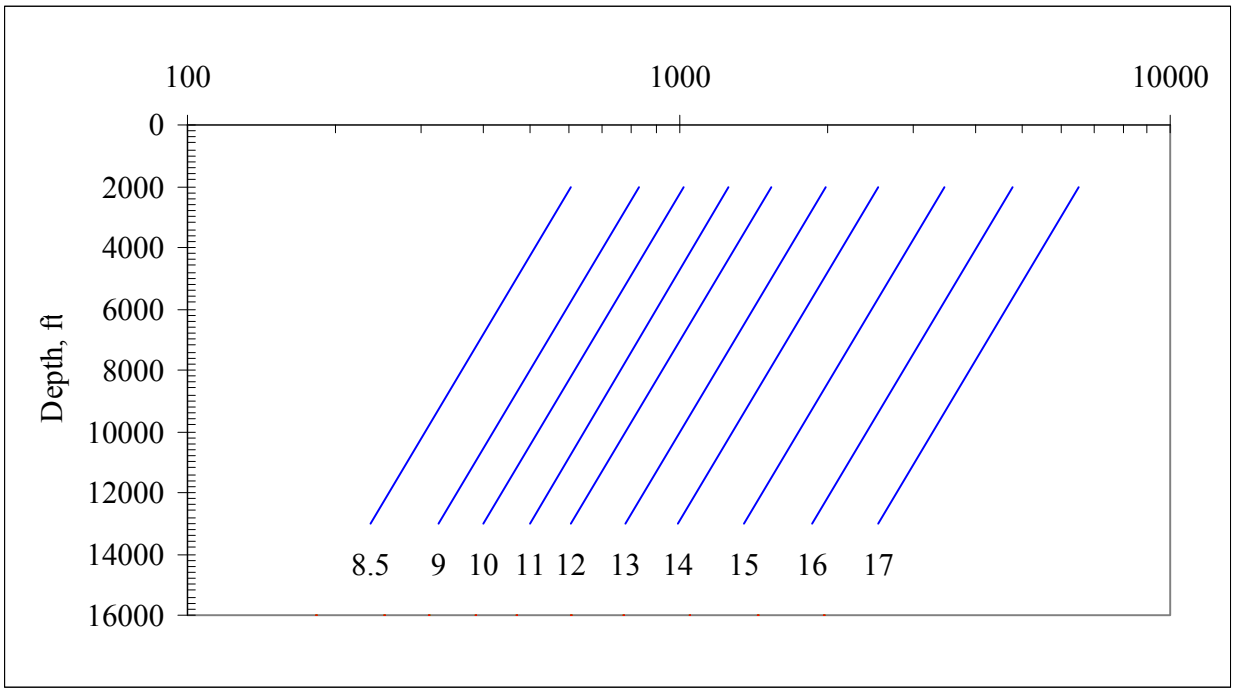

Fig. 2.6: Matthews' Pliocene/Pleistocene Conductivity vs Depth Overlay after MI Drilling Fluids[15]

2.2 Formation Fracture Gradient Prediction Strategy

The fracture gradient prediction strategy included in this literature review was also developed by Ben Eaton[7]. In 1996, Yoshida et al[24] published results of a study that investigated the current applied technologies used to predict, detect and evaluate the abnormal pressure and fracture pressure gradients in the earth's crust. This study revealed Ben Eaton's fracture gradient prediction strategy as the most widely used strategy worldwide. The fracture gradient prediction equation is

$$\frac{P_{FF}}{D} = \frac{\nu}{1-\nu}\left(\frac{\sigma_{ob}}{D} - \frac{P_F}{D}\right) + \frac{P_F}{D} \qquad \textit{(Equation 2.14)}$$

Eaton concludes that this relationship is applicable anywhere in the world as long as the following three steps are used:

1. Determine the area specific overburden stress gradient
2. Input an accurate pore pressure prediction for the subject well
3. Estimate the area specific Poisson's ratio

The area specific overburden stress can be determined using equation 2.7 and is easily converted to a gradient. The pore pressure can be determined using the methods described earlier. The only unknown variable in the fracture gradient prediction equation is Poisson's ratio.

Schlumberger[19] defines Poisson's ratio as "an elastic constant that is a measure of the compressibility of material perpendicular to the applied stress, or the ratio of latitudinal to longitudinal strain." As the value of the Poisson's ratio increases, more of the effective vertical stress, $\sigma_{EV,}$ will be transmitted in the horizontal direction, producing a higher fracture gradient. Eaton developed two Gulf of Mexico area Poisson's ratio versus burial depth relationships based on measured fracture gradient data. One curve is applicable to data gathered nearly forty years ago[7] and the second curve incorporates newer data[8], specifically data within deepwater drilling

environments. Figure 2.7 shows the two Poisson's ratio versus depth relationships. Note that Poisson's ratio does not exceed 0.5. A Poisson's ratio value of 0.5 is the upper limit since that is the value of an incompressible material in a plastic environment.

With Figure 2.7, Eaton provided a method to estimate the Poisson's ratio variable in his fracture gradient prediction equation if working in the Gulf of Mexico. He also provided a method to estimate Poisson's ratio for any area if sufficient fracture gradient data is present. Unless the potential well is a rank wildcat, there likely will be fracture gradient data available, whether from drilling operations (leak-off tests) or completion operations (hydraulic fracture stimulations).

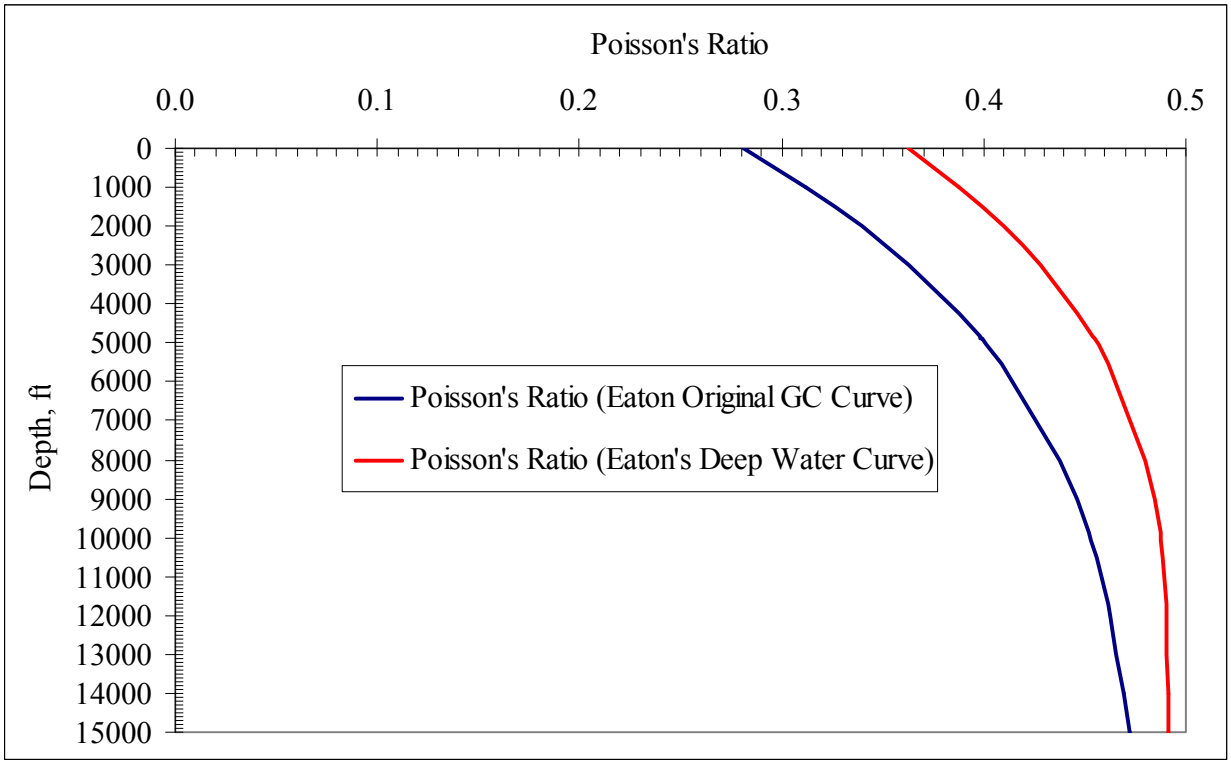

Fig. 2.7: Eaton's Poisson's Ratio Estimates[7]

If fracture gradient data is available, Eaton's equation can be rearranged for Poisson's ratio in the following manner:

$$\frac{\nu}{1-\nu} = \frac{\frac{P_{FF}}{D} - \frac{P_F}{D}}{\frac{\sigma_{ob}}{D} - \frac{P_F}{D}} \qquad \textit{(Equation 2.15)}$$

Depending upon how the leak-off test (LOT) was performed, Equation 2.15 may result in Poisson's ratio values much higher than reality. If the fracture initiation pressure is recorded as the leak-off, then a different approach must be taken to determine a Poisson's ratio relationship. For the majority of sedimentary basins, the effective stresses in the horizontal plane are approximately equal. With this assumption, the initiation pressure will occur when the tangential stress in the wellbore is zero. Roegiers[18] defined the initiation pressure as

$$P_{IF} = 3 * \sigma_{h-\min} - \sigma_{h-\max} - P_F \qquad \textit{(Equation 2.16)}$$

If the minimum and maximum stresses are assumed equal in the horizontal plane, Equation 2.16 can be rewritten as

$$P_{IF} = 2 * \sigma_{h-\min} - P_F \qquad \textit{(Equation 2.17)}$$

The effective minimum horizontal stress is defined by Eaton's fracture gradient relationship. So, the fracture initiation pressure can be rewritten as

$$P_{IF} = 2 * \left[\frac{\nu}{1-\nu} (\sigma_{OB} - P_F) \right] + P_F \qquad \textit{(Equation 2.18)}$$

Assuming the fracture initiation pressure was recorded as the LOT, then an estimate of Poisson's ratio can be determined from Equation 2.18 by rearranging and writing the equation as

$$\frac{\nu}{1-\nu} = \frac{P_{IF} - P_F}{2(\sigma_{OB} - Pf)} \qquad \textit{(Equation 2.19)}$$

Once a Poisson's ratio curve has been established for a specific well, it can typically be applied over a general area, providing a method to estimate fracture gradient, knowing pore pressure and overburden stress gradient.

One caveat to this approach is the failure of predicting initiation or breakdown pressures in inclined wellbores. Assuming isotropic effective horizontal stresses, as a wellbore deviates from vertical, the initiation pressure will be lower because the stresses are acting in parallel with the effective minimum stress.

2.3 Data Verification Techniques

Bourgoyne and Rocha[3] presented a method to correlate and estimate formation fracture gradients. Their method is based on the following relationship:

$$\frac{P_{FF}}{D} = F_{\sigma}\left(\frac{\sigma_{ob}}{D} - \frac{P_F}{D}\right) + \frac{P_F}{D} \qquad \textit{(Equation 2.20)}$$

where F_σ is the ratio of horizontal to vertical stress. Eaton based his relationship off the same equation, but he derived a relationship for the aforementioned stress ratio based on Poisson's ratio. The basis for Bourgoyne and Rocha's method is the assumption that in plastic environments, such as young, deepwater shale formations in the Gulf of Mexico, the F_σ term should be very close to 1.0. Therefore, fracture pressure is independent of pore pressure and solely dependent upon the formation overburden stress.

The authors chose to utilize the following procedure based on a compaction model to estimate the formation overburden stress:

- Describe formation porosity by the following relationship.

$$\phi = \phi_0 e^{-K_\varphi D_S} \qquad \textit{(Equation 2.21)}$$

- Formation bulk density is described by the following relationship.

$$\rho_b = \rho_{fluid}\phi + \rho_{matrix}(1-\phi) \qquad \textit{(Equation 2.22)}$$

- Solving the Equation 2.22 for φ and substituting it into the compaction model.

$$\rho_b = \rho_{fluid}\phi_0 e^{-K_\varphi D_S} + \left(1 - \phi_0 e^{-K_\varphi D_S}\right)\rho_{matrix} \qquad \textit{(Equation 2.23)}$$

- Overburden stress is defined as

$$\sigma_{ob} = \rho_w D_w + \int \rho_b dD_S \qquad \textit{(Equation 2.24)}$$

- The following expression for overburden stress is developed

$$\sigma_{ob} = g\rho_w D_w + g\rho_{matrix} D_S - \frac{(\rho_{matrix} - \rho_{fluid})g\phi_0}{K_\varphi}\left(1 - e^{-K_\varphi D_S}\right) \qquad \textit{(Equation 2.25)}$$

The relationship for overburden stress is used in Bourgoyne and Rocha's proposed method to correlate leak-off tests (LOT) data by the following procedure:

1. Collect many LOT data points.
2. Assume an initial value for Φ_0 and K_Φ. Solve the Bourgoyne and Rocha overburden stress equation for each LOT data point.
3. Create a table comparing the actual LOT data and the results of Bourgoyne and Rocha's equation.
4. Fit a function of the form $y = ax^b$. Iterate on the Φ_0 and K_Φ terms such that the constants *a* and *b* and the regression coefficients are close or equal to 1.0.

The above procedure will yield a plot correlating overburden stress and LOT pressure with a 45° line going through the origin. Therefore, the fracture gradient is equal to the overburden stress gradient.

Though the authors claim less than 4% average error using this method on wells from the offshore Gulf of Mexico, the inclusion of this method in the review is not as a fracture gradient prediction strategy, but rather as a method to provide or confirm a porosity compaction trendline for use in the pore pressure prediction strategies previously reviewed.

Bassiouni[2] describes the relationship between formation resistivity and porosity and how this relationship affects the formation resistivity factor, *F*.

$$F = \frac{R_o}{R_w} \qquad \textit{(Equation 2.26)}$$

where R_o is the formation resistivity of a rock fully saturated with water and R_w is the resistivity of the water contained in the pore throats of the formation.

Winsauer et al[23] introduced the following empirically-developed relationship between the formation resistivity factor and porosity:

$$F = a\phi^{-m} \qquad \textit{(Equation 2.27)}$$

where *a* and *m* are constants mainly related to pore geometry and are area specific. The best way to determine the values of *a* and *m* is by laboratory measurements on a large number of core samples.

There have been many area-specific relationships developed between formation resistivity factor and porosity. This review will contain four such relationships developed for the U.S. Gulf Coast area. Equations 2.28 – 2.31 were developed for clean sandstones[20,5,22,17]. Equation 2.32 was developed by Perez-Rosales[16] and though it was also developed for sandstones, it has been utilized to estimate the formation resistivity factor in shales[1]. These relationships will be utilized in an effort to provide or confirm a porosity compaction trendline for use in the pore pressure prediction equations.

$$F = \frac{0.81}{\phi^2} \text{ (Humble equation)} \qquad \textit{(Equation 2.28)}$$

$$F = \frac{1.45}{\phi^{1.54}} \text{ (Phillips equation)} \qquad \textit{(Equation 2.29)}$$

$$F = \frac{1.13}{\phi^{1.73}} \text{ (Chevron equation)} \qquad \textit{(Equation 2.30)}$$

$$F = \frac{1.97}{\phi^{1.29}} \text{ (Porter and Carothers equation)} \qquad \textit{(Equation 2.31)}$$

$$F = 1 + 1.85 * \frac{1-\phi}{\phi - 0.1} \text{ (Perez-Rosales equation)} \qquad \textit{(Equation 2.32)}$$

3. OFFSET WELL DATA REVIEW

One of the main requirements for developing a sound pore pressure and fracture gradient prediction strategy is using accurate offset well data in the application process. In this section, all pressure related data available from the operator's records of this area will be reviewed. Drilling data (mud weights, kicks, lost returns, LOTs, etc.) and measured pressures (MDT/RFT data) will be reviewed and analyzed.

3.1 Drilling Data Review

The drilling data being reviewed was obtained from drilling reports and drilling mud recaps. These reports and recaps were consolidated and included as a single "Well Recap", which is included in Appendix A1.

One of the most important pieces of drilling data available is the mud weight versus depth relationship for each well. This data can be obtained from either morning reports or mud recaps and is useful for representing the maximum expected value for pore pressure because the mud weight evidently exerted sufficient hydrostatic pressure to control formation pressures in permeable zones. Figure 3.1 is a plot of mud weight required versus true vertical depth for all of the eight offset wells. The scatter of the data is indicative of the significantly different operational strategies used and the apparent pore pressure differences throughout the area.

Typically, operators perform leak-off tests (LOTs) to provide real-time fracture gradient estimates at each casing point (usually in a shale formation). This provides the operator insight into the maximum mud weight that can be used in the hole section below. However, there are numerous instances where the open hole section below a casing point will not allow a hydrostatic pressure near the LOT. Due to Poisson's ratio differences, sands typically have a fracture gradient of 0.04 – 0.10 psi/ft lower than shales in the same pressure environments. Table 3.1 includes all of the LOTs obtained from the eight offset wells reviewed.

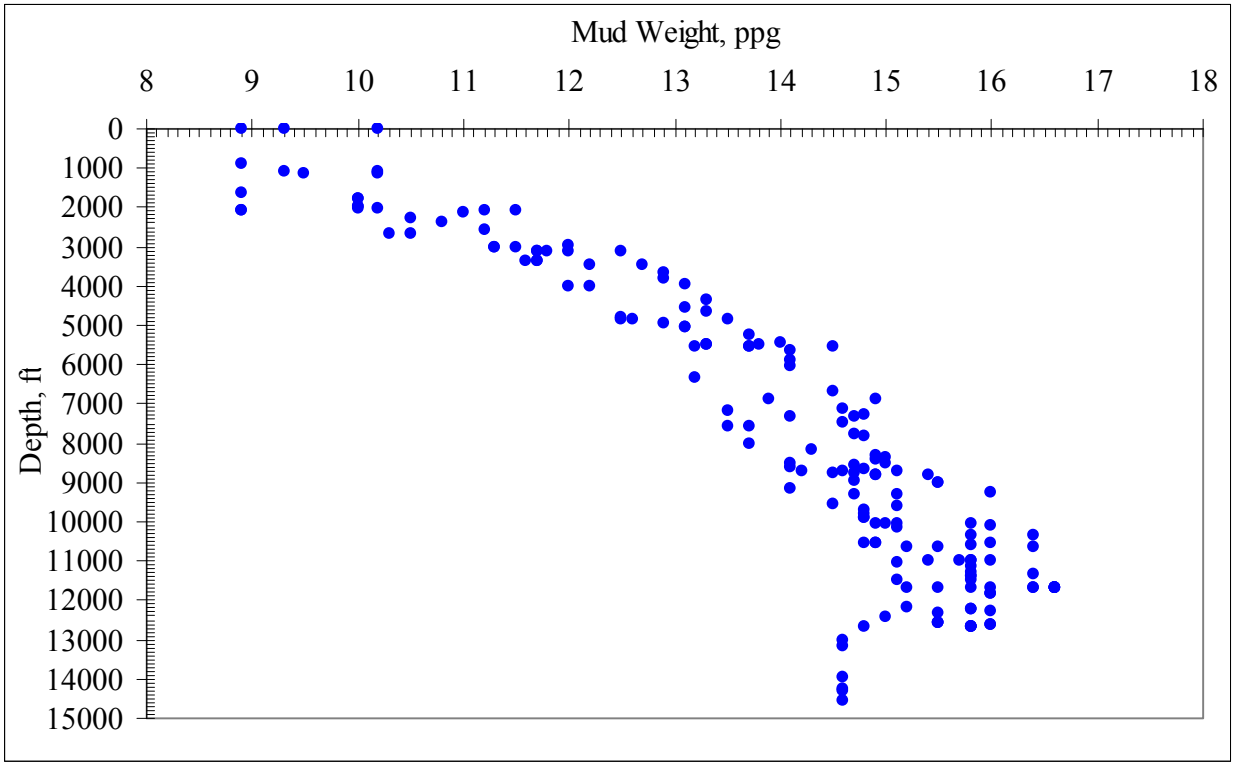

Fig. 3.1: Mud Weight vs. True Vertical Depth for Eight Offset Wells in EW 910 Area

Table 3.1: Leak Off Tests Obtained from Offset Well Data

Well	Depth	EMW	Pressure		Well	Depth	EMW	Pressure
EW 953 No. 1	4222	15.0	3290		ST 320 A4	2035	12.1	1279
						3375	14.2	2490
EW 910 A1BP	2108	12.0	1314			8015	16.6	6912
	3010	13.9	2173					
	5050	16.1	4224		EW 910 A5	2676	13.0	1807
	9000	18.5	8649			4893	15.8	4016
	11706	18.0	10946			10062	16.8	8781
EW 954 A2	2066	12.0	1288		EW 910 A6	4848	15.7	3954
	3148	14.2	2322			10058	17.2	8987
	5542	16.0	4606					
	9890	17.2	8837		EW 910 No. 4	2010	12.0	1253
						3110	14.4	2326
EW 910 A3	2659	13.1	1810			5510	15.9	4551
	4866	15.9	4019			10530	17.9	9792
	10042	17.6	9181					

Other important pressure data obtained from a review of the drilling records come from drilling problems. Well control events such as kicks and lost circulation events are great indicators of the minimum and maximum pressures allowed during drilling operations. These data are extremely helpful in developing a sound pore pressure and fracture gradient prediction strategy. Table 3.2 lists all pressure-related drilling problems experienced in the eight offset wells. Since all of this data is obtained from drilling records, details are missing in some cases which weakens the accuracy or conclusiveness relating to pore pressure and fracture gradient estimates. An example of a weak estimate is a fracture gradient based on a lost returns event. Due to a lack of data to describe the well geometry (i.e. bottom-hole assembly design), equivalent circulating density (ECD) calculations can not be performed. Therefore assuming a fracture gradient equal to the mud weight at the time of the event of the fluid loss event gives a weak estimate. The fracture gradient is at least the reported value, but the true value is unknown. The fracture gradient is less than the ECD when returns were lost but is at least equal to the mud weight for which the hole will stand full. Regardless, an inference of a pressure estimate is made, whether it is a pore pressure or fracture gradient estimate and included in Table 3.2. Most of these inferred values are considered weak and will only be used as guidelines in the model calibration process. If an inferred value is weak, an expected range of values based on minimum and maximum fracture gradient will be depicted on the pore pressure plots.

Table 3.2: Pressure-Related Drilling Problems Experienced in Offset Wells

Well	Depth (ft)	MW (ppg)	Problem	Inference	P_F	P_{FF}
EW 953 No. 1	3182	11.3	On choke.	Original MW = 10.8 ppg. Still on choke with MW = 11.3 ppg. Pf ≥ 11.3 ppg	≥11.3	-
	7374	14.7	Well flowing. Raise MW to 15.6 ppg.	Original MW = 14.7 ppg. Pf ≥ 14.7 ppg. Pf ≤ 15.6	≥14.7 ≤ 15.6	-

Table 3.2 (cont'd):

Well	Depth (ft)	MW (ppg)	Problem	Inference	P_F	P_{FF}
EW 953 No. 1	7477	15.6	Mud losses. Reduce MW to 15.3.	Insufficient data to calculate ECD. Pff ≥ 15.3	-	≥15.3
	9294	15.5	Circulate out kick.	Original MW = 15.5 ppg. Final MW = 15.7 ppg and drilled to TD with no problems.	15.6	-
EW 910 A1BP	11698	16.6	Drilling with losses of 20 – 30 BPH	Losing fluid while drilling. Was able to log hole and make conditioning trips without issue. Insufficient data to calculate ECD. Pff ≥ 16.6 ppg.	-	≥16.6
	11704	16.4	Drilling with no returns. Reduce MW to 16 ppg.	LOT = 18.0 ppg. Possible weak zone below shoe (sandy). Insufficient data to calculate ECD. Pff ≥ 16.0 ppg.	-	≥16.0
	12641	16.0	Circulate on bottom while losing returns.	See above.	-	≥16.0
EW 954 A2	2056	8.9	Well began flowing while circulating. Increase MW to 11.5 ppg.	Pf ≥ 8.9 ppg.	≥8.9	-
	3138	11.2	Circulate out gas. Increase MW to 11.8 ppg.	No flow. Pf ≤ 11.2 ppg.	≤11.2	-
	8694	15.1	Lost returns. Reduce MW to 14.6 ppg	Based on sea water additions, max allowable MW is 14.9 ppg. Insufficient data to calculate ECD.	-	14.9

Table 3.2 (cont'd):

Well	Depth (ft)	MW (ppg)	Problem	Inference	P_F	P_{FF}
EW 954 A2	10967	16	Losing returns – 120 BPH. Reduce MW to 15.8 ppg.	FIT = 17.2 ppg. Insufficient data to calculate ECD. Pff ≥ 15.8 ppg.	-	≥15.8
EW 910 A3	2340	10.0	Increase MW to 10.5 ppg due to high background gas.	Original MW = 10.0 ppg. No flow. Pf ≤ 10.0 ppg.	≤10.0	-
	6655	14.3	Increase MW to 14.3 ppg after 0.8 ppg mud cut while CBU due to rig repair.	Original MW = 14.0 ppg. High mud cut, but well not flowing. Pf ≤ 14.0 ppg.	≤14.0	-
ST 320 A4	1128	9.5	Lost total returns 9' below shoe of DP. Reduced MW from 10.2 and established full returns.	Insufficient data to calculate ECD. Pff ≥ 9.5 ppg	-	≥ 9.5
EW 910 A6	1500	10.5	Began losing fluid but hole healed on its own.	Insufficient data to calculate ECD. Pff ≥ 10.5 ppg	-	≥10.5
EW 910 No. 4	3100	11.7	Had 438 units of gas and a 0.4 ppg mud cut while CBU. Increased MW to 11.7 ppg.	Original MW = 11.5 ppg. No flow. Pf ≤ 11.5 ppg.	≤11.5	-

3.2 Measured Pressure Data Review

As revealed in Table 1.1, there are four wells that obtained measured reservoir pressures from either a Repeat Formation Test (RFT) tool or a Modular Dynamics Test (MDT) tool. Though these tools provide accurate reservoir pressures estimates, there are instances when the tool malfunctions or the reservoir's permeability is too low to provide accurate measurements. An analysis of the data must be performed to ensure that the pressures used in the pore pressure

prediction strategy are valid. The analysis consisted of eliminating the data that was reported as either “dry test”, “limited drawdown” or “lost seal” and using the remaining data (reported as either “normal pretest” or “volumetric pretest”). Also, an analysis of the hydrostatic pressure prior and after obtaining the pressure measurement was performed. If significant differences would have been reported (in this case, there were no significant differences), then that data would be eliminated, due to the likelihood of a tool malfunction.

All of the reported measured pressure data are included in tabular form in the Appendix A2. Figures 3.2 – 3.6 are plots showing the valid measured reservoir pressure versus true vertical depth for the four offset wells; EW 910 A1BP, EW 954 A2, EW 910 A3 and EW 953 No. 1.

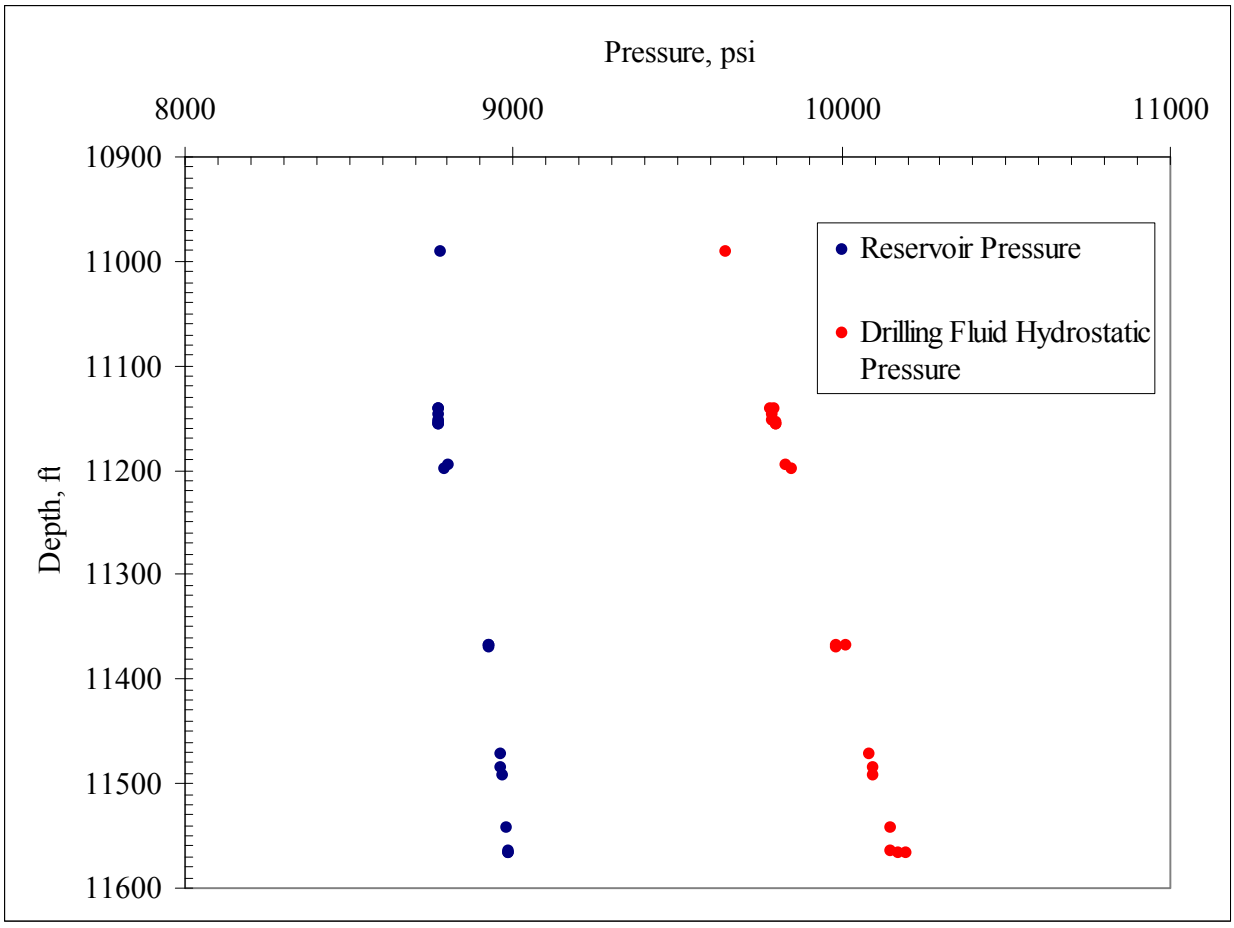

Fig. 3.2: RFT/MDT Pressures– EW 910 A1BP (Run 1)

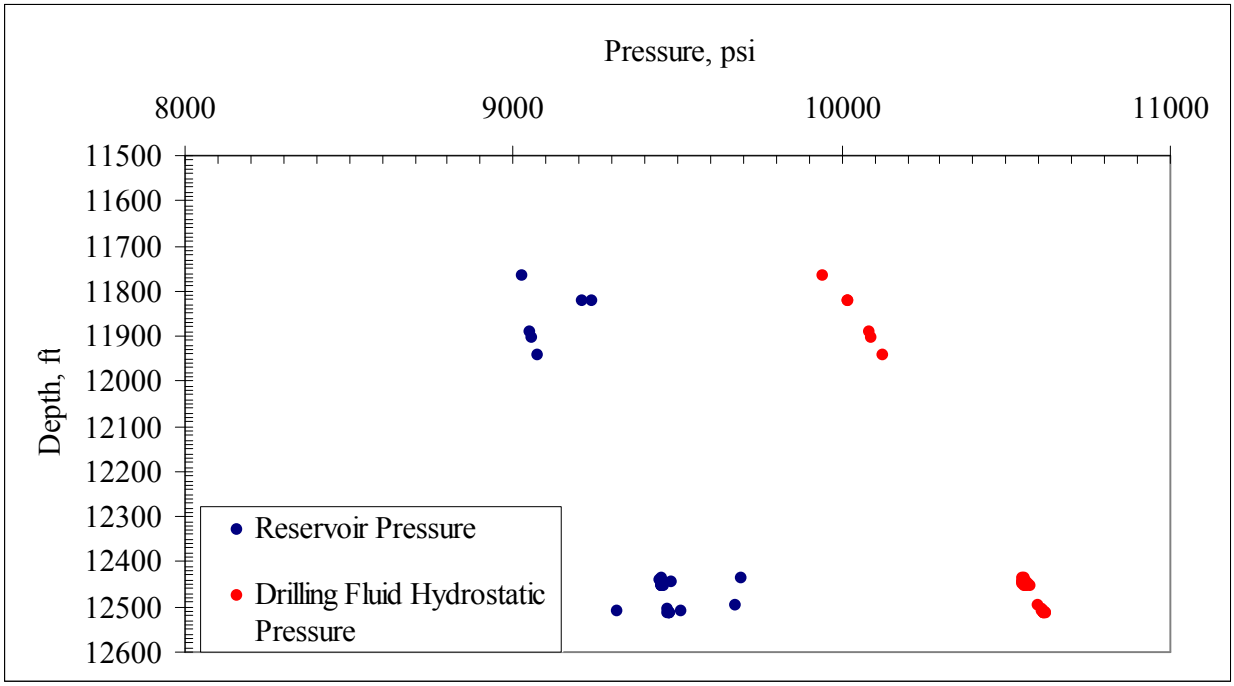

Fig. 3.3: RFT/MDT Pressures – EW 910 A1BP (Run 2)

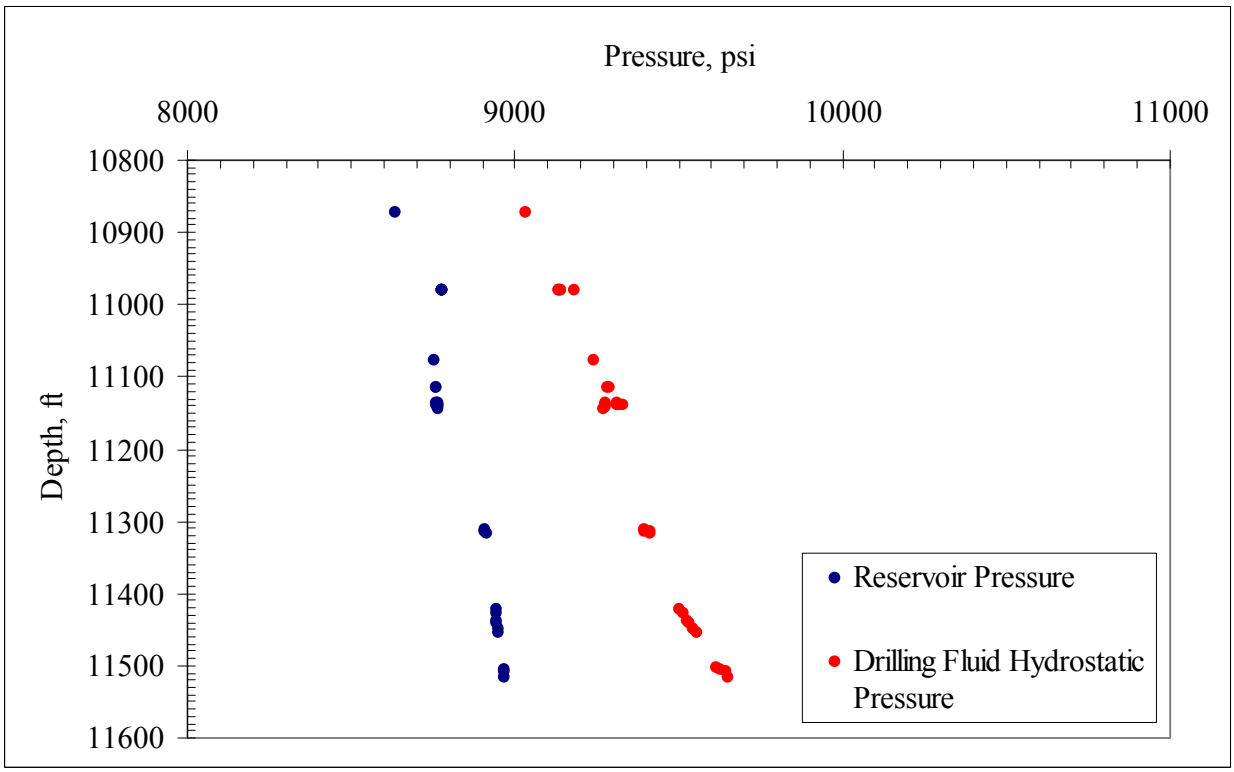

Fig. 3.4: RFT/MDT Pressures – EW 954 A2

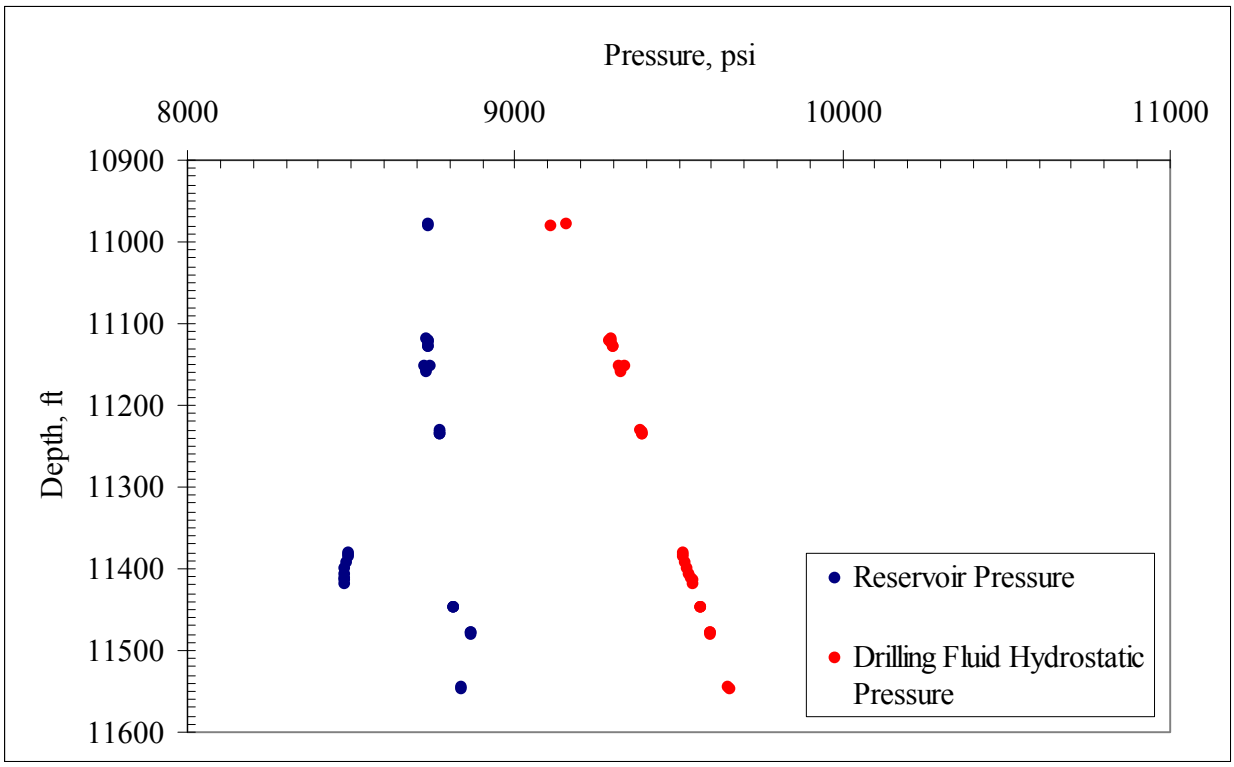

Fig. 3.5: RFD/MDT Pressures – EW 910 A3

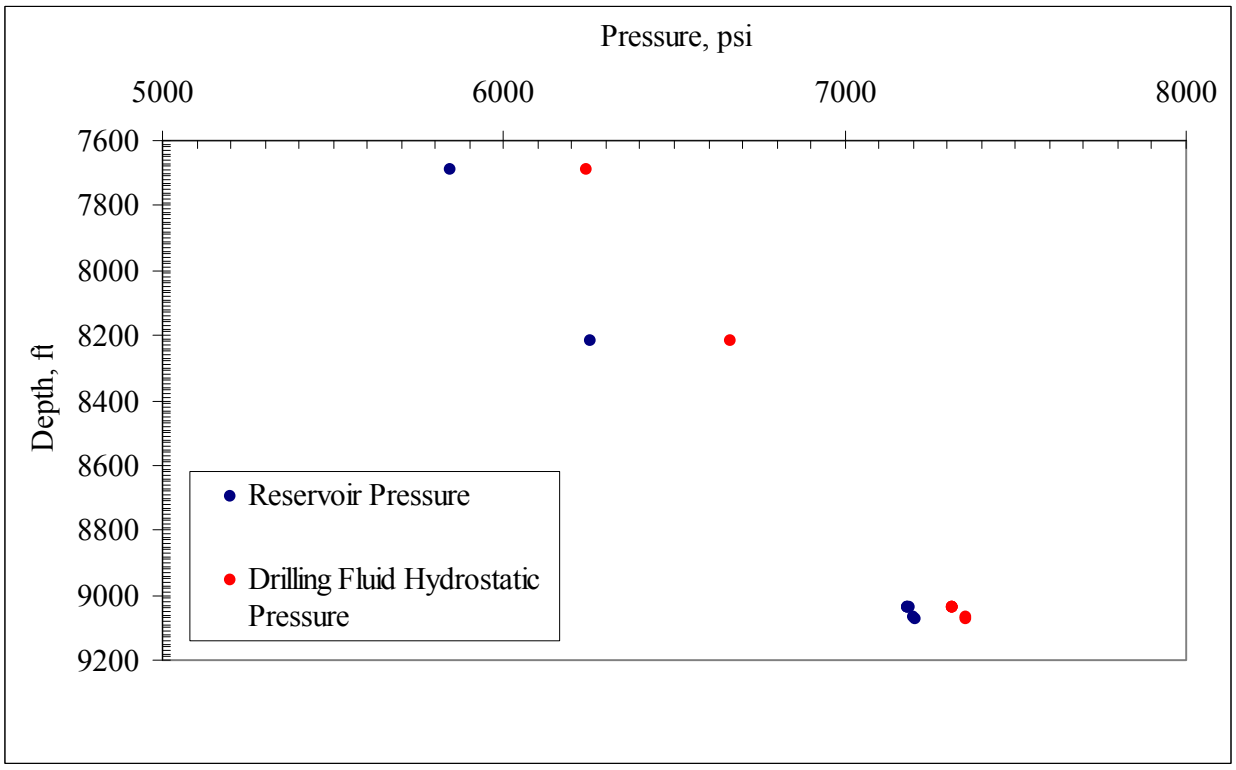

Fig. 3.6: RFD/MDT Pressures – EW 953 No. 1

As can be seen from Figures 3.2 through 3.6, there are some inconsistencies with the measured reservoir pressure data, specifically data scatter in the deeper sections of EW 910 A1BP and a lower pressured section at approximately 11400' in EW 910 A3. In an attempt to learn more about the general reservoir pressure trends in the area and determine the cause for these inconsistencies, the measured data from EW 910 A1BP, EW 954 A2 and EW 910 A3 have been included in a single plot and are shown in Figure 3.7.

As seen in Figure 3.7, though significant data scatter is present, a pressure gradient of approximately 0.48 psi/ft within these reservoirs from 10000' to 13000' can be estimated from the data. To further examine the inconsistencies of the pressure data, the data was sorted by reservoir. Table 3.3 is a listing of the geologic tops for the EW 910 A1BP, EW 954 A2 and EW 910 A3 wells in the intervals where measured reservoir pressure data was obtained. Figures 3.8 through 3.11 are plots of the measured reservoir pressure data sorted by the GA2, GA3, GA4 and GA5 reservoirs, respectively.

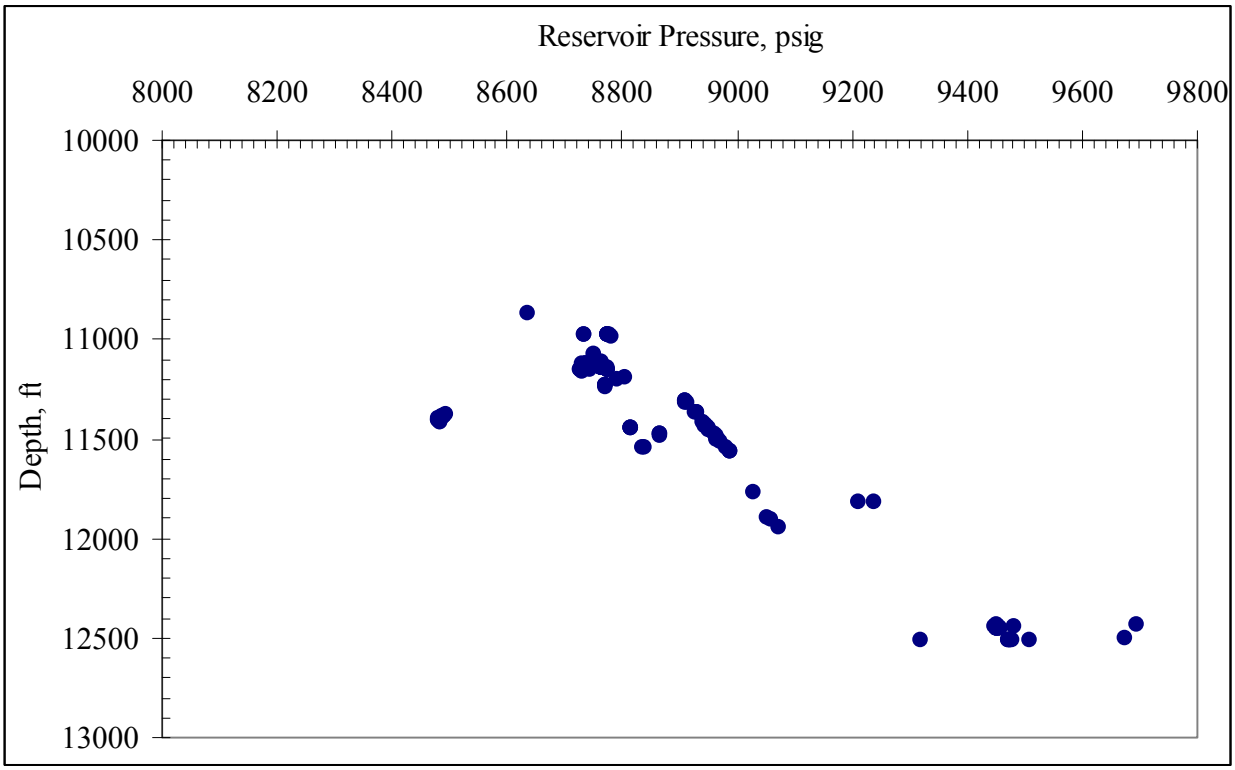

Fig. 3.7: RFT/MDT Pressures – EW 910 A1BP, EW 954 A2 and EW 910 A3

Table 3.3: Summary of Geologic Tops for EW 910 A1BP, EW 954 A2 and EW 910 A3

Reservoir	EW 910 A1BP	EW 954 A2	EW 910 A3
GA1	10792’	-	-
GA2	10980’	10966’	10958’
GA3	11143’	11113’	11118’
GA4	11373’	11310’	11227’
GA5	11490’	11410’	11372’
GA6	11750’	-	11635’
GA7	11890’	11820’	11750’
GA8	12088’	12000’	11995’
GA9	12342’	-	-
GA10	12430’	12270’	12295’

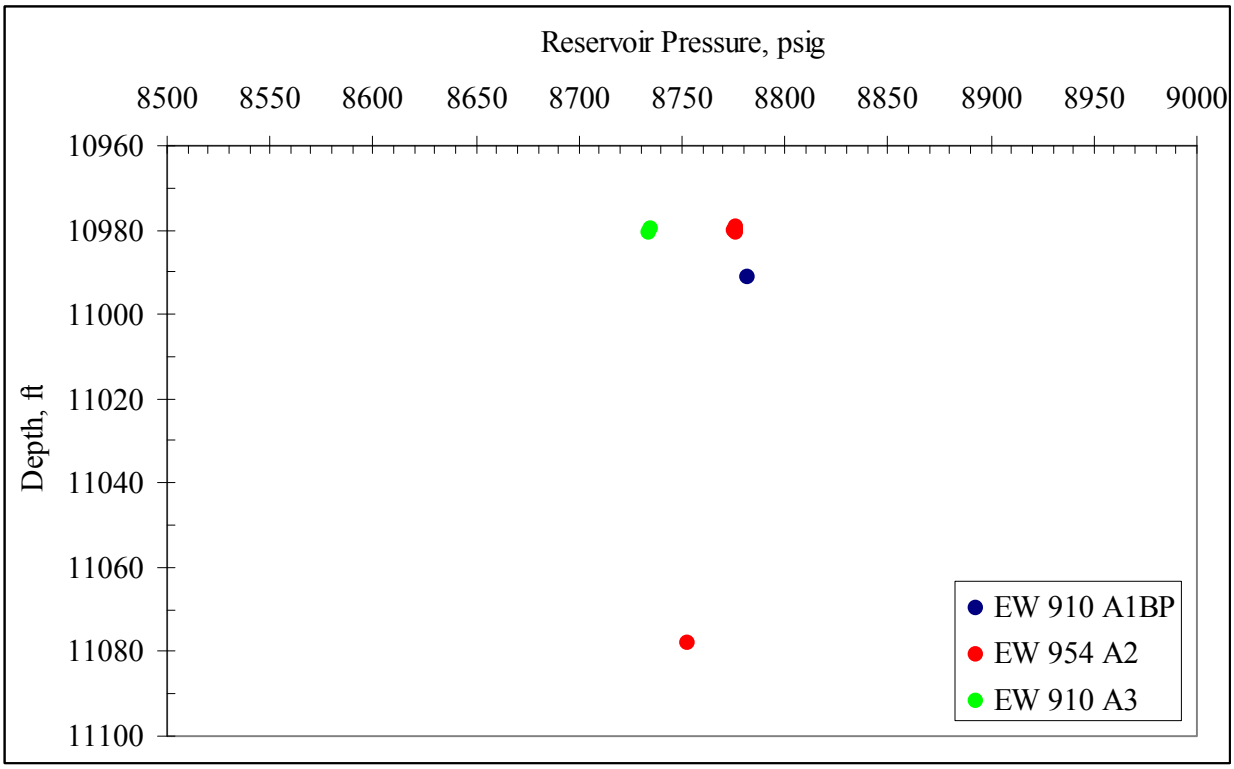

Fig. 3.8: RFT/MDT Pressures – GA 2 Reservoir

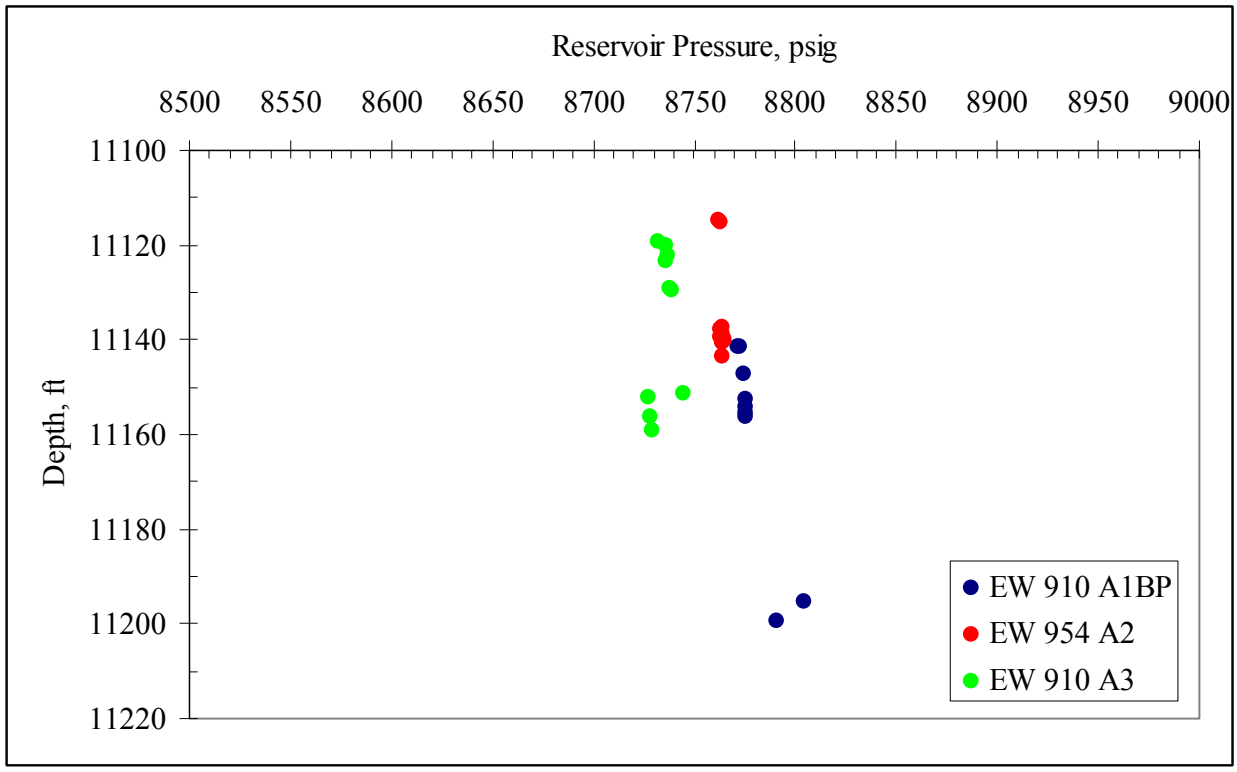

Fig. 3.9: RFT/MDT Pressures – GA3 Reservoir

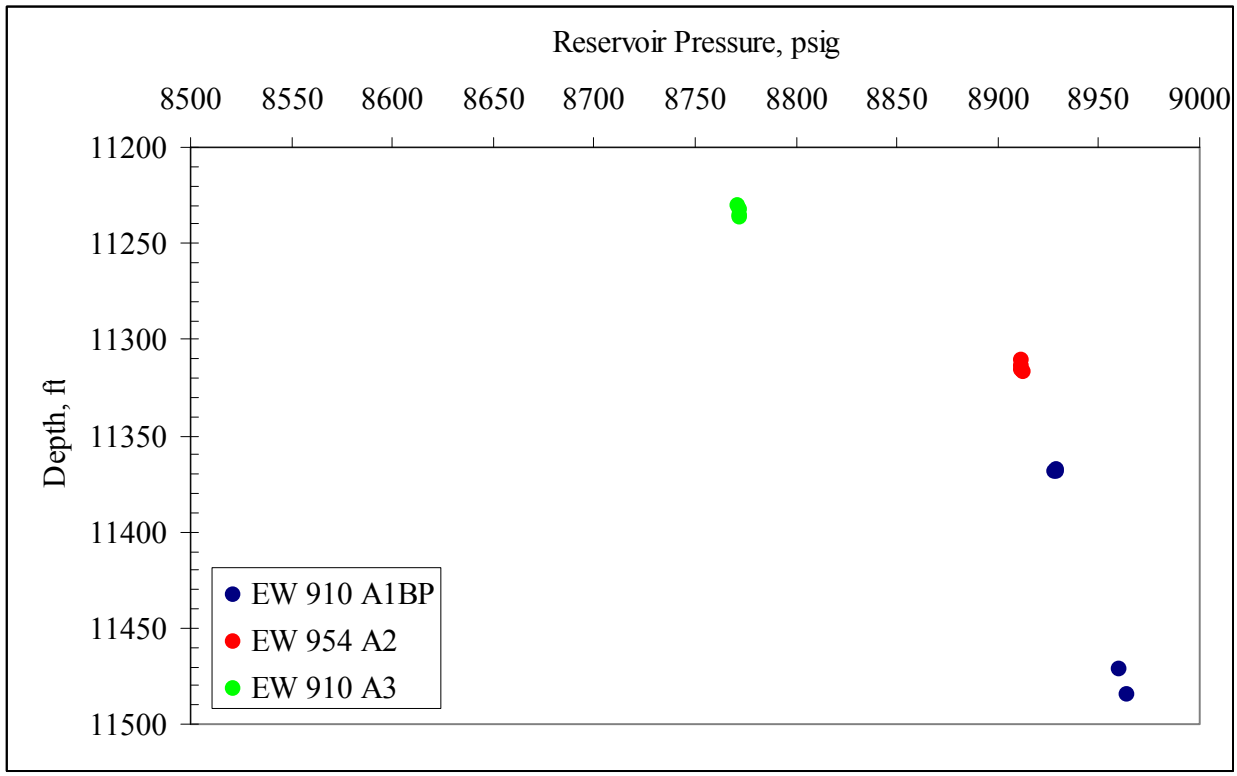

Fig. 3.10: RFT/MDT Pressures – GA4 Reservoir

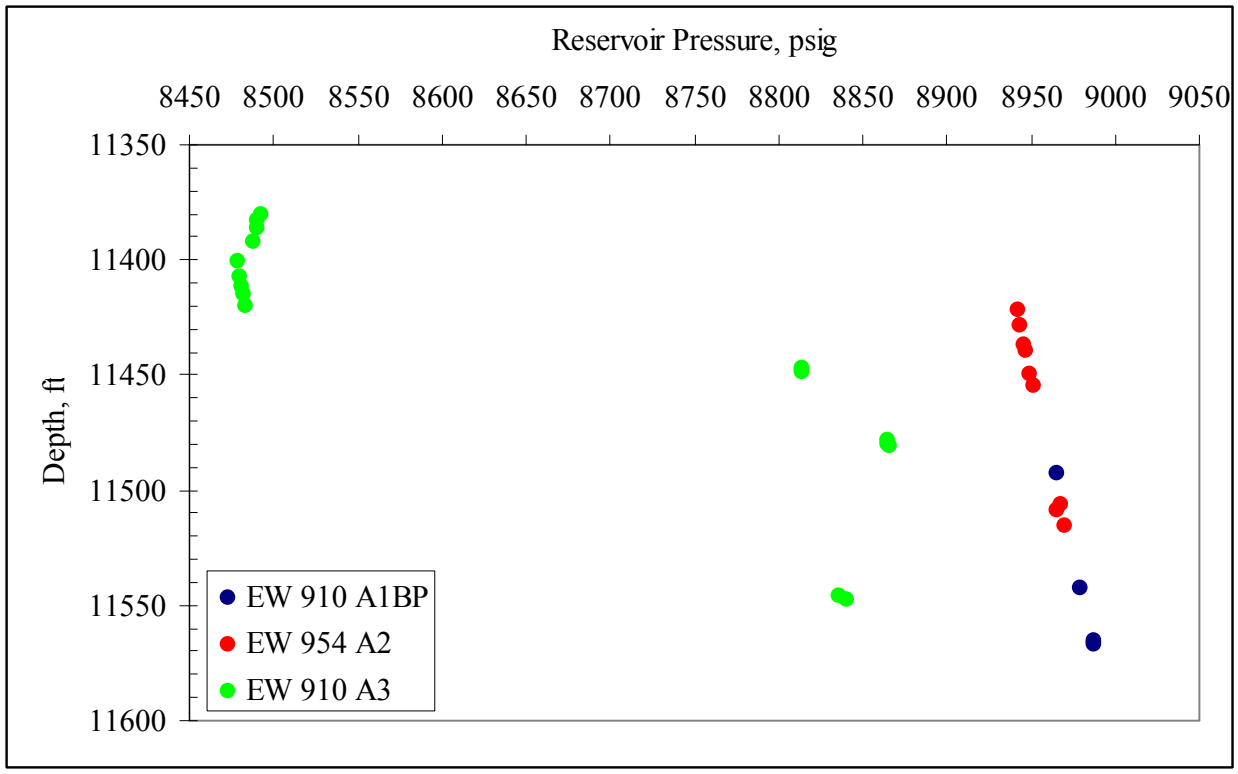

Fig. 3.11: RFT/MDT Pressures – GA5 Reservoir

As can be seen in Figures 3.8 through 3.11, the EW 910 A1BP and EW 954 A2 wellbores exhibit very similar reservoir pressures in all four of these reservoirs, whereas the EW 910 A3 typically has lower values. One important detail to note is that there is no known faulting between these three wellbores from the GA2 through the GA5 reservoirs. Therefore, with the close proximity to one another, the three wellbores should be in hydraulic communication. The GA5 reservoir pressure discrepancy between the EW 910 A3 in the ~11400' interval and the other two wellbores is concluded to be the result of pressure depletion. A review of the field exploitation history reveals that the EW 910 A1BP and EW 954 A2 were on production prior to drilling the remaining wells on the platform. Therefore, the reservoir pressures from the EW 910 A1BP and the EW 954 A2 wells should be virgin.

Table 3.4 summarizes the pressure gradients in each reservoir (GA2 – GA5) as calculated from the EW 910 A1BP and EW 954 A2 pressure data. This summary provides insight into the

reservoir contents; oil, water or gas. The reservoir content of the GA2 reservoir is inconclusive. As seen in Figure 3.8, the pressure gradient versus depth does not follow a typical trend. Whether this is due to gauge inaccuracy or lack of reservoir continuity, the difference in reservoir pressures is small and should not invalidate the measurements. The reservoir fluid pressure gradient in the other reservoirs matches the field production.

Table 3.4: Pressure Gradient Analysis in GA2 – GA5 Reservoirs

Reservoir	Reservoir Fluid Pressure Gradient, psi/ft	Reservoir Fluid Pressure Gradient, ppg	Reservoir Content
GA2	0.636	12.25	Inconclusive
GA3	0.321	6.19	Oil/Condensate
GA4	0.306	5.89	Oil/Condensate
GA5	0.310	5.97	Oil/Condensate

Because the EW 910 A1BP was the only well with measured reservoir pressures obtained in any reservoir below the GA5, the deeper reservoirs were not included in the previous analysis. To analyze the inconsistent data in the EW 910 A1BP well, several individual MDT files were examined. There were four data files that seemed anomalous (i.e. greater than 100 psi difference between it and adjacent pressure tests). A total of nine MDT files were analyzed and are included in the Appendix A3. Note that all nine of these files were classified as "normal pretest"; therefore they were not eliminated from the data set in the initial analysis. Table 3.5 describes the pertinent information for each test analyzed. The tests with a "*" next to the file number are the anomalous ones.

Table 3.5: MDT Pressures in Deeper Reservoirs

File No.	Depth	$P_{HYD(b)}$	$P_{HYD(a)}$	P_F	P_F
	ft	psi	psi	psi	ppg
119	11768	9945.83	9971.01	9028.57	14.77
111*	11820	10021.0	10020.4	9212.39	15.00
112*	11821	10021.6	10021.1	9238.03	15.04
105	11893	10084.9	10084.2	9053.37	14.65
78	11905	10091.6	10091.1	9057.88	14.65
77	11941	10123.6	10122.2	9073.72	14.63
102*	12437	10557.1	10556.4	9696.28	15.01
58*	12497	10600.5	10600.1	9676.30	14.91
91	12516	10622.1	10622.5	9473.85	14.57

After analyzing the files, only one file is obviously questionable. File No. 112 (15.04 ppg EMW @ 11821') is questioned due to the nature of the pressure buildup and falloff. After the packer is set and the probe inserted, the pressure abruptly increases approximately 650 psi to 9850 psig (16.04 ppg) and then falls as a logarithmic function of time, similar to reservoir pressure depletion. However, the initial pressure (9850 psig) as depicted on the chart is also unrealistic. Therefore, this test was eliminated from the data set.

The lessons learned from the in-depth analysis of the measured reservoir pressure data are as follows:

- The reservoir pressures from the EW 910 A1BP, EW 954 A2 and EW 953 No. 1 wells are indicative of virgin pressure.
- The EW 910 A3 pressure data from the GA4 and GA5 reservoirs are indicative of depletion with 0.19 ppg and 0.78 ppg gradient reductions, respectively, versus the virgin pressure of the EW 910 A1BP and EW 954 A2 wellbores.
- The reservoir pressures from the EW 910 A3 GA2 and GA3 reservoirs were probably still virgin when the pressure was measured. The EW 910 A3 reservoir pressures gradients were only lower by 0.074 ppg and 0.078 ppg EMW, respectively. This minor difference could be due to tool calibrations or possibly affected by a lower hydrostatic mud weight. The tool calibrations were not examined.

- The data scatter present in the pressures from the deeper sections of the EW 910 A1BP needed to be addressed, but only one of the suspicious pressure test files was eliminated. The cause or reason of the severe data scatter is unclear.

4. ANALYSIS OF W.R. MATTHEWS PORE PRESSURE PREDICTON STRATEGY

This chapter discusses the analysis of the pore pressure prediction method developed by W.R. Matthews[14]. This strategy utilizes geologic-age specific overlays developed empirically from measured pressure and petrophysical data as previously described in Section 2.1. The conductivity compaction trendlines for the Pliocene-Pleistocene overlay were depicted in a MS Excel spreadsheet for ease of use. The spreadsheet includes a "shifting factor" that allows the compaction trendlines to correlate with the known pore pressure data. In essence, the "shifting factor" changes the y-intercept of the compaction trendlines. The slope of the compaction trendlines remains unchanged since the trendlines represent the normal compaction for this specific age rock.

Once the normal compaction trendline has been determined, the pore pressures are transcribed from the conductivity plot and are plotted on a Cartesian scale versus true vertical depth. The pressure related data such as mud weights, measured reservoir pressures, kicks, etc. are included in this plot to develop confidence in the pore pressure prediction.

4.1 Calibration of Matthews' Normal Compaction Trendline and Application of the Pore Pressure Overlay

One idiosyncrasy with this offset-well data set is the absence of petrophysical data within a normally pressured section. Geopressures are developed prior to the depth at which the petrophysical data was obtained. Therefore, this prediction strategy was developed by calibrating the deep conductivity data to measured reservoir pressures. The RFT/MDT data from the EW 910 A1BP well was utilized in calibrating the deep conductivity data. Figure 4.1 is a plot of the observed formation conductivity versus depth including the RFT/MDT measured pressure data without a "shifting factor". Figure 4.2 is identical to Figure 4.1 except the overlay was shifted to calibrate the measured reservoir pressure with the observed conductivity. The

"shifting factor" used was "-7500". This "shifting factor" was applied to all eight offset well data sets.

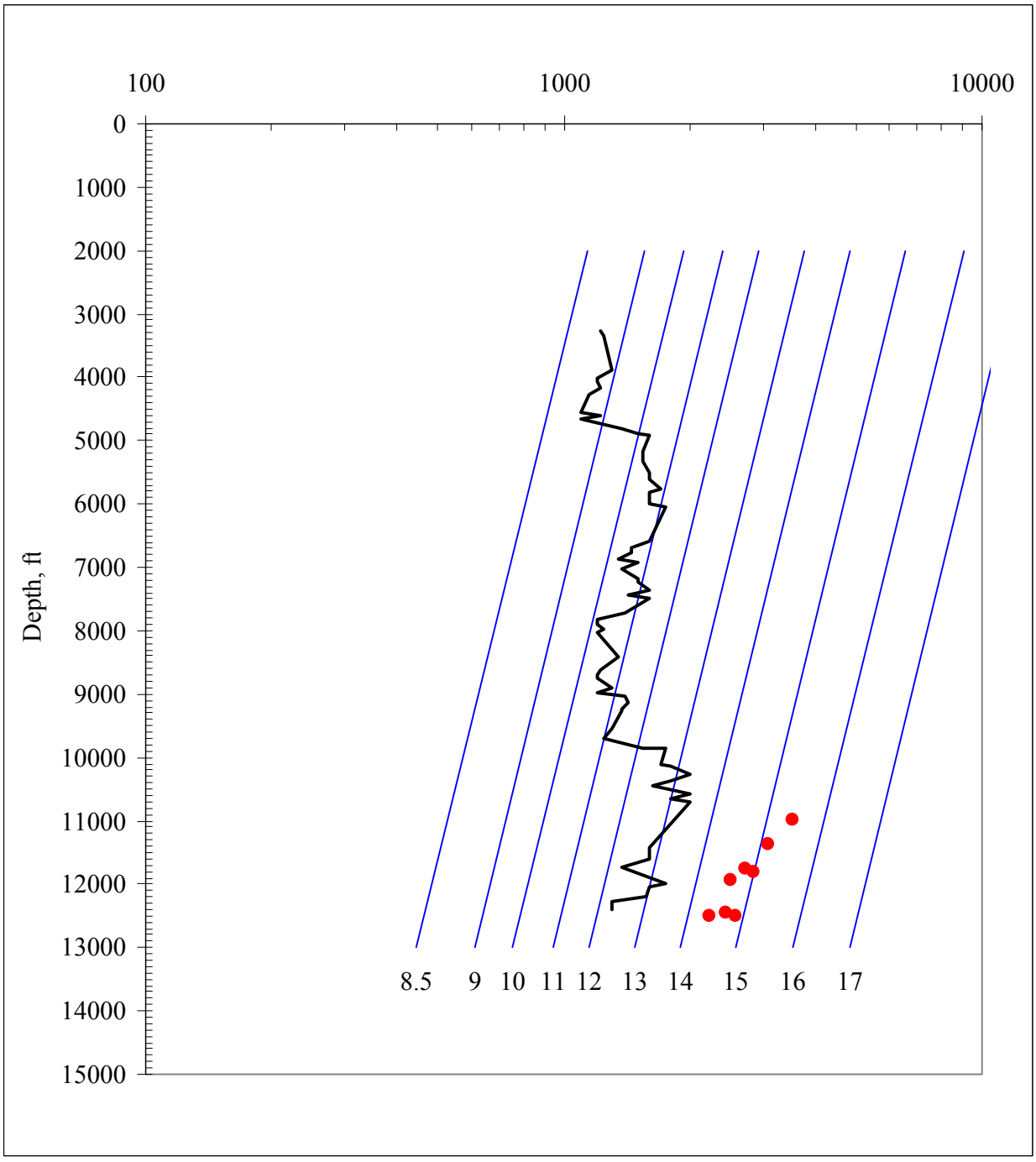

Fig. 4.1: Shale Conductivity vs True Vertical Depth with Matthews' Implied Pore Pressure Overlay (No "Shifting Factor") – EW 910 A1BP

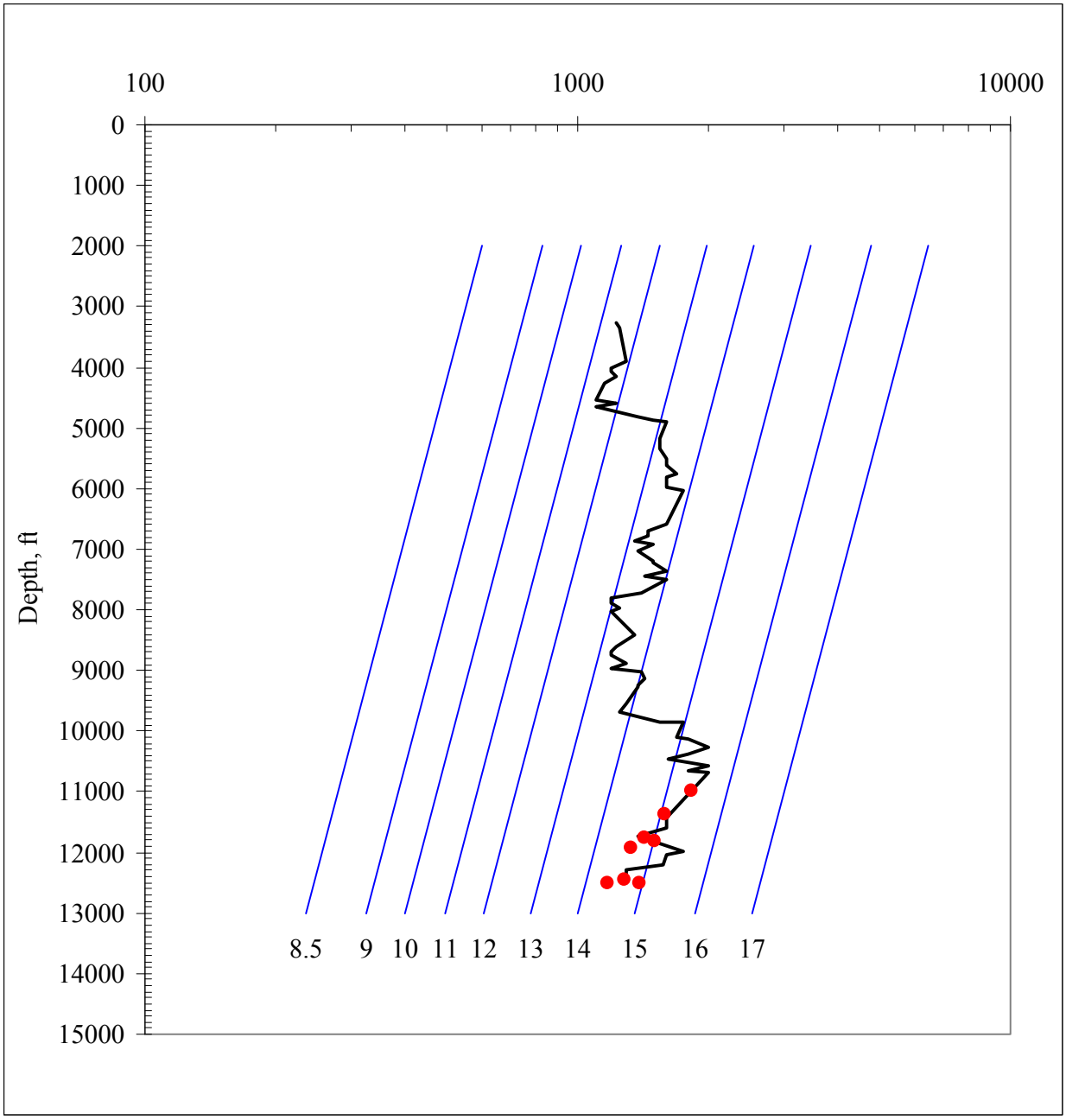

Fig. 4.2: Shale Conductivity vs True Vertical Depth with Matthews' Implied Pore Pressure Overlay (With "Shifting Factor") – EW 910 A1BP

Figures 4.3 – 4.10 show the formation shale conductivity versus depth for each well plotted against the Pliocene-Pleistocene overlay calibrated with the aforementioned shifting factor.

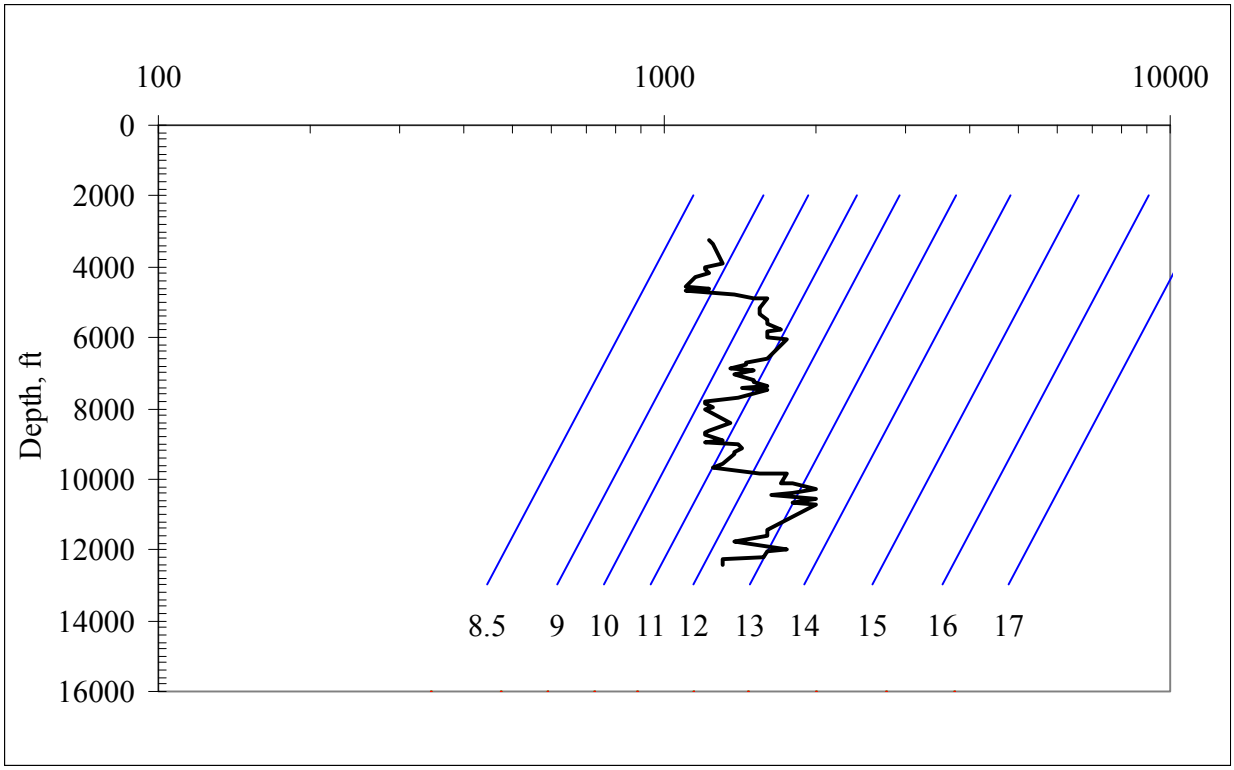

Fig. 4.3: Shale Conductivity vs True Vertical Depth with Matthews' Implied Pore Pressure Overlay– EW 910 A1BP

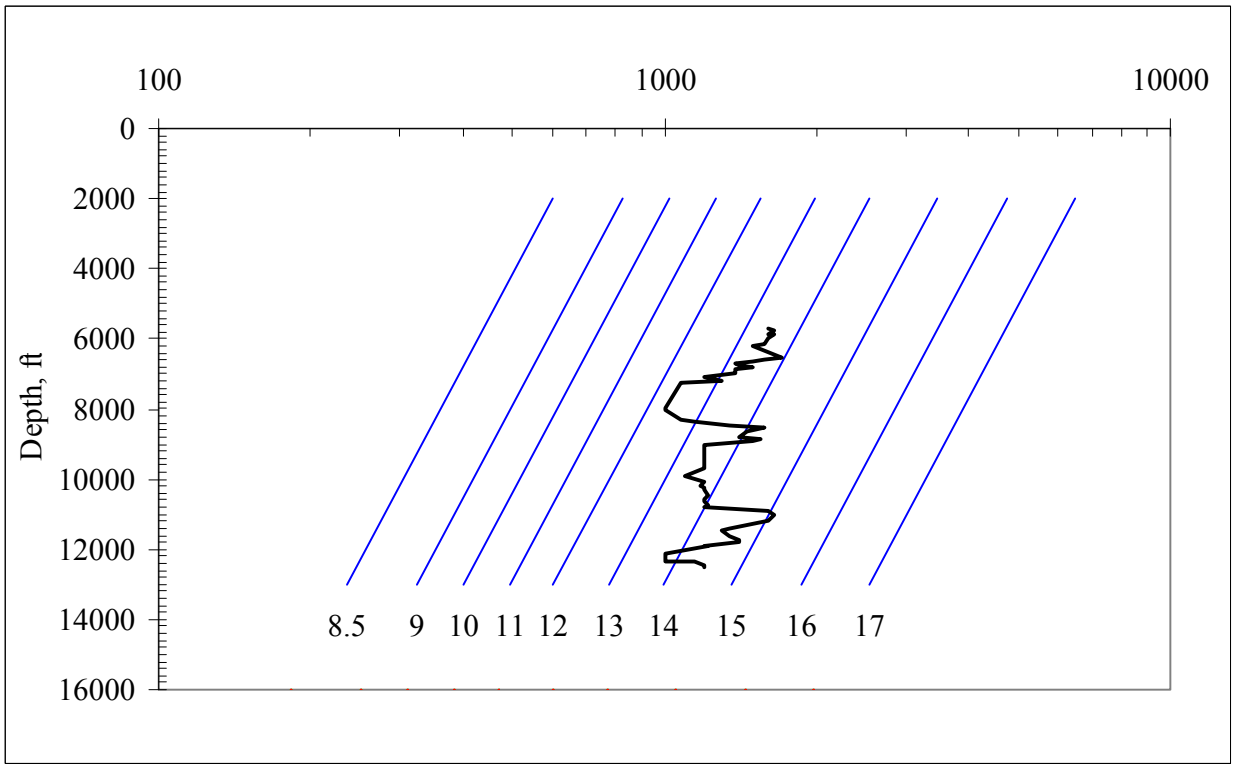

Fig. 4.4: Shale Conductivity vs True Vertical Depth with Matthews' Implied Pore Pressure Overlay – EW 954 A2

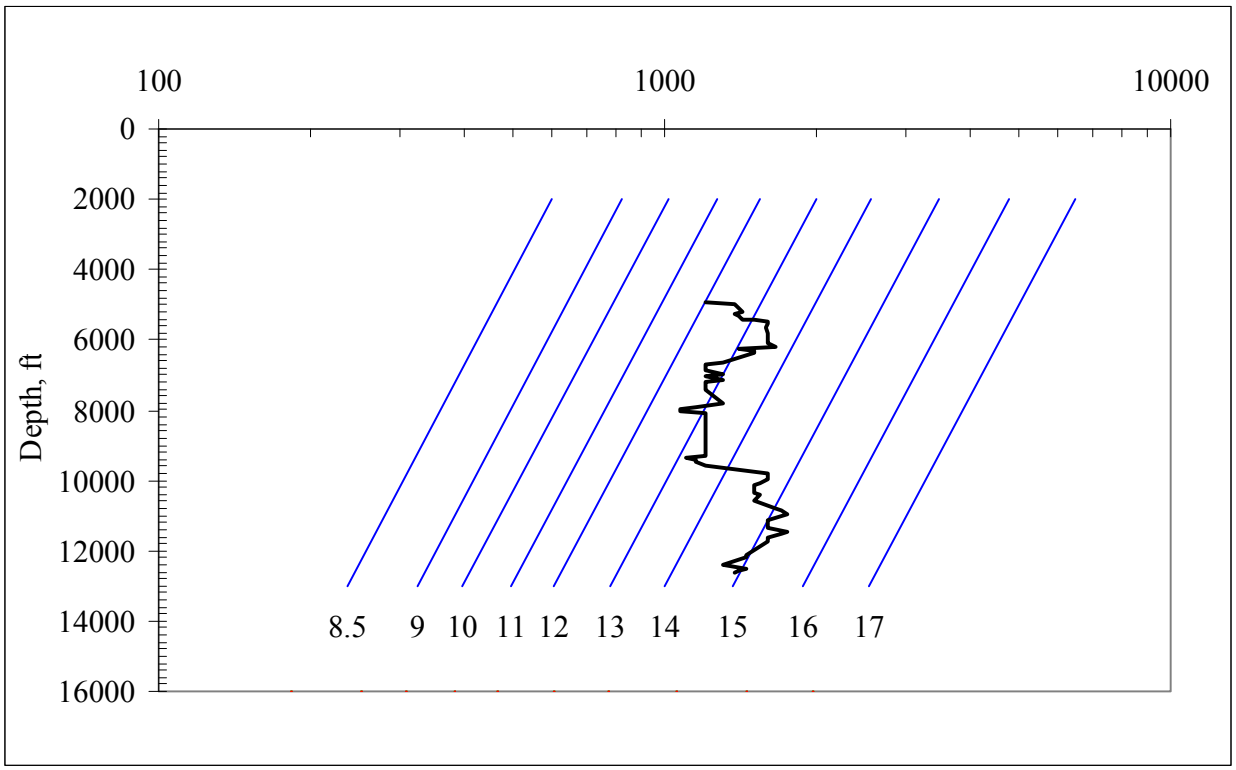

Fig. 4.5: Shale Conductivity vs True Vertical Depth with Matthews' Implied Pore Pressure Overlay – EW 910 A3

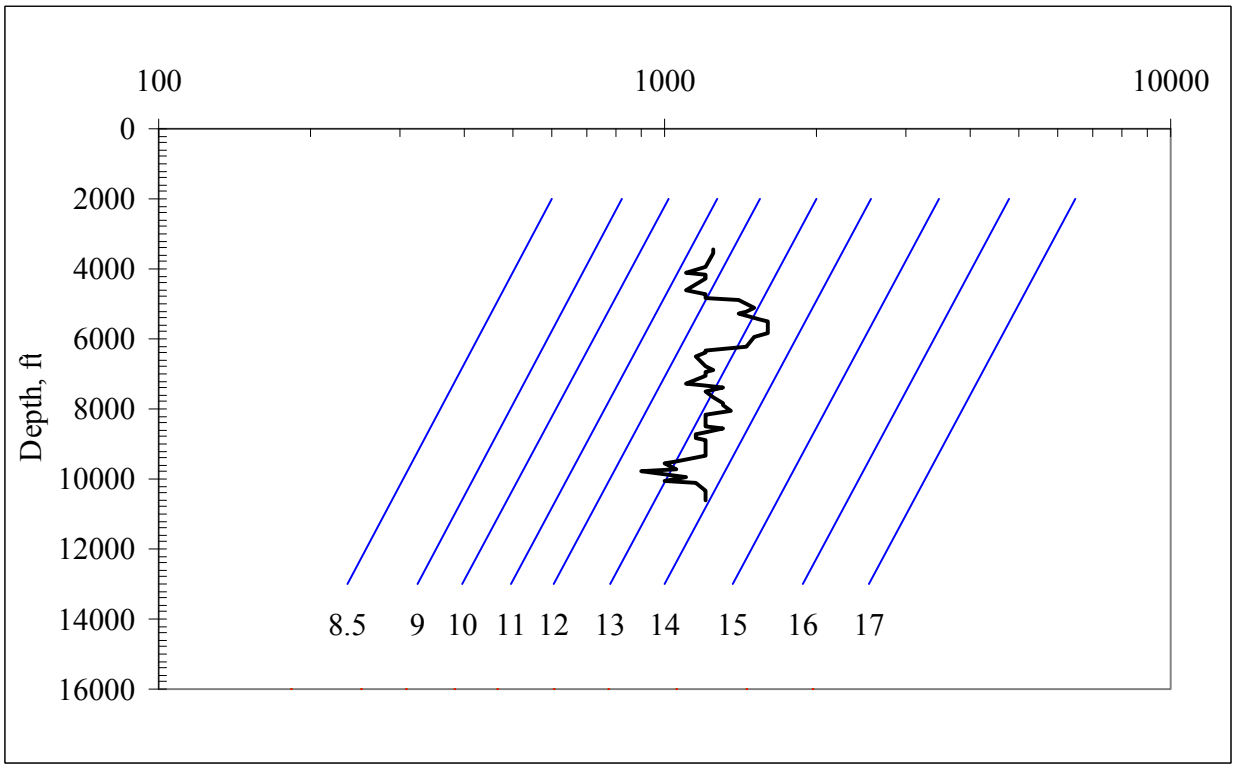

Fig. 4.6: Shale Conductivity vs True Vertical Depth with Matthews' Implied Pore Pressure Overlay – ST 320 A4

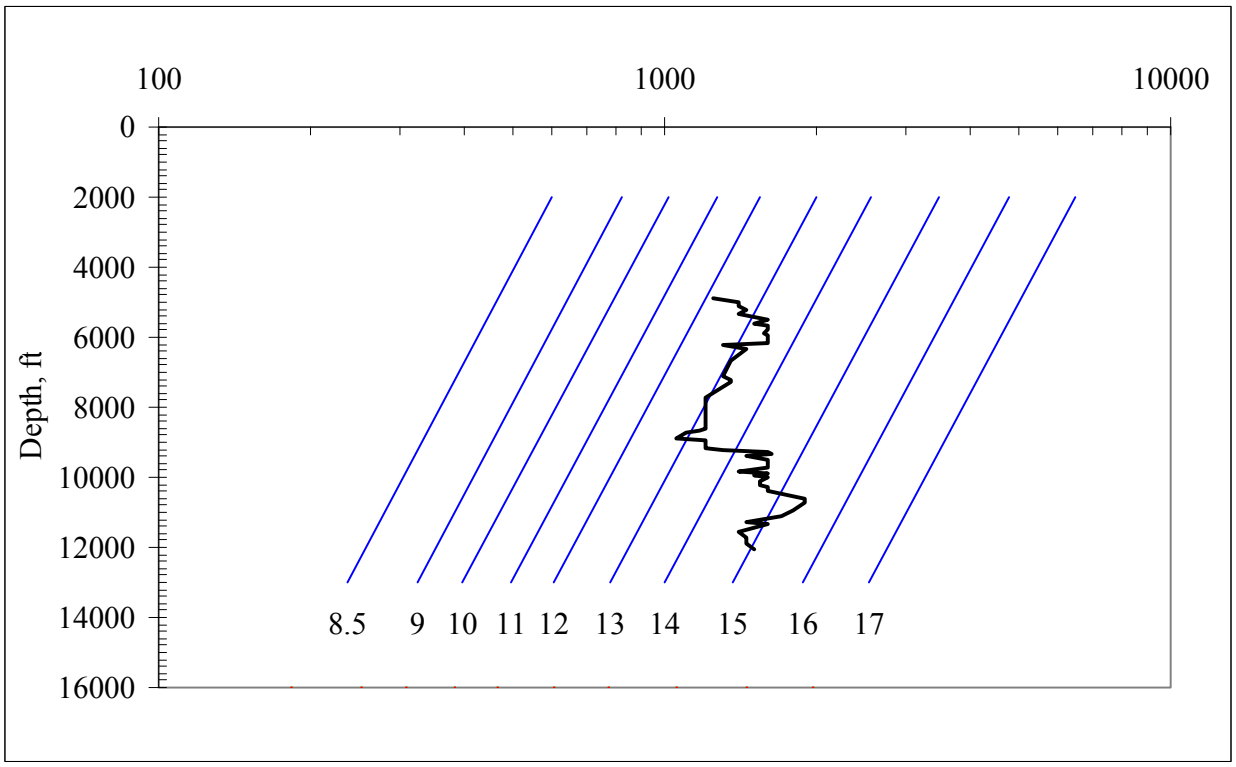

Fig. 4.7: Shale Conductivity vs True Vertical Depth with Matthews' Implied Pore Pressure Overlay – EW 910 A5

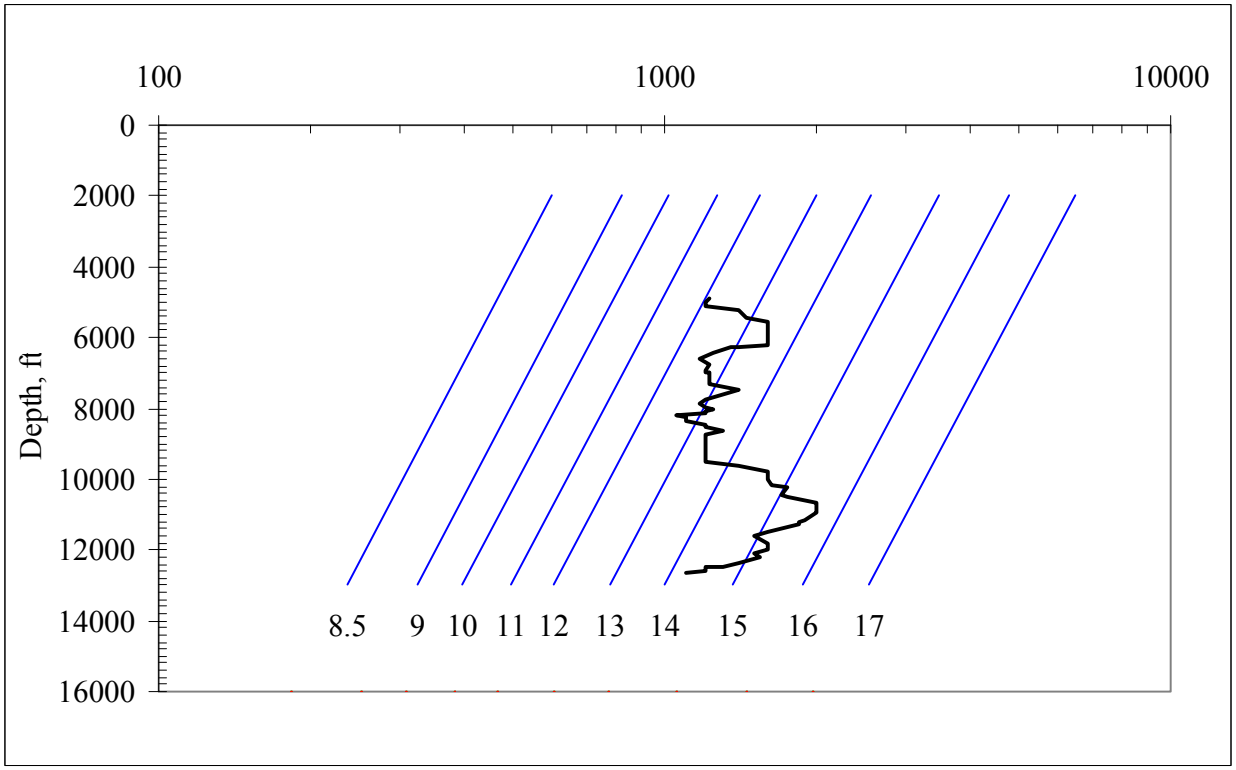

Fig. 4.8: Shale Conductivity vs True Vertical Depth with Matthews' Implied Pore Pressure Overlay – EW 910 A6

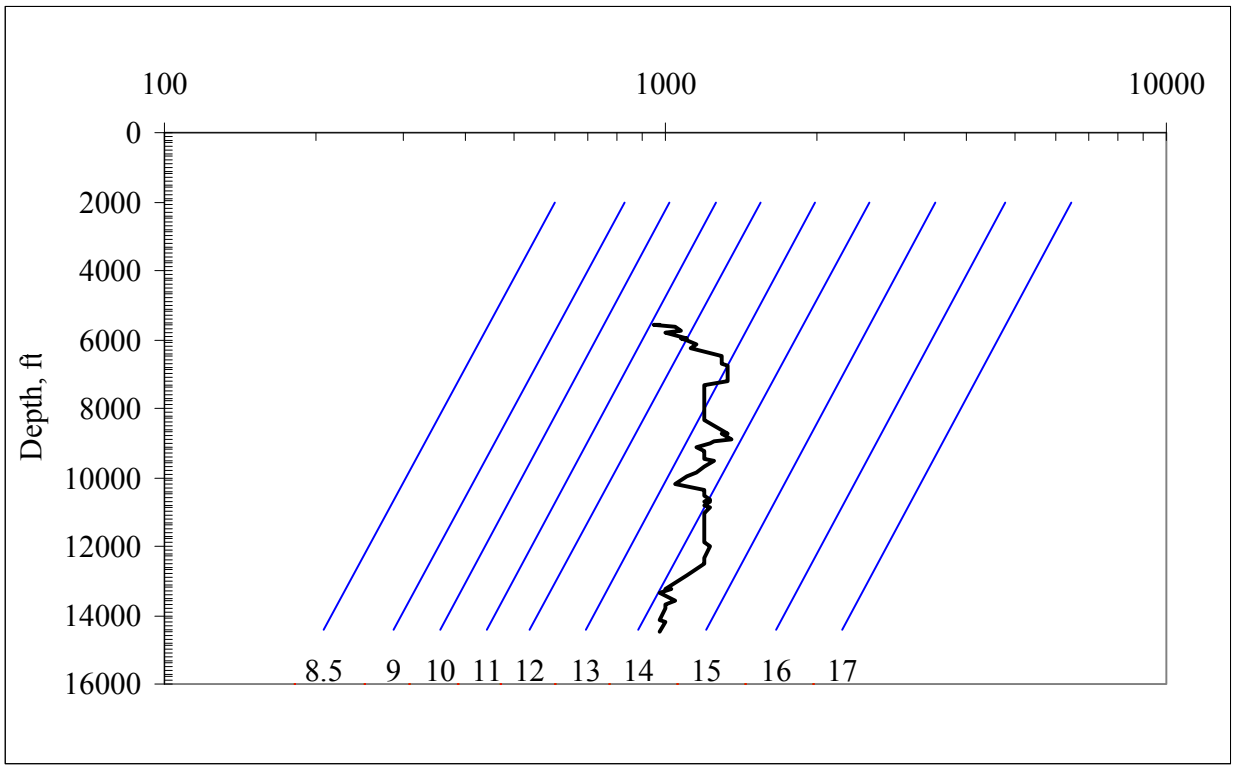

Fig. 4.9: Shale Conductivity vs True Vertical Depth with Matthews' Implied Pore Pressure Overlay – EW 910 No. 4

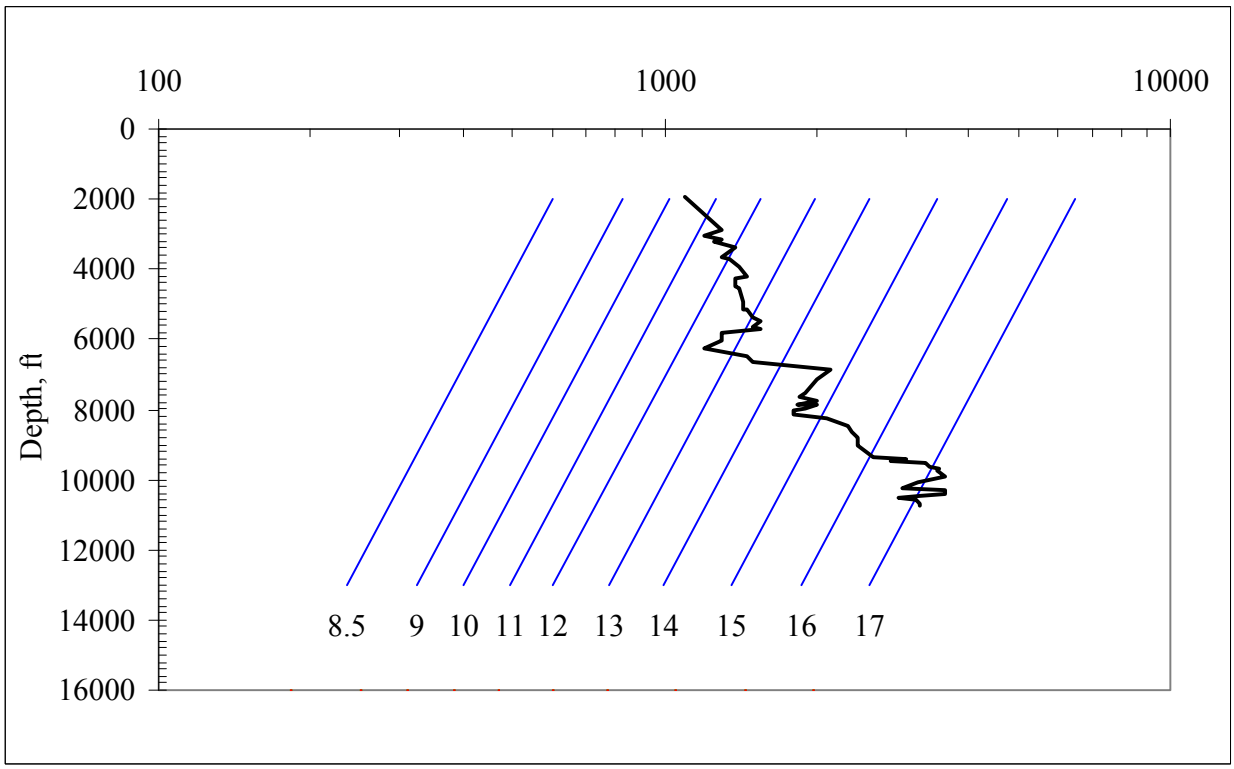

Fig. 4.10: Shale Conductivity vs True Vertical Depth with Matthews' Implied Pore Pressure Overlay – EW 953 No. 1

4.2 Analysis of Matthews' Pore Pressure Prediction Strategy

The pore pressures predicted from applying Matthews' compaction trendline and pore pressure gradient overlay were transcribed to a Cartesian plot and analyzed against the relevant available pressure data. The pressure data analyzed includes the mud weights, measured reservoir pressures, kicks, and other data described in Chapter 3. Mud weights and measured pressure data are plotted directly to the plot. The inferred pressure data is included on the plot, but has some uncertainty since assumptions were made due to the lack of details from the drilling records. This analysis results in Figures 4.11 – 4.18.

Figure 4.11 demonstrates that the deep measured pressure data correlates very well with the pore pressure predicted by the Matthews prediction strategy for the EW 910 A1BP well. This is by design, however, since the EW 910 A1BP well data was used for the development of the normal compaction trendline. The predicted pore pressure and mud weight follow a similar trend except in the interval from approximately 6000' – 10500', where the pore pressure prediction indicates that this zone is a pressure regression that was overbalanced by 1.0 – 2.0 ppg EMW when drilled. Unfortunately, there are no measured pressures in this interval to confirm this as reality. Nevertheless, it is a reasonable possibility given that the mud weight being used was required by the apparent pore pressures above the regression.

Figure 4.12 shows a similar pressure regression prediction for the EW 954 A2 well as seen in the EW 910 A1BP well in the interval of 6400' – 11000'. However, the regression appears to be more significant as the overbalance approaches 2.5 ppg EMW at approximately 8050'. Also, the pore pressure is under predicted by approximately 0.5 ppg EMW at 12450'.

Figure 4.13 also shows a pressure regression prediction in the interval of approximately 6200' – 9700' in the EW 910 A3 well. This plot may confirm that the predicted pressure regression may be due to questionable conductivity since there is a pore pressure estimated from inferred pressure data at 6655' in the 13.5 – 14.0 ppg range. The model predicts a pore pressure

of 12.8 ppg EMW at this depth, resulting in a pore pressure under prediction of 0.7 – 1.3 ppg EMW. Disregarding the depleted interval at approximately 11400', the pore pressure is under predicted by 0.5 ppg at approximately 11500'.

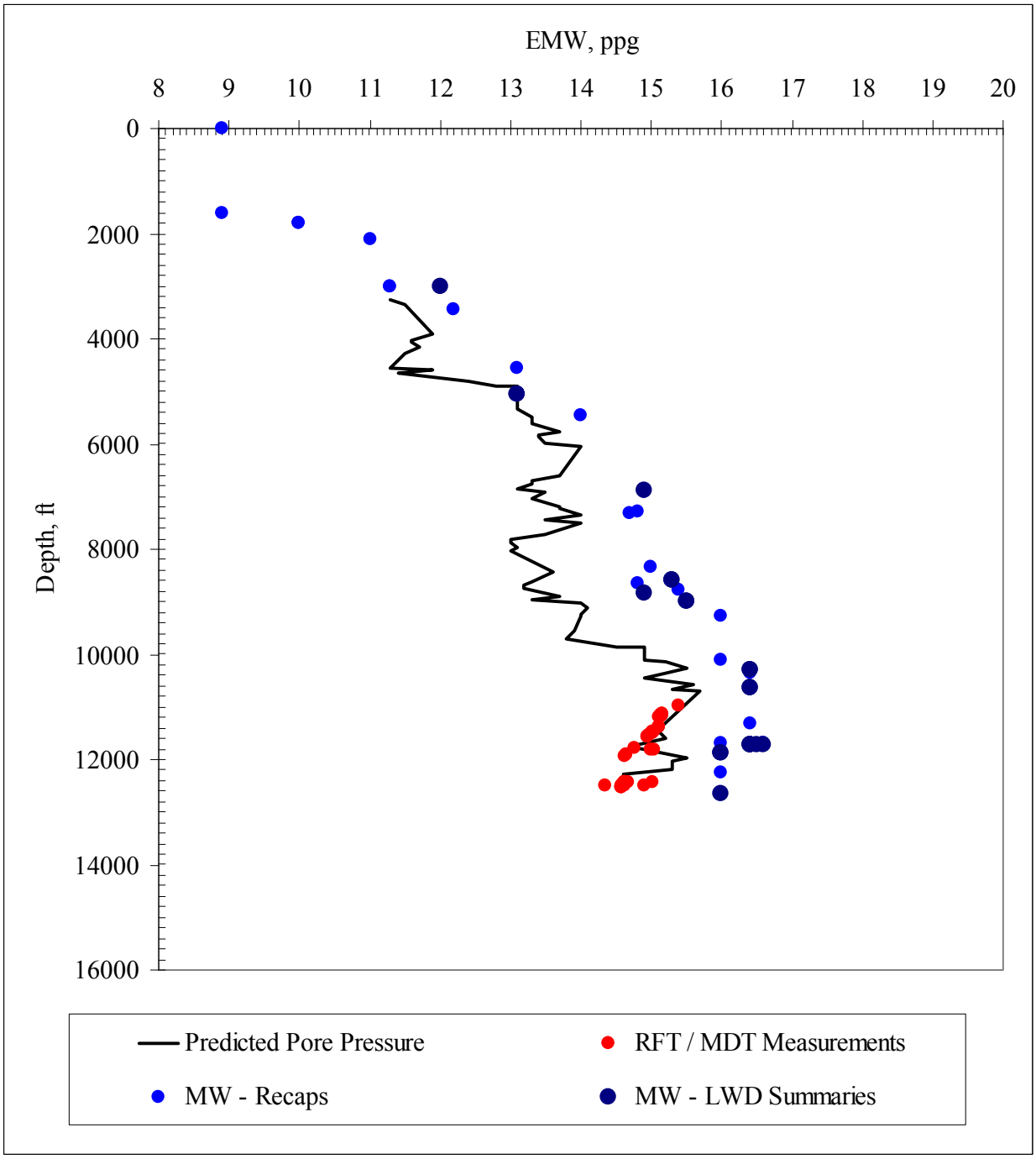

Fig. 4.11: Matthews' Pore Pressure Prediction – EW 910 A1BP

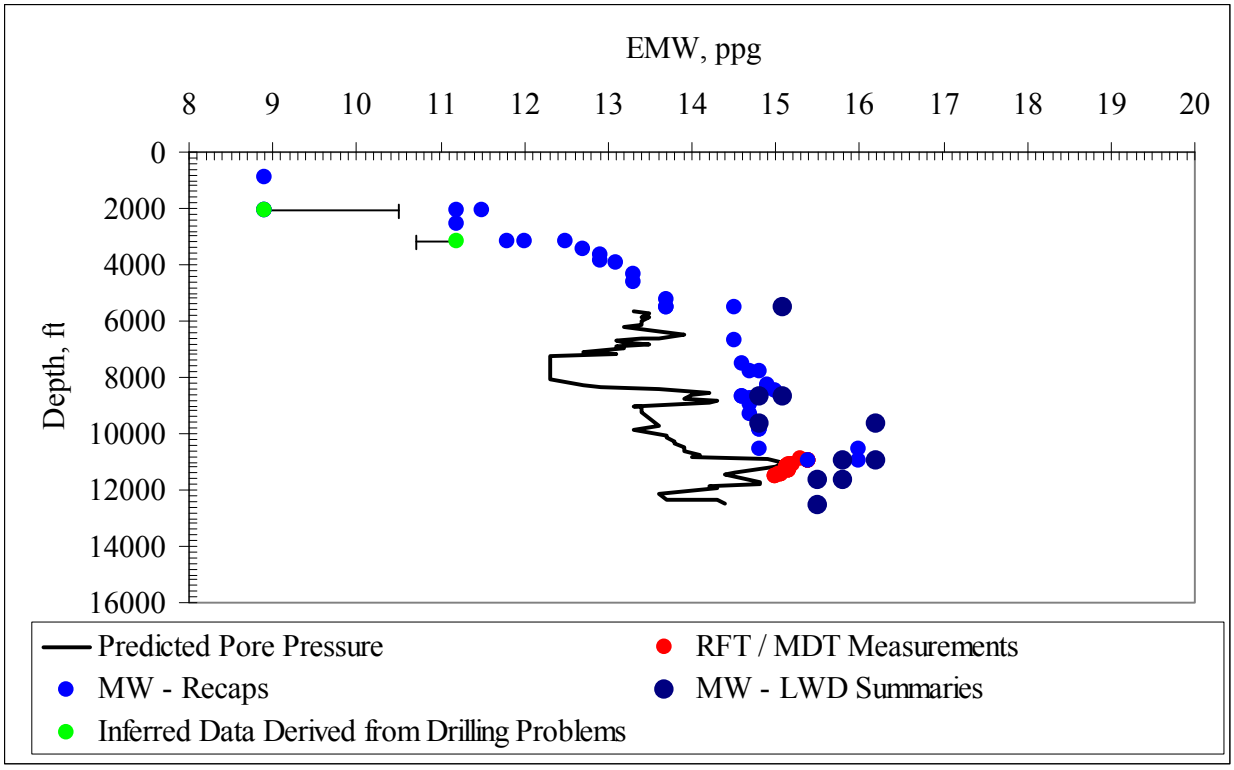

Fig. 4.12: Matthews' Pore Pressure Prediction – EW 954 A2

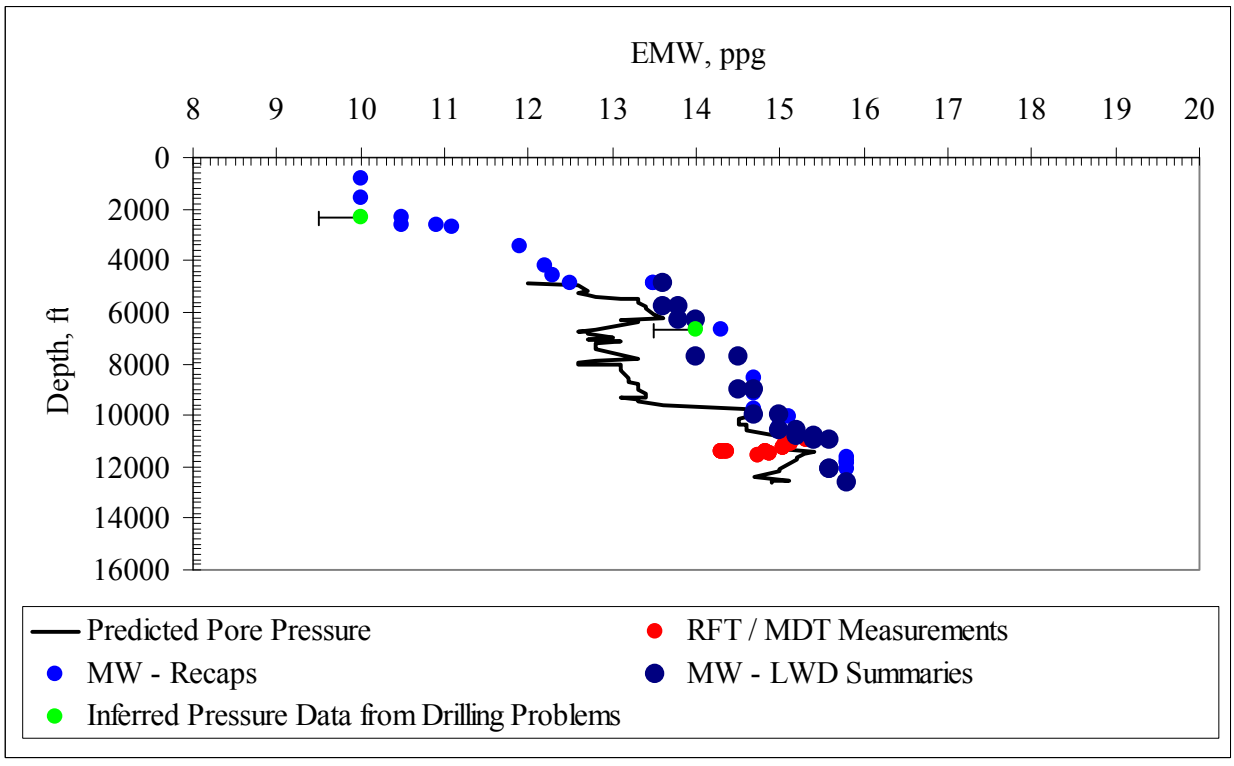

Fig. 4.13: Matthews' Pore Pressure Prediction – EW 910 A3

Figure 4.14 is a pore pressure prediction plot for the ST 320 A4 well. There is no measured reservoir pressure data for this well. The only pressure data available is the hydrostatic mud weight used during drilling operations. There were no drilling incidents leading to pore pressure inferences. This well appears to have a different pressure regime than the previously discussed wells. The maximum pore pressure predicted was 13.9 ppg EMW and occurred at 10585', less than 100' from total depth. Besides the EW 954 A2 well, which was predicted to be in a pressure regression at this depth, this predicted pore pressure is 0.7 ppg EMW less than the EW 910 A3 well and 1.3 ppg EMW less than the EW 910 A1BP well at similar true vertical depths. Also, there is not a significant pore pressure regression predicted.

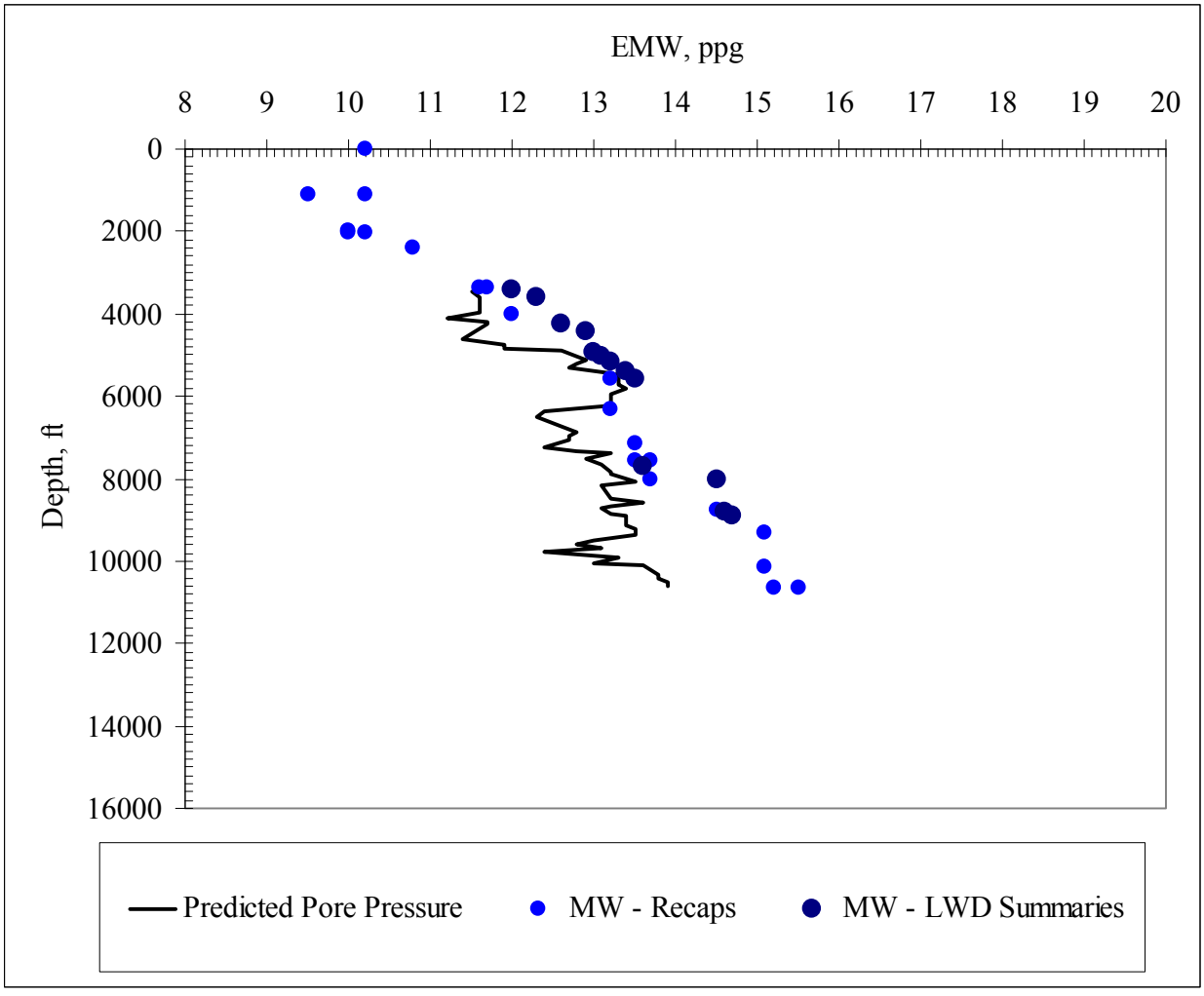

Fig. 4.14: Matthews' Pore Pressure Prediction – ST 320 A4

Figures 4.15 and 4.16 are the pore pressure prediction plots for the EW 910 A5 and A6 wells, respectively. These pore pressure plots are similar since neither well has measured reservoir pressure data. They were also both drilled with a maximum mud weight of 15.8 ppg. Both wells have pore pressure regressions predicted, though the regressions intervals differ slightly. The regression interval predicted in the EW 910 A5 well is from 6200' – 9300' and the interval predicted in the EW 910 A6 well is from 6200' – 9600'. Both wells have similar pore pressure prediction trends and were drilled with similar mud weight schedules.

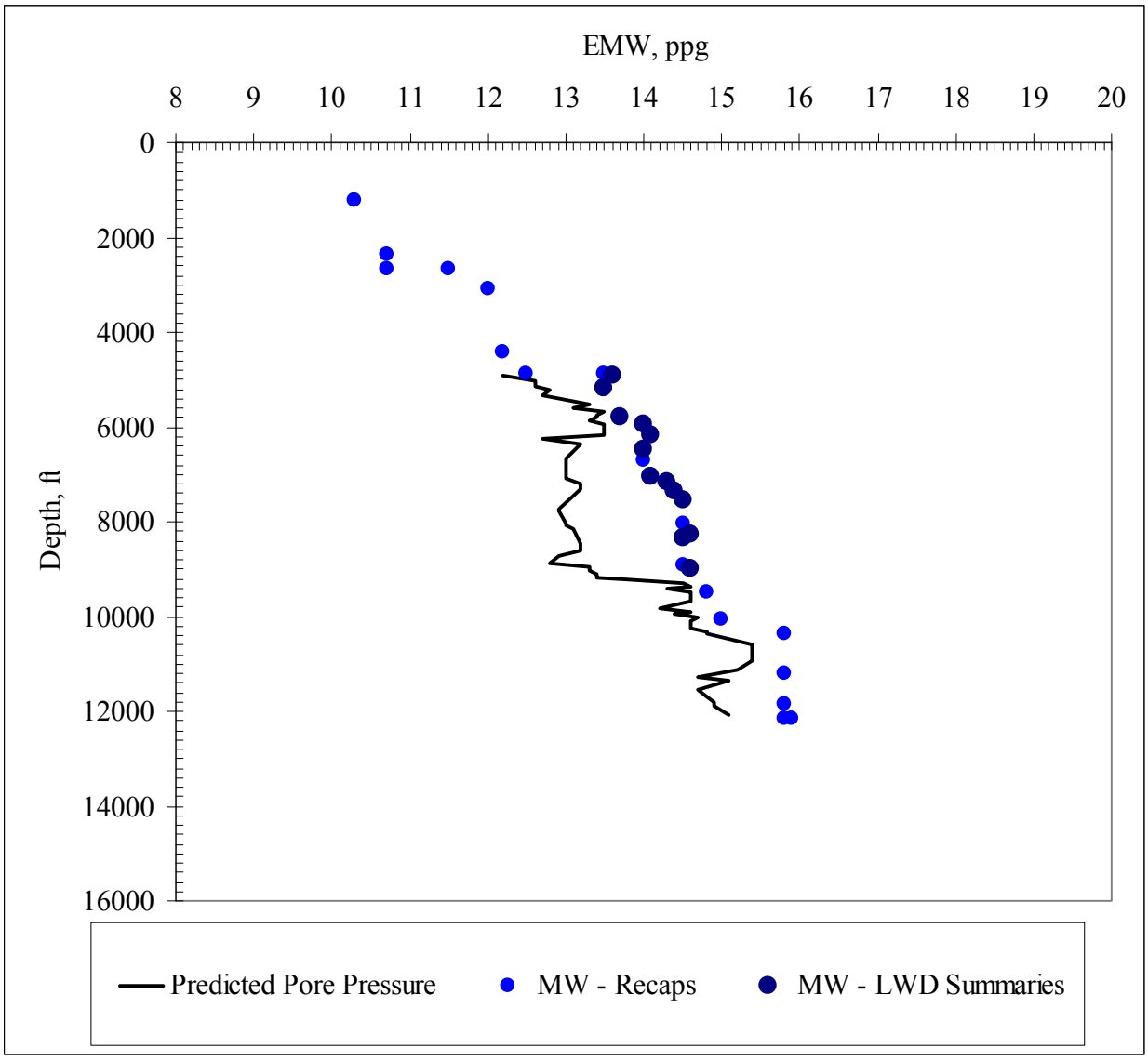

Fig. 4.15: Matthews' Pore Pressure Prediction – EW 910 A5

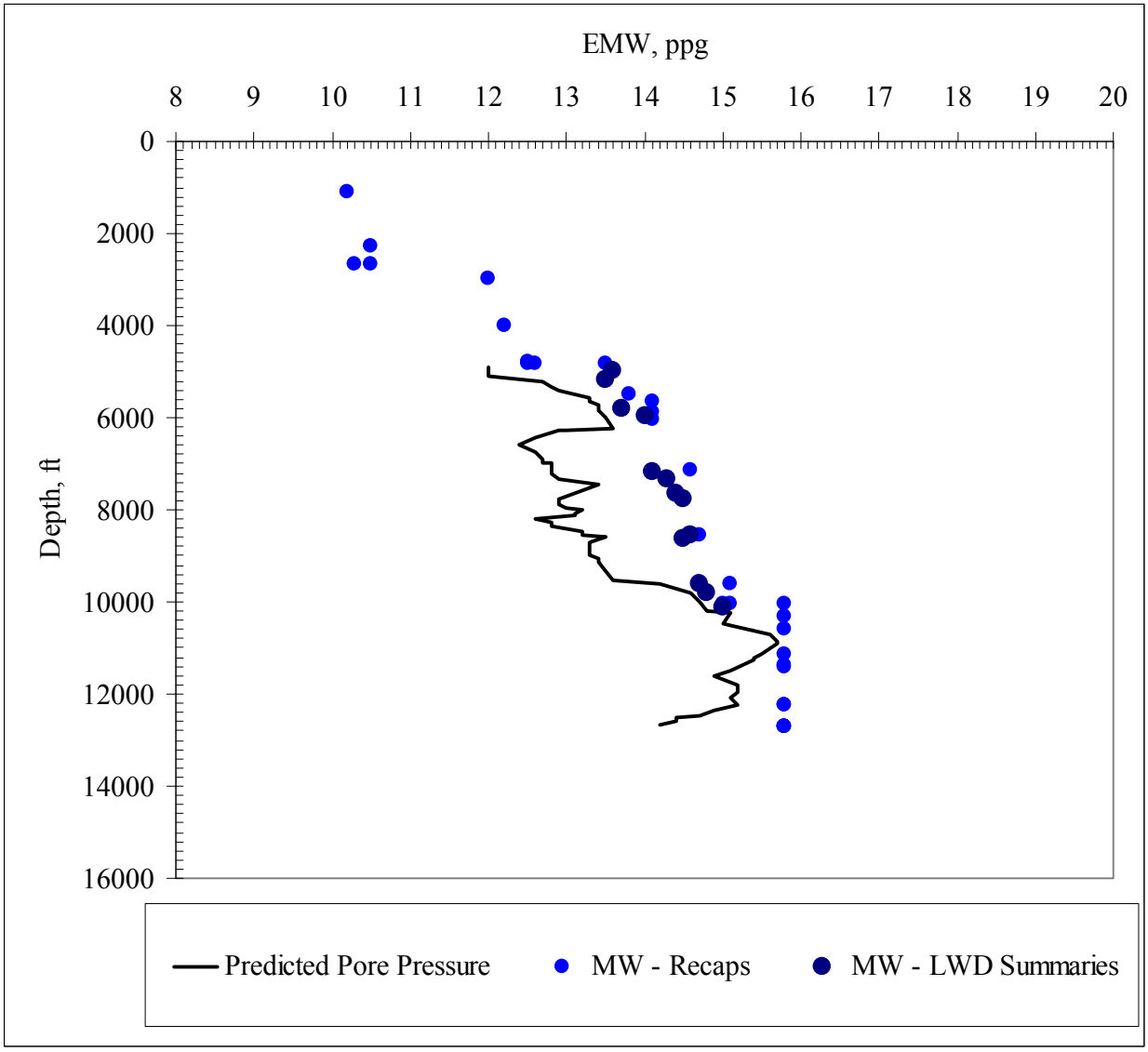

Fig. 4.16: Matthews' Pore Pressure Prediction – EW 910 A6

Figure 4.17 is the pore pressure prediction plot for the EW 910 No. 4 well. This well was drilled in the far eastern portion of the EW 910 block. Though this well was drilled with a maximum mud weight of 15.2 ppg, the well reached total depth with a mud weight of 14.6 ppg. This well has a similar pore pressure prediction profile as the ST 320 A4, which is the nearest offset well. Similar to the ST 320 A4 well, a significant pore pressure regression predicted does not exist as in the other wells discussed. There is no measured reservoir pressure data available for this well. There is one pore pressure inference at 3100' that corresponds well with the mud weight used in that interval.

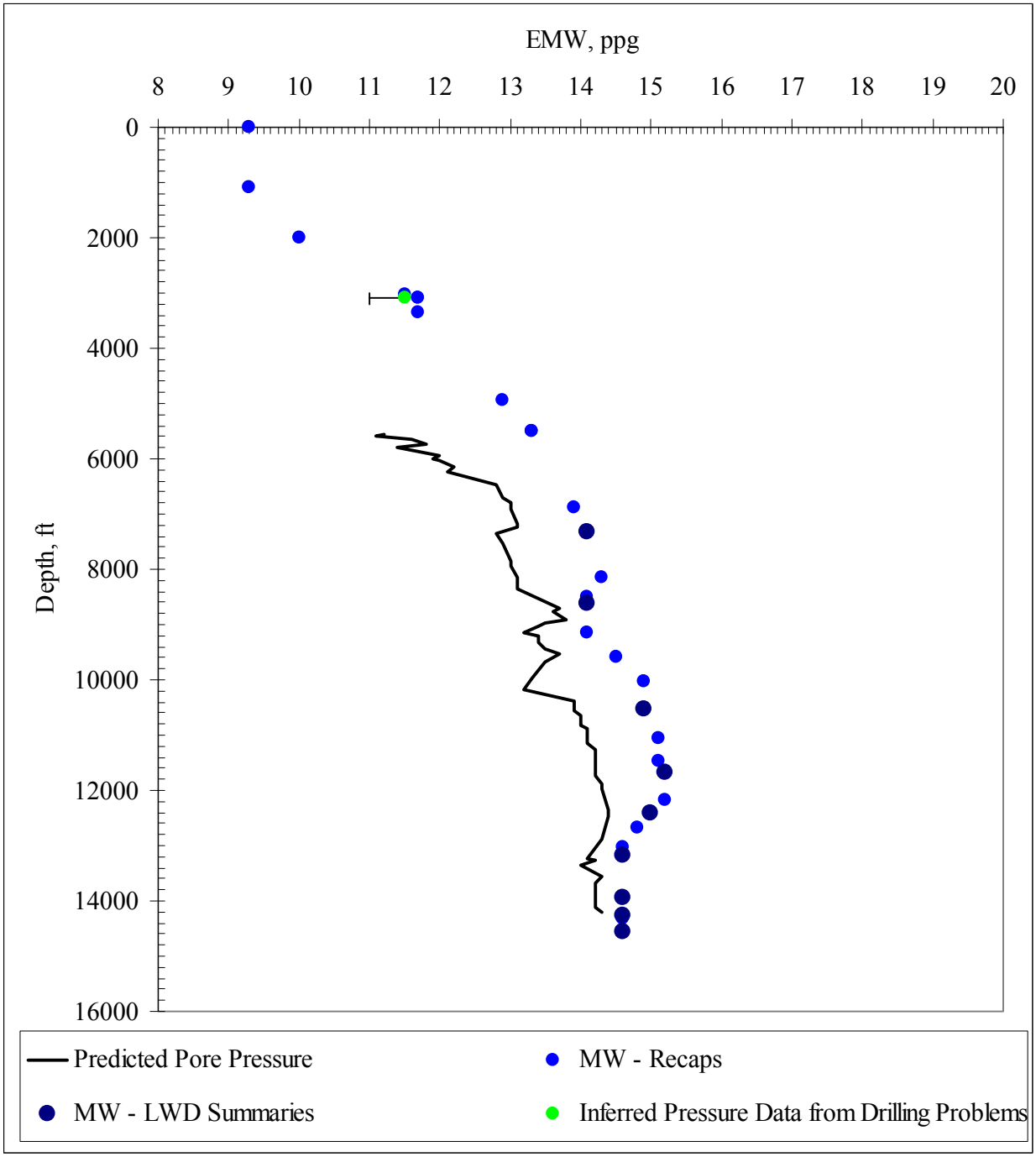

Fig. 4.17: Matthews' Pore Pressure Prediction – EW 910 No. 4

Figure 4.18 is the pore pressure prediction plot for the EW 953 No. 1 well. This is the furthest offset well from the main EW 910 area. This method does not predict the pore pressures very well for EW 953 No. 1 below approximately 8000'. This method predicts that the pore pressure is a maximum of 1.7 ppg EMW higher than the mud weight at approximately 10000'.

In addition, the method over predicts the measured pore pressure at 9000 feet by about 0.5 ppg EMW.

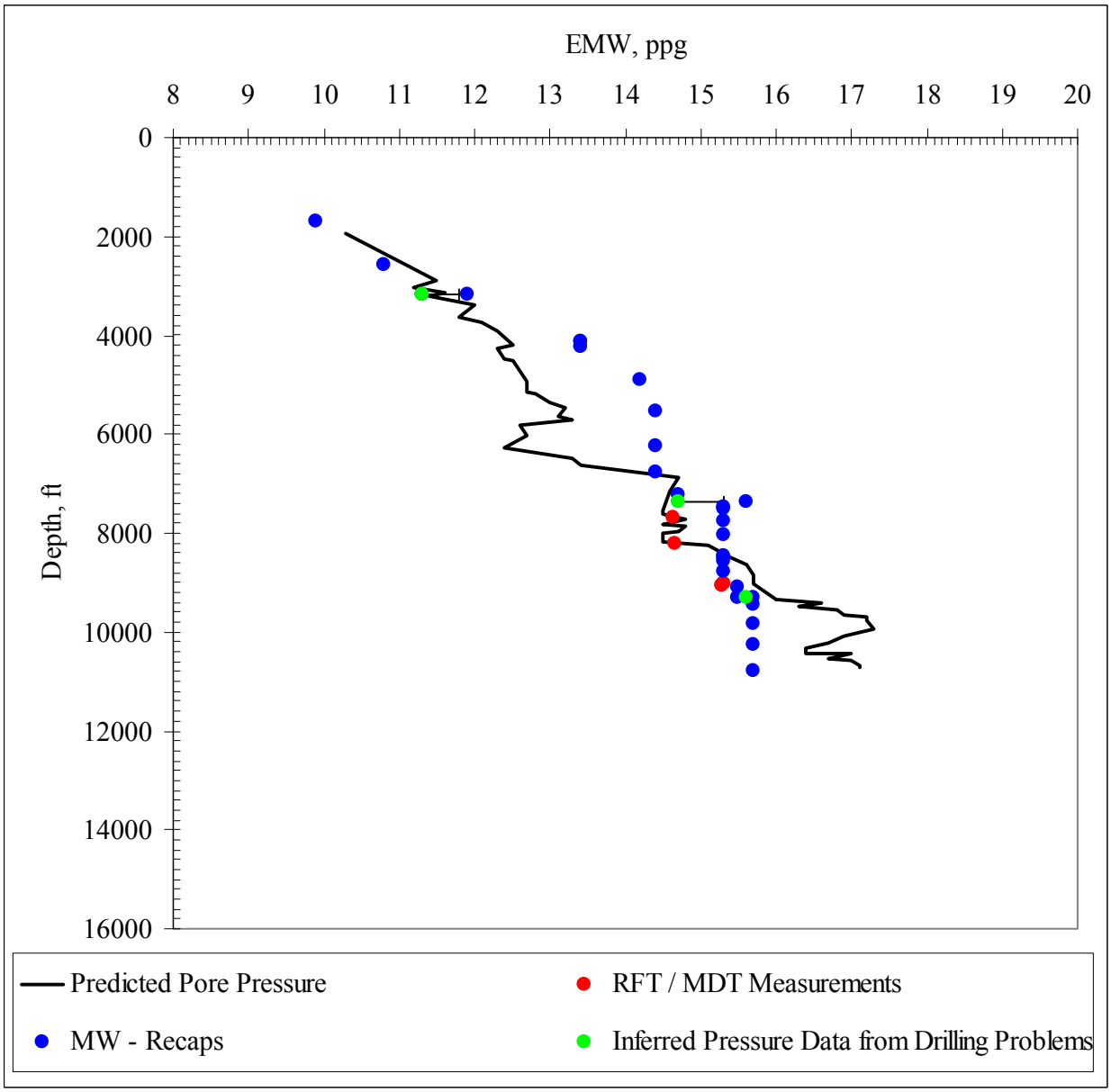

Fig. 4.18: Matthews' Pore Pressure Prediction – EW 953 No. 1

A possible explanation is implied by Hottman and Johnson's early publication[13] on estimating pore pressures from electric logs. One stated limitation of using conductivity as a pore pressure detecting parameter is assuming that the pore fluid content is of constant salinity. In many cases, this is a poor assumption. The formation water resistivity greatly affects the conductivity. Due to the significant shift in conductivity without a significant increase in mud

weight, the formation water resistivity of the deep (greater than 8000') formations was questioned and compared with the formation water resistivity of shallower formations. Figure 4.19 is a plot of calculated formation water resistivities, R_w, for different formation depths.

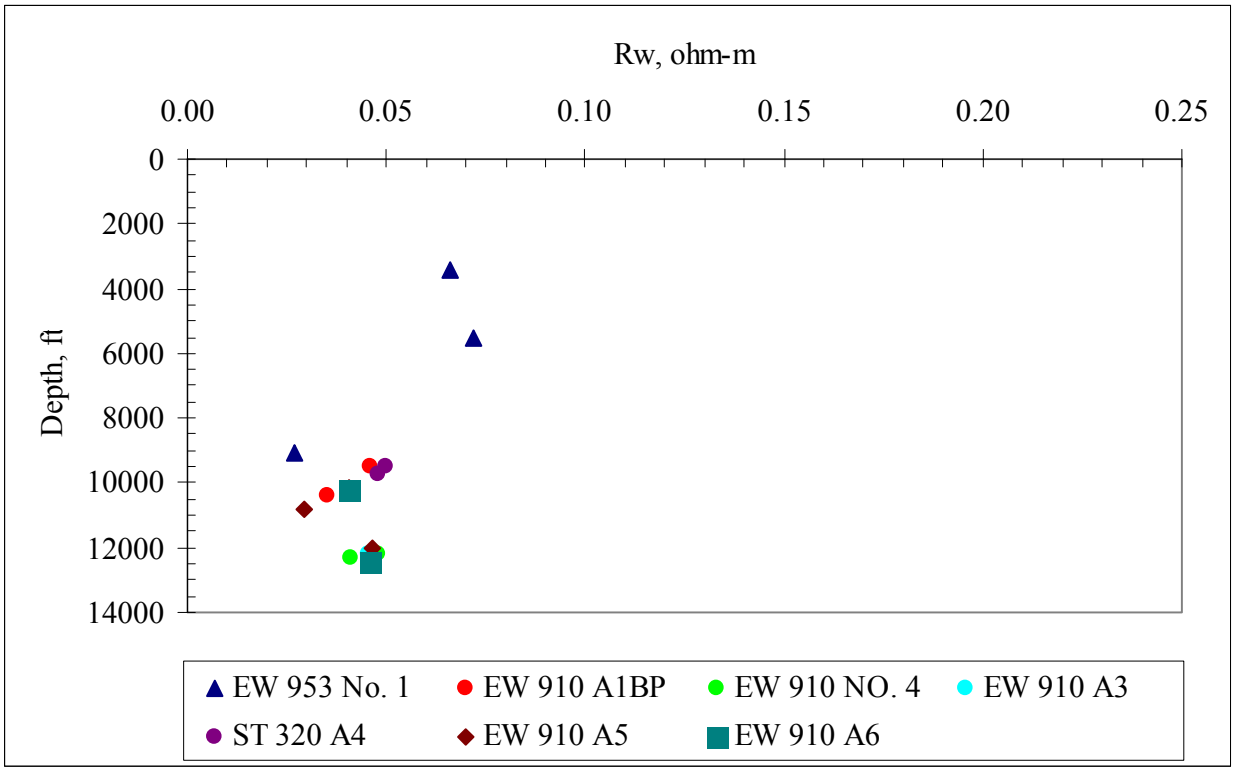

Fig. 4.19: Calculated Rw for Offset Wells Using Porter and Carother's Formation Resistivity Factor Relationship

This calculation was performed using the density data (EW 910 A1BP, EW 910 No. 4 and EW 953 No. 1) or density porosity (EW 910 A3, ST 320 A4, EW 910 A5 and EW 910 A6) and induction resistivity from the available logs. Though the only well with a questionable prediction is the EW 953 No. 1 well, calculated water resistivities from all of the other wells were used in the comparison to determine if the formation water resistivity data from the EW 953 No. 1 well is anomalous. The five formation resistivity factors for sandstone described in the literature review were applied (Equations 2.28 – 2.32). The Porter and Carothers[17] relationship was used in the final calculations. Both the Chevron[22] and the Phillips[5] relationships produced values similar to the Porter and Carothers, but the Humble[20] relationship produced

formation resistivity values consistently lower than the other three relationships at all depths. It is clear after examining Figure 4.19 that the formation water resistivity for the EW 953 No. 1 well is not constant versus depth.

One possible theory explaining the significant difference in actual versus predicted pore pressure in the EW 953 No. 1 well is this change in formation water resistivity. Figure 4.19 shows that the formation water resistivity varies significantly from the shallow to the deep sections. However, the only data available shallower than 8000 feet is from the EW 953 well. So, a comparison of this trend to the other wells is not possible.

It is potentially more relevant that the formation water resistivity calculated for the EW 953 No. 1 well at about 9000 feet is the lowest among all other wells in the EW 910 Area. A lower water resistivity implies a higher measured formation conductivity for the same formation porosity. The average water resistivity in the nearby wells is about 1.4 times higher than that in the EW 953 well and about 1.7 times higher in the zones nearest in depth to this zone. That implies that a formation in the EW 953 well with the same porosity, and therefore same pore pressure, as a formation in the other wells would have a conductivity 1.4 to 1.7 times higher. So, reducing the conductivity in the EW 953 by a factor of 1.4 to 1.7 should adjust the conductivity to be on the same basis as the other wells. Applying this adjustment provides more than enough difference to explain the apparent over prediction of formation pressure at 9000 feet. However, it still results in an interpreted pore pressure that is somewhat higher than the mud weight that was used at 10,000 feet. It is possible that the water resistivity in the EW 953 well continued to decrease with depth. If so, this might be the explanation for the higher than expected conductivities below 9000 feet in this well. However, there are no permeable formations below 9000 feet in which to calculate water resistivities. That may also be the reason that the well was drilled with mud weights less than the implied pore pressure, i.e. there were no permeable zones to cause kicks. In summary, the Matthews approach for calculating pore pressure from

conductivity, as applied herein, cannot be used for reliable pore pressure interpretations for the EW 953 No. 1 well below 8000 feet.

5. ANALYSIS OF BEN EATON'S PORE PRESSURE PREDICTION STRATEGY

This chapter discusses the implementation of a pore pressure prediction strategy developed by Ben Eaton[9]. The relationship empirically derived by Eaton is a simple relationship between pore pressure, formation overburden stress and the effective vertical stress:

$$P_F / D = \sigma_{OB} / D - \left(\sigma_{OB} / D - P_{F(n)} / D\right) * \left(\frac{Cn_{(sh)}}{Cob_{(sh)}}\right)^{1.2} \qquad \textit{(Equation 5.1)}$$

for conductivity data and

$$P_F / D = \sigma_{OB} / D - \left(\sigma_{OB} / D - P_{F(n)} / D\right) * \left(\frac{dTn_{(sh)}}{dTob_{(sh)}}\right)^{3} \qquad \textit{(Equation 5.2)}$$

for interval transit time data.

An implementation of both the conductivity and interval transit time (1/velocity) equations will be performed.

5.1 Development of the Overburden Stress Relationship

Integration of the formation bulk density data versus depth establishes the overburden stress relationship. As described in Table 1.1, there is formation bulk density data from multiple wells from 3000' to 14550'. With the water depth varying between 557' at the A Platform, 650' at the EW 953 No. 1 and 630' at the EW 910 No. 4 well, there's a significant amount of sediments without bulk density measurements above 3000'.

There is long spaced sonic data available from 2000' to 3000' in the EW 953 No. 1 wellbore. Gardener et al[12] developed the following relationship between average interval velocity, *V*, and bulk density:

$$\rho_b = 0.23 * V^{0.25} \qquad \textit{(Equation 5.3)}$$

where velocity is in ft/sec. This relationship was applied to the long spaced sonic data to estimate bulk density data for the interval.

With the velocity relationship described above, the only interval requiring a bulk density estimate is from the surface to 2000'. Eaton assigns a bulk density of 1.06 g/cc from the sea level to the mudline and 1.6 g/cc from the mudline to 500' below the mudline (BML). With the available data, it isn't possible to estimate the bulk density for the remaining interval. A straight line from the bulk density value at 500' BML to the bulk density value at 2000' is assumed. This should provide a fairly accurate estimate of bulk density which can be integrated to determine the overburden stress relationship. Figure 5.1 is a plot of formation bulk density versus depth for the EW 910 area based on these assumptions and the available measured data. The data was obtained from the EW 953 No. 1, EW 910 A1BP and EW 910 No. 4 wells.

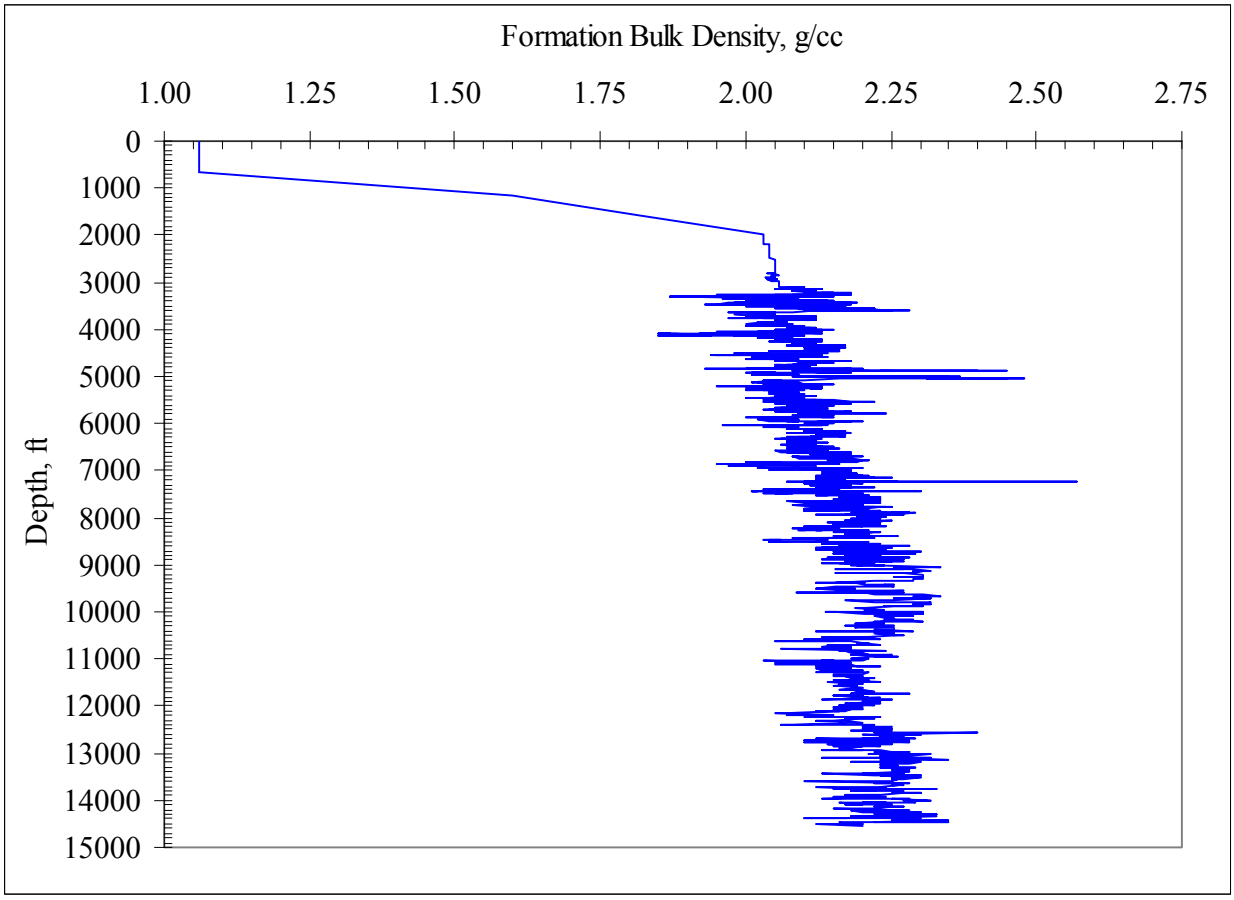

Fig. 5.1: Formation Bulk Density for the EW 910 Area

After integration of the bulk density shown in Fig. 5.1, a relationship for overburden stress was determined. Fig. 5.2 is a plot the overburden stress gradient versus true vertical depth

for the EW 910 Area. Eaton published two overburden stress gradient versus depth relationships for Gulf Coast formations[7,8]. The first was developed nearly forty years ago for normally compacted formations and the second, developed most recently, utilized deepwater data with abnormal pore pressures included in the data set. As a comparison, they are also shown in Figure 5.2. The overburden stress calculated herein is seen to be similar to the Eaton deepwater overburden stress, which is reasonable given the similar age of the sediments for these two relationships.

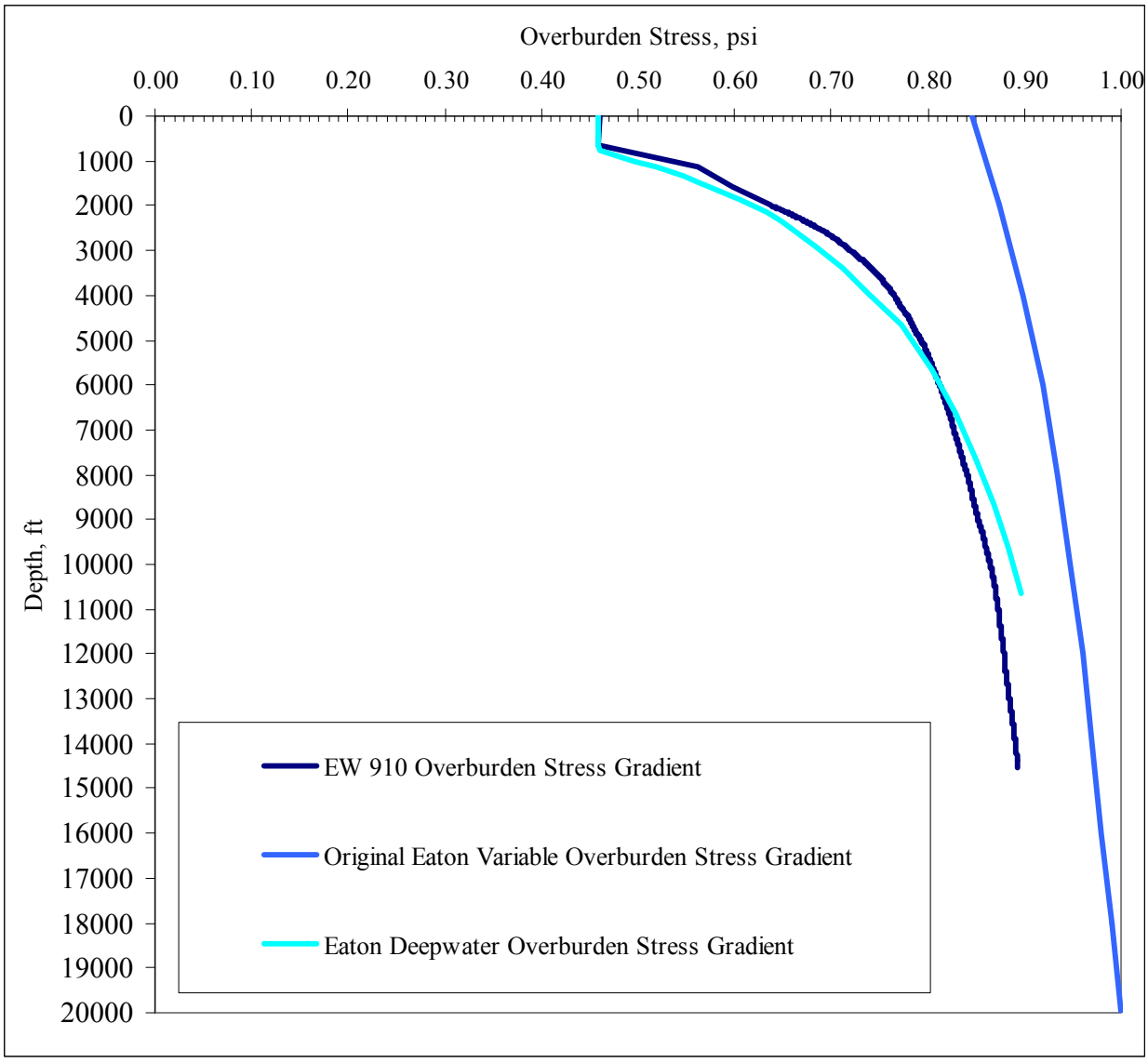

Fig. 5.2: Overburden Stress Relationship for EW 910 Area Compared to Ben Eaton's Published Relationships

The overburden stress versus depth relationship was fit to a polynomial curve in Excel and is described by the following equation:

$$\sigma_{OB} = a_1 D^6 + a_2 D^5 + a_3 D^4 + a_4 D^3 + a_5 D^2 + aD + a_7 \qquad \textit{(Equation 5.4)}$$

where,

a_1 = 4.092542229E-21
a_2 = -1.91276937109725E-16
a_3 = 3.46041193695536E-12
a_4 = -3.07205791465204E-08
a_5 = 1.44604224757927E-04
a_6 = 5.53568356670439E-01
a_7 = - 48.7022134214639

5.2 Development of the Effective Vertical Stress Parameter

Eaton defined the effective vertical stress term using three different petrophysical parameters; conductivity, resistivity and interval transit time. The effective vertical stress term relates the value of an observed petrophysical property to the expected value for that property in a normally compacted formation at the same depth, (i.e. normal compaction trendline). Typically, a normal trendline is established from the petrophysical data in the normally pressured section of the wellbore. As discussed in Chapter 4, the abnormality with this data set is the onset of geopressures shallower than any recorded petrophysical data. Therefore, an iterative process was required to develop the normal trendline for both conductivity and sonic data. The procedure for this process is described below.

1. Input petrophysical values (either conductivity or interval transit time) of "clean shales" into pore pressure prediction model.
2. Plot all available pressure data on a Cartesian plot of pressure gradient (psi/ft) versus true vertical depth.
3. Assume an equation of the form $D = m * \ln(PP) + b$ for the normal pressure trendline, where "PP" is a petrophysical parameter, using either conductivity or interval transit time. Rewrite

the equation in the form $PP = \exp\left(\frac{D-b}{m}\right)$ to help determine the estimated value of the petrophysical parameter in normally pressured shale at any depth.

4. Calculate the effective vertical stress term, σ_v, by the relationship between the observed petrophysical parameter value and the normal petrophysical parameter value calculated in Step 3.
5. Calculate pore pressure by utilizing Eqns. 5.1 or 5.2.
6. Compare the resulting pore pressure relationship versus depth. If the prediction does not compare favorably with the pressure data choose a new equation for the normal pressure trend line and repeat Steps 3 – 6 until a satisfactory result is obtained.

5.3 Results and Conclusions of the Eaton Pore Pressure Prediction Strategy Using Formation Conductivity Measurements

The previously described procedure was followed resulting in the following normal pressure trendline for conductivity data:

$$D = -13600 * \ln(COND) + 96000 \qquad \textit{(Equation 5.5)}$$

As performed with the Matthews' strategy discussed in Chapter 4, the calibration of the model was determined from one well, and the result applied to the remaining wells. For the formation conductivity approach, the equation for the normal trendline was determined by comparing the pore pressure predicted by Equation 5.1 to the observed pressure data for the EW 910 A1BP well. Equation 5.4 was defined and then utilized in all other well predictions.

Figures 5.3 through 5.10 are the pore pressure plots resulting from implementation of Equation 5.1 and the aforementioned procedure. In general, the results appear very similar to the results obtained using Matthews' prediction strategy.

Figure 5.3 is a plot of the pore pressures predicted by the Eaton conductivity method for the EW 910 A1BP well. The measured pressure data correlate very well with the predicted pore

pressure except in the interval from 6600' – 9900', where the pore pressure prediction indicates a pressure regression of approximately 0.6 ppg – 1.0 ppg EMW.

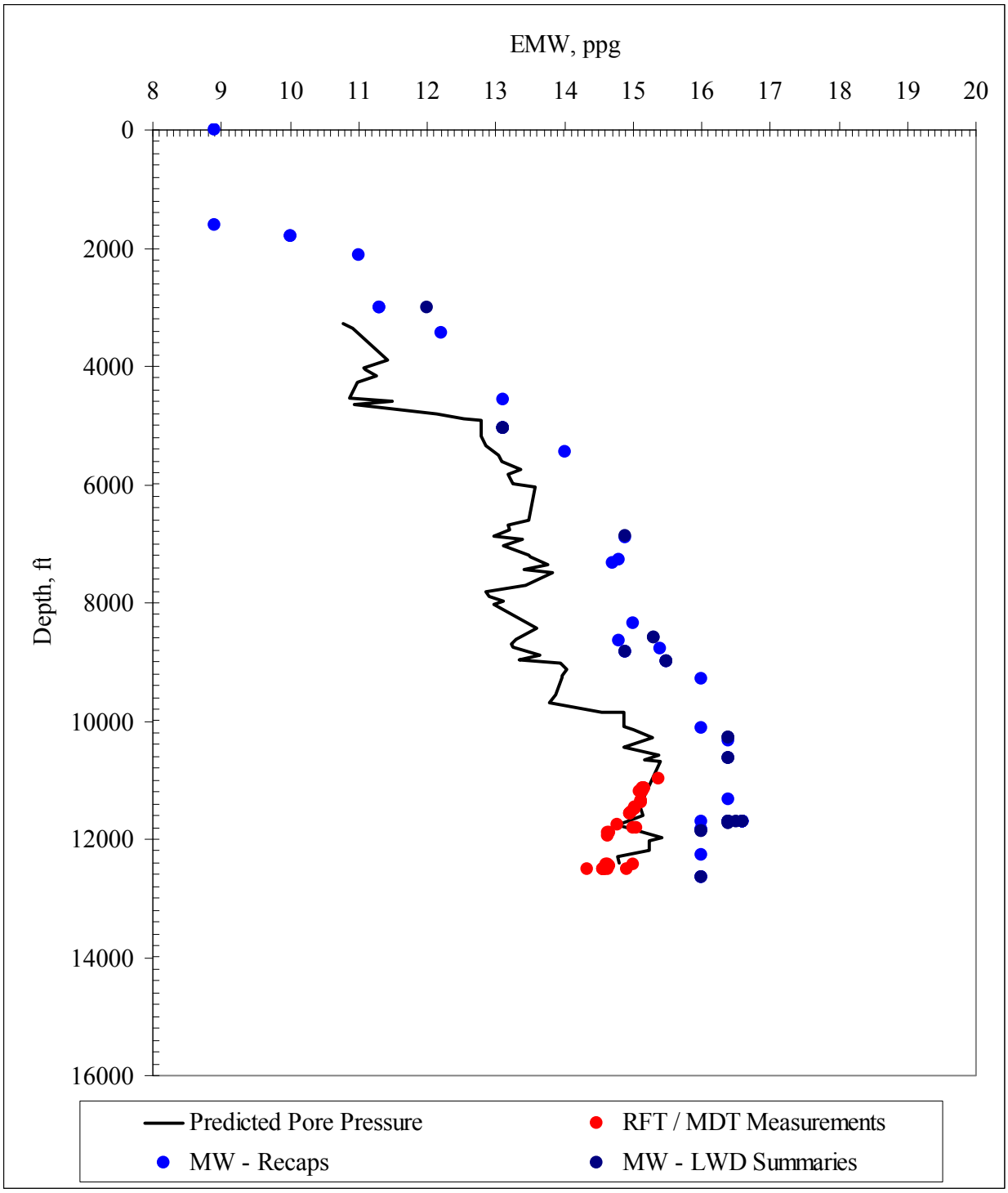

Fig. 5.3: Eaton's Pore Pressure Prediction (Conductivity Based) – EW 910 A1BP

Figure 5.4 is the pore pressures predicted for the EW 954 A2 well. This prediction includes a pressure regression similar to the EW 910 A1BP well, except the interval is from 6500' – 11000'. Also, the model slightly under predicts the pore pressures as compared to the measured pressure data.

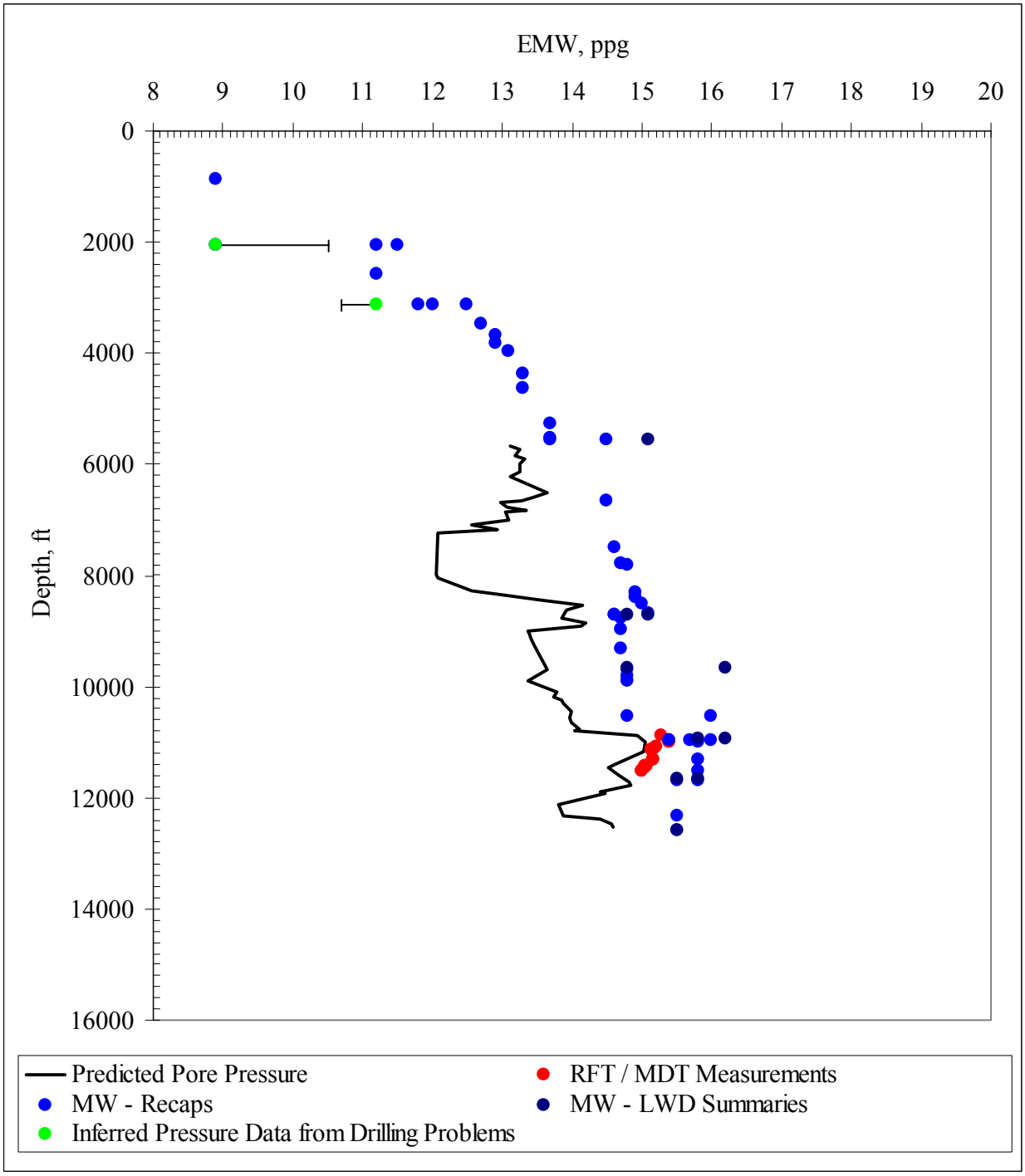

Fig. 5.4: Eaton's Pore Pressure Prediction (Conductivity Based) – EW 954 A2

Figure 5.5 is the predicted pore pressure plot for the EW 910 A3 well. This well also includes a predicted pressure regression. However, unlike the EW 910 A1BP and the EW 954 A2 well, this plot includes pore pressure data inferred from drilling problems at 6655', which is within the predicted pressure regression interval (6200' – 9800'). This inferred pressure estimate is weak as it was based on the need to increase the mud weight from 14.0 – 14.3 ppg after circulating high amounts of background gas. Since the well was not flowing, the only conclusive determination is that the pore pressure is not greater than 14.0 ppg. However, the predicted pore pressure at this point is 12.7 ppg EMW. The "true" pore pressure is estimated to be in the 13.5 – 14.0 ppg EMW range, indicating an under prediction of the pore pressure by 0.8 – 1.3 ppg EMW. Disregarding the depleted interval at approximately 11400', the pore pressure is under predicted by 0.5 ppg at approximately 11500'.

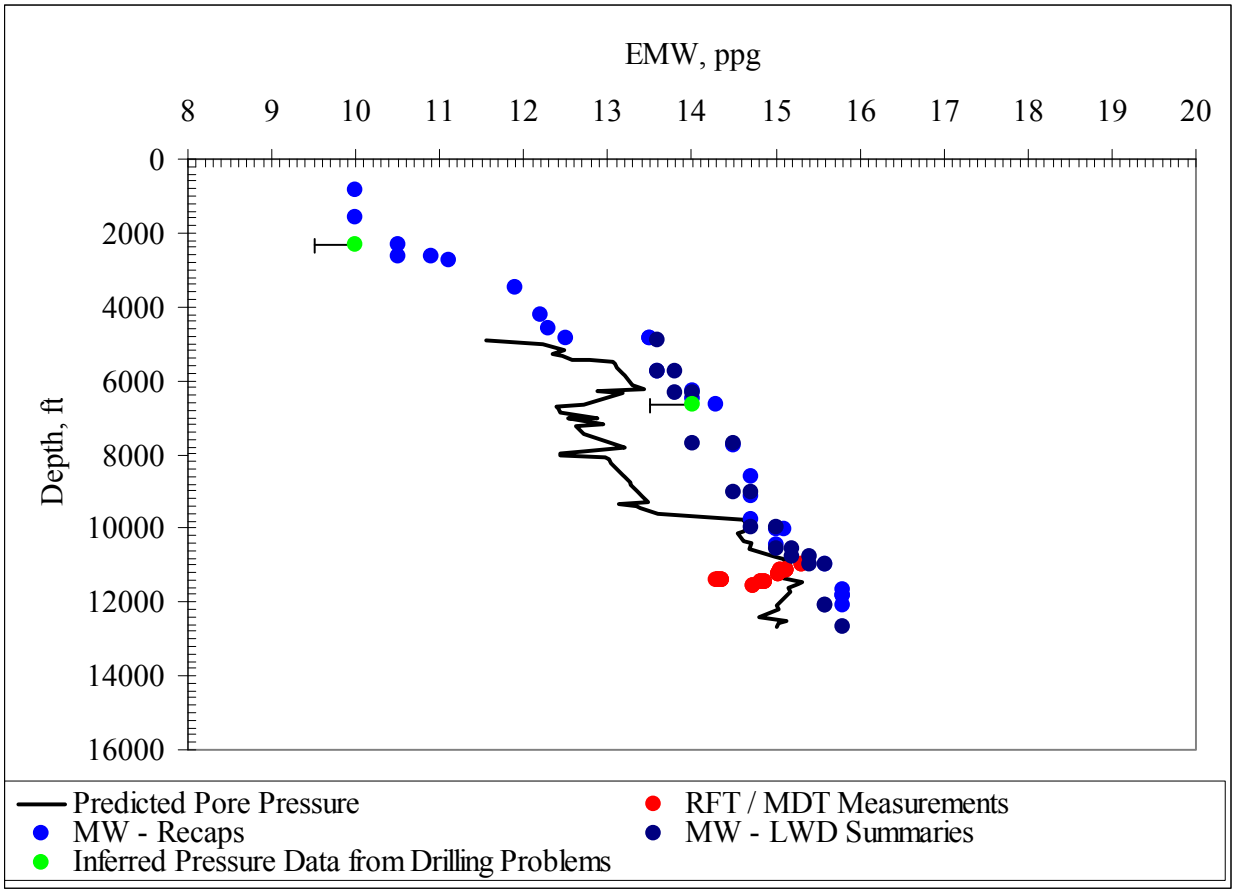

Fig. 5.5: Eaton's Pore Pressure Prediction (Conductivity Based) – EW 910 A3

Figure 5.6 is a plot of the pore pressures predicted for the ST 320 A4 well. As discussed in the Matthews' prediction Chapter, this well appears to have a different pore pressure regime than the other wells discussed, as both the predicted pore pressures and the maximum mud weights are lower. Also, there is not a significant pore pressure regression predicted.

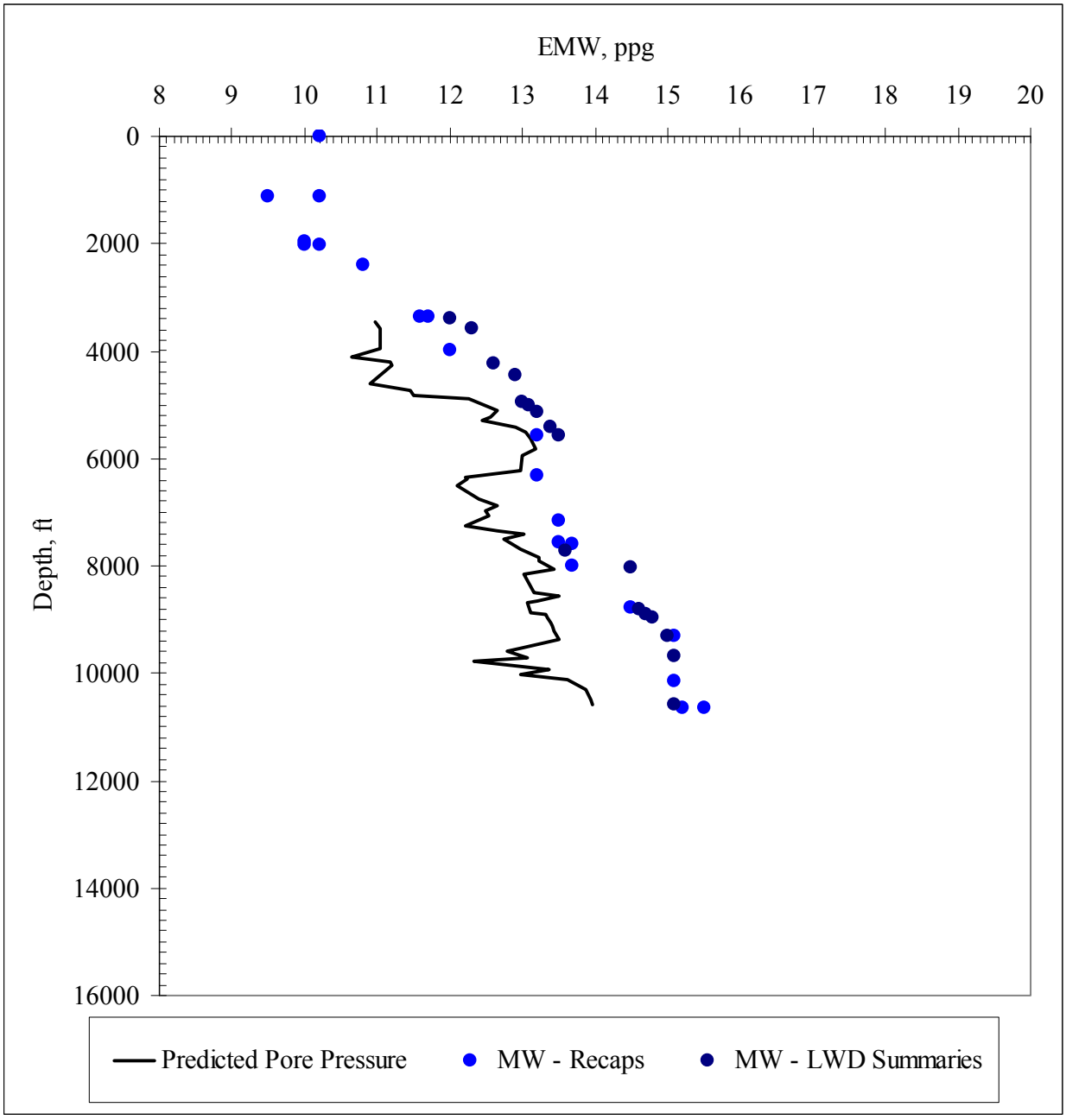

Fig. 5.6: Eaton's Pore Pressure Prediction (Conductivity Based) – ST 320 A4

Figures 5.7 and 5.8 are the pore pressure prediction plots for the EW 910 A5 and A6 wells, respectively. These pore pressure plots are similar in both predicted pore pressures and mud weights used during drilling operations. They were both drilled with a maximum mud weight of 15.8 ppg. Both wells have pore pressure regressions predicted, though the regression intervals differ slightly. The regression interval predicted in the EW 910 A5 well is from 6200' – 9300' and the interval predicted in the EW 910 A6 well is from 6200' – 9800'.

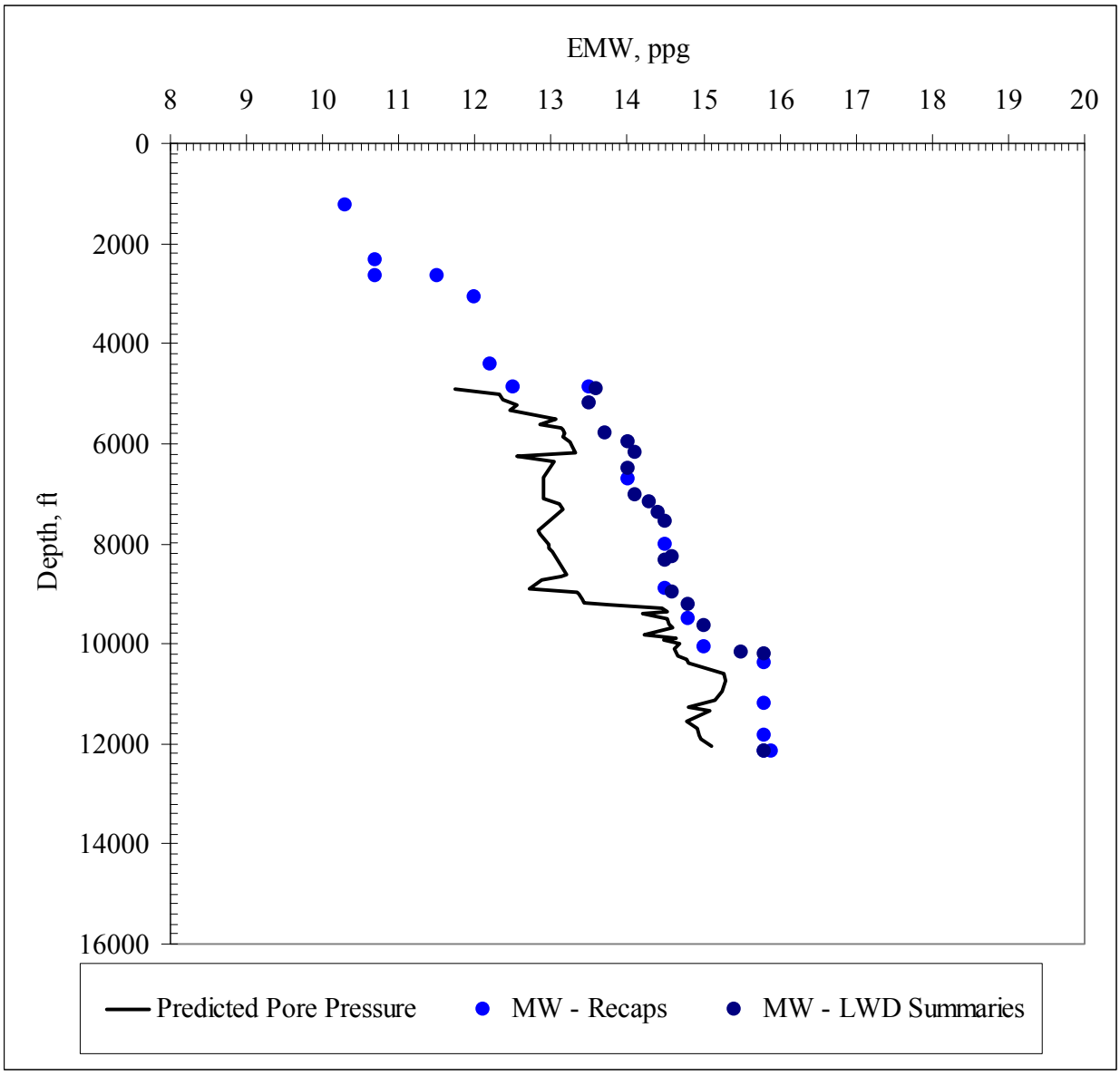

Fig. 5.7: Eaton's Pore Pressure Prediction (Conductivity Based) – EW 910 A5

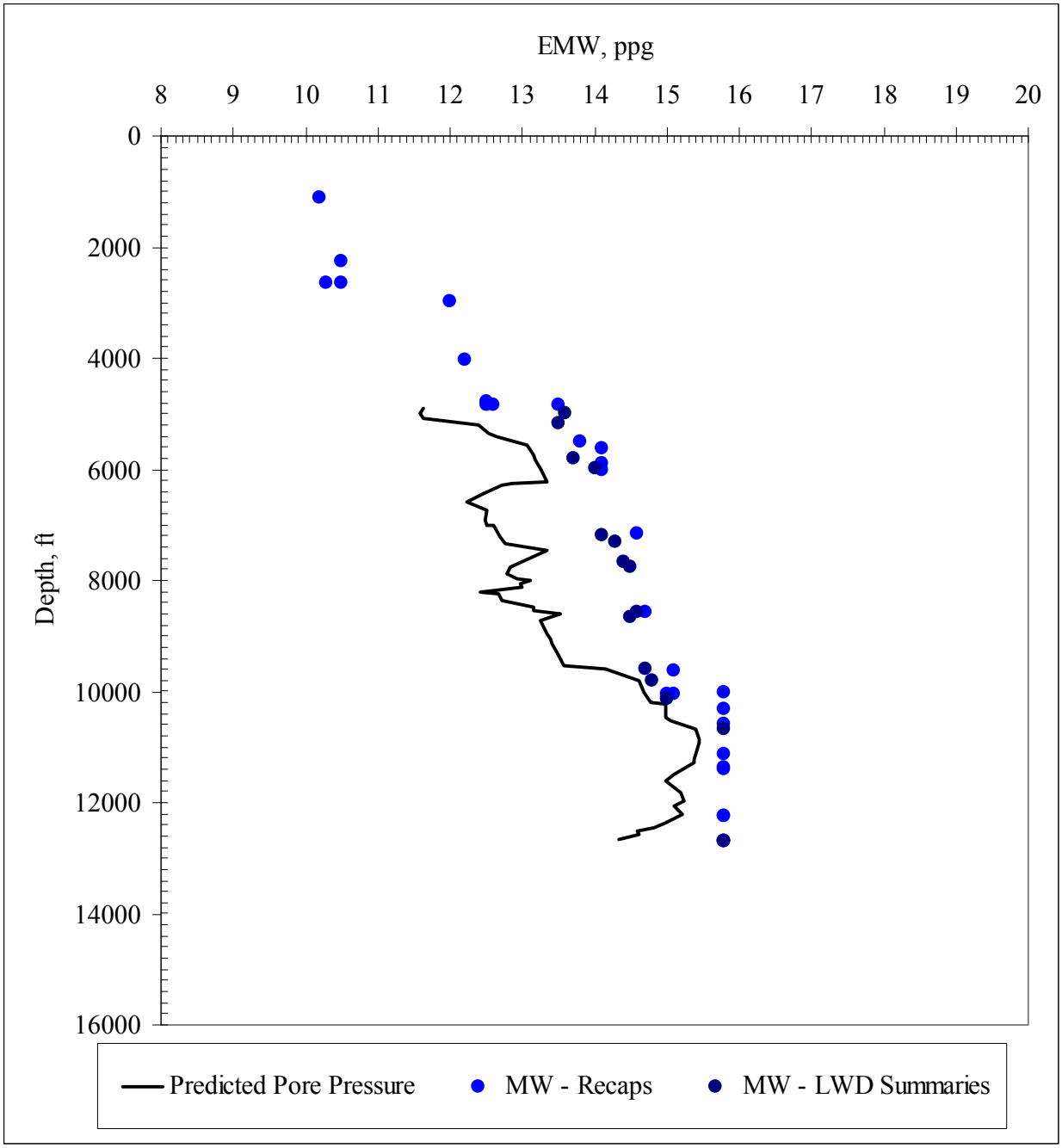

Fig. 5.8: Eaton's Pore Pressure Prediction (Conductivity Based) – EW 910 A6

Figure 5.9 is the pore pressure prediction plot for the EW 910 No. 4 well. As discussed in the Matthews' pore pressure prediction plot review, this well is located in the far eastern side of the EW 910 block and has a different pore pressure profile than the other wells discussed. This profile appears most similar to the ST 320 A4 well, its closest offset.

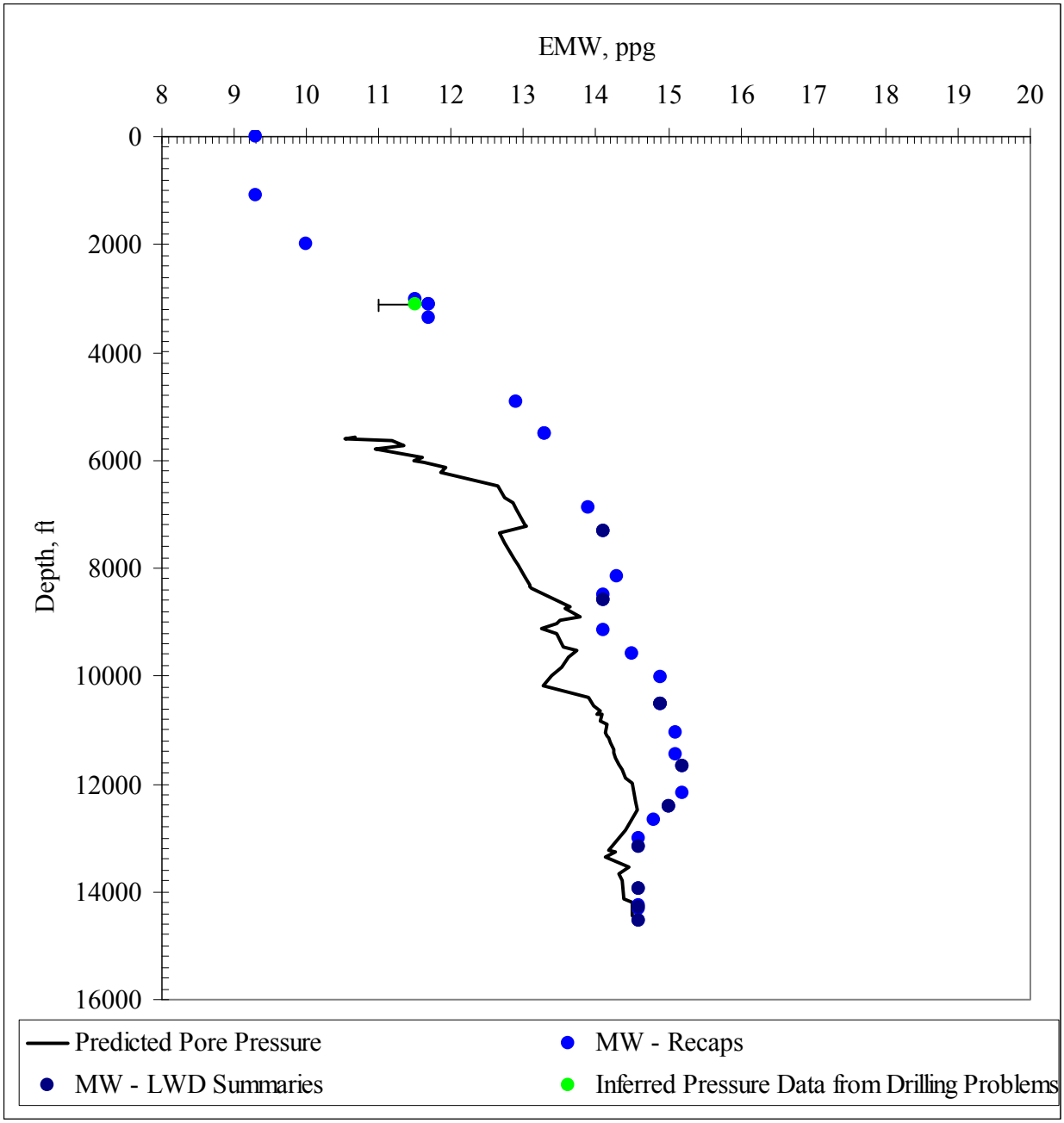

Fig. 5.9: Eaton's Pore Pressure Prediction (Conductivity Based) – EW 910 No. 4

Figure 5.10 is the plot of predicted pore pressures for the EW 953 No. 1 well. As discussed in the Matthews' pore pressure prediction analysis, the pore pressures below approximately 9500' are over predicted, though not as significantly as for the Matthews' approach. However, the pore pressures predicted in EW 953 No. 1 are accurate for the known and inferred pressures above 9000' and are over predicted by a maximum of only 0.5 ppg based

on the mud weights below 9500'. As shown in Figure 4.19, the R_w estimates are significantly different between shallow and deeper formations and one would expect a different normal compaction trendline to be required for accurate pore pressure estimation. Nevertheless, all of the pore pressure estimates are within an acceptable range of accuracy.

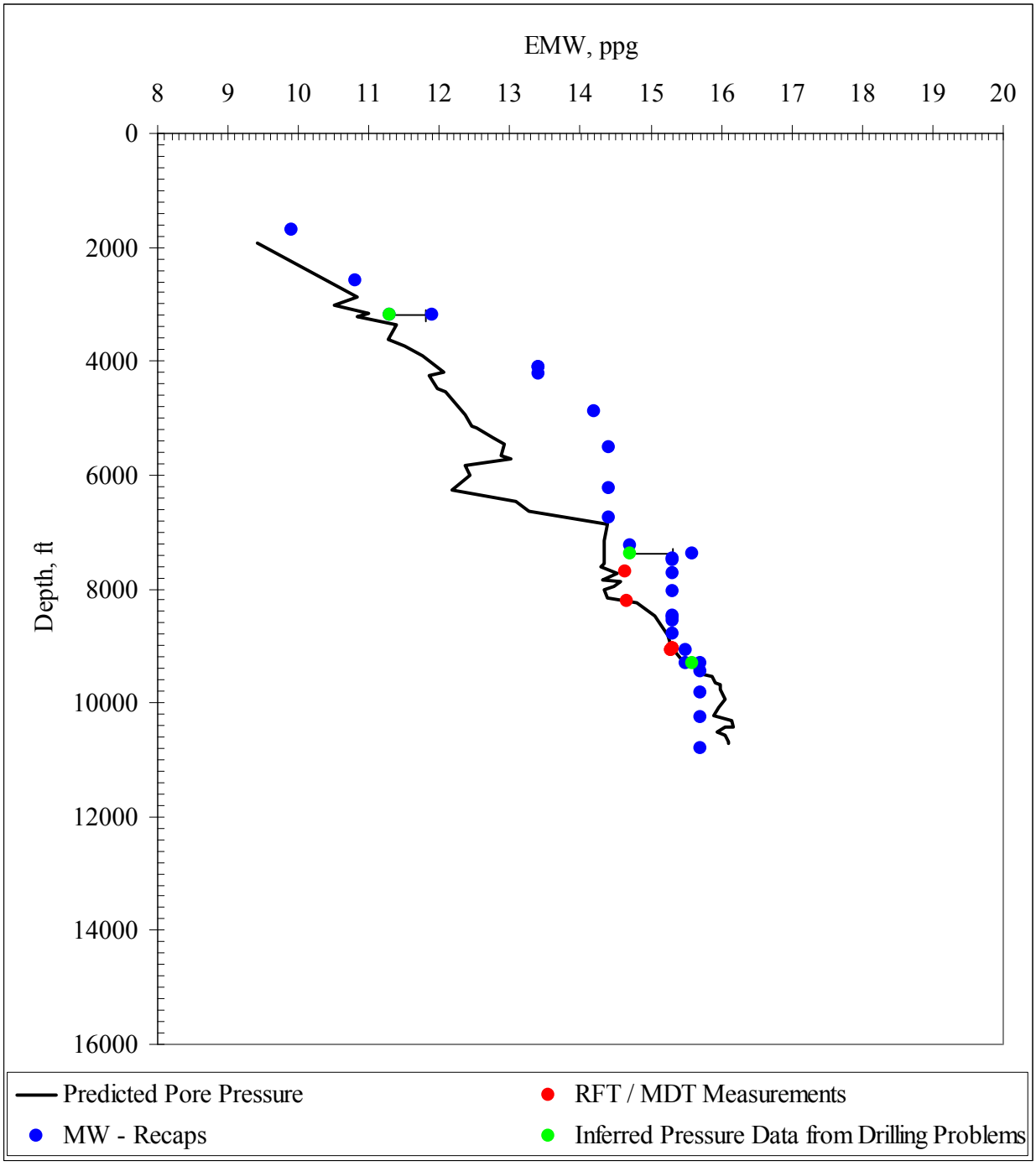

Fig. 5.10: Eaton's Pore Pressure Prediction (Conductivity Based) – EW 953 No. 1

5.4 Verification of the Normal Conductivity Trendline

The absence of normally pressured petrophysical data casts doubt into the validity of this pore pressure prediction model. The development of the normal conductivity trendline described in section 5.2 is very different than the original concept for this approach. Ideally, one would base the normal trendline on normally pressured data, and the divergence from the line would be used as indicative of abnormal formation pressures.

However, an attempt was made to verify the normal conductivity trendline in the absence of normally pressured conductivity data. Two verification techniques were used in this attempt.

Utilization of Bourgoyne and Rocha's[3] "method of estimating fracture gradient," was the first technique applied. This technique is based on fracture gradient being equal to overburden stress gradient in deepwater sediments, and the actual LOT data as representative of fracture gradient. Using these assumptions one can estimate the surface porosity, ϕ_0, and the porosity decline constant, K_ϕ, in equation 2.25 using regression analysis. Using ϕ_0 and K_ϕ, an equation of the form $\phi = \phi_0 e^{-K_\varphi D_S}$ relating porosity versus depth can be developed for the area. This porosity versus depth relationship is based on compaction theory and provides an estimate of the porosities in a normally compacted environment. Using this porosity versus depth relationship, one can estimate a formation resistivity factor, F, at any depth provided a formation resistivity factor relationship for shale is known. In this case, F was calculated using the Perez-Rosales[16] formation resistivity factor (Equation 2.32). Alixant[1] concluded that the Perez-Rosales formation resistivity factor relationship is applicable to shale environments, even though it was developed for sandstone environments. Once F is determined and an estimate of water resistivity is available, conductivity can be estimated by the following relationship[2]:

$$C_n = \frac{1000}{F * R_w} \qquad \textit{(Equation 5.5)}$$

C_n was calculated for an applicable depth range and compared against the normal conductivity trendline determined from implementation of Eaton's approach described in section 5.2. Figure 5.11 is a plot comparing the Eaton-derived and Bougoyne and Rocha-derived normal compaction trendlines. The resulting trendlines are very different. The only point where the conductivity values are similar is at about 12,000 feet. This may have some relevance because the data used to calibrate the Eaton trendline is from a depth of about 12,000 feet. Therefore if the Eaton method is correct, the prediction of the conductivity for a normal pressure trendline should be correct at that depth.

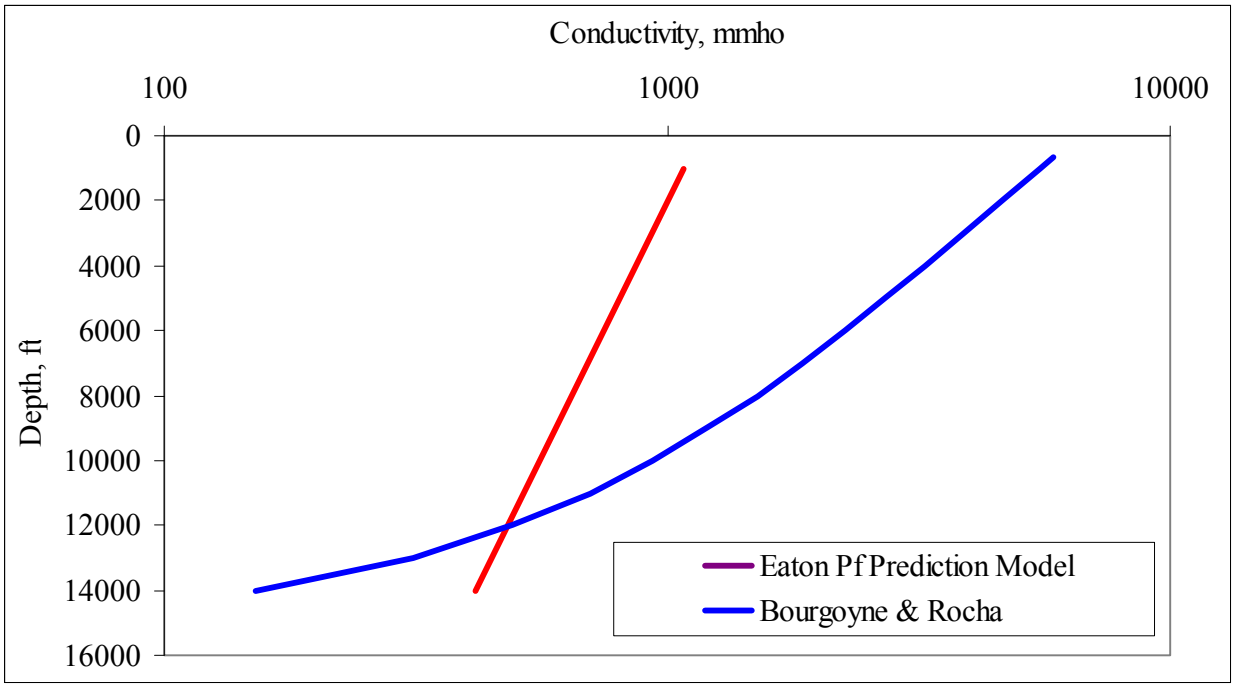

Fig. 5.11: Comparison of Calculated Normal Conductivity Curve vs Normal Conductivity Curve Utilized in Eaton's Pore Pressure Prediction Method

As seen in Figure 5.11, the normal compaction curve verification was unsuccessful. There may be a multitude of problems with the technique implemented, but the following are items that are probably incorrect and may need further research in order to apply this concept.

- Bourgoyne and Rocha's fundamental assumption for their method is that the Poisson's ratio is 0.5 for shallow, deepwater sediments, and therefore, fracture pressure is independent of

pore pressure. Fracture gradient prediction will be discussed in Chapter 7, but as described in the literature review, Eaton's fracture gradient equation is a function of pore pressure in his approach for deepwater sediments.

- The formation resistivity factor is definitely questionable since it was developed for sandstones. A relationship derived from shaly-sand analysis may prove more correct.

The second verification technique utilized porosity versus depth relationships for two pure clay minerals, bentonite and illite, as determined Chilingar and Knight[6]. Assuming an R_w value of 0.05 ohm-m, porosity can be calculated by using the Eaton-derived normal conductivity compaction trendline and the formation resistivity factor relationships described in the Literature Review. Figure 5.12 is a plot of porosity versus depth for the two pure clay minerals and the porosity calculated from the Eaton normal conductivity trendline and all of the formation resistivity factor relationships included in the Literature Review.

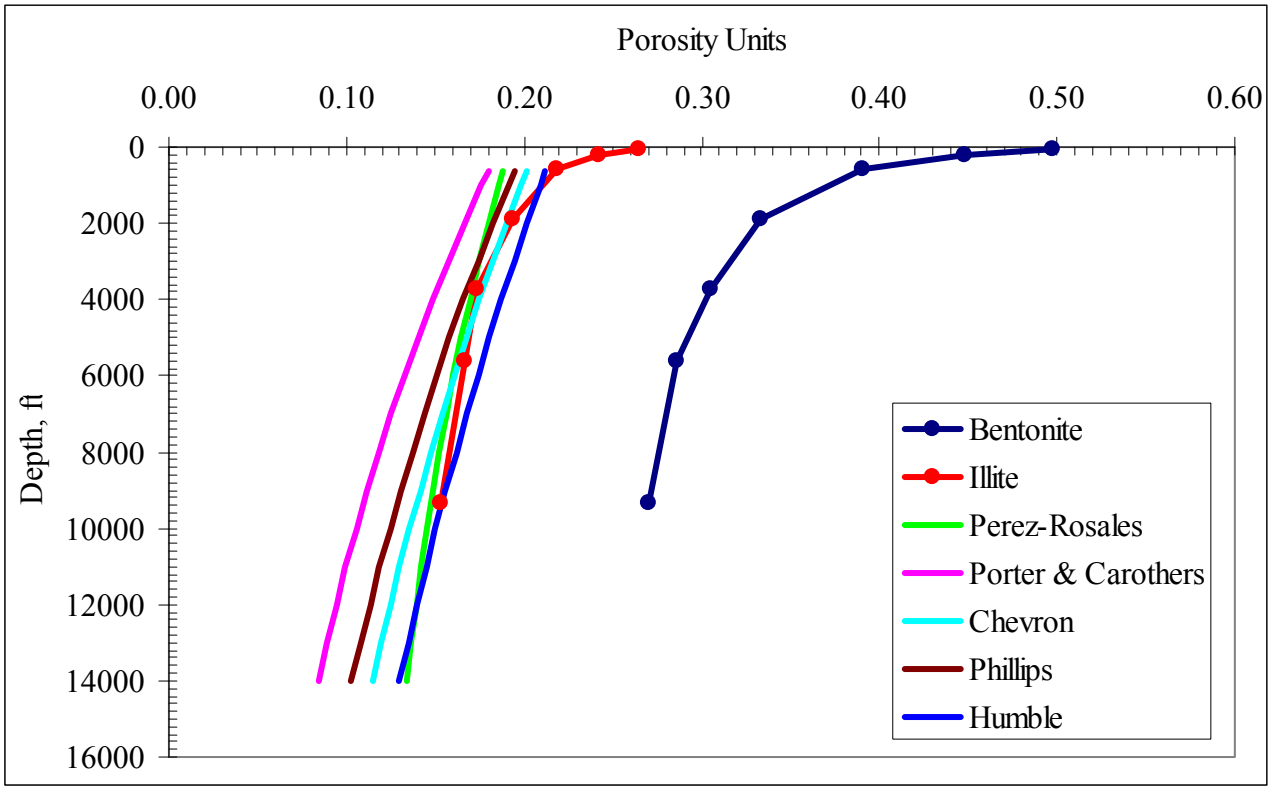

Figure 5.12: Porosity vs Depth Relationships for Bentonite, Illite and the Eaton-Derived Normally Compaction Trendline

As demonstrated in Figure 5.12, the porosity derived from the Eaton normal trendline agrees very well with the illite pure clay porosity relationship. However, it is very unlikely that illite was the clay mineral present during the depositional process or that only clays are present in the sediments. Typically, illite is present in the Gulf of Mexico only after the clay diagenesis transformation. This process requires temperatures in excess of 200 °F, and this geologic environment does not have temperatures in that range.

The validity of this kind of approach to predicting a realistic normal pressure trendline could be improved. The porosity-depth relationship for a normally-compacted shale sequence in this area could be improved by measuring the relationship using a 1-D consolidation test for a sample prepared from cuttings from the EW 910 area. Likewise, a formation resistivity factor relationship for this shale, or at least representative of a shaly-sand, might provide a better prediction of resistivity from porosity.

These approaches have not provided a reliable validation of the normal pressure trendline used herein with the Eaton conductivity-based pore pressure prediction model. However, the conductivity predicted for normal pressure at a depth of 12,000 feet is reasonable based on the Bourgoyne-Rocha porosity at that depth, and the slope of the porosity versus depth trend used herein is similar to that for a pure illite or bentonite clay. Consequently, it is concluded that the normal pressure trendline defined for the Eaton method is reasonable based on these considerations, and more importantly, on the fact that it provides reasonable pore pressure predictions for all of the zones with measured pressures.

5.5 Results and Conclusions of the Eaton Pore Pressure Prediction Strategy Using Acoustic Velocity Measurements

Hottman and Johnson[13] discussed some limitations to utilizing formation resistivity or conductivity as a means to predict pore pressures. If zones of considerable depth contain fresh or brackish water, the resistivity approach may prove useless. In such cases, the velocity

interpretation technique may be more valid. In general, the correlation of acoustic velocity versus depth is more easily established than resistivity since there are more factors that influence formation resistivity such as: salinity of the formation fluid, mineral composition and temperature.

The most significant drawback to using velocity data is data availability. Most wells drilled will have formation resistivity or conductivity data. This is not true with velocity data. Also, more and more operators are obtaining the required petrophysical data while drilling as a costs saving measure. This is accomplished via logging-while-drilling (LWD) methods. The extra expense and risk of including a sonic tool in the LWD logging suite is a deterrent to some operators. Therefore a pore pressure prediction strategy based on velocity data is not as desirable as one based on resistivity or conductivity.

However, an attempt was made to develop a pore pressure prediction model based on Eaton's velocity relationship previously described in section 2.1 and included in this chapter as Equation 5.2. The only change to the procedure is the petrophysical parameter utilized. The overburden stress relationship was previously discussed.

Unfortunately, there was only one well analyzed with significant velocity data, and it is the EW 953 No. 1 well. Thus far, pore pressures in this well have been difficult to predict in comparison to the other seven wells in the area. However, using Equation 5.2 and the available pressure data, a normal velocity trendline was developed as follows:

$$D = -1000 * \ln(dT) + 57000 \qquad \textit{(Equation 5.6)}$$

Figure 5.13 is the pore pressure plot generated utilizing Eaton's velocity equations and the available pressure data. As can be seen, the model performs very well in predicting formation pressures compared to the pressure data from both MDT measurements and drilling problems.

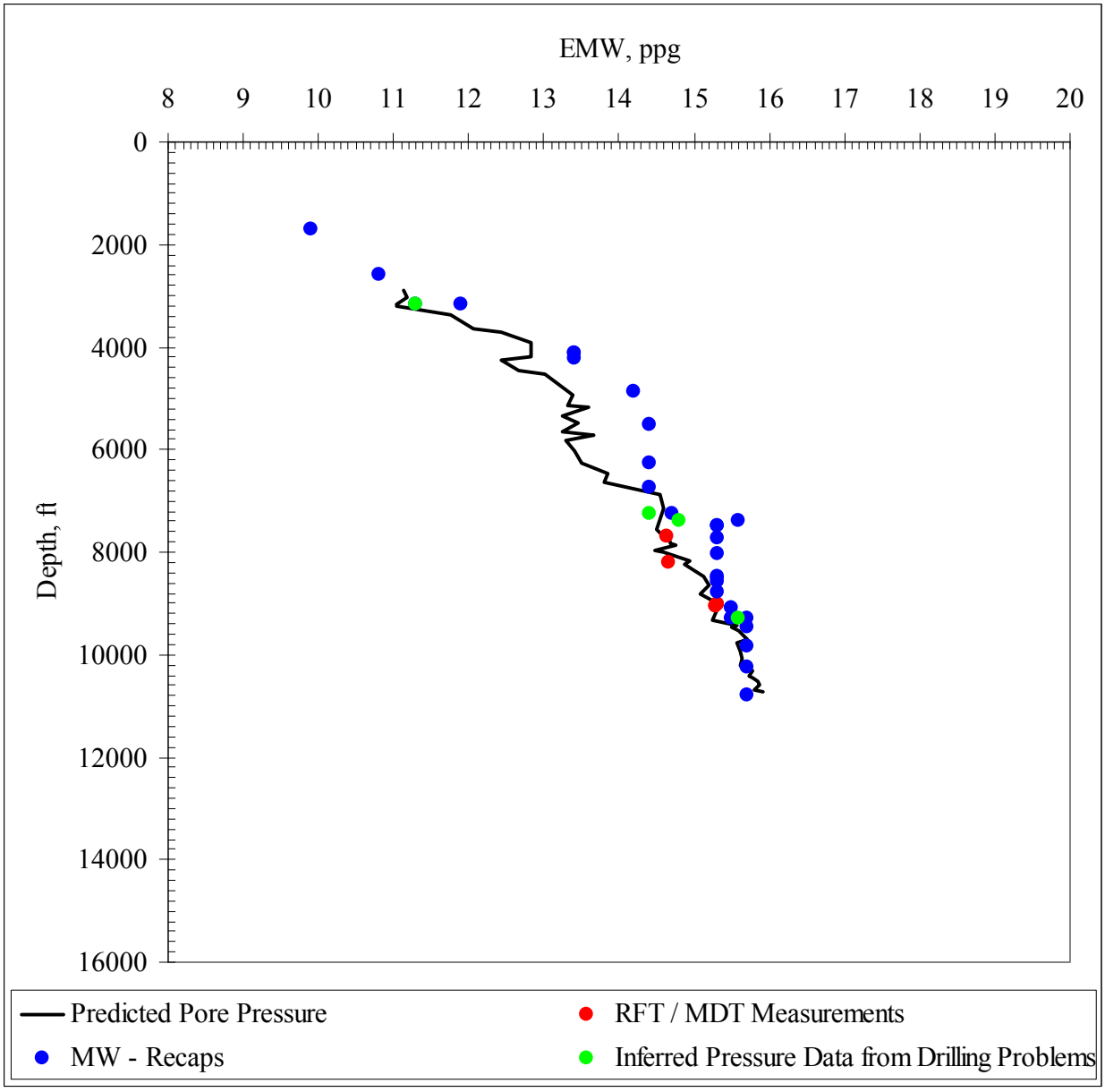

Fig. 5.13: Eaton's Pore Pressure Prediction (Interval Velocity Based) – EW 953 No. 1

Figure 5.14 is a comparison of the pore pressure predicted by Eaton's relationship using both velocity and conductivity data. Both relationships match very well with the pressure data. However, there are significant differences in the models in other places. From approximately 5700' to 6700' the pore pressure predicted from conductivity data is much less than that predicted from velocity data. Also, the deep pore pressures are predicted to within 0.15 ppg EMW of the measured and inferred pressure data using the velocity data as opposed to the 0.50 ppg EMW over prediction using the conductivity approach.

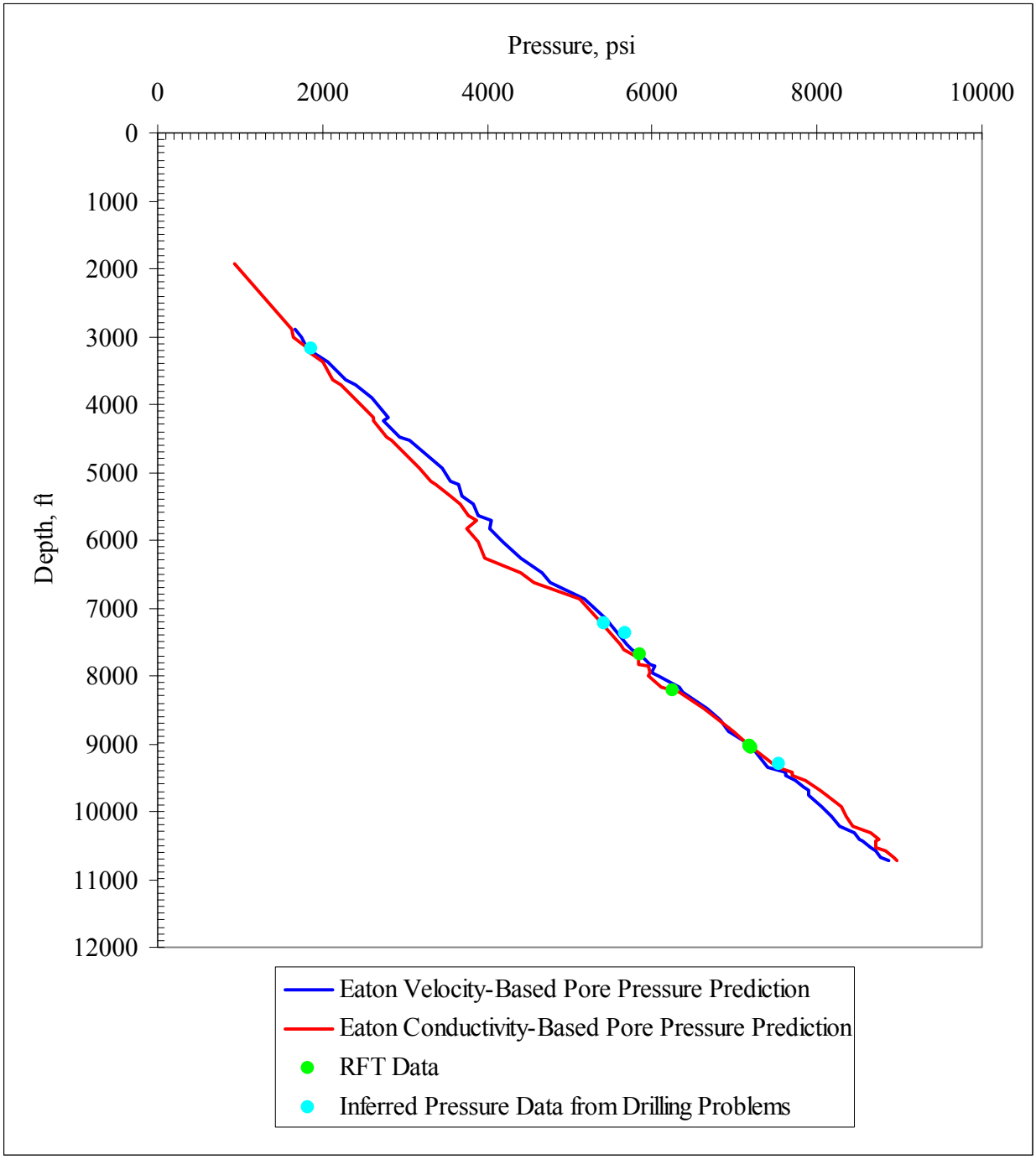

Fig. 5.14: Pore Pressure Prediction Comparison Between Eaton Conductivity- and Velocity-Based Approaches – EW 953 No. 1

Equation 5.6 was utilized in an attempt to predict pore pressures in the EW 910 A3 well using the available velocity data. Besides the EW 953 No. 1 well, this well recorded the longest interval of velocity data (2620' true vertical depth) of the other wells in the area. As can be seen

in Figure 5.15 the velocity model developed for EW 953 No. 1 does not predict pore pressures very well in the EW 910 A3 well.

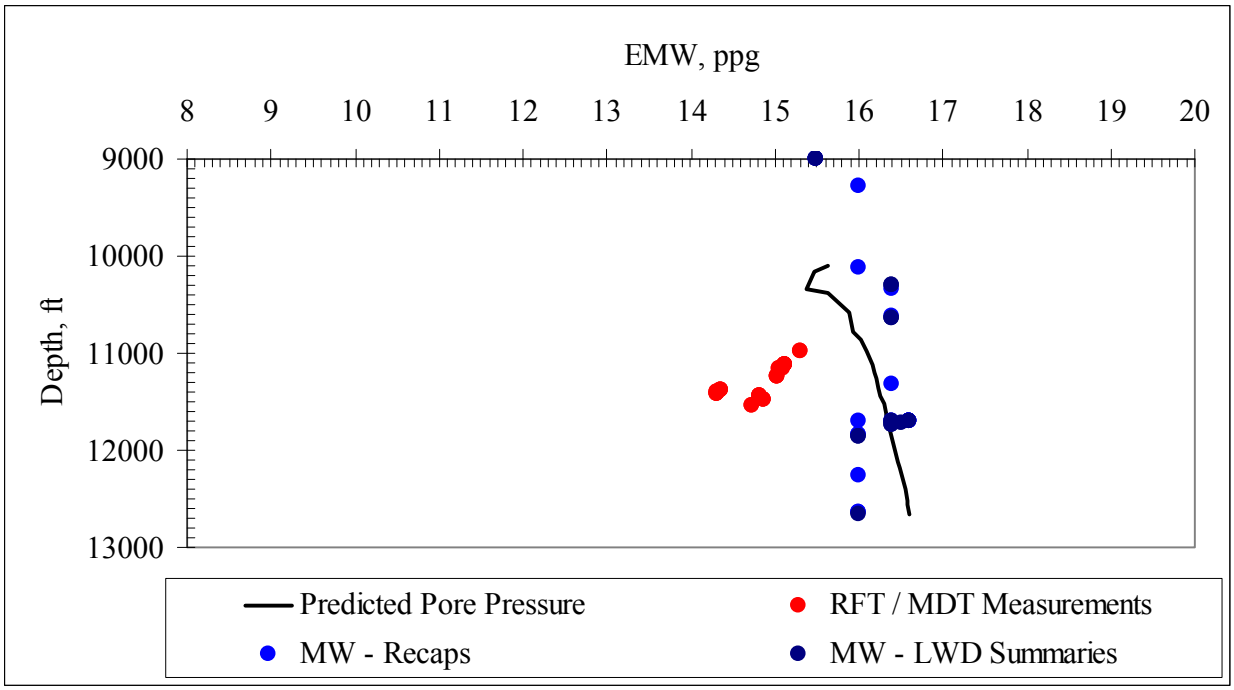

Fig. 5.15: Pore Pressure Plot Including Pressure Data Developed from Eaton's Velocity Approach – EW 910 A3

Initially, there was optimism that the results of the test case would help determine the reason for the significant difference in the accuracy of the pore pressure predictions for the deep data between the EW 953 No. 1 well and the other offsets. The thought was that changes in formation water salinity, formation temperature or formation mineral composition may have been the reason for the difference in predictions. These factors could have affected the conductivity but not the acoustic velocity.

6. COMPARISON OF THE MATTHEWS AND EATON PORE PRESSURE PREDICTION STRATEGIES

As mentioned in the introduction, the purpose of this project is to develop a pore pressure and fracture gradient prediction strategy for the EW 910 area. Therefore, a comparison will be made in this chapter to determine what the best strategy for estimating pore pressure going forward will be.

6.1 Comparison Technique

The comparison technique is very simple. Figures 6.1 through 6.8 are pore pressures predicted by both Matthews' and Eaton's relationships versus depth. Included on the plots is the measured pressure data obtained from the RFT tool and the hydrostatic pressure of the MW column. The plots were analyzed for substantial differences between the prediction methods and how each prediction compared to the measured pressure data.

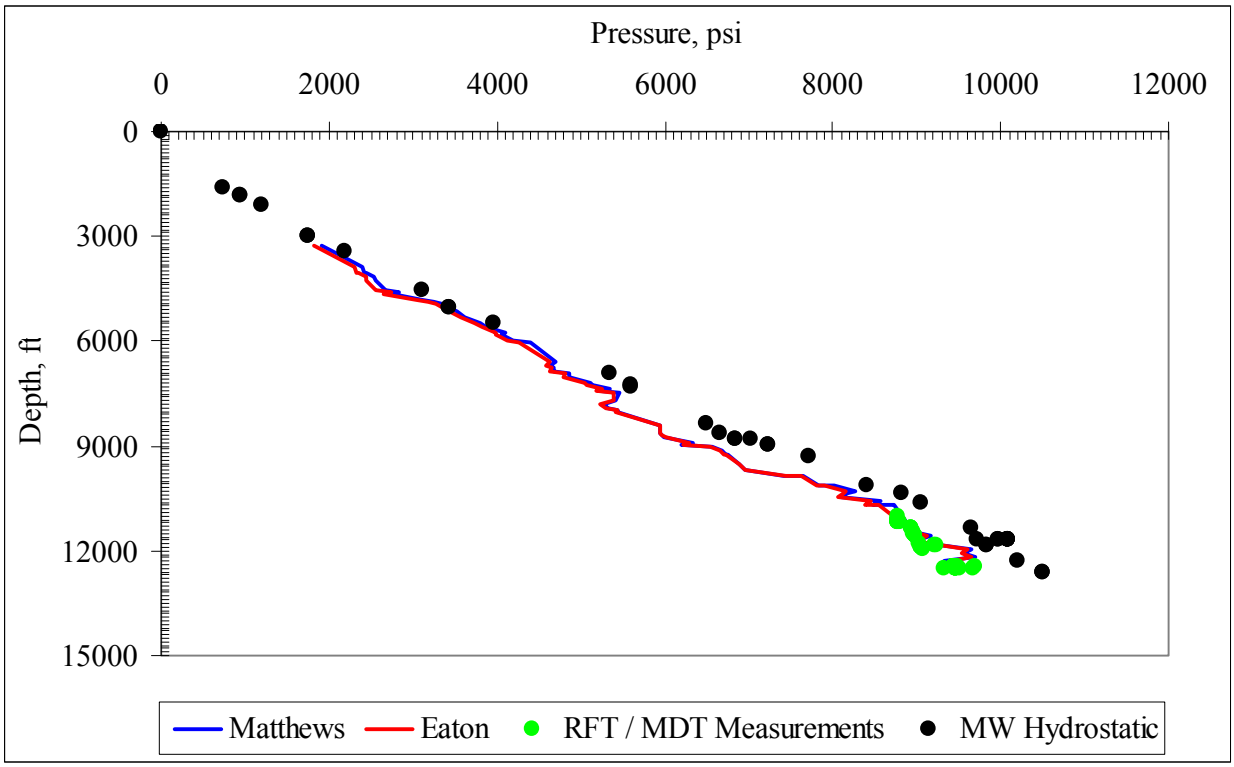

Fig. 6.1: Pore Pressure Prediction Strategy Comparison – EW 910 A1BP

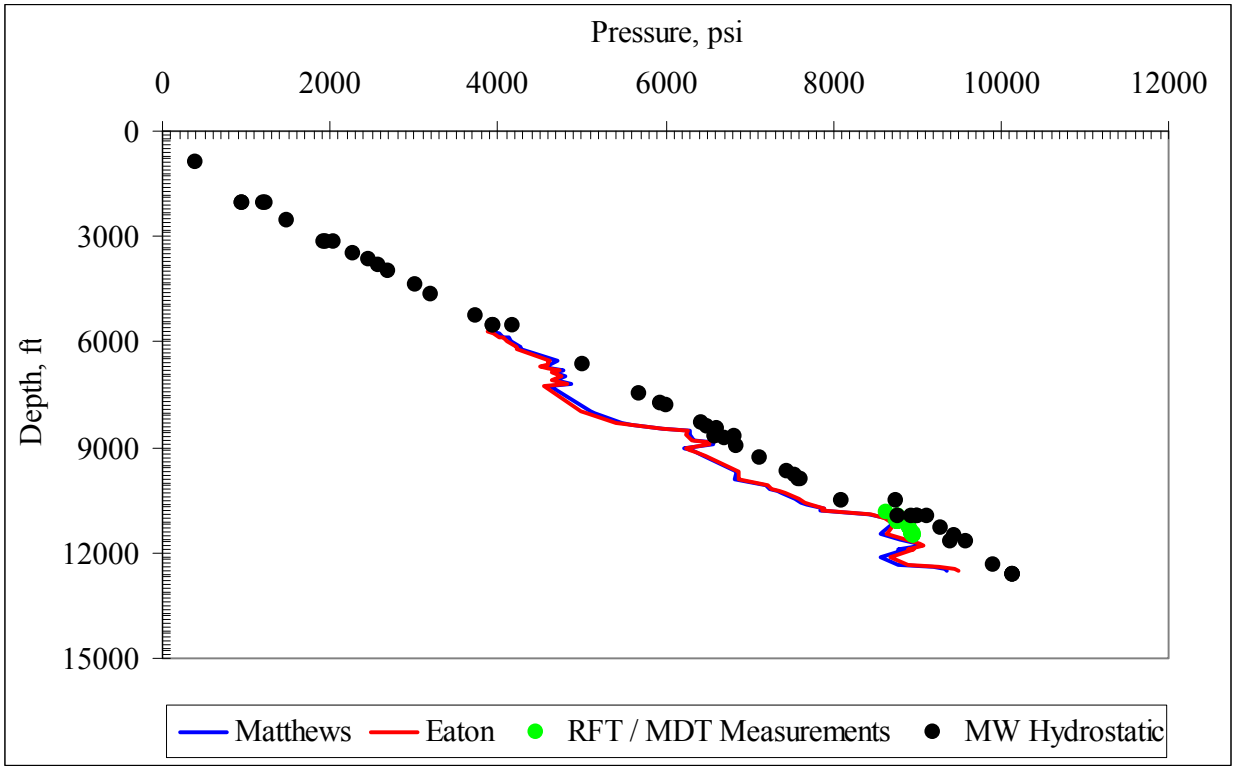

Fig. 6.2: Pore Pressure Prediction Strategy Comparison – EW 954 A2

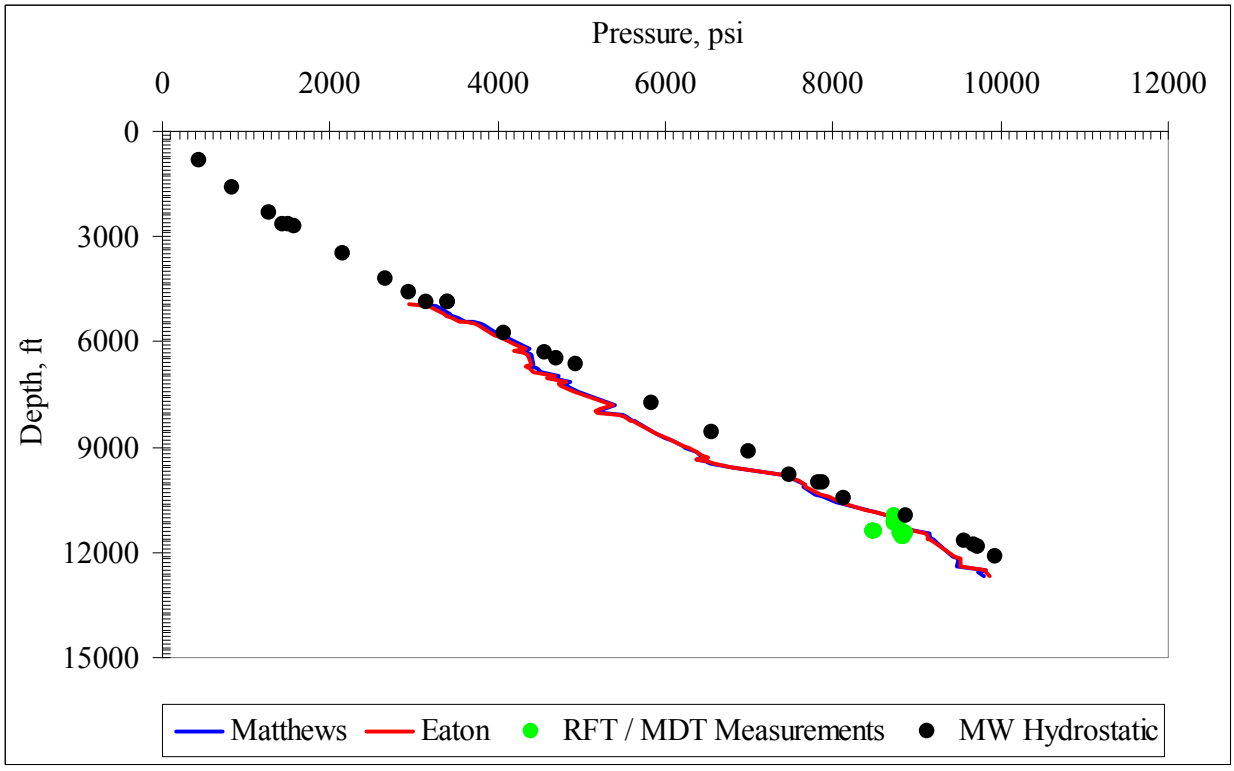

Fig. 6.3: Pore Pressure Prediction Strategy Comparison – EW 910 A3

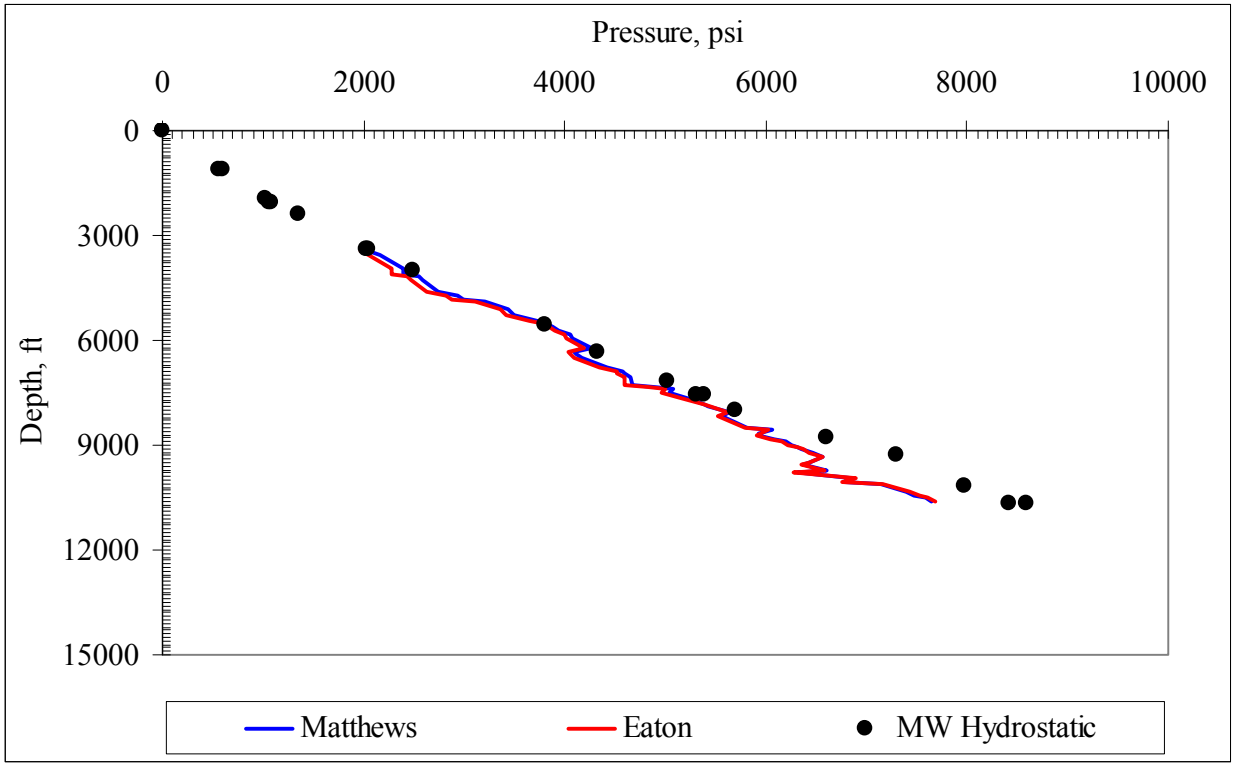

Fig. 6.4: Pore Pressure Prediction Strategy Comparison – ST 320 A4

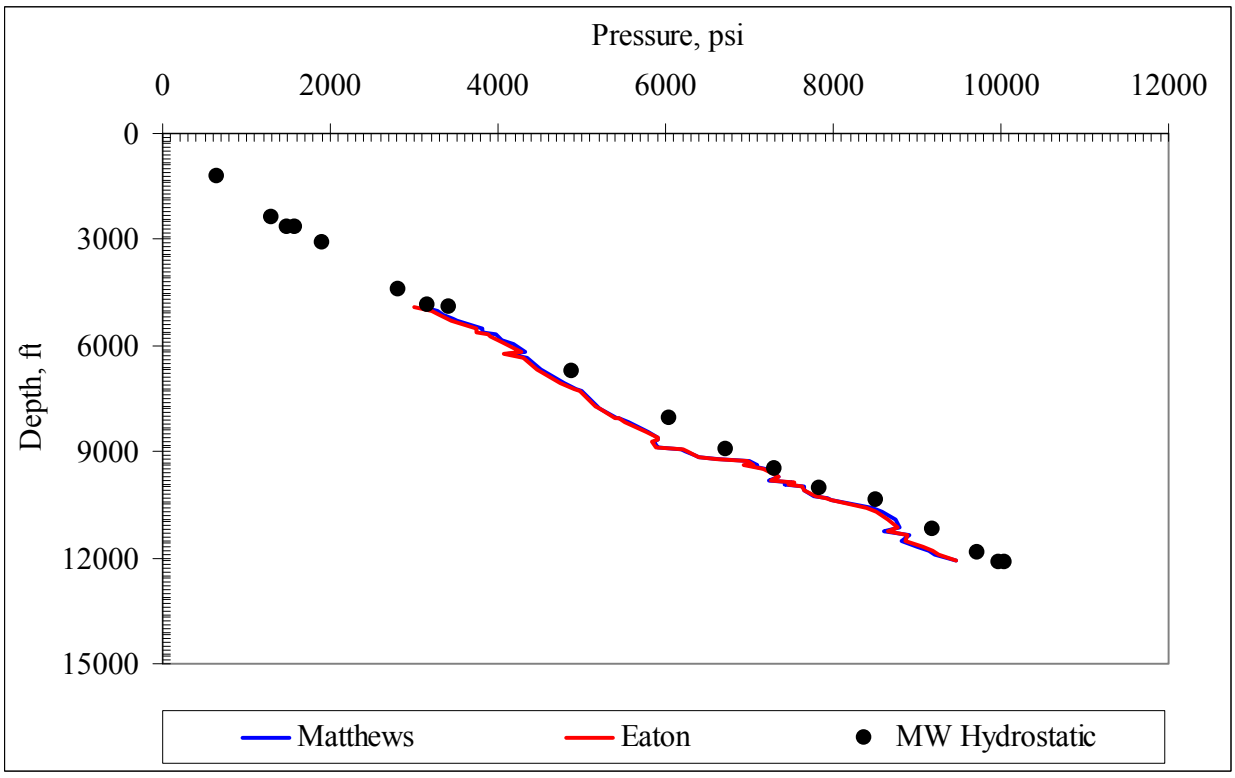

Fig. 6.5: Pore Pressure Prediction Strategy Comparison – EW 910 A5

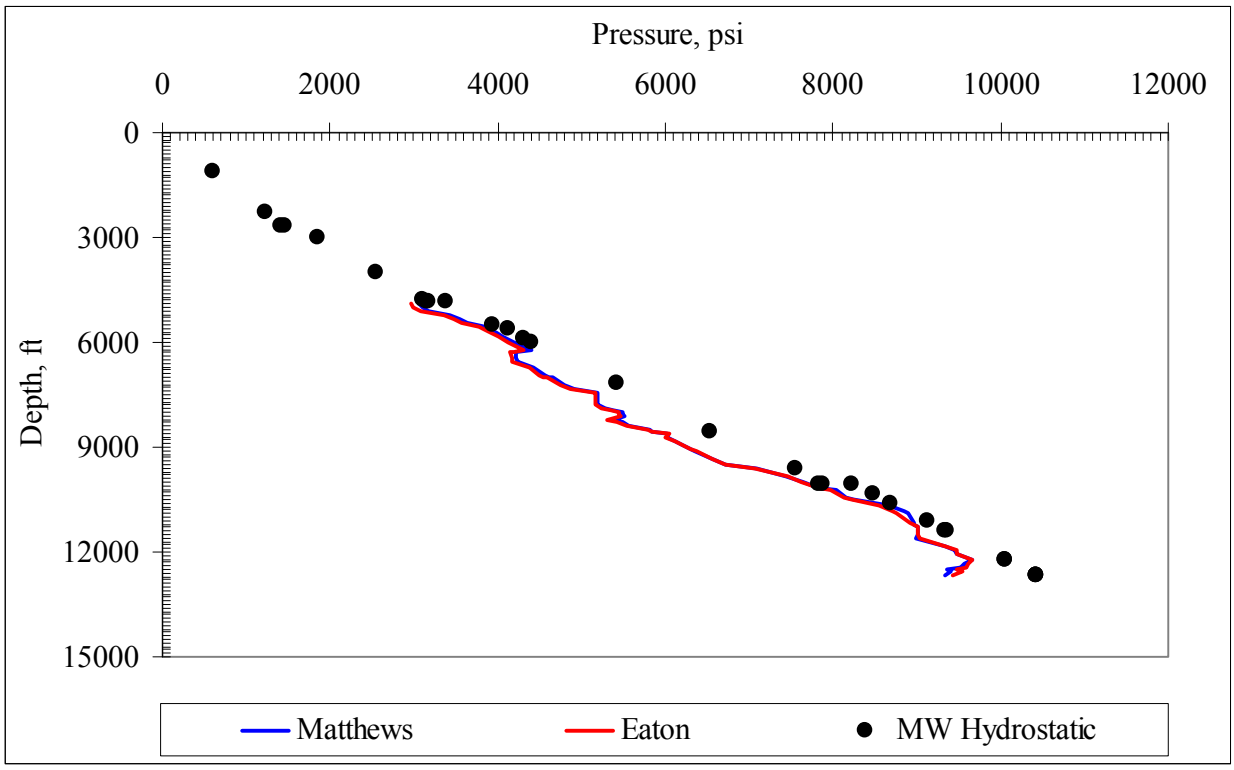

Fig. 6.6: Pore Pressure Prediction Strategy Comparison – EW 910 A6

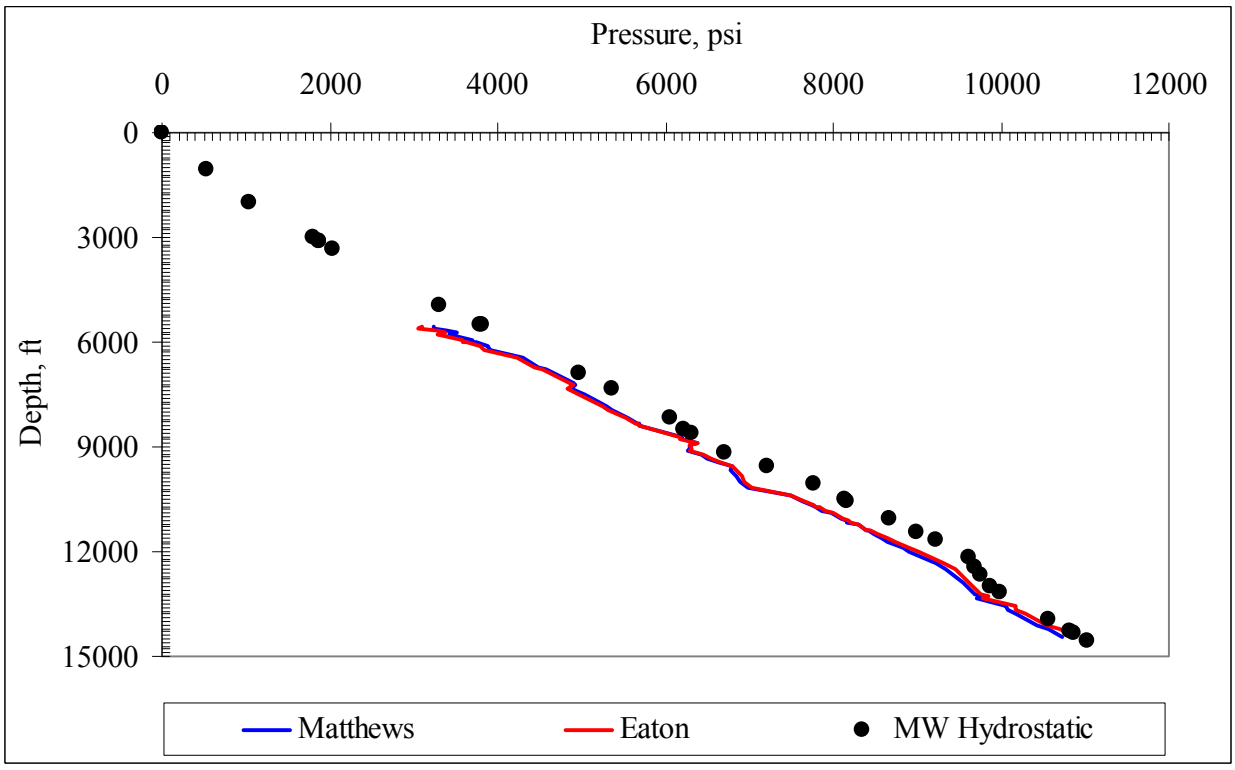

Fig. 6.7: Pore Pressure Prediction Strategy Comparison – EW 910 No. 4

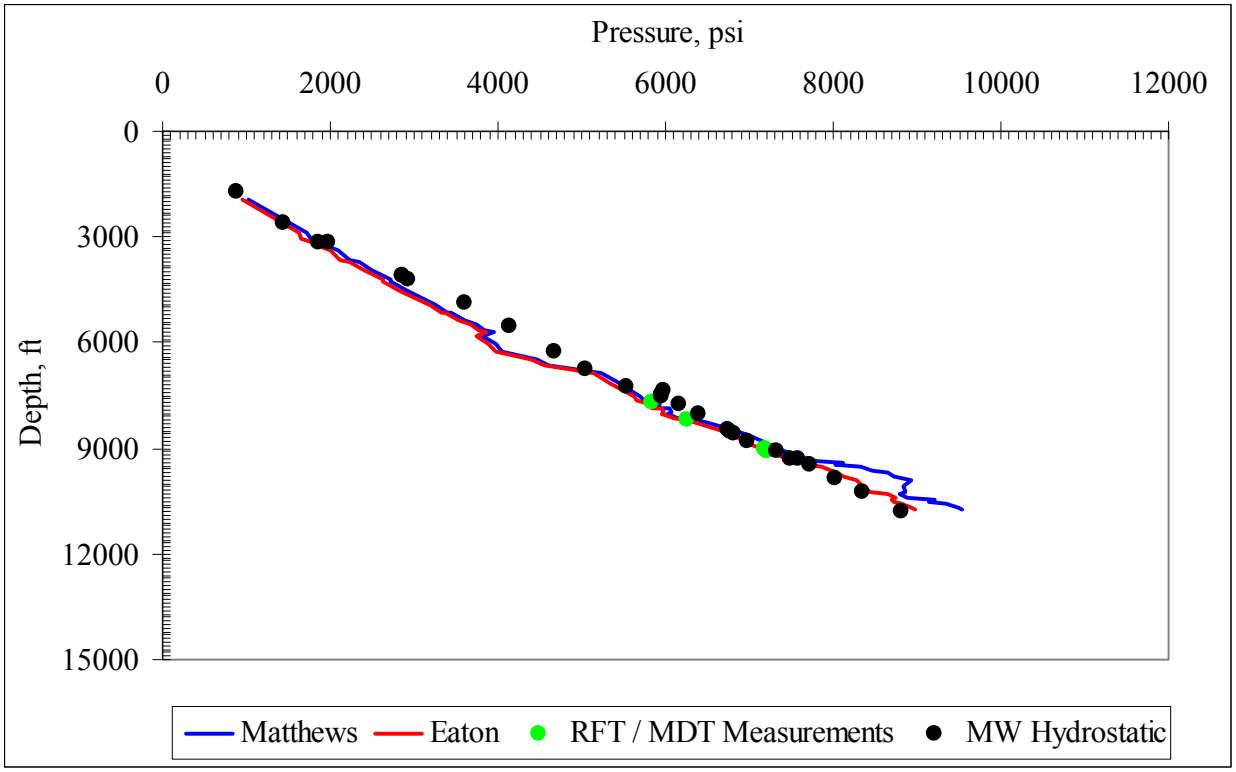

Fig. 6.8: Pore Pressure Prediction Strategy Comparison – EW 953 No. 1

6.2 Comparison Results

As seen in Figures 6.1 – 6.8, both the Matthews and Eaton conductivity-based prediction techniques provide similar results. As noted in the previous chapter, both methods were more applicable for this study than the Eaton sonic velocity-based approach due to data availability, although the Eaton sonic velocity-based approach provided a somewhat better prediction for the EW 953 No. 1 well after being calibrated against that data. The Eaton conductivity-based strategy predicts the deep pressures in the EW 953 No. 1 well much more realistically than the Matthews method.

In an effort to determine the cause for the significant difference between the two conductivity-based prediction methods, the mathematics behind each method was analyzed. As in Hottman and Johnson's method, Matthews developed a direct relationship between the ratio of observed conductivity to the conductivity of the normally compacted sediments and pore

pressure gradient. Essentially, rather than creating a curve similar to Figure 2.3, Matthews created pore pressure gradient trendlines based on the aforementioned conductivity ratio (C_{ob}/C_n) to make the pore pressure prediction process more user-friendly. To determine why there was a significant difference between the pore pressure prediction methods demonstrated in Figure 6.8, Figure 6.9 was developed by plotting the pore pressure gradient versus the aforementioned conductivity ratio for both the Matthews and Eaton prediction techniques. Since the Eaton prediction technique requires an overburden stress gradient, two curves were generated reflecting overburden stress gradients of 0.85 psi/ft and 0.90 psi/ft. The overburden stress gradient for the EW 910 Area, as shown in Figure 5.2, ranges between 0.85 psi/ft and 0.90 psi/ft for the depth intervals where the measured pressure data was obtained. Included in Figure 6.9 is the measured pressure data calculated using the respective method's normal conductivity trendline.

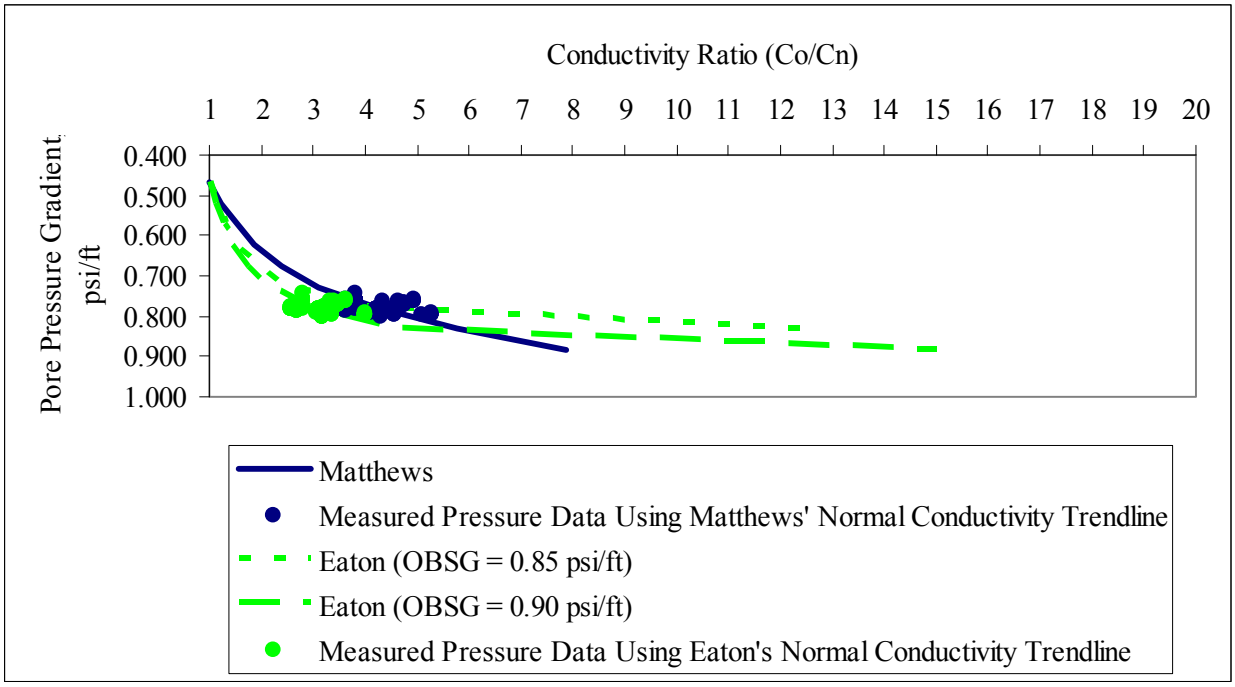

Figure 6.9: Pore Pressure Gradient vs Conductivity Ratio For Each Conductivity-Based Prediction Strategy

One disparity in Figure 6.9 is that though all three curves are offset from one another, they track each other fairly well until a conductivity ratio of approximately four is reached, where the curve generated using the Matthews' prediction method has an entirely different slope than the curves generated from the Eaton method as the value of the conductivity ratio increases beyond four. Conductivity ratios were calculated for every conductivity data point in all eight wells. The conductivity ratio was calculated using the normal pressure conductivity trendline utilized in the Matthews pore pressure prediction strategy, since this prediction technique was more erroneous than the Eaton technique when predicting pore pressures in the EW 953 No. 1 well. Figure 6.10 is a plot of the conductivity ratio versus depth for all eight wells in the EW 910 Area using the Matthews normal compaction trend.

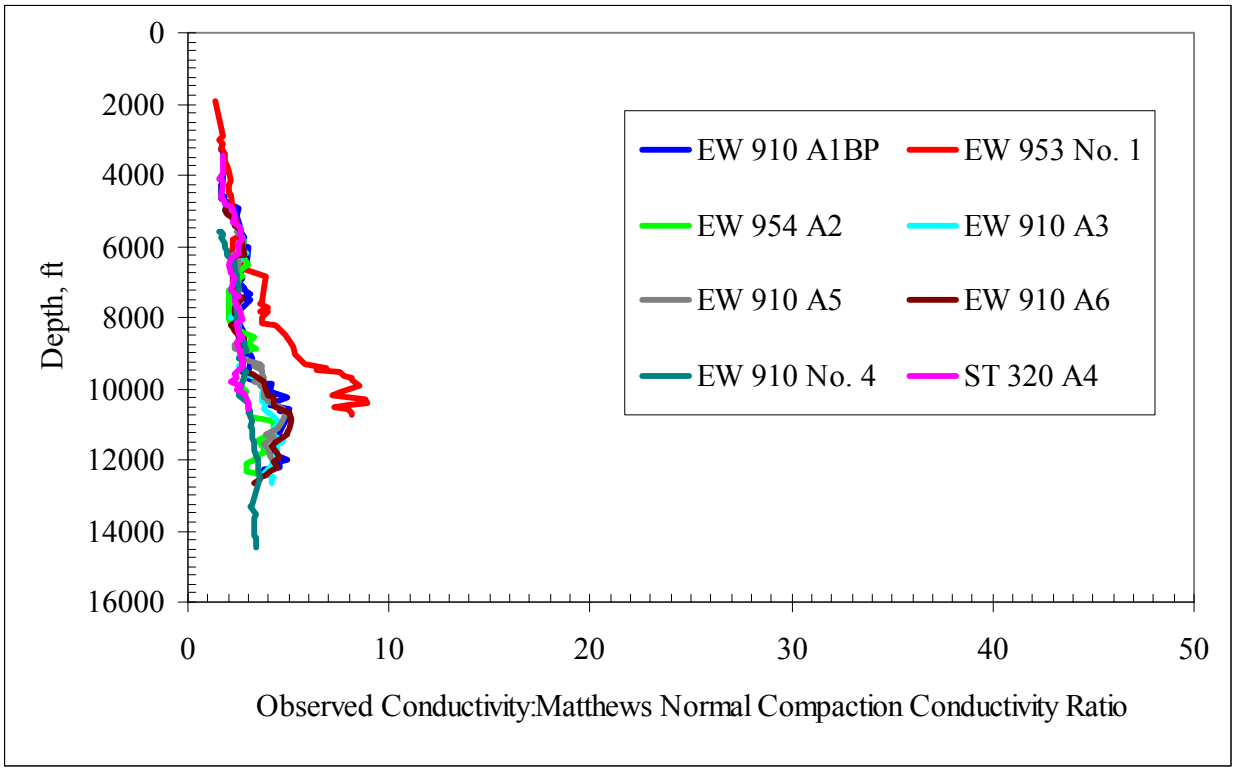

Figure 6.10: Conductivity Ratio vs Depth for All Wells in EW 910 Area

As demonstrated in Figure 6.10, the conductivity ratios for the EW 953 No. 1 well are much higher than the other wells in the area. Since the Matthews pore pressure prediction is

based directly on the conductivity ratio, it's understandable to expect the predicted pore pressures to be significantly higher than the other wells in the field.

A similar process was performed with the Eaton conductivity-based prediction method, but rather than analyzing the aforementioned conductivity ratio, the analysis was performed on the last term in Eaton's pore pressure prediction equation $\left(\frac{C_n}{C_{ob}}\right)^{1.2}$ resulting in Figure 6.11. Again, the Matthews normal conductivity trendline is used in the calculations for comparison's sake. As shown in Figure 6.11, the EW 953 No. 1 relationship is not as much of an outlier as previously demonstrated in Figure 6.10.

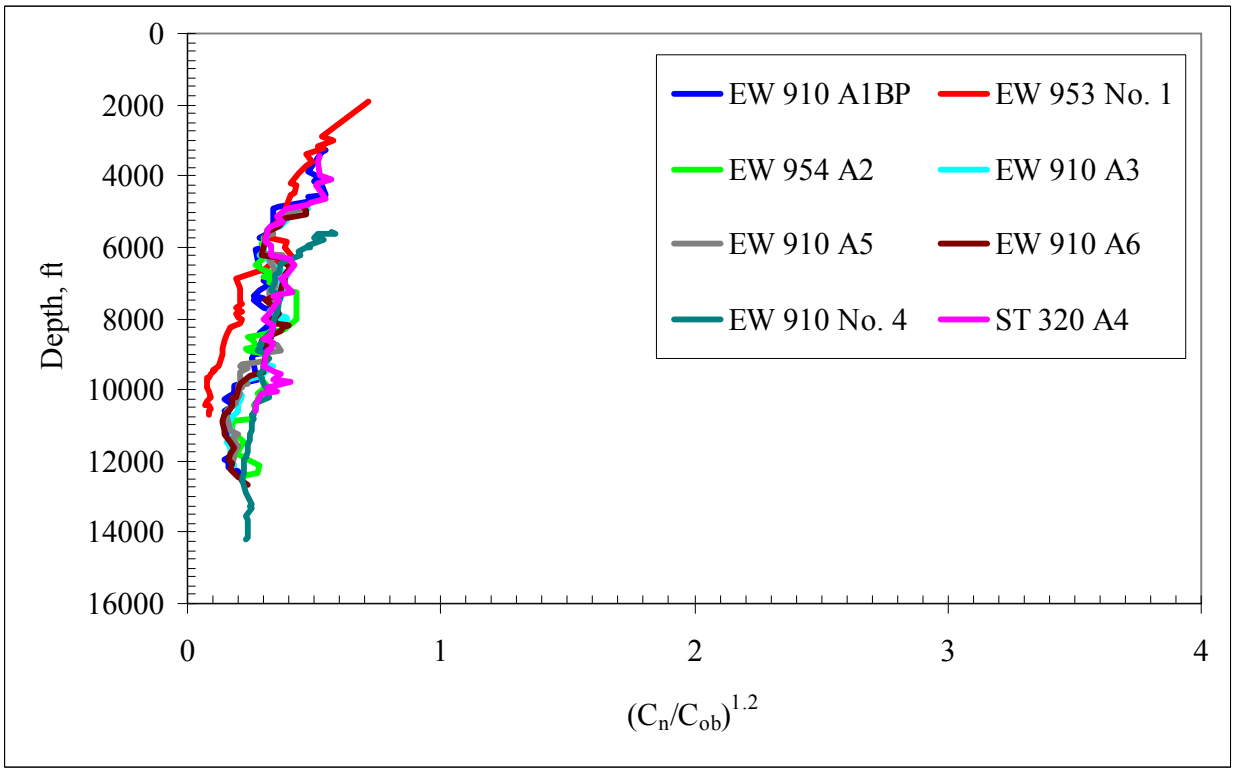

Figure 6.11: Eaton's Conductivity Ratio vs Depth for EW 910 Area Wells

After analyzing Figure 6.9, the difference between Figures 6.10 and 6.11 can be explained intuitively due to the fact that the pore pressure gradient is more variable with respect to the conductivity ratio used in Matthews' approach versus Eaton's approach.

At this time, the most plausible explanation for the significant difference in predicted pore pressures for the EW 953 No. 1 well is that the Matthews pore pressure gradient trendlines above approximately 15 ppg are invalid. The 15 ppg EMW trendline is calculated from a conductivity ratio of approximately 5.8.

Based on the comparison of each pore pressure prediction method against the available pressure data (both measured and inferred) and the mathematical analysis described above, the more accurate and therefore preferred pore pressure prediction strategy for future use in the EW910 area is the Eaton conductivity-based approach.

7. FRACTURE GRADIENT PREDICTION STRATEGY DEVELOPMENT

This chapter focuses on the development of an accurate fracture gradient prediction strategy. The method reviewed was developed by Ben Eaton[7]. As discussed in the literature review, Eaton's relationship is based on overburden stress, Poisson's ratio and pore pressure as follows:

$$\frac{P_{FF}}{D} = \frac{\nu}{1-\nu}\left(\frac{\sigma_{ob}}{D} - \frac{P_F}{D}\right) + \frac{P_F}{D} \qquad \textit{(Equation 7.1)}$$

The overburden stress determination discussed in Chapter 5, which was required for Eaton's pore pressure prediction strategy, will also be used for the fracture gradient calculations. The remaining variable required for fracture gradient prediction is Poisson's ratio. This chapter will include the following:

- A thorough discussion of several alternative methods for the estimation of Poisson's ratio.
- A comparison between the fracture gradient predictions based on the alternative methods for estimating Poisson's ratio and observed fracture gradient data (LOTs, loss of returns while drilling, etc.)

7.1 Poisson's Ratio Estimation

Poisson's ratio, or some other basis for determining the horizontal to vertical stress ratio, is necessary for calculating fracture gradient. This section will discuss various ways to obtain an estimated value of Poisson's ratio.

The simplest way to estimate Poisson's ratio, if operating in the Gulf of Mexico, is by using one of Ben Eaton's Poisson's ratio versus depth relationships. There are two relationships, which are significantly different. The first relationship, which indicates lower Poisson's ratio values versus depth, is described as a "Gulf Coast Variable Overburden Stress Relationship" and was developed nearly 40 years ago. This was introduced in Eaton's original publication[7]. The

second relationship, published in 1997 [8], includes much more data, including data from deep water drilling environments and is described as "Eaton's Deep Water Gulf of Mexico Poisson's Raito Relationship". Figure 7.1 is a plot of each Poisson's ratio versus depth relationship.

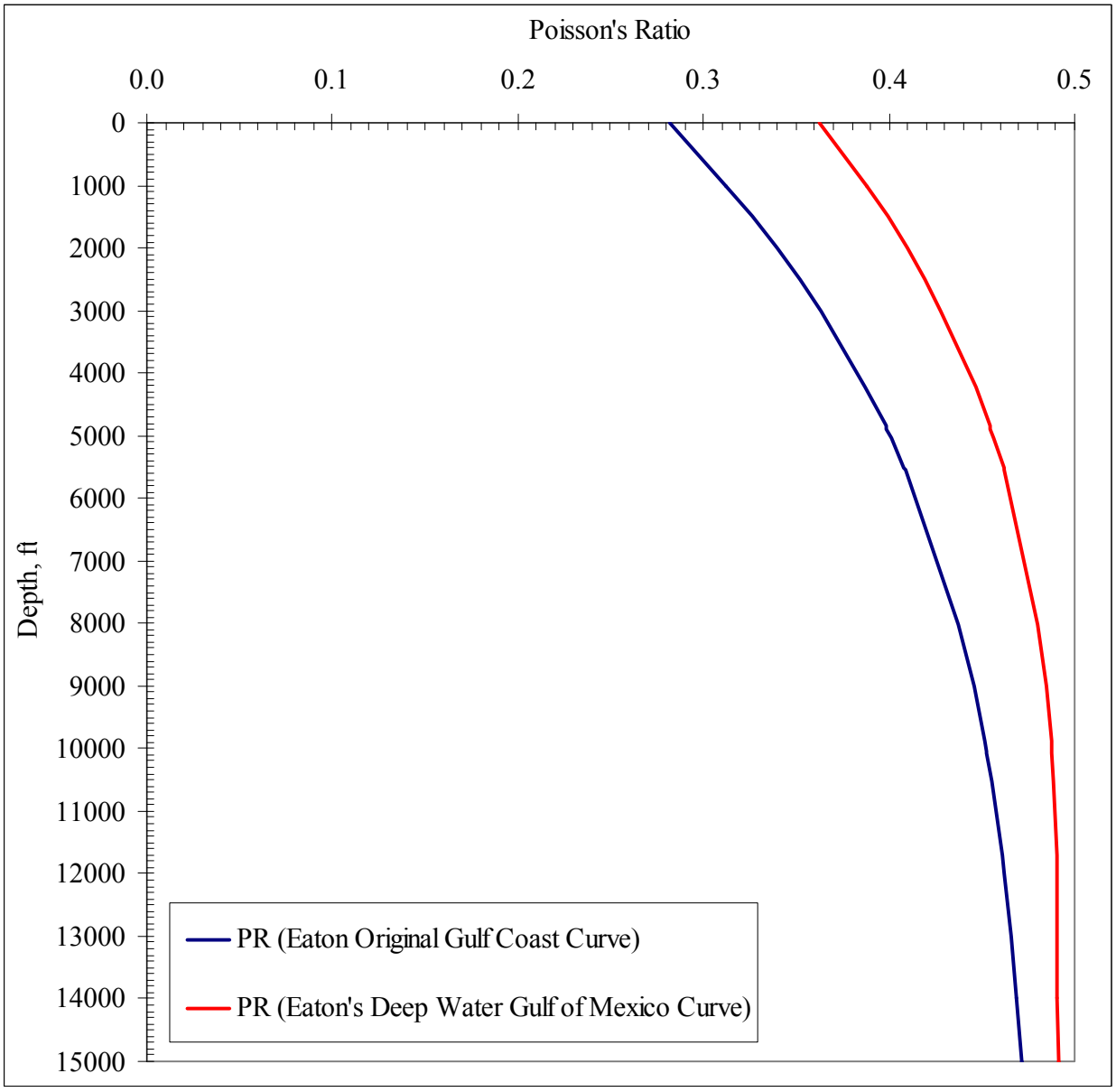

Fig. 7.1: Eaton's Correlations of Poisson's Ratio vs. True Vertical Depth

However, if the area of interest is not the Gulf of Mexico or U.S. Gulf Coast, then Eaton's Poisson's ratio relationships must be determined based on local knowledge.

Another source of Poisson's ratio is from the dipole sonic log obtained during the evaluation of the EW 954 A2 well. Poisson's ratio is determined from a relationship of compressional-wave and shear-wave velocities by the following relationship defined as[19]

$$\nu = \frac{1}{2} * \frac{\left(\frac{V_p}{V_s}\right)^2 - 2}{\left(\frac{V_p}{V_s}\right)^2 - 1} \qquad \textit{(Equation 7.2)}$$

where, V_p is the compressional-wave velocity and V_s is the shear-wave velocity of the formation.

Eaton describes a technique to calculate Poisson's ratio if there are measured fracture gradients available in the field data. Equation 7.1 can be rewritten and solved in terms of Poisson's ratio as

$$\frac{\nu}{1-\nu} = \frac{\frac{P_{FF}}{D} - \frac{P_F}{D}}{\frac{\sigma_{OB}}{D} - \frac{P_F}{D}} \qquad \textit{(Equation 7.3)}$$

This equation can be solved for a Poisson's ratio for any measurement of fracture gradient, such as a LOT or instance of lost returns, to provide the basis for an area specific Poisson's ratio versus depth relationship.

Rock mechanics and fracture stimulation experts also utilize another strategy to estimate Poisson's ratio from LOTs[10]. Fracturing mechanics experts assume that the LOT pressure is directly related to fracture initiation pressure. For the majority of sedimentary basins, the stresses in the horizontal plane are approximately equal. With this assumption, the initiation pressure will occur when the tangential stress in the wellbore is zero. Roegiers[18] defined the fracture initiation pressure as

$$P_{IF} = 3 * \sigma_{\min} - \sigma_{\max} - P_F \qquad \textit{(Equation 7.4)}$$

Since in the horizontal plane the minimum and maximum stresses are often approximately equal, Equation 7.4 can be rewritten in the following manner:

$$P_{IF} = 2 * \sigma_{\min} - P_F \qquad \textit{(Equation 7.5)}$$

The minimum horizontal stress is defined by Eaton's fracture gradient relationship. So, the fracture initiation can be rewritten as

$$P_{IF} = 2 * \left[\frac{\nu}{1-\nu} \left(\sigma_{OB} - P_F \right) \right] + P_F \qquad \textit{(Equation 7.6)}$$

Assuming the fracture initiation pressure was recorded as the LOT, then an estimate of Poisson's ratio can be determined from Equation 7.6 by rearranging and writing the equation as

$$\frac{\nu}{1-\nu} = \frac{P_{IF} - P_F}{2\left(\sigma_{OB} - Pf\right)} \qquad \textit{(Equation 7.7)}$$

Figure 7.2 is a plot comparing the following Poisson's ratio estimates:

- The two curves established by Eaton and also shown in Fig. 7.1
- Poisson's ratio as calculated by Equation 7.3 with the assumption that the LOT data is equal to the fracture gradient.
- Poisson's ratio as calculated by Equation 7.7 with the assumption that the maximum and minimum horizontal stresses are approximately equal and the tangential stress in the wellbore is zero.
- Poisson's ratio as determined from a dipole sonic log. A dipole sonic tool was included in the logging suite on the EW 954 A2 well which provided direct estimates of Poisson's ratio.

Figure 7.2 shows that, the different Poisson's ratio estimation methods give very different results with some results that are probably not valid. One issue is data validity. The LOT data was obtained from reviewing well histories and mud recaps. There was no detailed LOT pressure data available to review.

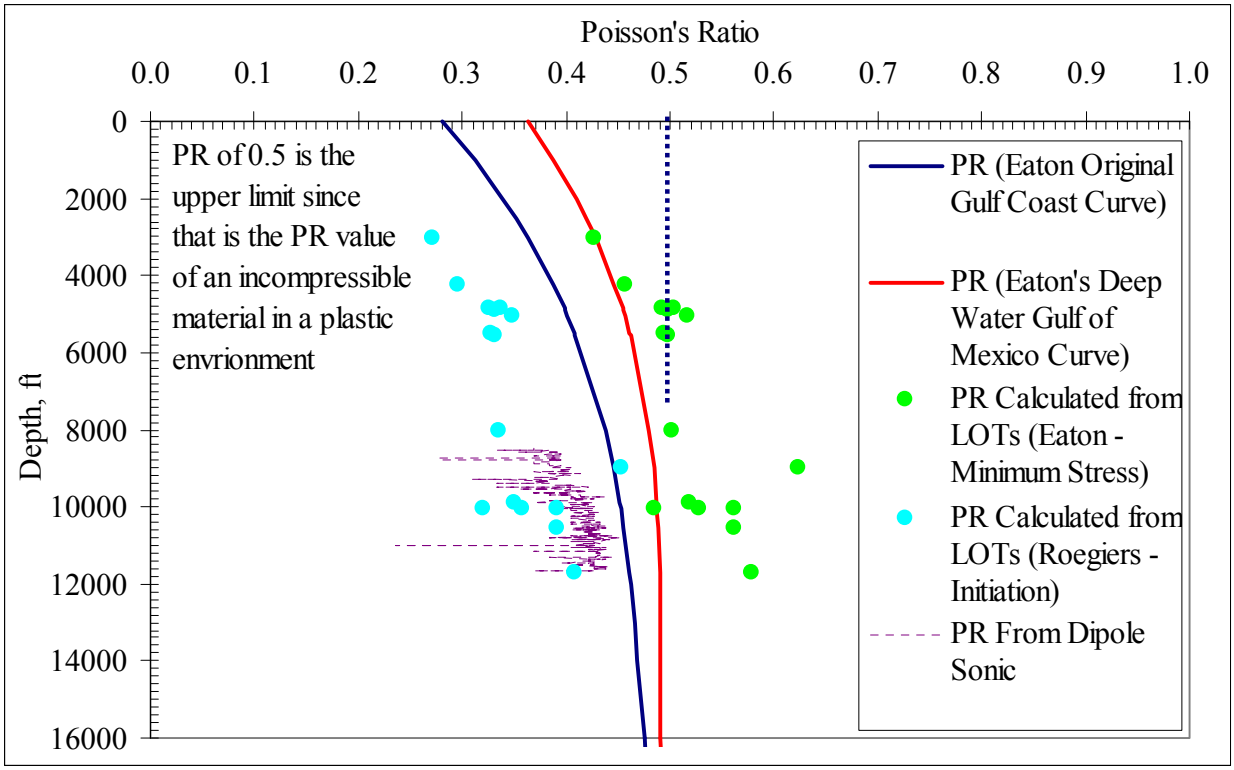

Fig 7.2: Poisson's Ratio Calculation Comparison for the EW 910 Area

Therefore, there is an open question as to what technique was used to produce the LOT data, specifically whether leak off occurred at all, and if so, what criteria was used for selecting the leak off pressure from the test data.

Two of the three interpretations (Poisson's ratio calculated by Roegiers' fracture initiation equations and Poisson's ratio determined by the dipole sonic log) of the area-specific Poisson's ratio are similar therefore use of the generalized Gulf of Mexico relationships established by Eaton is not necessary. Also, if we assume the LOT data to be valid, six of the fourteen Poisson's ratio values calculated from Eaton's method should be disregarded as well due to being greater than 0.5, which is impossible. It appears that the LOT data was measured based on fracture initiation rather than actual leak off or fracture extension pressure. Therefore, an area-specific estimate of Poisson's ratio versus depth was derived from using the fracture initiation pressure calculations and the dipole sonic values. Figure 7.3 shows the relationship of

Poisson's ratio versus depth that will be utilized for the fracture gradient prediction method proposed for this area.

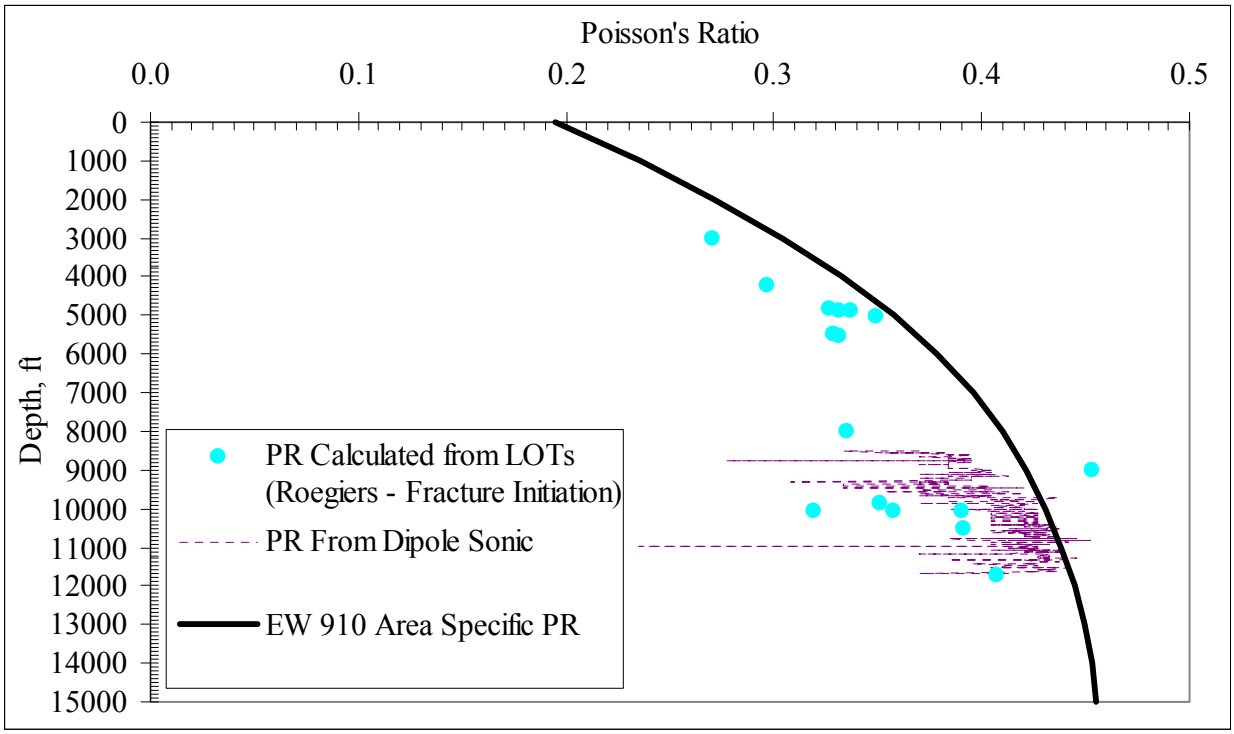

Fig. 7.3: Area Specific Poisson's Ratio vs Depth Relationship

Figure 7.3 demonstrates the area specific Poisson's ratio estimate based on the data with the higher Poisson's ratio value for similar depths. This is due to shales being expected to have a higher Poisson's ratio value than sandstones. This is important because this strategy is being developed for wells drilled with water base muds. Although sandstones typically have a lower Poisson's ratio and fracture gradient than the adjacent shales, the fluid loss characteristics of a water base mud will generally prevent formation fracture development and propagation in the sandstone. Therefore, the data furthest to the right in Figure 7.3 is considered to be the most likely to be representative for the shales that should control the fracture gradient. The EW 910 Area Specific PR is defined by the following equation.

$$\nu = a_1 D^3 + a_2 D^2 + a_3 D + a_4 \qquad \textit{(Equation 7.8)}$$

where,

a_1 = 4.55371017870928E-14
a_2 = -1.92071678321704E-09
a_3 = 2.71158119658153E-05
a_4 = 3.628666666663E-01

7.2 Fracture Gradient Calculation

The aforementioned area specific Poisson's ratio relationship will be implemented into both Eaton's equation to provide an estimate of fracture gradient and Rogiers' equation to provide an estimate of fracture initiation pressure. As noted in the previous section, when the LOT data was used to calculate Poisson's ratio using Eaton's method, many of the Poisson's ratio values were impossibly high. Therefore with a reduced Poisson's ratio value, the predicted fracture gradient will be less than the LOT data. This is because the fracture gradient calculated using Eaton's relationship is related to the true closure pressure of the fracture, or the minimum horizontal stress. The fracture initiation pressure calculated by Roegiers' relationship will yield results matching the LOT data, since it was this relationship from which the Poisson's ratio data was calculated. Both the fracture gradient and initiation pressure will be calculated and compared against the LOT data, and the fracture gradient data inferred from drilling problems. Applying Eaton's fracture gradient relationship and Roegiers' fracture initiation relationship should provide upper and lower limits to the maximum mud weights allowed while drilling.

Figures 7.4 to 7.11 are plots of the following; pore pressures, mud weights, inferred fracture gradients from drilling problems, calculated fracture gradient, LOTs and calculated fracture initiation pressure. The red curve is the fracture gradient predicted from Eaton's relationship and the purple curve is the fracture initiation pressure predicted by Roegiers' relationship. The red and purple dashed lines are the minimum fracture gradients and fracture initiation pressures predicted for each hole section, respectively. Note that there should never be

lost returns at ECDs lower than the lowest fracture gradient in the interval and also a mud weight greater than the fracture initiation pressure should always cause losses. A mud weight greater than the fracture gradient prediction, yet lower than the fracture initiation prediction may or may not cause losses. The casing setting depths are highlighted on the far right side of the plot.

Figure 7.4 is the predicted fracture gradient plot for the EW 910 A1BP. With the exception of one LOT data point at 9000', all of the LOT data fall between the upper and lower limits of fracture pressure established by Eaton's and Roegiers' relationships. The data point at 9000' is questionable. The LOT data point of 18.5 ppg EMW is the highest data point in all of the wells reviewed, regardless of depth. The next highest recorded LOT data point among all of the wells was an 18.0 ppg EMW test at 11706' in this well.

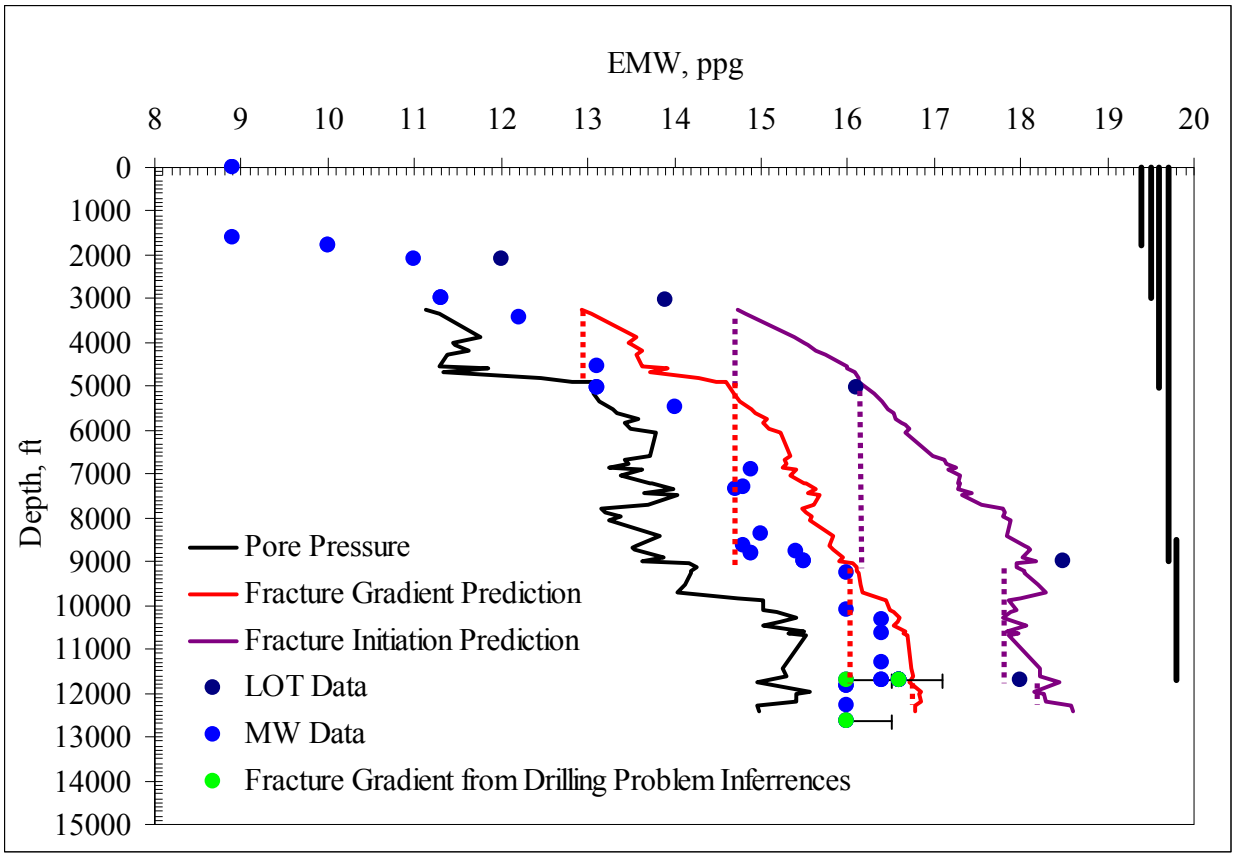

Fig. 7.4: Fracture Gradient Plot Using Area Specific Poisson's Ratio – EW 910 A1BP

There are also three fracture gradient data points inferred from drilling operations. All three events were lost returns, either partial or total losses. Though the ECDs can't be calculated

due to insufficient data, it's clear that the pressures exerted on the formation were greater than the minimum fracture gradient prediction. It's conceivable that a fracture could occur somewhere in the open hole interval with minimal initiation pressure.

Figure 7.5 is the predicted fracture gradient plot for the EW 954 A2 well. In this well, all of the LOT data points fall between the upper and lower limits of the predicted fracture gradient. As in Figure 7.4, there are two fracture gradient data points inferred from drilling operations. Though the ECDs aren't calculated, the value of the inferred data point is near the minimum fracture gradient predicted for the open hole interval. With minimal ECDs, it's conceivable that a fracture could be initiated exceeding the minimum fracture gradient prediction.

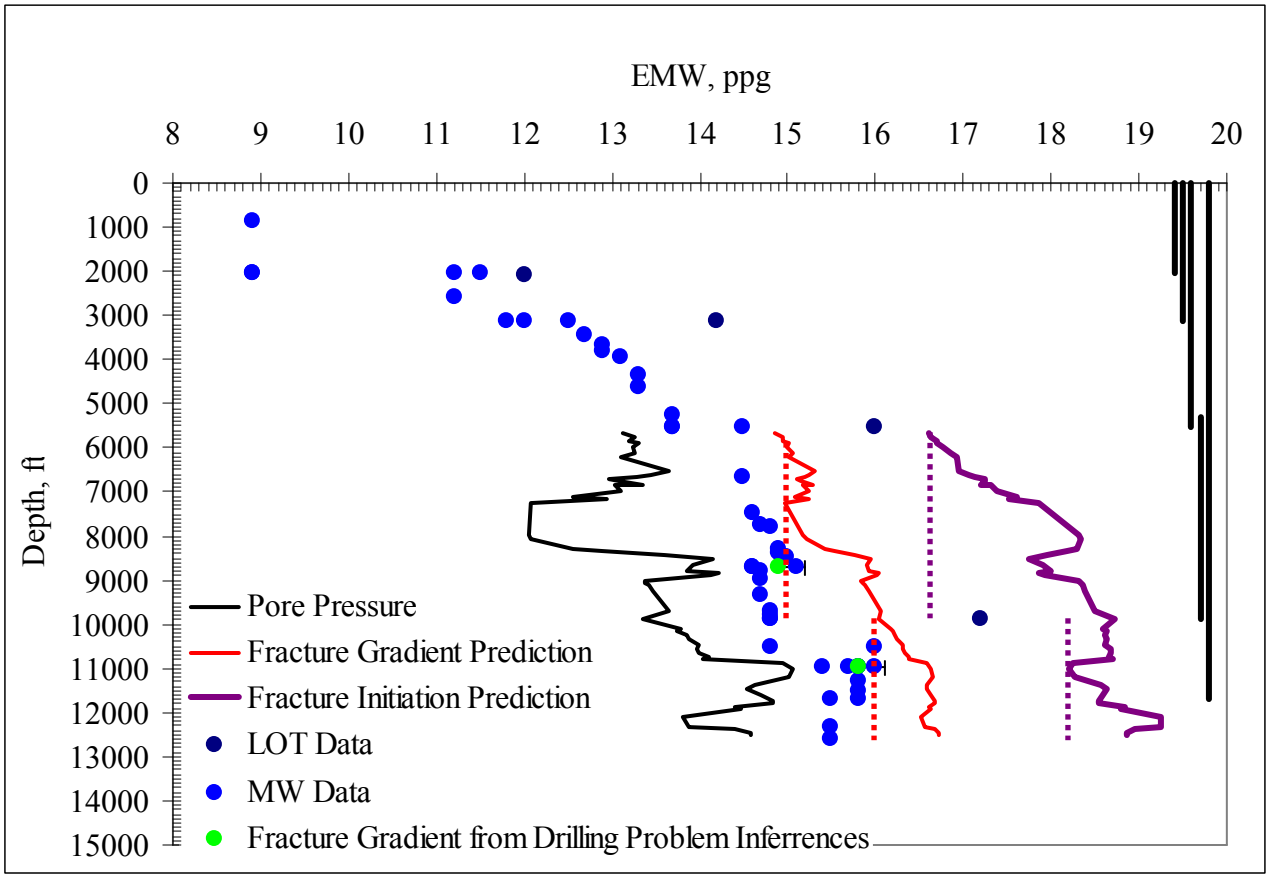

Fig. 7.5: Fracture Gradient Plot Using Area Specific Poisson's Ratio – EW 954 A2

Figure 7.6 is the predicted fracture gradient plot for the EW 910 A3 well. As in the EW 954 A2 well, all LOT data points are within the minimum and maximum fracture gradient

curves. There are no drilling events to infer fracture gradients. Note that from below 9700', to the next casing point at 10000', the predicted pore pressure exceeds the minimum fracture gradient curve. Well control was maintained because full returns were maintained, apparently because the minimum fracture initiation pressure was not exceeded. Nevertheless, presuming that these interpretations are correct there was a substantial risk of losing control of the well while drilling that interval.

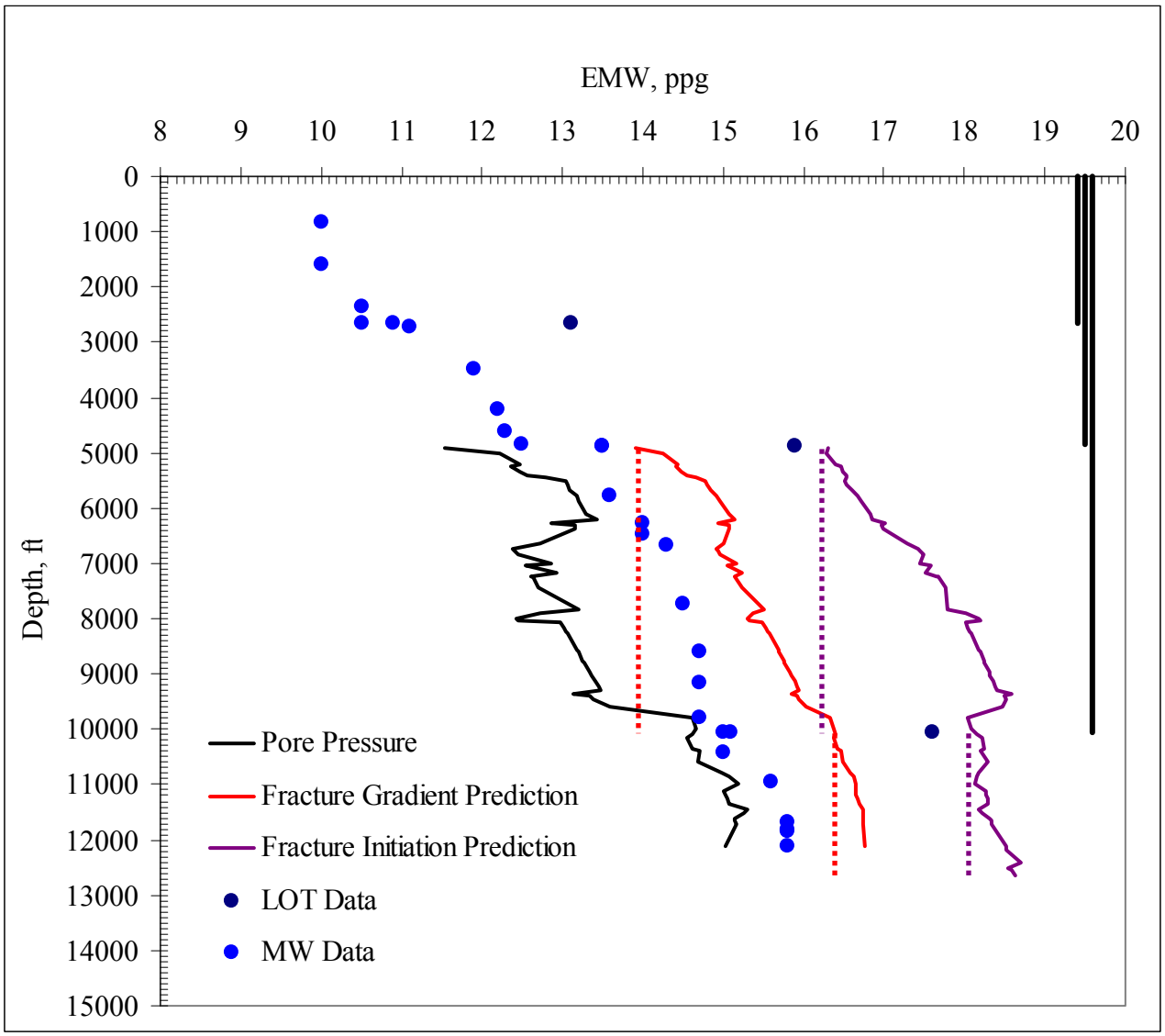

Fig. 7.6: Fracture Gradient Plot Using Area Specific Poisson's Ratio – EW 910 A3

Figure 7.7 is the predicted fracture gradient plot for ST 320 A4. The LOT data falls within the minimum and maximum fracture gradient curves. The only data point inferred from a

drilling event occurred shallow in the well where there is no pore pressure or fracture gradient prediction due to a lack of petrophysical data. Note that there are multiple intervals where the predicted pore pressure and mud weights exceed the minimum fracture gradient curve, similar to the situation described in the A3 well.

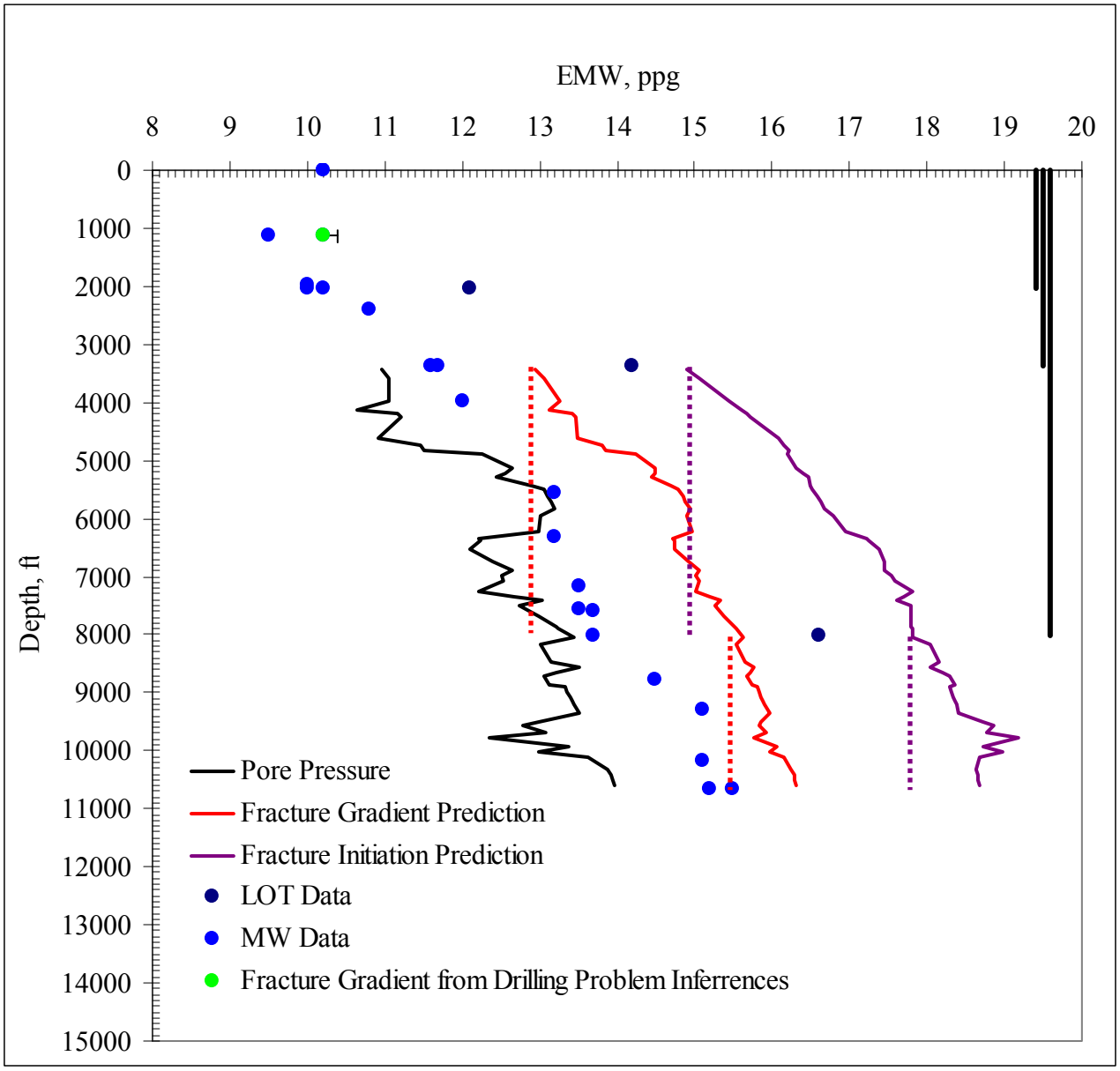

Fig. 7.7: Fracture Gradient Plot Using Area Specific Poisson's Ratio – ST 320 A4

Figure 7.8 is the predicted fracture gradient plot for the EW 910 A5 well. As in all wells, except EW 910 A1BP, the LOT data falls between the minimum and maximum fracture gradient curves. There were no drilling events to infer fracture gradient data. As in the EW 910 A3 and

ST 320 A4 wells, there is an interval below 9300' where the predicted pore pressure exceeds the minimum fracture gradient curve.

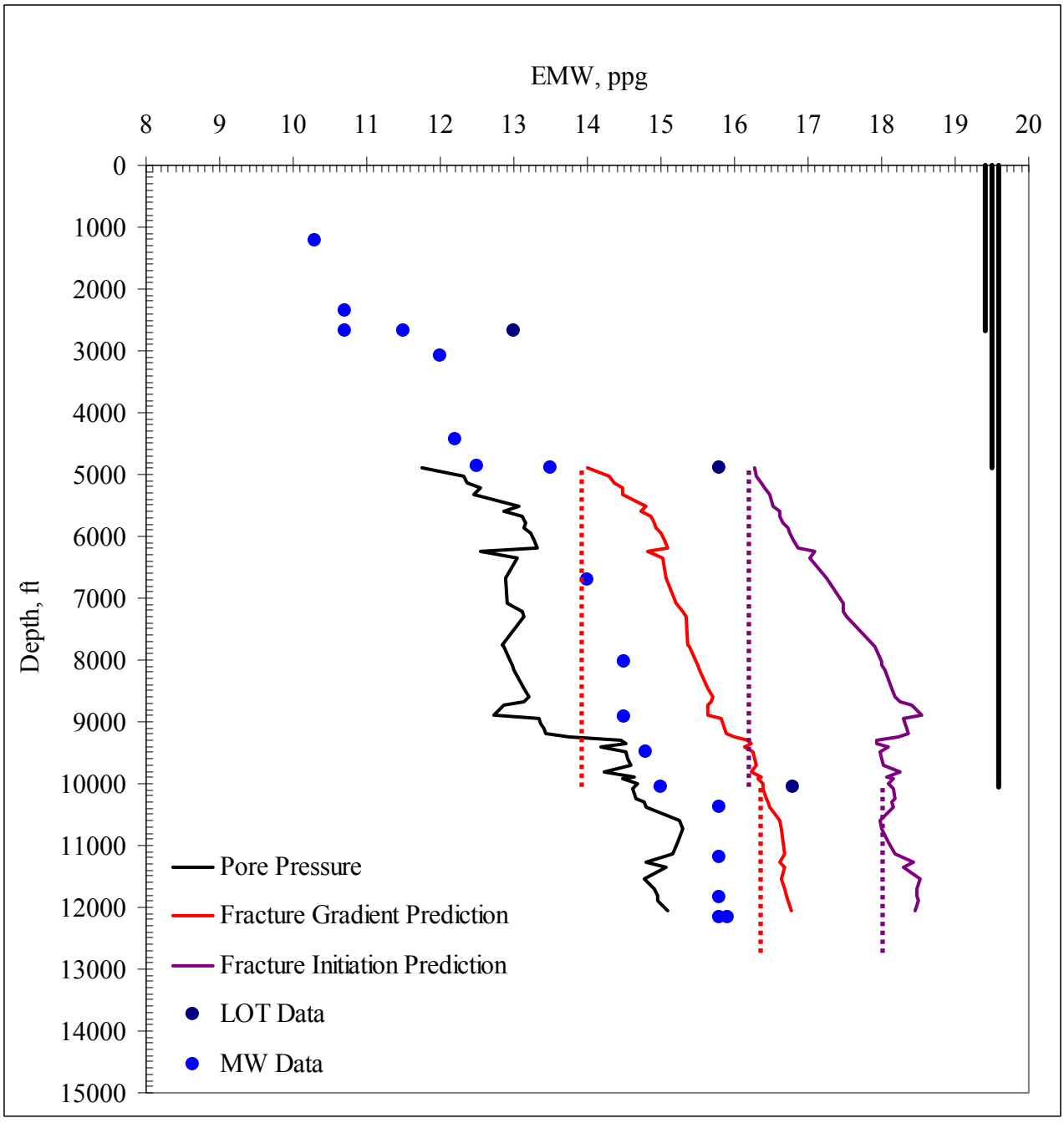

Fig. 7.8: Fracture Gradient Plot Using Area Specific Poisson's Ratio – EW 910 A5

Figure 7.9 is the predicted fracture gradient plot for EW 910 A6. The conclusions from this plot are almost identical to the EW 910 A5 plot, except the depth at which the predicted pore pressure exceeds the minimum fracture gradient curve occurs at approximately 9600'. Also,

there is an inferred fracture gradient data point shallow in the well, but there is no pore pressure or fracture gradient prediction since there are no petrophysical data.

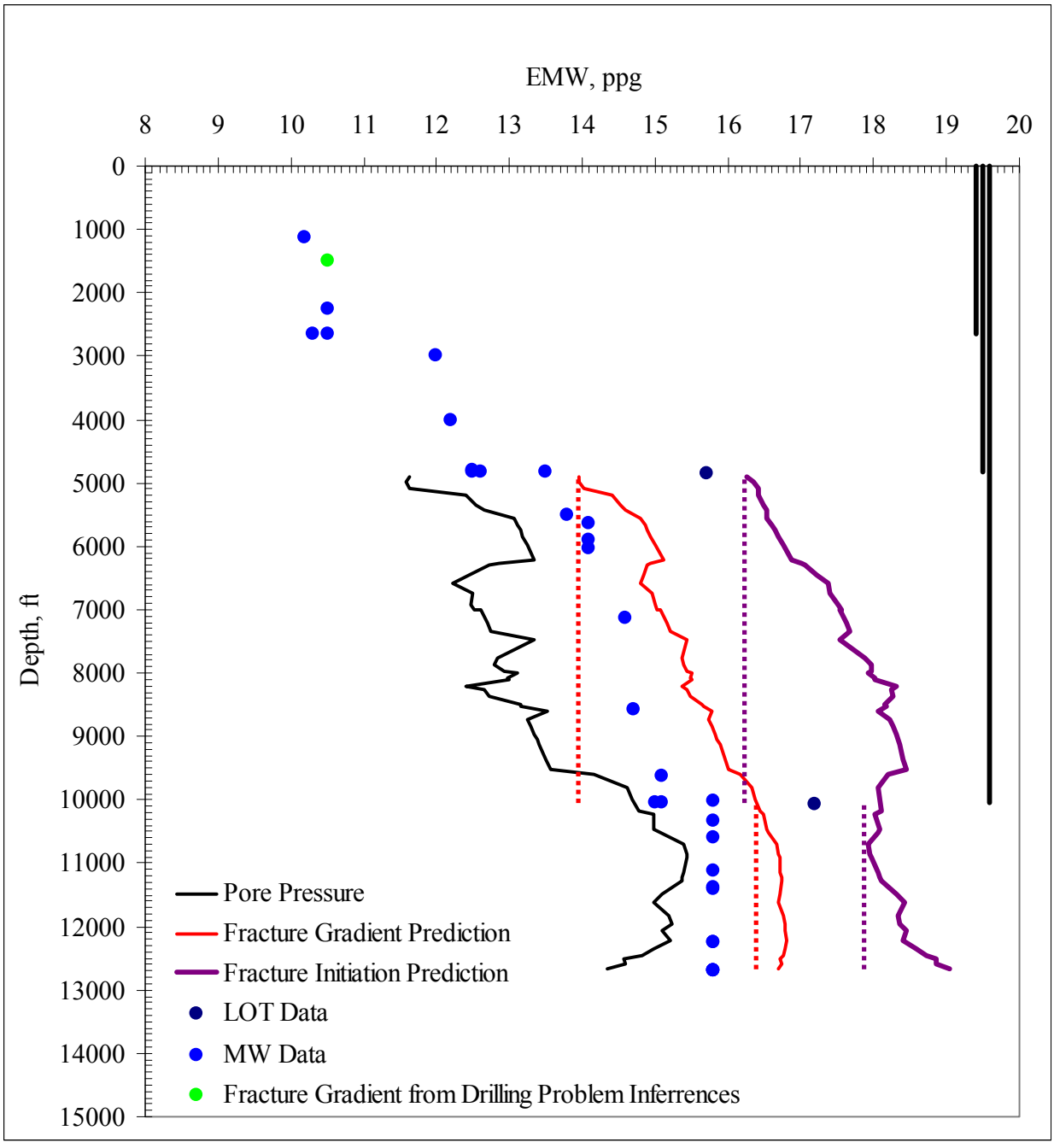

Fig. 7.9: Fracture Gradient Plot Using Area Specific Poisson's Ratio – EW 910 A6

Figure 7.10 is the predicted fracture gradient plot for the EW 910 A4 well. All of the LOT data points fall between the minimum and maximum predicted fracture gradient curves. There are no data points inferred from drilling events.

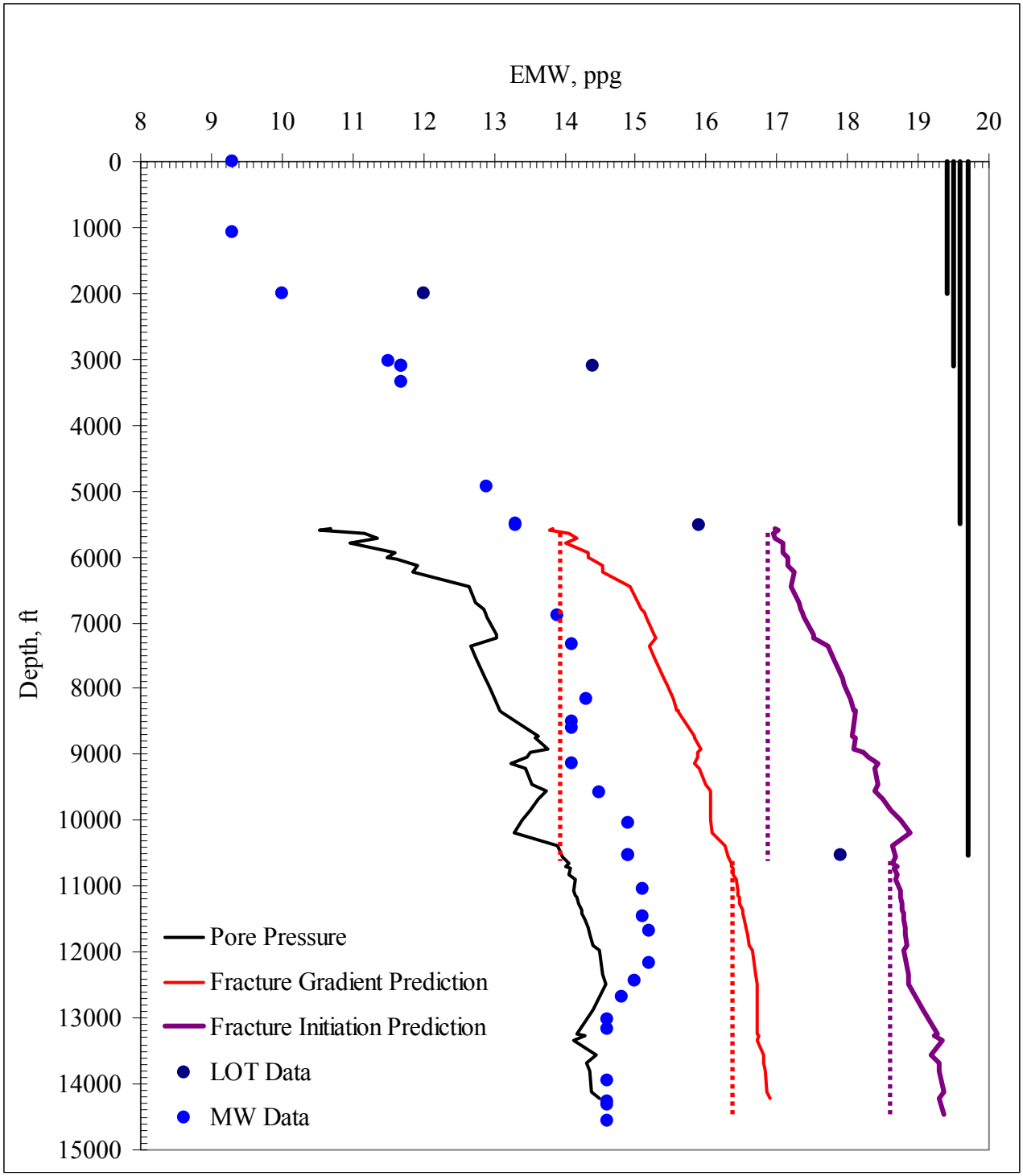

Fig. 7.10: Fracture Gradient Plot Using Area Specific Poisson's Ratio – EW 910 No. 4

Figure 7.11 is the predicted fracture gradient plot for the EW 953 No. 1 well. The single LOT data point falls between the minimum and maximum fracture gradient curves. There is one data point inferred from a drilling event at 7477'. The well history report is missing detail and

reports only that the hole was experiencing mud losses with a mud weight of 15.6 ppg. The mud weight was reduced to 15.3 ppg and the well drilled without experiencing subsequent losses. Since there is no bottom-hole assembly data present, ECDs can't be calculated. Therefore, the only conclusion that can be made is that the fracture gradient is greater than or equal to 15.3 ppg. The data point on the plot includes an error bar representing an 0.4 ppg EMW ECD. This value approaches the minimum predicted fracture gradient at that depth.

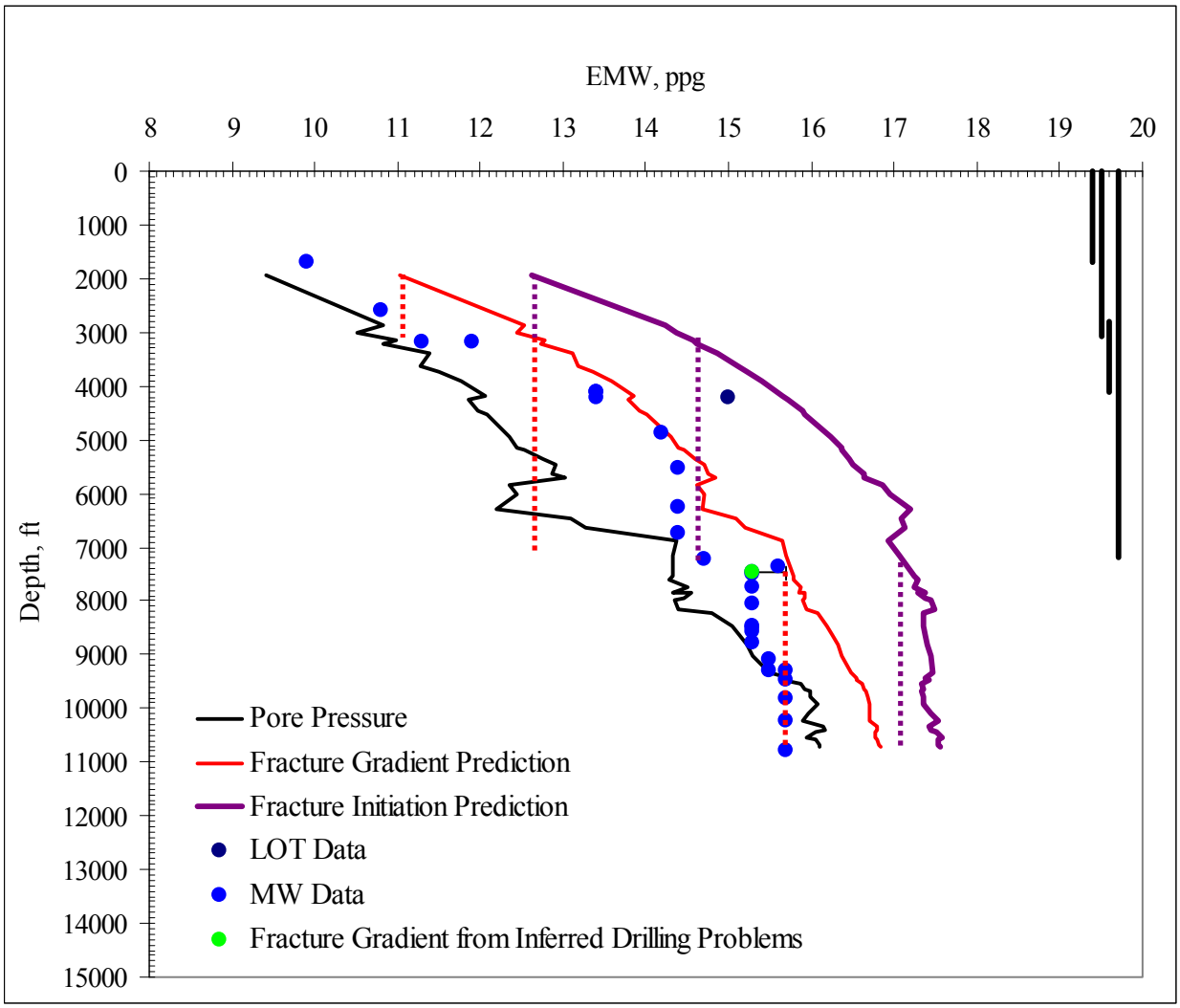

Fig. 7.11: Fracture Gradient Plot Using Area Specific Poisson's Ratio – EW 953 No. 1

7.3 General Conclusion Regarding the Fracture Gradient Prediction Strategy

Utilization of these fracture gradient and fracture initiation pressure predictions should provide good estimates of expected LOT values and maximum allowable mud weights for

drilling in the EW 910 area. With the exception of the EW 910 A1BP well, all LOT data points fell between the minimum and maximum predicted fracture gradient curves. The mud loss events described in Section 3.2 correlate extremely well with the minimum fracture gradient prediction for each respective hole interval.

8. SUMMARY, CONCLUSIONS AND RECOMMENDATIONS

8.1 Summary and Conclusions

The purpose of this project was to develop a pore pressure and fracture gradient prediction strategy for the Ewing Banks 910 area. The offset well data consisted of eight wells in EW 910 or neighboring blocks. Multiple pore pressure prediction strategies were reviewed with the implementation of three that gave reasonable results: W. R. Matthews' formation conductivity overlay approach and Ben Eaton's geopressure prediction equation for both formation conductivity and velocity data. Attempts were made to verify the validity of these approaches by comparing the empirically derived normal compaction trend line to an independently based prediction of conductivity versus depth for normally compacted sediments. Those attempts did not provide confirmation of the validity of the methods used. Nevertheless, the use of an implied area specific normal compaction trend line and the Eaton conductivity relationships provided the best match between predicted and actual pore pressures for the wells in this area. The predictions were generally within 0.2 ppg EMW of the actual pore pressure gradient and always within 0.5 ppg EMW. Therefore, the Eaton conductivity method was concluded to be the best pore pressure interpretation method for future use in this area.

The fracture gradient prediction method proposed by Ben Eaton was also applied using area specific data and an independent basis for the relationship between Poisson's ratio relationship and depth. The relationship for Poisson's ratio versus depth that was utilized is based on a combination of fracture initiation data from leak off tests and dipole sonic log data from wells where it was available. This method allows prediction of both fracture gradient and fracture initiation pressure and was concluded to be appropriate for future use in this area.

8.2 Pore Pressure and Fracture Gradient Methodology

Table 8.1 includes the set of equations and relationships for the EW 910 area to predict formation pore pressure and fracture gradients based on these Eaton methods. These equations result in a strategy that has been tailored to this area due to a high amount of offset well data. Chapters 5 – 7 demonstrates the validity of these equations when utilized in the EW 910 area.

Table 8.1: EW 910 Area Pore Pressure and Fracture Gradient Prediction Equations

Pore Pressure Prediction Equation	**Eaton's Fracture Gradient Equation**
$P_F / D = \sigma_{OB} / D - \left(\sigma_{OB} / D - P_{F(n)} / D\right) * \left(\frac{Cn_{(sh)}}{Cob_{(sh)}}\right)^{1.2}$	$\frac{P_{FF}}{D} = \frac{\nu}{1-\nu}\left(\frac{\sigma_{ob}}{D} - \frac{P_F}{D}\right) + \frac{P_F}{D}$
Normal Conductivity Trendline Equation	**Rogiers' Fracture Initiation Equation**
$Cn_{(sh)} = \exp\left[\frac{96000 - D}{13600}\right]$	$P_{IF} = 2 * \left[\frac{\nu}{1-\nu}\left(\sigma_{OB} - P_F\right)\right] + P_F$
Area Specific Overburden Stress Gradient Equation	**Area Specific Poisson's Ratio Equation**
$\sigma_{OB} = a_1 D^6 + a_2 D^5 + a_3 D^4 + a_4 D^3 + a_5 D^2 + a\ D + a_7$	$\nu = a_1 D^3 + a_2 D^2 + a_3 D + a_4$
a_1 = 4.092542229E-21	*a_1 = 4.55371017870928E-14*
a_2 = -1.91276937109725E-16	*a_2 = -1.92071678321704E-09*
a_3 = 3.46041193695536E-12	*a_3 = 2.71158119658153E-05*
a_4 = -3.07205791465204E-08	*a_4 = 3.628666666663E-01*
a_5 = 1.44604224757927E-04	
a_6 = 5.53568356670439E-01	
a_7 = - 48.7022134214639	

8.3 Recommendations

Although the aforementioned pore pressure and fracture gradient prediction techniques work well for the majority of the data, there is some uncertainty in the accuracy of the predictions. The following recommendations regarding those uncertainties should be addressed when planning and conducting future drilling operations.

- Normal Compaction Trendline – Since geopressures were developed at a shallower depth than logs or other petrophysical data was obtained in the existing wells, formation evaluation

logs should be obtained on future wells for all intervals below the shoe of the drive pipe/conductor. On the initial well, running a full quad combo suite, including density/neutron and sonic porosity, is recommended. With this petrophysical data, it should be possible to establish a normal pressure trendline. On subsequent wells, it is recommended to only obtain resistivity logs to minimize cost.

- Pore Pressure Prediction in the 6000' – 11000' Interval – The pore pressure prediction in this interval is questionable and cannot be verified with the existing data. The pore pressure prediction models indicate a pressure regression. There are multiple formation properties that could influence the formation conductivity leading to an apparent pressure regression. These include, but are not limited to, formation water salinity, i.e. water resistivity, clay mineralogy and sorting of the clay minerals. Any of those properties could result in a decrease in porosity yielding abnormally low formation conductivity. If the petrophysical data is obtained based on the previous recommendation, an analysis of the data could confirm that the formation properties in this interval are different than those directly above and below. If there formation properties found within this interval are not anomalous, it is recommended that pressure measurements within this interval be obtained to establish a true pore pressure to compare to the current predictions and potentially improve future predictions. Realistic pore pressures are required to make reliable fracture gradient calculations.

REFERENCES

1. Alixant, J.L. and Desbrandes, R.: "Explicit Pore-Pressure Evaluation: Concept and Application," SPEDE (September 1991) p. 182.

2. Bassiouni, Z.: "Theory, Measurement, and Interpretation of Well Logs," SPE, Richardson, TX, 1994, pp. 1 – 19.

3. Bourgoyne, A.T. Jr, and Rocha, A.L. Jr.: "A New, Simple Way to Estimate Fracture Pressure Gradient," SPEDC, September 1996, pp. 153 – 159.

4. Bourgoyne A.T. Jr, et al.: "Applied Drilling Engineering," SPE, Richardson, TX, 1991, pp. 246 – 252.

5. Carothers, J.W.: "A Statistical Study of the Formation Factor Relationship," The Log Analyst, September – October 1948, pp. 14 – 20.

6. Chilingar, G.V. and Knight, L.: "Relationship Between Pressure and Moisture Content of Kaolinite, Illite and Montmorillonite Clays," AAPG Bulletin, 1960, V. 44, No. 1, pp. 100 – 106.

7. Eaton, B.A.: "Fracture Gradient Prediction and Its Application in Oilfield Operations," JPT, October 1969, p. 246

8. Eaton, B.A., and Eaton, L.E.: "Fracture Gradient Prediction for the New Generation," World Oil, October 1997, p. 93.

9. Eaton, B.A.: "The Equation for Geopressure Prediction from Well Logs," paper SPE 5544 presented at the 1975 SPE Annual Technical Conference and Exhibition, Dallas, TX, September 28 – October 1.

10. Economides, M.J., and Martin, T.:" Modern Fracturing – Enhancing Natural Gas Production," ET Publishing, Houston, TX, 1997, pp. 116 – 124.

11. Fricke, H.: "A Mathematical Treatment of the Electrical Conductivity and Capacity of Disperse Systems," Physical Review, 1924, 24, pp. 525 – 587.

12. Gardner, G.H.F., et al.: "Formation Velocity and Density – The Diagnostic Basis for Stratigraphic Traps," Geophysics, Vol. 39, No. 6, December 1974, pp.2085 – 2095.

13. Hottman, C.E., and Johnson, R.K.: "Estimation of Formation Pressures from Log-derived Shale Properties," JPT, June 1965, p. 717

14. Matthews, W.R.: "Here is How to Calculate Pore Pressure from Logs," OGJ, November 15, 1971 – January 24, 1972.

15. MI Drilling Fluids, Inc.: "Plotting Pressures From Electric Logs," 1999.

16. Perez-Rosales, C.: "Generalization of Maxwell Equation for Formation Factor," paper SPE 5502 presented at the 1975 SPE Annual Technical Conference and Exhibition, Dallas, TX, September 18 – October 1.

17. Porter, C.R., and Carothers, J.W.: "Formation Factor-Porosity Relation Derived from Well Log Data," SPWLA, 1970, Paper A.

18. Roegiers, J-C.: "Rock Mechanics," Chapter 3 or Reservoir Stimulation, ed. Economides, M.J. and Nolte, K.G., Schlumberger Educational Services, 1987.

19. Schlumberger: "Oilfield Glossary – Where the Oilfield Meets the Dictionary," http://www.glossary.oilfield.slb.com.

20. Schlumberger: "Log Interpretation Charts," Houston, Tx, 1979.

21. Terzaghi, K.: "Theoretical Soil Mechanics," John Wiley and Sons, New York City, NY, 1943.

22. Timur. A., et al.: "Porosity and Pressure Dependence on Formation Resistivity Factor for Sandstones," Cdn. Well Logging Soc., 1972, 4, paper D.

23. Winsauer, H.M., et al.: "Resistivity of Brine-Saturated Sands in Relation to Pore Geometry," AAPB Bulletin 36, No. 2, February 1952, pp. 253 – 277.

24. Yoshida, C., et al.: "An Investigative Study of Recent Technologies Used For Prediction, Detection, and Evaluation of Abnormal Formation Pressure and Fracutre Pressure in North and South America," IADC/SPE 36381 presented at the 1996 IADC/SPE Asia Pacific Drilling Technology Conference, Kuala Lumpur, Malaysia, September 9 – 11.

Drilling Operations Recap - EW 910 A1 BP

Recap Information				FIT / LOT	
Depth	MW	Comments		Depth	Pff
0	8.9			2108	12.0
1612	8.9			3010	13.9
1800	10.0	Ran & cmt'd 20".		5050	16.1
1800	10.0			9000	18.5
2108	11.0	FIT = 12.0 ppg @ 2108'.		11706	18.0
3000	11.3	Ran & cmt'd 16".			
3000	11.3	LOT = 13.9 ppg @ 3010'.			
3448	12.2				
4553	13.1				
5040	13.1	Cmt 13-3/8" w/ no returns.			
5040	13.1	LOT = 16.1 ppg @ 5050'.			
5455	14.0				
7322	14.7				
8645	14.8	ST @ 7427' w/ slight drag at 5660 - 5700'. NO drag on TIH.			
8825	14.9	Hole packed off while making connection. POOH until stuck. Pipe stuck @ 7889'.			
8825	14.9	Severed pipe at 7491'.			
6900	14.9	Set S/T plug.			
7278	14.8	S/T around fish @ 7020'.			
8348	15.0	ST @ 8100' w/ some drag. Ream & wash to bottom.			
8788	15.4	POOH to shoe w/ gumbo on BHA. Wash & ream to bottom with excessive torque on bottom. POOH 1 stand and circulate clean.			
8992	15.5	ST to 8500' w/ slight drag.			
8992	15.5	Ran & cmt'd 9-5/8". LOT = 18.5 ppg @ 9000'.			
9277	16.0				
10121	16.0	ST @ 10121'. POOH w/ 50-60K drag from 10129 - 9665'. Pipe stuck. Worked free and established returns. POOH to 9-5/8" shoe. Wash & ream to bottom.			

Drilling Operations Recap - EW 910 A1 BP

Recap Information				FIT / LOT	
Depth	MW	Comments		Depth	Pff
10348	16.4	Hole packing off while drilling. POOH w/ 60K drag. Clean gumbo off BHA.			
10625	16.4	Drill to 10422' w/ seepage losses. Drill to 10625' losing 25 - 35 bph. Add LCM - hole packed off. POOH and clean BHA.			
11324	16.4	ST @ 11238'. Drag reduced after adding "aqua magic" sweeps.			
11698	16.6	Drill to 11698' losing at 20 - 30 bph. ST and POOH.			
11698	16.6	Log.			
11698	16.6	Perform conditioning trip with no problems.			
11698	16.6	Log. Make conditioning trip with no problems.			
11698	16.6	Shoot SWC's. Make conditioning trip with no problems. POOH and PU 7" liner. RIH w/ liner.			
11698	16.6				
11698	16.4	Cut MW to 16.4 ppg prior to drilling out.			
11702	16.4	LOT = 18.0 ppg. POOH for MWD failure.			
11704	16.0	Drill to 11704 with no returns. Hole taking 40 - 50 bph while static. Spot LCM pill on bottom. Reduce MW to 16.0 ppg.			
11830	16.0				
11830	16.0				
12263	16.0				
12641	16.0	Circulate on bottom while losing returns. Increase LCM additions.			
12641	16.0				

Drilling Operations Recap - EW 954 A2

Recap Information				FIT / LOT	
Depth	MW	Comments		Depth	Pff
869	8.9	Jet 30" casing to 869'.		2066	12.0
2056	8.9			3148	14.2
2056	8.9	Drilled to 2056'. Circulated prior to taking survey. Well flowing. Pumped 12.0 ppg kill mud and sea water. EMW = 11.5 ppg.		5542	16.0
2056	11.5	Ran and cemented 20" casing.		9890	17.2
2056	11.2	Lowered MW to 11.2 prior to drilling out. LOT = 12.0 ppg EMW @ 2066'.			
2563	11.2				
3138	11.8	Drilled to 3138'. Circulate out gas. Max Gas = 550 units. Raise MW to 11.8 ppg.			
3138	12.0				
3138	12.5	Ran and cemented 16" casing. Raise MW to 12.5 ppg prior to drilling out. LOT = 14.2 ppg EMW @ 3148'			
3462	12.7				
3662	12.9				
3828	12.9				
3962	13.1				
4362	13.3	ST @ 4020'. No problems or fill on bottom.			
4638	13.3				
5262	13.7				
5532	13.7	No problems or fill on ST. Ran and cemented 13-5/8" casing. No returns while cementing.			
5542	13.7	LOT = 16.0 ppg EMW @ 5542.			
5542	14.5	Displaced to SBM.			
6668	14.5				
7491	14.6				
7770	14.7	ST @ 7607'. No problems or fill on bottom.			
7808	14.8				
8297	14.9				

Drilling Operations Recap - EW 954 A2

Recap Information				FIT / LOT	
Depth	MW	Comments		Depth	Pff
8403	14.9				
8496	15.0				
8694	15.1	Lost returns after increasing the MW to 15.1 ppg. Fill hole with sea water. Based on volume of sea water pumped, it was determined that the Max MW is 14.9 ppg. Cut MW to 14.6 ppg.			
8704	14.6				
8704	14.6				
8773	14.7				
8956	14.7				
9322	14.7				
9694	14.8				
9804	14.8	ECD = 14.9 ppg.			
9883	14.8	Running 11-3/4" liner. Lost displacement returns @ 700'. Cemented liner with no returns.			
9890	14.8	FIT = 17.2 ppg EMW.			
10533	14.8				
10533	16.0	Raise MW to 16.0 ppg per WU schedule.			
10967	16.0	Began losing returns. Static losses as high as 120 bph.			
10967	15.8	Cut MW to 15.8 ppg.			
10967	15.4				
10967	15.7				
10985	15.8				
11300	15.8				
11508	15.8	Drilled to 11367'. Large amounts of cutting on sweep.			
11679	15.8	Ran and cemented 9-5/8" casing. Cemented with no returns.			
11686	15.5	Cut MW to 15.5 ppg on drill out. FIT = 16.7 ppg EMW.			
12320	15.5				

Drilling Operations Recap - EW 954 A2

Recap Information			FIT / LOT	
Depth	MW	Comments	Depth	Pff
12595	15.5			
12595	15.5	RIH w/ liner. Max Gas = 96 units on BU.		
12595	15.5	Cemented liner.		

Drilling Operations Recap - EW 910 A3

Recap Information				FIT / LOT	
Depth	MW	Comments		Depth	Pff
846	10.0			2659	13.1
1598	10.0			4866	15.9
2340	10.5	Increased MW to 10.5 ppg due to 200 units gas.		10042	17.6
2649	10.5	Ran and cemented 20" with no problems.			
2649	10.9	Increased MW prior to drill out. LOT = 13.1 ppg at 2659'.			
2721	11.1				
3477	11.9	Control drilling. WU per schedule. Some gas circulated out.			
4219	12.2	ST @ 3928' - No problems.			
4616	12.3				
4856	12.5	Ran and cemented 13-3/8". Well flowing on annulus after cement job. Pumped 12.5 ppg and 17.1 ppg on annulus to kill well.			
4866	13.5	LOT = 15.9 ppg. Marginal test. Squeeze shoe.			
4866	13.5				
5761	13.6				
6286	14.0				
6477	14.0				
6655	14.3	After rig repair, TIH. CBU w/ low mud cut of 13.2 ppg. Raise MW to 14.3 ppg.			
7740	14.5				
8597	14.7	Experiencing tight hole. (Hole angle problems?) Back ream out of hole.			
9149	14.7				
9792	14.7				
10042	15.0	Ran and cemented 9-5/8".			
10042	15.1	LOT = 17.6 ppg.			
10435	15.0				
10958	15.6	Drill to 10958 and hole packed off. Worked pipe free. Increased MW to 15.6 ppg.			
11844	15.8				

APPENDIX A1: OFFSET WELL RECAPS

Drilling Operations Recap - EW 910 A3

Recap Information			FIT / LOT	
Depth	MW	Comments	Depth	Pff
11667	15.8			
11806	15.8			
12113	15.8			

Drilling Operations Recap - ST 320 A4

Recap Information				FIT / LOT	
Depth	MW	Comments		Depth	Pff
0	10.2			2035	12.1
1113	10.2	Drive 30" to 1114'		3375	14.2
1128	9.5	Spudded well. 9' below shoe of DP, lost full returns. MW was 10.2 ppg. Eventually cut MW to 9.5 ppg and established full returns.		8015	16.6
1964	10.0				
2034	10.2	Drilling ahead fighting losses.			
2034	10.0	Run and cement 20" conductor. No returns during cmt job.			
2396	10.8	Drilled out with 10 ppg. LOT = 12.1 ppg.			
3365	11.6	Drilling ahead fighting gumbo.			
3365	11.7	Make wiper trip at casing point. Large amounts of gumbo on BU (after trip). Ran and cemented 13-3/8" with no problems.			
3989	12.0	LOT = 14.2 ppg EMW.			
5559	13.2				
6315	13.2				
7156	13.5				
7557	13.5	Attempted ST @ 6788', but hole was swabbing (4.5 bbl gain). 1145 units of gas on BU. Mud cut from 13.5 - 13.2 ppg.			
7580	13.7	Increased MW to 13.7 ppg to trip. BHA severly balled.			
8005	13.7	Ran and cemented 9-5/8' casing. Full returns througout cement job.			
8770	14.5	LOT = 16.6 ppg EMW.			
9299	15.1	Drilled to 8964'. Made ST. Backreaming required to TOOH. Hole trying to pack off. MW @ 14.7 ppg. Increase MW to 15.1 ppg. Drill to 9299'. Attempt to POOH. Well swabbing. Backreamed 9 stands fighting packing off issues. After 9 stands, POOH w/out reaming.			
10163	15.1				
10659	15.2	TD'd. Needed to pump out of hole.			

APPENDIX A1: OFFSET WELL RECAPS

Drilling Operations Recap - ST 320 A4

Recap Information					FIT / LOT	
Depth	MW		Comments		Depth	Pff
10659	15.5	Run logs and evaluate.				

Drilling Operations Recap - EW 910 A5

Recap Information				FIT / LOT	
Depth	MW	Comments		Depth	Pff
1220	10.3			2676	13.0
2345	10.7			4893	15.8
2666	10.7	Ran and cemented 20" casing.		10062	16.8
2666	11.5	LOT = 13.0 ppg EMW @ 2676'.			
3077	12.0				
4429	12.2				
4858	12.5	Ran and cemented 13-3/8" casing.			
4883	13.5	LOT = 15.8 ppg @ 4893'.			
6716	14.0	ST at 6716' with no problems.			
8030	14.5				
8912	14.5				
9494	14.8				
10052	15.0	Ran and cemented 9-5/8" casing with no returns. LOT = 16.8 ppg @ 10062'.			
10381	15.8				
11187	15.8	ST at 11187'. Hole swabbing. TIH to 10823' - wash and ream tight spot.			
11831	15.8				
12158	15.8				
12158	15.9				

Drilling Operations Recap - EW 910 A6

Recap Information				FIT / LOT	
Depth	MW	Comments		Depth	Pff
1117	10.2			4848	15.7
2257	10.5	At approximately 1500' the hole seemed to be taking mud, but healed on it's on.		10058	17.2
2661	10.5				
2661	10.3	Ran and cemented 20" casing.			
2984	12.0				
4017	12.2				
4788	12.5				
4838	12.6				
4838	12.5				
4838	13.5	Ran and cemented 13-5/8" casing. LOT = 15.7 ppg @ 4848'.			
5496	13.8				
5628	14.1				
5890	14.1				
6025	14.1				
7145	14.6				
8562	14.7				
9621	15.1				
10048	15.1				
10048	15.0	Ran and cemented 9-5/8" casing with no returns. LOT = 17.2 ppg @ 10058'			
10585	15.8				
11376	15.8				
12240	15.8				
12242	15.8				
12691	15.8				
12691	15.8				
12691	15.8				

Drilling Operations Recap - EW 910 A6

Recap Information				FIT / LOT	
Depth	MW	Comments		Depth	Pff
12691	15.8				
10030	15.8				
10329	15.8				
11132	15.8	Trip for new bit. Had 597 units of gas with mud cut to 15.5 ppg on BU.			
11398	15.8	Lost returns at TD. Log and sidetrack well for exploration.			

Drilling Operations Recap - EW 910 No. 4

Recap Information				FIT / LOT	
Depth	MW	Comments		Depth	Pff
0	9.3			2010	12.0
1077	9.3	Jet in 30" to 954'. Drill to 1077'.		3110	14.4
2000	10.0	Run and cement 20" casing. LOT = 12.0 ppg.		5510	15.9
3025	11.5	LOT = 12.0 ppg @ 2010'.. Drill to 3025'.		10530	17.9
3100	11.7	Drill to 3100'. CBU (gcm f/ 11.5 - 11.1 w/ max gas of 438 units). Raise MW to 11.7 ppg.			
3100	11.7	Run and cement 16" casing. LOT = 14.4 ppg @ 3110'.			
3350	11.7				
4933	12.9				
5500	13.3	Run and cement 13-3/8".			
5510	13.3	Finish testing BOPs. LOT = 15.9 ppg.			
6880	13.9				
7326	14.1				
8160	14.3				
8501	14.1				
8607	14.1				
9145	14.1				
9576	14.5				
10030	14.9				
10520	14.9	Ran and cemented 9-5/8" casing.			
10530	14.9	LOT = 17.9 ppg EMW.			
11054	15.1				
11462	15.1	Drill to 11082'. Make ST. Improper fill. No other signs of pressure. Drill to 11462'.			
11676	15.2				
12170	15.2				
12425	15.0				
12680	14.8				

Drilling Operations Recap - EW 910 No. 4

Recap Information				FIT / LOT	
Depth	MW	Comments		Depth	Pff
13016	14.6				
13165	14.6				
13943	14.6				
14268	14.6				
14319	14.6				
14550	14.6	Log well. Begin P&A operations.			

Drilling Operations Recap - EW 953 No. 1

Recap Information				FIT / LOT	
Depth	MW	Comments		Depth	Pff
1700	9.9			4222	15.0
2582	10.8				
3182	11.9	On choke.			
3182	11.3	Circulate out on choke.			
4115	13.4	Gas cut mud.			
4122	13.4	LOT = 15.0 ppg @ 4122'.			
4222	13.4				
4882	14.2				
5526	14.4	Swabbing on trip.			
6247	14.4				
6755	14.4				
7237	14.7	Increase MW for connection gas.			
7374	15.6	Well flowing.			
7477	15.3	Decrease MW for mud losses.			
7501	15.3				
7740	15.3				
8040	15.3				
8474	15.3				
8504	15.3				
8563	15.3				
8778	15.3				
9085	15.5				
9294	15.5	Circulate out kick.			
9294	15.7				
9454	15.7				
9825	15.7				

APPENDIX A1: OFFSET WELL RECAPS

Drilling Operations Recap - EW 953 No. 1

Recap Information				FIT / LOT	
Depth	MW	Comments		Depth	Pff
10243	15.7				
10800	15.7				

RFT/MDT MEASURED RESERVOIR PRESSURE ANALYSIS - EW 910 A1BP

EW 910 A1BP - 7/14/96
MW = 16.6 ppg
Probe Type - Conventional
Gauge Resolution - 0.01 psi

Test #	TVD	Drawdown	Phyd (b)	Phyd (a)	Pf	Comments	Phyd Diff	Pf (grad)	Phyd - Pf	MW_{BH}
35	10974.49		9635.83	9630.21		Dry Test	5.62		9635.83	16.90
33	10996.37		9659.09	9649.71		Dry Test	9.38		9659.09	16.91
21	11171.52		9812.03	9802.75		Dry Test	9.28		9812.03	16.91
19	11172.48		9817.35	9814		Dry Test	3.35		9817.35	16.92
10	11493.37		10103.03	10094.39		Dry Test	8.64		10103.03	16.92
5	11507.31		10115.45	10112		Dry Test	3.45		10115.45	16.92
8	11508.35		10117.37	10101.08		Dry Test	16.29		10117.37	16.92
6	11509.28		10112.04	10118.8		Dry Test	-6.76		10112.04	16.91
31	10997.42		9656.1	9646.98		Lost Seal	9.12		9656.1	16.90
32	10998.48		9656.67	9641.35		Lost Seal	15.32		9656.67	16.90
34	10991.42	109.15	9648.02	9638.67	8782.36	Normal Pretest	9.35	15.38	865.66	16.90
27	11141.33	1.92	9782.21	9767.07	8772.41	Normal Pretest	15.14	15.16	1009.8	16.90
28	11141.44	4.08	9794.82	9770.24	8772.14	Normal Pretest	24.58	15.16	1022.68	16.92
26	11147.4	20.99	9789.23	9789.37	8774.33	Normal Pretest	-0.14	15.15	1014.9	16.90
25	11152.48	4.07	9791.86	9791.51	8775.75	Normal Pretest	0.35	15.15	1016.11	16.90
24	11154.41	62.34	9800.98	9794.11	8775.72	Normal Pretest	6.87	15.14	1025.26	16.91
22	11155.45	1.13	9799.66	9787.53	8775.38	Normal Pretest	12.13	15.14	1024.28	16.91
23	11156.43	3.76	9802.8	9786.51	8775.91	Normal Pretest	16.29	15.14	1026.89	16.91
18	11195.36	73.15	9831.15	9825.77	8804.72	Normal Pretest	5.38	15.14	1026.43	16.90
17	11199.42	10.93	9850.36	9836.75	8790.55	Normal Pretest	13.61	15.11	1059.81	16.93
16	11367.36	8.23	9986.13	9987.11	8929.21	Normal Pretest	-0.98	15.12	1056.92	16.91
14	11368.38	63.76	10011.26	9990.38	8928.63	Normal Pretest	20.88	15.12	1082.63	16.95
15	11369.22	4.45	9984.39	9987.94	8929.13	Normal Pretest	-3.55	15.12	1055.26	16.91

RFT/MDT MEASURED RESERVOIR PRESSURE ANALYSIS - EW 910 A1BP

EW 910 A1BP - 7/14/96
MW = 16.6 ppg
Probe Type - Conventional
Gauge Resolution - 0.01 psi

Test #	TVD	Drawdown	Phyd (b)	Phyd (a)	Pf	Comments		Phyd Diff	Pf (grad)	Phyd - Pf	MW_{BH}
13	11471.29	1.94	10082.03	10065.5	8960.28	Normal Pretest		16.53	15.04	1121.75	16.92
12	11484.35	131.41	10096.24	10079.37	8964.45	Normal Pretest		16.87	15.03	1131.79	16.92
11	11492.39	33.58	10098.92	10089.43	8965.8	Normal Pretest		9.49	15.02	1133.12	16.92
4	11542.29	1.56	10147.57	10136.46	8979.96	Normal Pretest		11.11	14.98	1167.61	16.92
3	11565.24	33.15	10151.2	10158.63	8987.33	Normal Pretest		-7.43	14.96	1163.87	16.90
1	11566.33	178.34	10194.09	10177	8987.79	Normal Pretest		17.09	14.96	1206.3	16.97
2	11567.25	180.05	10173.76	10154.62	8987.69	Normal Pretest		19.14	14.96	1186.07	16.93

RFT/MDT MEASURED RESERVOIR PRESSURE ANALYSIS - EW 910 A1BP

EW 910 A1BP - 7/29/96
MW = 16 ppg
Probe Type - Conventional
Gauge Resolution - 0.04 psi

Test #	TVD	Drawdown	Phyd (b)	Phyd (a)	Pf	Comments	Phyd Diff	Pf (grad)	Phyd - Pf	MW_{BH}
109	11832.06	-	10032.04	10029.83	-	Dry Test	2.21	-	-	16.32
80	11889.98	-	10078.22	10077.47	-	Dry Test	0.75	-	-	16.32
66	12479.07	-	10578.79	10579.51	-	Dry Test	-0.72	-	-	16.32
52	12508.00	-	10606.51	10604.83	-	Dry Test	1.68	-	-	16.32
113	11818.07	1.60	10019.33	10018.72	9216.25	Limited Drawdown	0.61	15.01	803.08	16.32
79	11888.98	1.34	10077.91	10076.96	9545.59	Limited Drawdown	0.95	15.46	532.32	16.32
96	12451.04	0.74	10569.07	10568.06	9421.86	Limited Drawdown	1.01	14.57	1147.21	16.34
94	12486.02	1.68	10598.34	10597.83	9479.29	Limited Drawdown	0.51	14.61	1119.05	16.34
61	12488.08	0.71	10579.91	10546.73	8992.39	Limited Drawdown	33.18	13.86	1587.52	16.31
115	11789.05	-	9994.11	9994.13	-	Lost Seal	-0.02	-	-	16.32
114	11790.08	-	9995.27	9994.89	-	Lost Seal	0.38	-	-	16.32
110	11829.08	-	10028.61	10028.54	-	Lost Seal	0.07	-	-	16.32
108	11834.05	-	10034.21	10033.66	-	Lost Seal	0.55	-	-	16.32
107	11850.98	-	10048.38	10048.22	-	Lost Seal	0.16	-	-	16.32
106	11853.04	-	10050.56	10050.12	-	Lost Seal	0.44	-	-	16.32
50	12445.10	126.92	10550.13	10549.03	2615.08	Depleted (?)	1.10	4.04	7935.05	16.32
65	12480.04	-	10576.81	10555.83	-	Lost Seal	20.98	-	-	16.31
119	11768.08	40.03	9945.83	9971.01	9028.57	Normal Pretest	-25.18	14.77	917.26	16.27
111	11820.13	9.81	10021.04	10020.37	9212.39	Normal Pretest	0.67	15.00	808.65	16.32
112	11821.08	191.92	10021.61	10021.09	9238.03	Normal Pretest	0.52	15.04	783.58	16.32
105	11893.08	34.86	10084.91	10084.15	9053.37	Normal Pretest	0.76	14.65	1031.54	16.32
78	11905.02	250.93	10091.62	10091.07	9057.88	Normal Pretest	0.55	14.65	1033.74	16.32
77	11941.14	604.20	10123.59	10122.22	9073.72	Normal Pretest	1.37	14.63	1049.87	16.32

RFT/MDT MEASURED RESERVOIR PRESSURE ANALYSIS - EW 910 A1BP

EW 910 A1BP - 7/29/96
MW = 16 ppg
Probe Type - Conventional
Gauge Resolution - 0.04 psi

Test #	TVD	Drawdown	Phyd (b)	Phyd (a)	Pf	Comments	Phyd Diff	Pf (grad)	Phyd - Pf	MW_{BH}
70	12437.04	354.08	10551.85	10551.18	9449.83	Normal Pretest	0.67	14.63	1102.02	16.33
102	12437.08	21.16	10557.09	10556.36	9696.28	Normal Pretest	0.73	15.01	860.81	16.34
69	12441.07	2.96	10554.97	10553.87	9449.59	Normal Pretest	1.10	14.62	1105.38	16.33
100	12446.02	32.38	10564.51	10563.36	9451.03	Normal Pretest	1.15	14.62	1113.48	16.34
49	12446.10	17.18	10548.92	10548.98	9455.22	Normal Pretest	-0.06	14.62	1093.70	16.32
48	12447.10	155.01	10548.61	10549.17	9481.00	Normal Pretest	-0.56	14.66	1067.61	16.31
68	12447.17	50.71	10554.46	10559.67	9451.76	Normal Pretest	-5.21	14.62	1102.70	16.32
51	12448.00	468.97	10552.89	10553.81	9452.94	Normal Pretest	-0.92	14.62	1099.95	16.32
72	12450.02	14.30	10561.88	10561.85	9451.28	Normal Pretest	0.03	14.61	1110.60	16.33
99	12451.08	219.85	10569.18	10567.75	9453.25	Normal Pretest	1.43	14.62	1115.93	16.34
73	12451.10	265.61	10563.72	10563.63	9452.64	Normal Pretest	0.09	14.61	1111.08	16.33
71	12451.98	207.19	10564.72	10560.75	9454.54	Normal Pretest	3.97	14.62	1110.18	16.33
67	12452.03	33.62	10554.94	10554.75	9451.90	Normal Pretest	0.19	14.61	1103.04	16.32
76	12452.08	1672.08	10563.45	10562.63	9453.79	Normal Pretest	0.82	14.61	1109.66	16.33
95	12455.06	89.08	10572.33	10571.35	9456.69	Normal Pretest	0.98	14.62	1115.64	16.34
58	12496.92	10.71	10600.52	10600.08	9676.30	Normal Pretest	0.44	14.91	924.22	16.33
56	12507.00	20.45	10607.83	10607.59	9472.02	Normal Pretest	0.24	14.58	1135.81	16.33
55	12508.00	79.81	10607.99	10606.54	2319.73	Normal Pretest	1.45	3.57	8288.26	16.33
89	12510.98	139.98	10614.38	10614.03	9510.47	Normal Pretest	0.35	14.63	1103.91	16.33
88	12511.97	181.56	10613.76	10614.02	9472.74	Normal Pretest	-0.26	14.57	1141.02	16.33
93	12513.02	218.23	10620.56	10620.59	9473.53	Normal Pretest	-0.03	14.57	1147.03	16.34
90	12514.03	314.51	10618.09	10618.24	9476.98	Normal Pretest	-0.15	14.58	1141.11	16.33
87	12515.98	587.54	10615.82	10614.99	9474.24	Normal Pretest	0.83	14.57	1141.58	16.33

RFT/MDT MEASURED RESERVOIR PRESSURE ANALYSIS - EW 910 A1BP

EW 910 A1BP - 7/29/96											
MW = 16 ppg											
Probe Type - Conventional											
Gauge Resolution - 0.04 psi											
Test #	TVD	Drawdown	Phyd (b)	Phyd (a)	Pf	Comments		Phyd Diff	Pf (grad)	Phyd - Pf	MW_{BH}
91	12515.98	67.02	10622.06	10622.50	9473.85	Normal Pretest		-0.44	14.57	1148.21	16.34
103	12436.02	-	-	-	-	Unrecognizable			-	-	
60	12490.02	-	-	-	-	Unrecognizable			-	-	
57	12496.10	-	-	-	-	Unrecognizable			-	-	
59	12498.10	-	-	-	-	Unrecognizable			-	-	

RFT/MDT MEASURED RESERVOIR PRESSURE DATA ANALYSIS - EW 954 A2

EW 954 A2 - 5-6-97											
MW = 15.8 ppg											
Probe Type - Large Diameter											
Gauge Resolution - 0.010 psi											
File #	TVD	Drawdown	Phyd (b)	Phyd (a)	Pf	Comments		Phyd Diff	Pf (grad)	Phyd - Pf	MWBH
58	10872.52	6.89	9040.68	9042.88		Dry Test		-2.2	0.00	9040.68	16.01
59	10873.18	3.96	9049.99	9048.10		Dry Test		1.89	0.00	9049.99	16.02
61	10875.36	58.30	9089.26	9085.42		Dry Test		3.84	0.00	9089.26	16.09
18	11113.94	77.10	9285.23	9282.98		Dry Test		2.25	0.00	9285.23	16.08
21	11454.03	0.10	9558.30	9554.43		Dry Test		3.87	0.00	9558.3	16.06
19	11501.69	0.72	9618.29	9615.37		Dry Test		2.92	0.00	9618.29	16.10
13	11507.20	1.69	9637.62	9633.67		Dry Test		3.95	0.00	9637.62	16.12
17	11507.21	1.01	9482.27	9628.50		Dry Test		-146.23	0.00	9482.27	15.86
10	11514.15		9655.85	9645.32		Dry Test		10.53	0.00	9655.85	16.14
20	11502.29	0.14	9616.03	9611.91		Lost Seal		4.12	0.00	9616.03	16.09
31	11314.29	108.49	9413.18	9408.74	8911.37	Normal Pretest		4.44	15.16	501.81	16.02
30	11315.66	1666.16	9398.35	9410.21	8911.52	Normal Pretest		-11.86	15.16	486.83	15.99
32	11317.16	2810.02	9414.09	9426.34	8912.50	Normal Pretest		-12.25	15.16	501.59	16.01
57	10873.95	49.46	9032.57	9032.50	8634.94	Volumetric Pretest		0.07	15.29	397.63	15.99
55	10979.41	21.76	9136.72	9135.16	8776.09	Volumetric Pretest		1.56	15.39	360.63	16.02
54	10980.08	20.79	9139.64	9138.34	8776.42	Volumetric Pretest		1.3	15.39	363.22	16.02
56	10980.13	13.14	9135.23	9129.92	8776.23	Volumetric Pretest		5.31	15.39	359	16.02
65	10980.15	5.62	9184.09	9181.68	8775.37	Volumetric Pretest		2.41	15.38	408.72	16.10
53	10980.79	956.25	9140.03	9140.27	8776.59	Volumetric Pretest		-0.24	15.39	363.44	16.02
50	11078.08	2450.38	9241.16	9240.81	8752.60	Volumetric Pretest		0.35	15.21	488.56	16.06
49	11114.67	6.51	9284.13	9281.33	8762.34	Volumetric Pretest		2.8	15.18	521.79	16.08
17	11115.36	165.61	9291.43	9287.31	8763.05	Volumetric Pretest		4.12	15.18	528.38	16.09
44	11137.36	5731.47	9314.84	9309.06	8763.87	Volumetric Pretest		5.78	15.15	550.97	16.10

RFT/MDT MEASURED RESERVOIR PRESSURE DATA ANALYSIS - EW 954 A2

EW 954 A2 - 5-6-97											
MW = 15.8 ppg											
Probe Type - Large Diameter											
Gauge Resolution - 0.010 psi											
File #	TVD	Drawdown	Phyd (b)	Phyd (a)	Pf	Comments		Phyd Diff	Pf (grad)	Phyd - Pf	MWBH
37	11138.00	3.31	9276.35	9263.28	8763.19	Volumetric Pretest		13.07	15.15	513.16	16.03
43	11138.74	263.31	9320.57	9315.19	8764.11	Volumetric Pretest		5.38	15.15	556.46	16.11
36	11139.44	370.30	9279.27	9271.33	8763.30	Volumetric Pretest		7.94	15.14	515.97	16.04
45	11140.00	4605.63	9312.48	9318.91	8764.73	Volumetric Pretest		-6.43	15.15	547.75	16.09

RFT/MDT MEASURED RESERVOIR PRESSURE DATA ANALYSIS - EW 954 A2

EW 954 A2 - 5-6-97
MW = 15.8 ppg
Probe Type - Large Diameter
Gauge Resolution - 0.010 psi

File #	TVD	Drawdown	Phyd (b)	Phyd (a)	Pf	Comments	Phyd Diff	Pf (grad)	Phyd - Pf	MWBH
42	11140.20	708.88	9330.59	9323.00	8764.80	Volumetric Pretest	7.59	15.15	565.79	16.12
35	11140.84	948.57	9276.04	9268.52	8763.60	Volumetric Pretest	7.52	15.14	512.44	16.03
34	11143.65	147.01	9271.82	9275.12	8763.77	Volumetric Pretest	-3.3	15.14	508.05	16.02
29	11311.16	1533.02	9395.87	9396.51	8911.66	Volumetric Pretest	-0.64	15.17	484.21	15.99
27	11421.64	355.62	9505.83	9502.77	8942.22	Volumetric Pretest	3.06	15.07	563.61	16.02
26	11428.58	15.84	9513.55	9512.03	8943.69	Volumetric Pretest	1.52	15.06	569.86	16.02
25	11437.13	3.04	9526.65	9522.78	8945.46	Volumetric Pretest	3.87	15.06	581.19	16.03
24	11439.93	4.10	9531.26	9529.29	8946.81	Volumetric Pretest	1.97	15.05	584.45	16.04
23	11449.82	9.00	9547.39	9543.37	8949.41	Volumetric Pretest	4.02	15.05	597.98	16.05
22	11454.73	78.12	9556.16	9553.29	8951.89	Volumetric Pretest	2.87	15.04	604.27	16.06
18	11506.45	1.99	9629.58	9623.70	8968.49	Volumetric Pretest	5.88	15.00	661.09	16.11
12	11508.57	62.13	9646.87	9637.33	8965.93	Volumetric Pretest	9.54	15.00	680.94	16.14
11	11515.62	139.37	9650.81	9650.44	8970.47	Volumetric Pretest	0.37	15.00	680.34	16.13

RFT/MDT MEASURED RESERVOIR PRESSURE ANALYSIS - EW 910 A3

EW 910 A3											
MW = 15.8 ppg											
Probe Type - Large Diameter											
Gauge Resolution - 0.010 psi											
File #	TVD	Drawdown	Phyd (b)	Phyd (a)	Pf	Comments		Phyd Diff	Pf (grad)	Phyd - Pf	MWBH
90	11096.10		9206.01	9221.02		Dry Test		-15.01	0.00	9206.01	15.97
84	11096.13		9272.58	9244.87		Dry Test		27.71	0.00	9272.58	16.09
83	11096.35	0.54	9273.51	9284.37		Dry Test		-10.86	0.00	9273.51	16.09
88	11096.43		9278.67	9244.19		Dry Test		34.48	0.00	9278.67	16.10
89	11096.72		9248.36	9212.94		Dry Test		35.42	0.00	9248.36	16.04
78	11123.83		9282.62	9296.60		Dry Test		-13.98	0.00	9282.62	16.06
77	11124.36		9298.49	9287.56		Dry Test		10.93	0.00	9298.49	16.09
73	11130.80		9303.31	9302.84		Dry Test		0.47	0.00	9303.31	16.09
65	11230.17	3.71	9386.21	9385.49		Dry Test		0.72	0.00	9386.21	16.09
61	11245.48		9400.92	9399.53		Dry Test		1.39	0.00	9400.92	16.09
38	11545.60		9653.86	9651.93		Dry Test		1.93	0.00	9653.86	16.10
74	11130.32	0.59	9303.71	9299.39	7853.29	Limited Drawdown		4.32	13.58	1450.42	16.09
96	10964.64		9155.20	9156.05		Lost Seal		-0.85	0.00	9155.2	16.07
95	10965.15		9163.72	9156.72		Lost Seal		7	0.00	9163.72	16.09
93	10965.60		9161.42	9166.71		Lost Seal		-5.29	0.00	9161.42	16.08
94	10966.15		9165.33	9163.24		Lost Seal		2.09	0.00	9165.33	16.09
72	11131.30		9302.86	9303.85		Lost Seal		-0.99	0.00	9302.86	16.09
60	11236.99		9388.86	9392.70		Lost Seal		-3.84	0.00	9388.86	16.08
57	11379.87		9513.53	9512.46		Lost Seal		1.07	0.00	9513.53	16.09
58	11380.33		9512.99	9512.66		Lost Seal		0.33	0.00	9512.99	16.09
55	11382.34		9514.18	9513.73		Lost Seal		0.45	0.00	9514.18	16.09
54	11382.86		9514.47	9514.26		Lost Seal		0.21	0.00	9514.47	16.09
52	11386.82		9518.13	9517.65		Lost Seal		0.48	0.00	9518.13	16.09

RFT/MDT MEASURED RESERVOIR PRESSURE ANALYSIS - EW 910 A3

EW 910 A3											
MW = 15.8 ppg											
Probe Type - Large Diameter											
Gauge Resolution - 0.010 psi											
File #	TVD	Drawdown	Phyd (b)	Phyd (a)	Pf	Comments		Phyd Diff	Pf (grad)	Phyd - Pf	MWBH
92	10979.64	55.88	9155.92	9176.47	8734.86	Normal Pretest		-20.55	15.31	421.06	16.05
91	10980.57	4.43	9110.56	9168.00	8733.83	Normal Pretest		-57.44	15.31	376.73	15.97
82	11119.37	148.16	9293.92	9294.27	8732.21	Normal Pretest		-0.35	15.12	561.71	16.09
81	11120.33	231.55	9288.70	9294.38	8736.47	Normal Pretest		-5.68	15.12	552.23	16.08
80	11122.34	131.86	9295.21	9290.71	8736.79	Normal Pretest		4.5	15.12	558.42	16.09
79	11123.33	8.97	9296.00	9296.26	8736.12	Normal Pretest		-0.26	15.12	559.88	16.09
76	11129.32	82.43	9302.05	9304.55	8737.73	Normal Pretest		-2.5	15.11	564.32	16.09

RFT/MDT MEASURED RESERVOIR PRESSURE ANALYSIS - EW 910 A3

EW 910 A3											
MW = 15.8 ppg											
Probe Type - Large Diameter											
Gauge Resolution - 0.010 psi											
File #	TVD	Drawdown	Phyd (b)	Phyd (a)	Pf	Comments		Phyd Diff	Pf (grad)	Phyd - Pf	MWBH
75	11129.76	12.68	9298.07	9310.14	8739.06	Normal Pretest		-12.07	15.12	559.01	16.08
71	11151.21	340.98	9338.78	9338.60	8744.22	Normal Pretest		0.18	15.09	594.56	16.12
70	11152.30	75.41	9321.30	9321.44	8727.40	Normal Pretest		-0.14	15.06	593.9	16.09
68	11156.28	40.99	9325.18	9324.86	8728.20	Normal Pretest		0.32	15.06	596.98	16.09
67	11159.27	175.76	9324.67	9327.28	8729.60	Normal Pretest		-2.61	15.06	595.07	16.09
66	11230.61	659.93	9386.80	9386.50	8771.80	Normal Pretest		0.3	15.04	615	16.09
64	11232.29	195.12	9387.77	9381.55	8771.95	Normal Pretest		6.22	15.03	615.82	16.09
63	11235.17	170.38	9390.33	9390.06	8772.47	Normal Pretest		0.27	15.03	617.86	16.09
62	11236.42	25.31	9391.29	9391.32	8772.62	Normal Pretest		-0.03	15.03	618.67	16.09
59	11380.82	52.75	9513.41	9513.05	8492.61	Normal Pretest		0.364	14.36	1020.804	16.09
56	11383.36	13.74	9515.52	9514.36	8490.46	Normal Pretest		1.16	14.36	1025.06	16.09
53	11386.38	305.91	9517.31	9517.05	8490.31	Normal Pretest		0.26	14.35	1027	16.09
51	11391.85	85.55	9522.48	9522.19	8488.21	Normal Pretest		0.29	14.34	1034.27	16.09
50	11400.86	282.56	9529.56	9529.35	8478.95	Normal Pretest		0.21	14.32	1050.61	16.09
49	11407.84	1638.48	9535.46	9535.28	8480.52	Normal Pretest		0.18	14.31	1054.94	16.09
48	11411.78	86.21	9539.17	9538.98	8481.43	Normal Pretest		0.19	14.31	1057.74	16.09
47	11414.82	146.98	9541.97	9541.96	8482.34	Normal Pretest		0.01	14.30	1059.63	16.09
46	11419.77	570.14	9545.4	9546.43	8484.01	Normal Pretest		-1.03	14.30	1061.39	16.09
45	11446.76	1047.12	9568.99	9568.89	8813.73	Normal Pretest		0.1	14.82	755.26	16.09
44	11447.73	95.66	9570.11	9570.13	8813.99	Normal Pretest		-0.02	14.82	756.12	16.09
43	11448.69	263.28	9569.01	9570.75	8814.41	Normal Pretest		-1.74	14.82	754.6	16.09
42	11478.72	20.52	9596.06	9595.88	8864.73	Normal Pretest		0.18	14.87	731.33	16.09
41	11479.71	45.51	9596.16	9596.42	8865.33	Normal Pretest		-0.26	14.87	730.83	16.09

RFT/MDT MEASURED RESERVOIR PRESSURE ANALYSIS - EW 910 A3

EW 910 A3											
MW = 15.8 ppg											
Probe Type - Large Diameter											
Gauge Resolution - 0.010 psi											
File #	TVD	Drawdown	Phyd (b)	Phyd (a)	Pf	Comments		Phyd Diff	Pf (grad)	Phyd - Pf	MWBH
40	11480.68	16.85	9596.98	9597.93	8865.99	Normal Pretest		-0.95	14.87	730.99	16.09
39	11546.09	3.05	9652.63	9652.14	8836.10	Normal Pretest		0.49	14.73	816.53	16.09
37	11547.88	549.64	9656.86	9655.59	8840.37	Normal Pretest		1.27	14.74	816.49	16.10

RFT/MDT MEASURED RESERVOIR PRESSURE ANALYSIS - EW 953 No. 1

EW 953 No. 1 - 2/12/86					
MW = 15.6 ppg					
Probe Type - Conventional					
Gauge Resolution - Unknown					
TVD	Phyd	Pf	Pf (grad)	Phyd - Pf	MWBH
2000	1616	-	-	-	15.55
3000	2430	-	-	-	15.59
4000	3230	-	-	-	15.54
5000	4040	-	-	-	15.55
6000	4901	-	-	-	15.72
7000	5716	-	-	-	15.72
8000	6477	-	-	-	15.59
8365	6786	-	-	-	15.62
9000	7300	-	-	-	15.61
9091	7364	-	-	-	15.59
9071.5	7355	7207	15.29	148.00	15.61
9071	7355	7203	15.29	152.00	15.61
9038	7317	7189	15.31	128.00	15.58
9036.5	7316	7187	15.31	129.00	15.58
9037.5	7317	7186	15.31	131.00	15.59
9037	7317	7185	15.30	132.00	15.59
8215	6668	6256	14.66	412.00	15.62
7689	6244	5845	14.63	399.00	15.63

APPENDIX A3: MDT FILES

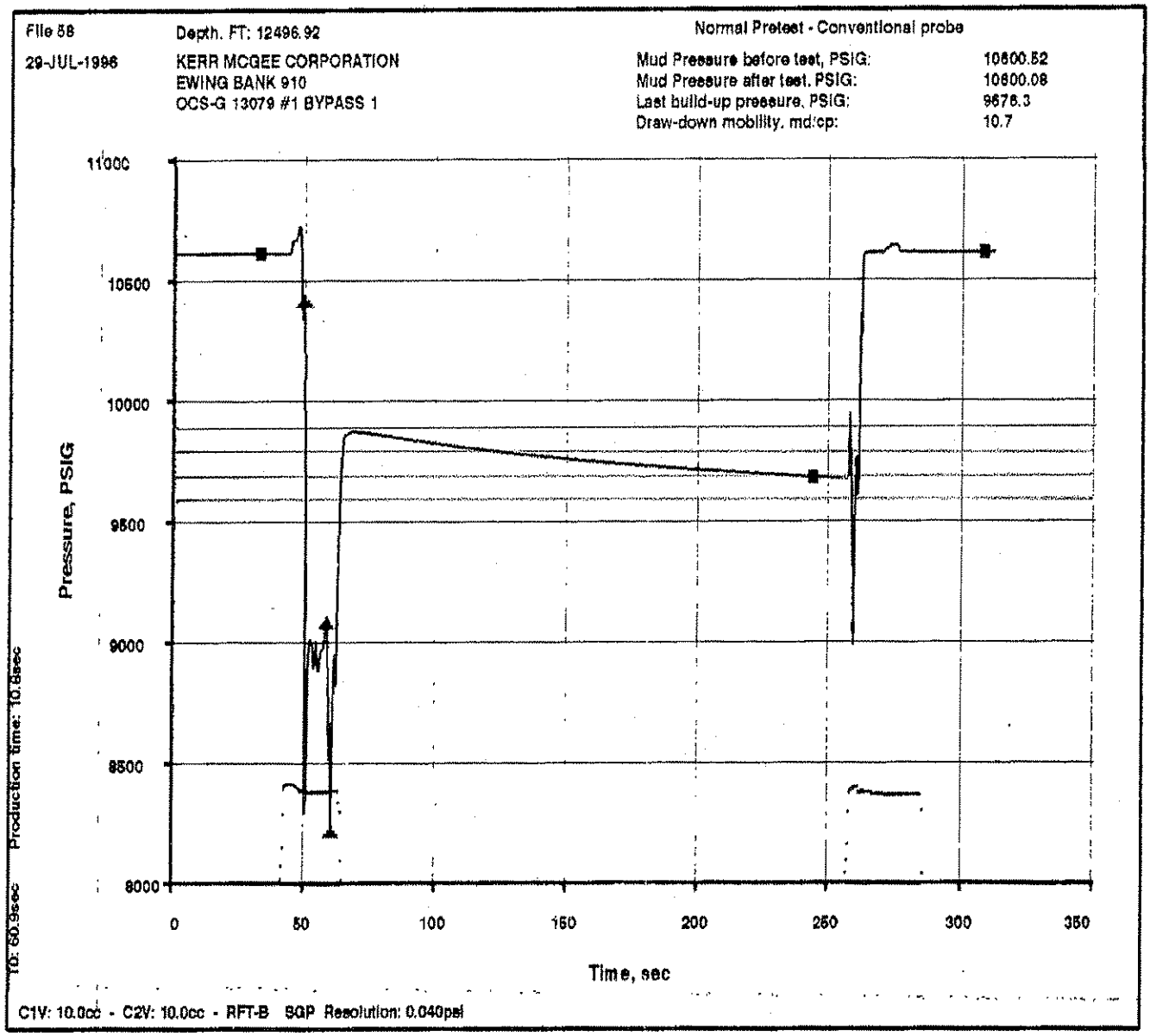

APPENDIX A3: MDT FILES

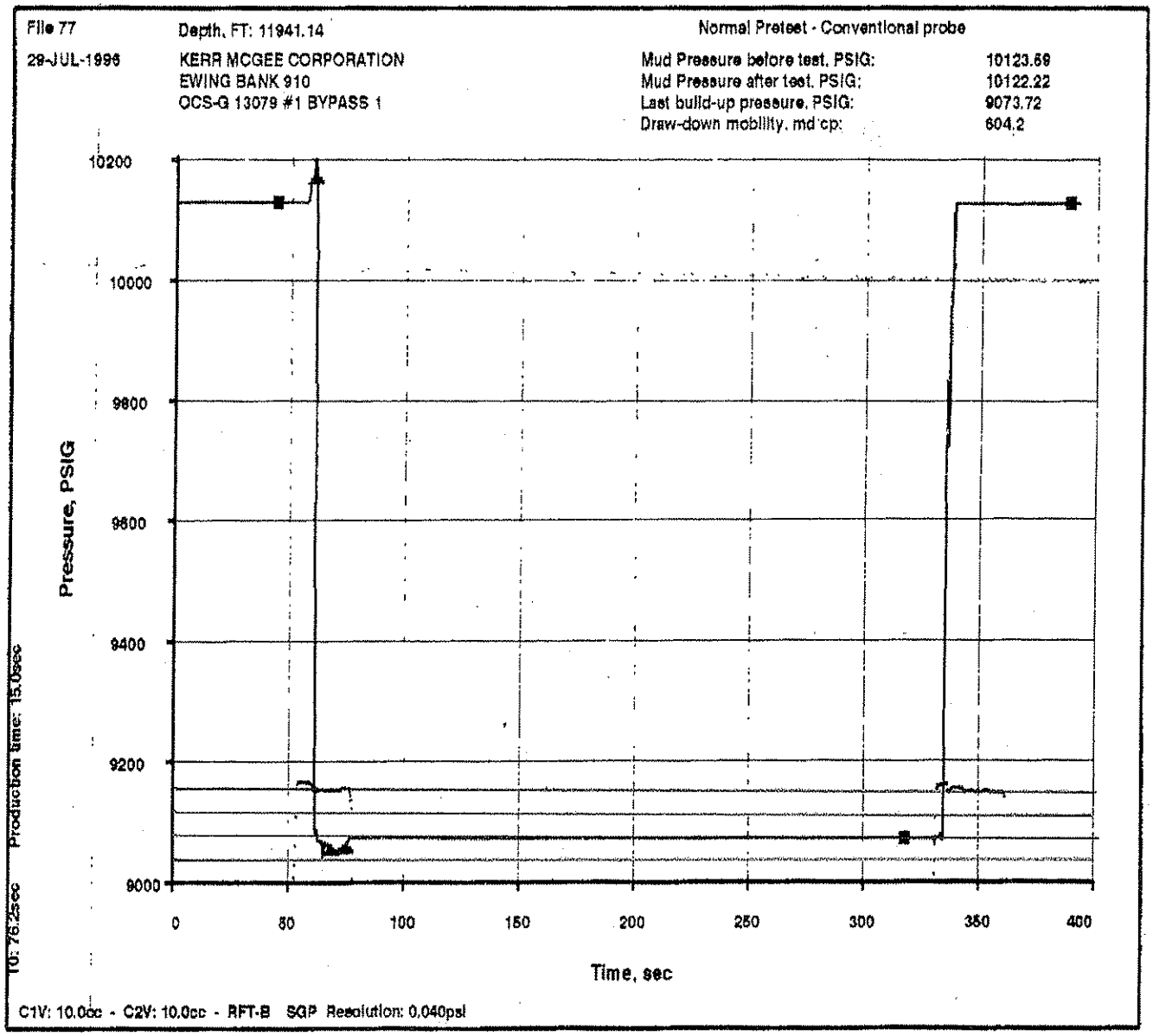

APPENDIX A3: MDT FILES

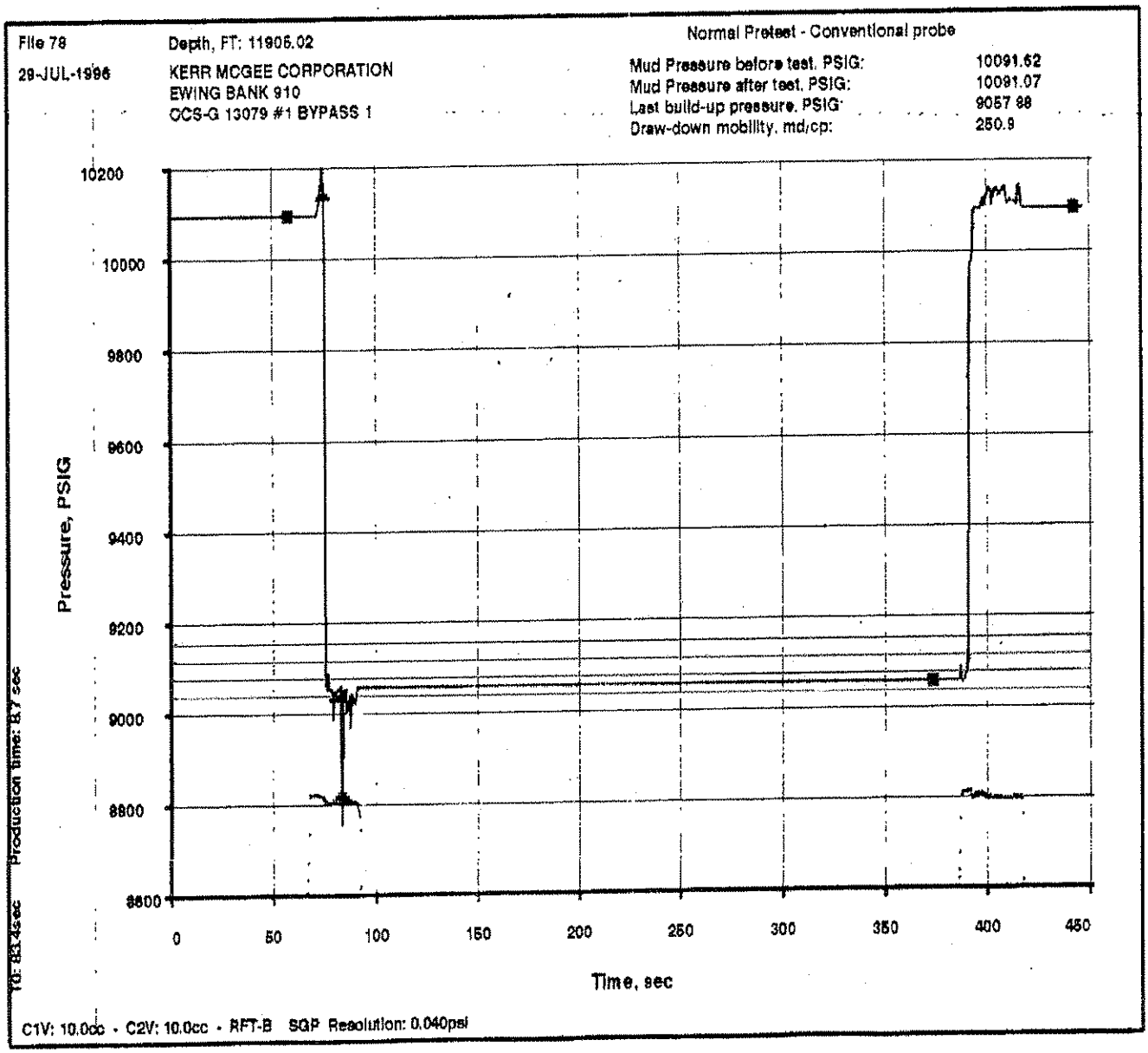

APPENDIX A3: MDT FILES

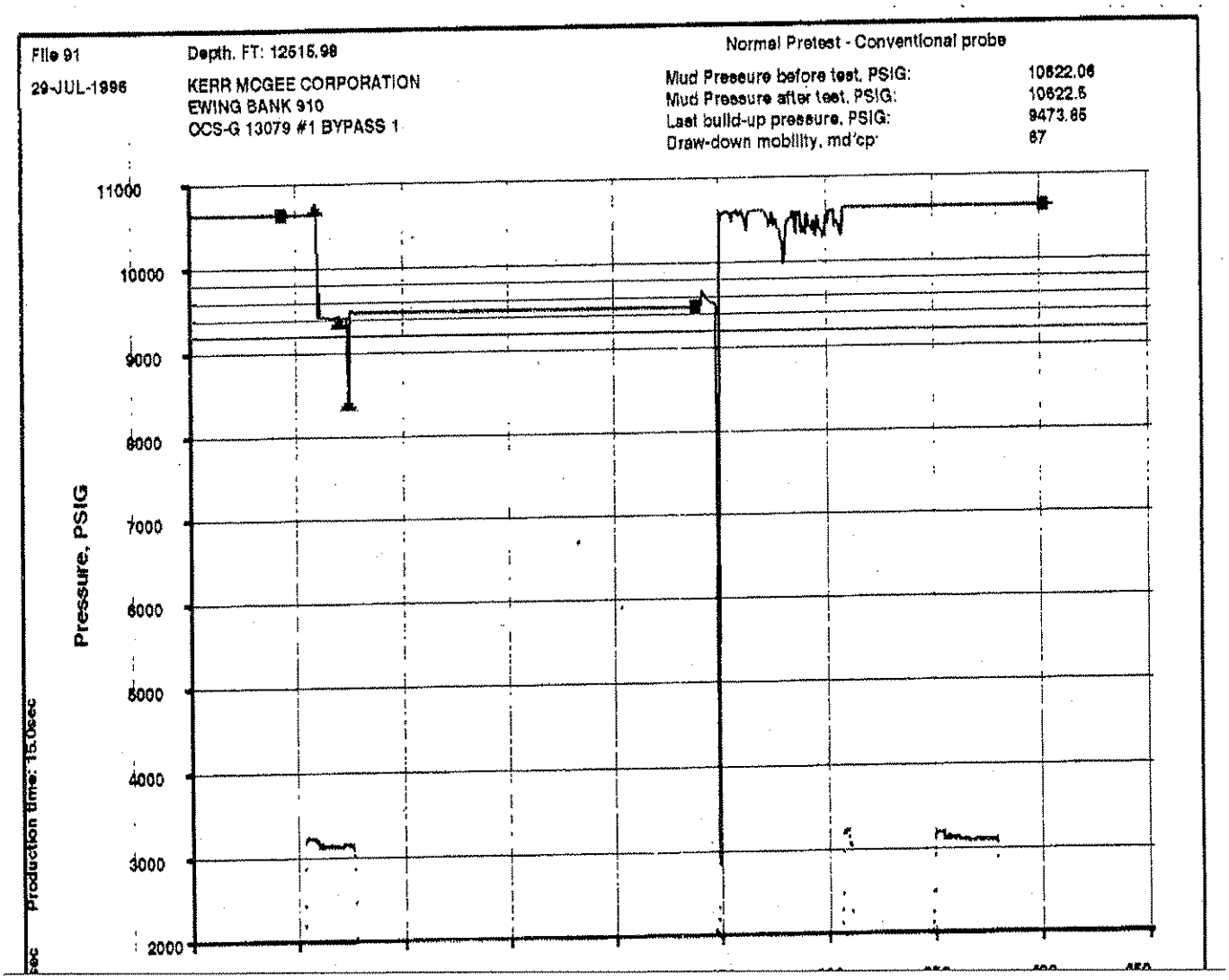

APPENDIX A3: MDT FILES

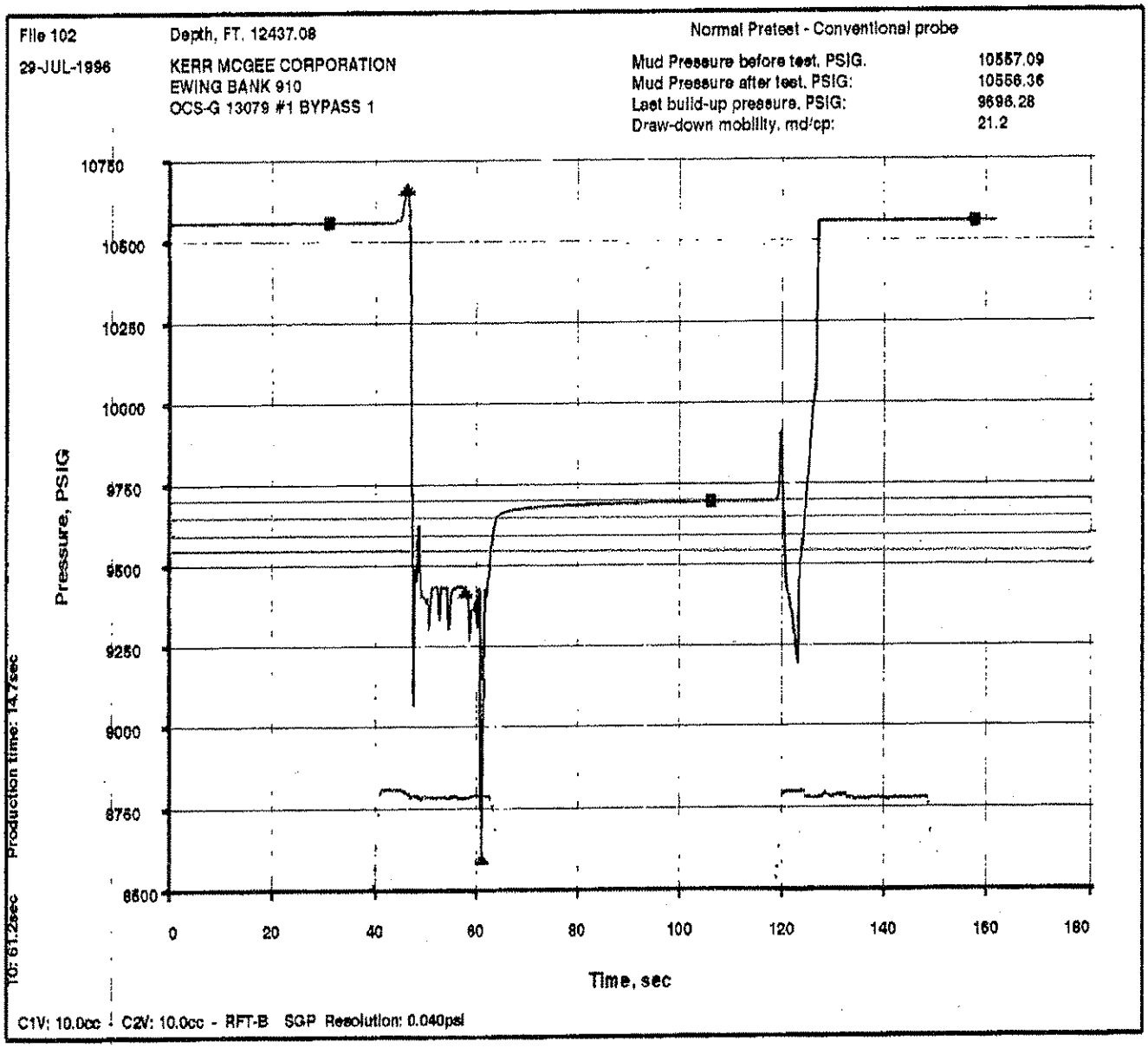

APPENDIX A3: MDT FILES

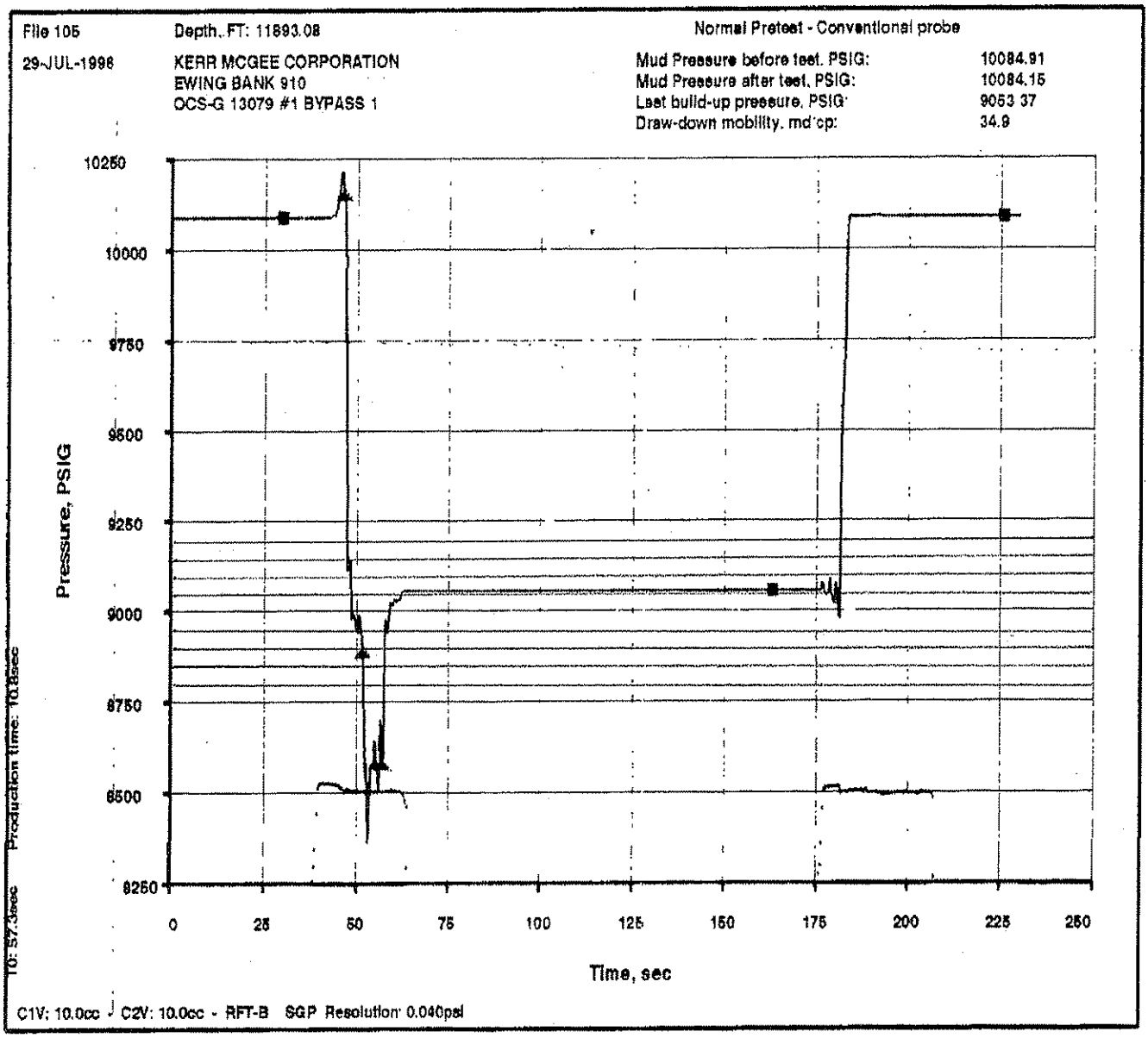

APPENDIX A3: MDT FILES

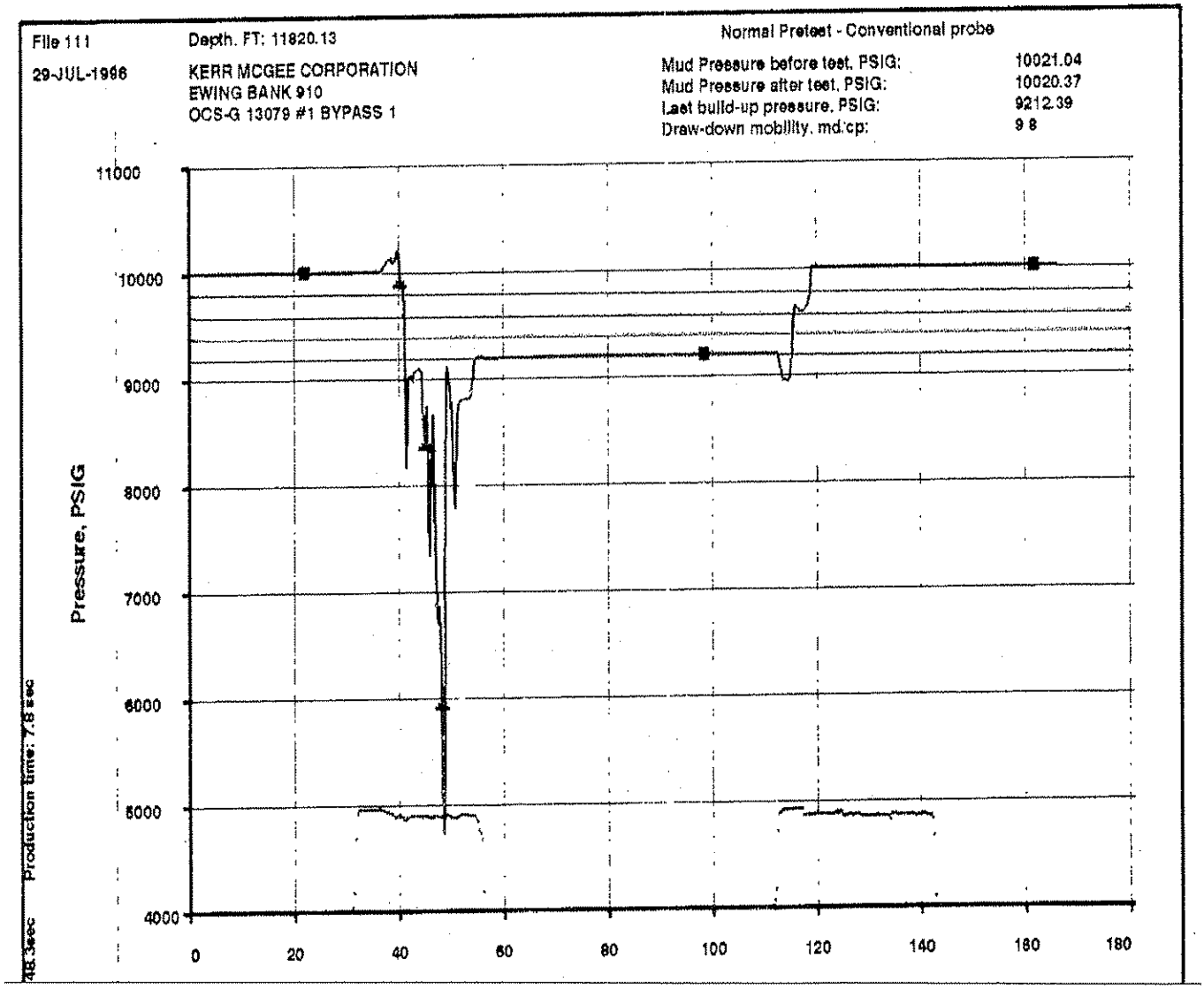

APPENDIX A3: MDT FILES

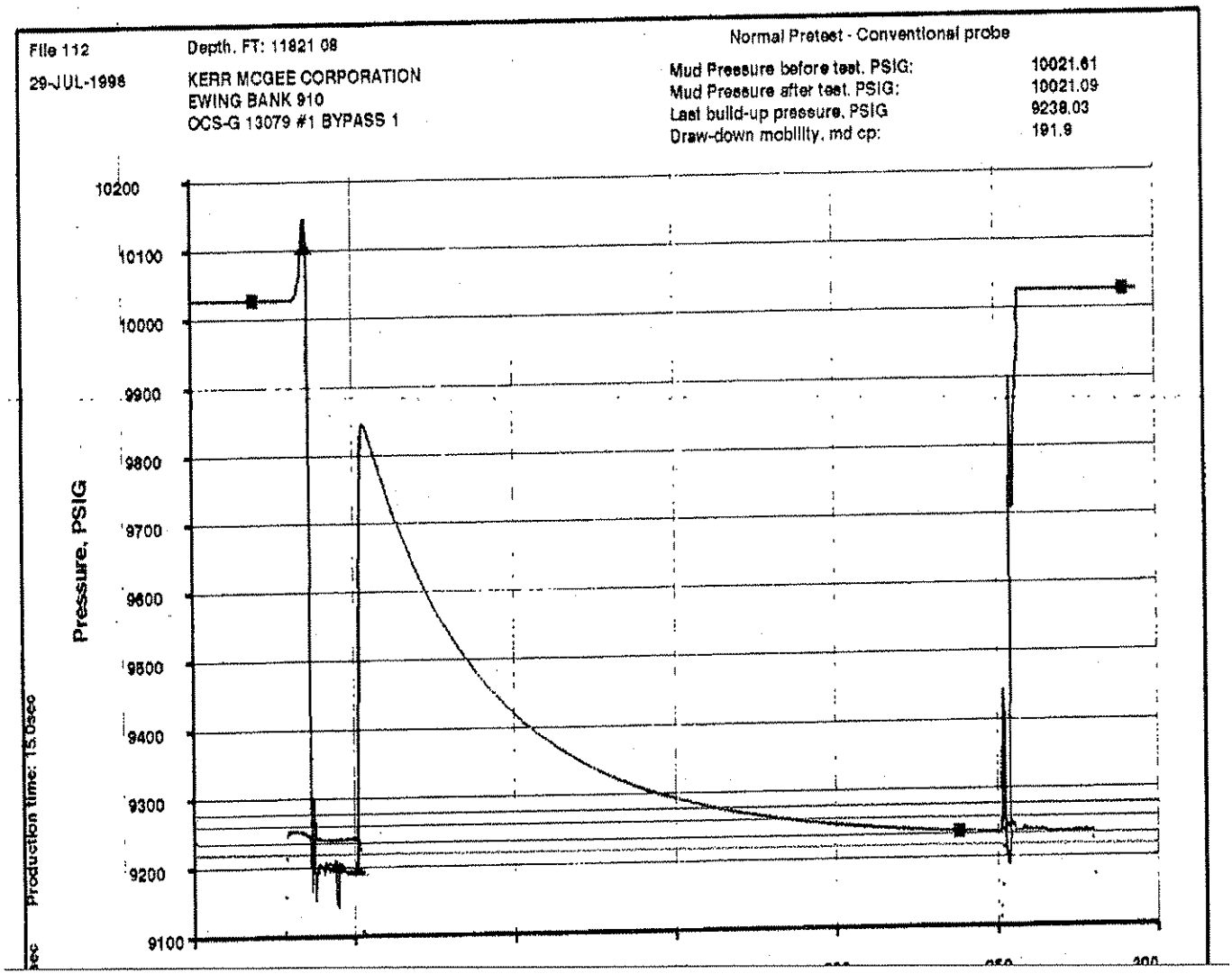

APPENDIX A3: MDT FILES

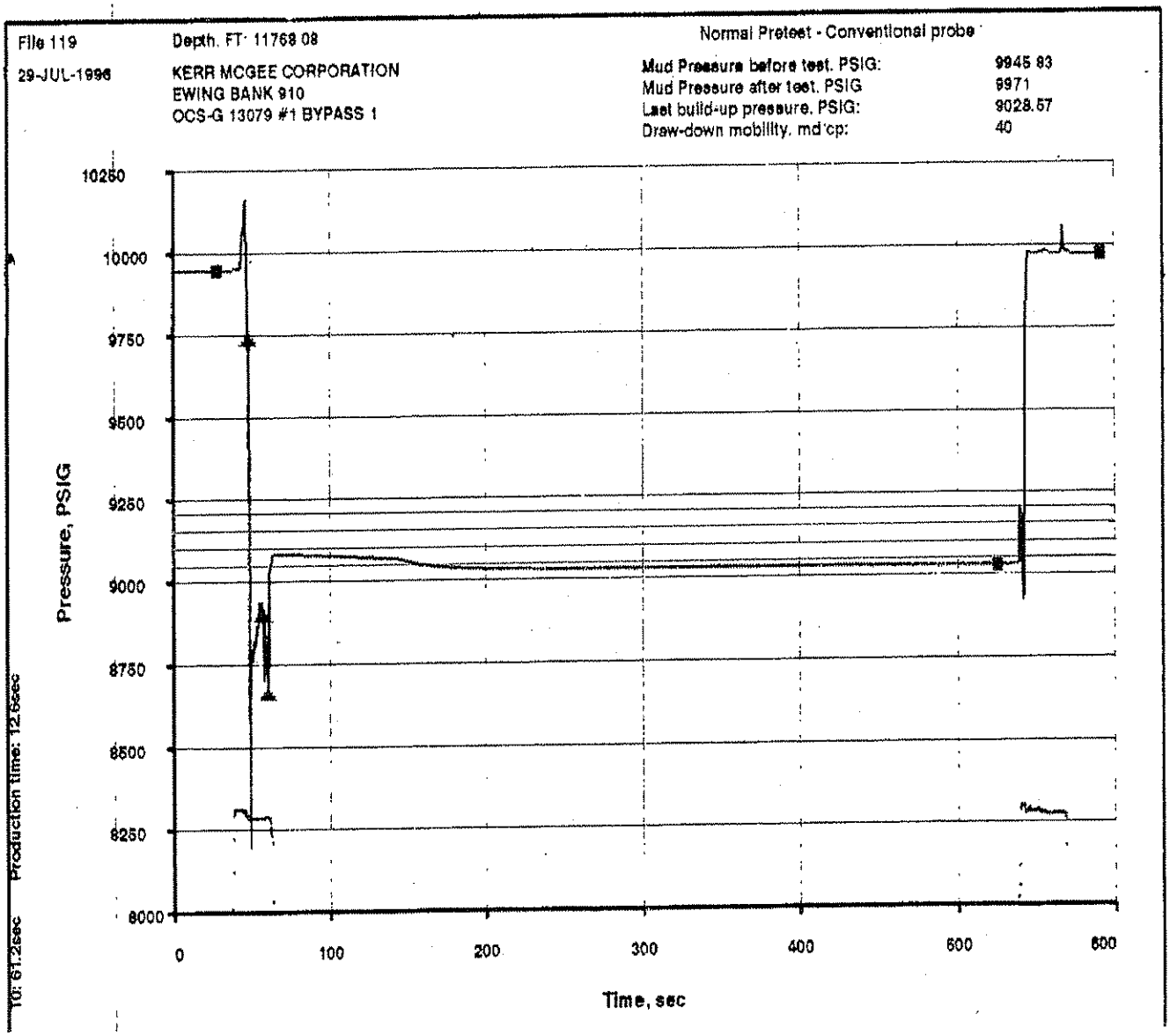

VITA

Jeffrey S. Fooshee is a native of Louisiana, being born in Baton Rouge and raised in Walker. After attending Live Oak High School, he began his secondary education studying Petroleum Engineering at Louisiana State University. While attending LSU, he was a member of the LSU Golden Band from Tiger Land and participated in many musical activities and ensembles.

After graduating with a Bachelor of Science in Petroleum Engineering in December, 2000, he began his engineering career for Bass Enterprises Production Company as a drilling engineer. While working as a full time engineer, he began pursuing his Master of Science of Petroleum Engineering Degree as a part-time student.

Pursuant to obtaining his Master's degree, his future plans are to progress into managerial roles within the oil and gas industry.